MINISTRY OF EDUCATION

TECHNICAL UNIVERSITY
OF CLUJ-NAPOCA, ROMANIA

FACULTY OF CIVIL ENGINEERING

Eng. Adina-Ana MUREȘAN

PhD THESIS

GBT analysis of the linear and buckling behavior of thin-walled conical shells

Scientific Main Supervisor:
Associate Professor PhD Eng. Mihai NEDELCU
Scientific co-Supervisor:
Associate Professor PhD Eng. Rodrigo de Moura Gonçalves

2019

Disclaimer

The content of the following PhD thesis may be viewed, transmitted and printed only for personal, didactic, research and non-commercial purposes. The copyright for the information presented in this PhD thesis is owned by the author and by the scientific supervisors. The information presented in the PhD thesis cannot be partially, respectively integrally reproduced or modified without the explicit permission, by written agreement, of the author and the scientific supervisors.

The content of the following PhD thesis, namely the text, the mathematical expressions, the figures and any other material found in the thesis are protected by the copyright law from Romania, Law no. 8/1996, with modifications brought by Law no. 74/2018 and by European Parliament and Council Directive 2004/48/CE from 29th April 2004 regarding copyright of intellectual property.

Acknowledgements

I would like to express sinciere gratitude to:

Associate Professor Mihai Nedelcu, from Structural Mechanics Department at Faculty of Civil Engineering, Technical University of Cluj-Napoca, Romania, for all of his support, for his valuable suggestions and encouragements that I received during my doctoral studies. All of these have helped me develop my career as civil engineer and researcher. It was a pleasure and honor to work with him.

Associate Professor Rodrigo Gonçalves, from Civil Engineering Department at Faculdade de Ciências e Tecnologia, Universidade NOVA de Lisboa, Portugal, for all the support I received and for the many explanations and advices he gave me. Also, I am grateful for showing me the life and culture of Portugal during my stay as Erasmus+ student. It has been a pleasure and an honor to work with him.

I would also like to express my gratitude to my family who supported me on the journey of becoming a civil engineer.

Table of Contents

List of Symbols and Abbreviations

Small Case Letters

$\{d^{(e)}\}$: the displacement vector;

$\{d_b\}$: the eigen vector corresponding to the eigenvalue λ_b;

$\{f^{(e)}\}$: the vector of equivalent nodal forces;

a_j: a coefficient whose value depends on the deformation mode j. Therefore, $a_j=0$ for $j=1$ and $a_j=1$ for $j=2…4$;

d_{free}: the vector of free displacements;

d_k: the eigen vector corresponding to the eigen value λ_k associated with deformation mode k;

d_{total}: the vector of total displacements (i.e. of all the finite elements);

f : the global vector of equivalent nodal forces;

f_{red}: the reduced global vector of equivalent nodal forces after the elimination of the columns corresponding to blocked degrees of freedom;

$j=1…4$: the global deformation mode having the following meanings: $j=1$ is axial extension, $j=2$ is bending with respect the major axis, $j=3$ is bending with respect the minor axis and $j=4$ is torsion;

k: the number of the deformation mode;

m: the number of circumferential waves;

n: the total number of deformation modes;

n_{hw}: the number of longitudinal half-waves;

s: the coordinate with respect the cross section's middle line in GBT for prismatic bars;

t: the thickness of the cross section's wall;

u: the conical shell's displacement on meridional direction;

u: the displacement with respect the bar's longitudinal axis in GBT for prismatic bars;

$u_k(s)$: the warping component of the middle line displacement profile corresponding to deformation mode k;

$u_k(\theta)$: the cross section warping displacement component of the conical shell's circumference corresponding to deformation mode k;

v: the conical shell's displacement on circumferential direction;

v: the displacement with respect the cross section's middle line in GBT for prismatic bars;

$v_k(s)$: the transverse component of the middle line displacement profile corresponding to deformation mode k;

$v_k(\theta)$: the cross section transverse displacement component of the conical shell's circumference corresponding to deformation mode k;

w: the conical shell's displacement on normal direction;

w: the displacement with respect the wall's thickness in GBT for prismatic bars;

$w_k(s)$: the flexural component of the middle line displacement profile corresponding to deformation mode k;

$w_k(\theta)$: the cross section normal displacement component of the conical shell's circumference corresponding to deformation mode k;

x: the coordinate with respect the bar's longitudinal axis in GBT for prismatic bars;

x: the local meridional coordinate of the conical shell;

x_g: the global coordinate of the conical shell with respect the longitudinal axis;

y_g: the global coordinate of the conical shell with respect its cross section;

z: the coordinate with respect the wall's thickness in GBT for prismatic bars;

z: the local normal coordinate of the conical shell;

z_g: the global coordinate of the conical shell with respect its cross section.

Upper Case Letters

$\widetilde{X}_j$: the modal geometric matrix which takes into account the influence of the pre-buckling stresses associated with deformation mode j;

$\widetilde{B}$: the modal stiffness matrix associated with cross section deformation;

$\widetilde{C}$: the modal stiffness matrix associated with general warping;

C_{ik}^1: the linear stiffness tensor associated with generalized primary warping;

C_{ik}^2: the linear stiffness tensor associated with generalized secondary warping;

$\widetilde{D}$: the modal stiffness matrix associated with torsion;

D_{ik}^1: the linear stiffness tensor associated with generalized torsion;

D_{ik}^2: the linear stiffness tensor associated with generalized flexural Poisson's effect;

$\widetilde{U}$: the global transformation matrix;

W_j^0: the vector of the pre-buckling stress resultants associated with deformation mode j.

X_{jik}^{σ}: the geometrical stiffness tensor associated with normal stresses;

$X_{jik}^{\sigma x}$: the geometrical stiffness tensor which takes into account the second order effects of the pre-buckling meridional stresses associated with deformation mode j;

$X_{jik}^{\sigma\theta}$: the geometrical stiffness tensor which takes into account the second order effects of the pre-buckling hoop stresses associated with deformation mode j;

X^{τ}_{jik}: the geometrical stiffness tensor which takes into account the second order effects of the pre-buckling shear stresses associated with deformation mode *j*;

$[G^{(e)}]$: the finite element geometric matrix;

$[K^{(e)}]$: the finite element stiffness matrix;

∂W: the variation of strain energy;

B: the bending component;

B: the stiffness matrix associated with cross section deformation;

B_{ik}: the linear stiffness tensor associated with generalized transversal bending;

C: the stiffness matrix associated with general warping;

C_{ik}: the linear stiffness tensor associated with generalized warping;

C_{jj}: the cross section's stiffness associated with deformation mode *j*;

D: the stiffness matrix associated with torsion;

E: the Young modulus of elasticity;

F_{ik}: the linear stiffness tensor associated with cross section distorsion of the conical shell, in the first order analysis;

G: the global geometric matrix;

G: the transversal modulus of elasticity;

G_{ik}: the linear stiffness tensor associated with cross section distorsion of the conical shell;

G_{red}: the reduced global stiffness matrix, respectively geometric matrix after the elimination of the lines and columns corresponding to blocked degrees of freedom;

H_{ik}: the linear stiffness tensor associated with cross section distorsion of the conical shell;

K: the global stiffness matrix;

K_{red}: the reduced global stiffness matrix after the elimination of the lines and columns corresponding to blocked degrees of freedom;

L: the length of the conical shell;

L: the matrix of localization which is used to transfer the degrees of freedom from finite element level to global level;

L_e: the length of the finite element;

M: the membrane component;

U_I: matrix resulted from the 1st GBT eigen problem;

U_{II}: matrix resulted from the 2nd GBT eigen problem;

U_{III}: matrix resulted from the 3rd GBT eigen problem;

$W_{j,x}$: the resultant of the pre-buckling shear stresses associated with mode *j*;

W_j: the resultant of the pre-buckling normal stresses associated with mode *j*;

X_j: the geometric matrix which takes into account the influence of the pre-buckling stresses associated with deformation mode *j*.

Greek Letters

$\gamma_{xs}^{B.L}$: the linear bending shear strain component for prismatic cross sections;

γ_{xs}^{M} : the shear membrane strain for prismatic cross sections;

$\gamma_{xs}^{M.NL}$: the non-linear membrane shear strain component for prismatic cross sections;

$\gamma_{x\theta}^{M.L}$: the linear membrane shear strain of conical shells;

$\gamma_{x\theta}^{M.NL}$: the non-linear membrane shear strain of conical shells;

$\varepsilon_{ss}^{B.L}$: the linear bending strain component along the cross section's middle line;

ε_{ss}^{M}: the transverse membrane strain for prismatic cross sections;

$\varepsilon_{xx}^{B.L}$: the linear bending strain component along the member's longitudinal axis;

$\varepsilon_{xx}^{M.L}$: the linear membrane meridional strain of conical shells;

$\varepsilon_{xx}^{M.L}$: the linear membrane strain component along the member's longitudinal axis;

$\varepsilon_{xx}^{M.NL}$: the non-linear membrane meridional strain of conical shells;

$\varepsilon_{xx}^{M.NL}$: the non-linear membrane strain component along the member's longitudinal axis;

$\varepsilon_{\theta\theta}^{M.L}$: the linear membrane hoop strain of conical shells;

$\varepsilon_{\theta\theta}^{M.NL}$: the non-linear membrane hoop strain of conical shells;

$\sigma_{ss}^{B.L}$: the linear bending normal stress component along the cross section's middle line;

σ_{xx}^{0}: the pre-buckling normal meridional stresses;

σ_{xx}^{0}: the pre-buckling normal stress along the member's longitudinal axis;

$\sigma_{xx}^{B.L}$: the linear bending normal stress component along the member's longitudinal axis;

$\sigma_{xx}^{M.L}$: the linear membrane normal stress component along the member's longitudinal axis;

$\sigma_{\theta\theta}^{0}$: the pre-buckling normal hoop stresses;

τ_{xs}^{0}: the pre-buckling shear stress for members with prismatic cross sections;

$\tau_{xs}^{B.L}$: the linear bending shear stress component for prismatic cross sections;

$\tau_{x\theta}^{0}$: the pre-buckling shear stresses;

$\{\varepsilon^{B}\}$: the conical shell's bending strains;

$\{\varepsilon^{M}\}$: the conical shell's membrane strains;

$\{\chi\}$: the vector of curvature variation with respect the middle surface;

α: the angle of the semi-vertex of the conical shell;

θ: the local circumferential coordinate of the conical shell;

λ: the load parameter;

λ_b: the eigenvalue corresponding to eigen vector $\{d_b\}$;

λ_c: the lowest eigenvalue called the critical buckling coefficient;

λ_k: the eigenvalues corresponding to deformation mode k;

μ: Poisson's ratio;

σ_c: the critical normal stress;

τ_c: the critical shear stress;

ϕ: the vector of modal amplitude functions defined along the bar's longitudinal axis;

$\phi_k(x)$: the modal amplitude function defined with respect the bar's longitudinal axis;

Abbreviations

cFSM: constrained Finite Strip Method;

DOF: degree of freedom;

DSM: Direct Strength Method;

FE: Finite Element;

FEM: Finite Element Method;

FSM: Finite Strip Method;

GBT: Generalized Beam Theory;

SFEA: Shell Finite Element Analysis;

TWB: thin walled bars;

TWS: thin walled structures.

Chapter I
Introduction

1.1. The Context of Research

Steel bars are often divided into two categories. The first category is represented by either hot-rolled or welded profiles. The second category which is less known, but with an increased importance, is represented by cold formed profiles. These structural members may come in the form of corrugated sheets, strips or thin walled bars and are manufactured by industrial processes which involve cold pressing, bending or embossing. The thickness of thin walled bars range, in general, between *0.378 mm* and *6.35 mm* [1].

Thin walled structures (TWS) are widely used in civil and mechanical engineering, from industrial buildings, showrooms, storage facilities, bridges to vechicle components, engines, naval and aerospace industry. Generally, the structural members formed by thin walled bars have the following advantages:

(i) Unlike thick hot rolled profiles, thin walled bars may be used for relatively small loads and/or spans.

(ii) Cross sections with unusual shapes may be manufactured economically using cold formed procedures, thus obtaining a favorable strength-to-weight ratio.

(iii) Thin walled structures may be manufactured as embbedable elements allowing compact packing and an easier transport.

(iv) Load-carrying panels may be used for floors, roofs and walls. In other conditions, these panels may provide closed spaces for electric wires and pipes.

(v) Load-carrying panels do not only take loads normal to their surface, but can also act as diafragms to take the in-plane loads, if the panels are properly connected between them and the main structural elements.

(vi) The large variety of cross section shapes results in various architectural configurations.

(vii) The slenderness of thin walled bars provides large reductions in building and material costs.

Besides thin walled bars (TWB) with prismatic flat-walled cross sections and corrugated sheets, in the same category enter also TWB with circular cross sections. The last one may appear as cylindrical bars or conical structures. Conical structures are often used as structural columns, cooling towers, pillars for oil platforms, pillars for wind turbines and in the aerospace industry. Also, truncated conical shells are used as transition elements between cylindrical bars having different diameters.

Conical structures are extremily efficient when it comes to strength and stability. Their most important property is the fact that the membrane stiffness is a few orders higher than the bending stiffness. Even though conical and cylindrical shells are used in many fields of engineering, the buckling of these structures is less studied than in case of prismatic TWB.

Even though the bearing capacity of TWB is high despite the low thickness of their walls, this type of structural elements are prone to buckling and excessive vibrations. The calculations to estimate the bearing capacity, the stability and the vibration behavior of TWB are one of the most complex structural analysis problems. Therefore, design codes are developed based on simplified, approximate and very often empirical formulae, which often lead to unjustified costs and a waste of material. Even nowadays, the design of some thin walled structures extensively used in current practice is exclusively based on experimental procedures (for example, TWB with variable cross sections or perforations).

Due to the slenderness of the walls, the collapse of compressed TWB usually takes the form of a coupled instability. The study of this complex phenomenon begins, generally, with the decomposition of the general buckling into pure deformation modes as follows (see Figure 1.1):

(i) Global deformation modes, where the cross section has a rigid body behavior;

(ii) Distortional deformation modes, where relative displacements of the corners of the section occur in the transversal plane,

(iii) Local deformation modes, where local buckling of the walls occur.

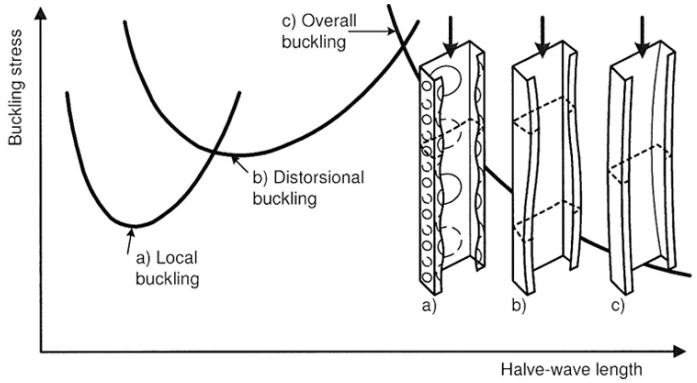

Figure 1.1: Pure buckling modes for thin walled bars [2].

Every pure buckling mode is represented by its own post-critical behavior:

(i) Local buckling has considerable post-critical capacity;

(ii) Global buckling doesn't have significant post-critical capacity;

(iii) Distortional buckling is an intermediary case.

The coupling of the GDL (global, distortional, local) deformation modes is often seen in TWB columns and beams. Therefore the determination of the degree of participation of the pure GDL modes in the general buckling mode (modal decomposition) is an important step in the determination

of the design bearing capacity of the structural member. But this is a difficult problem. For this reason, buckling analysis methods for thin walled structures are still being developed.

1.2. The Objectives of the Thesis

The purpose of the following study is to develop new numerical analysis methods for thin walled structures which are superior to the existent ones. The study focuses on the buckling behavior of circular cylindrical and conical shells. Also, the study extends the methods introduced by Nedelcu [3], [4]. The main objective is to create a Generalized Beam Theory (GBT) based Finite Element (FE) formulation for the analysis of circular cylindrical and conical shells. In the presented work, the proposed formulation was developed to handle 1st order and linear buckling analyses with various classic bar boundary conditions and various loading, namely axial compression, torsion and bending.

1.3. The Methodology of the Scientific Research

In order to correctly evaluate the buckling behavior of cylindrical and conical shells it is necessary not only to understand the buckling process of this type of structures, but also the GBT adapted for them. Therefore, the first step was the literature review and the study of the GBT formulation for thin walled bars with prismatic cross section, more exactly the original GBT developed by Schardt [5]. This step was followed by the literature review and study of the GBT extension to thin walled bars with circular cross section and with variable cross section. Once this task was completed, , the next step was the literature review of the GBT-based FE formulations, **developed until the present work only for prismatic members.**

After the literature review phase, the following step was the adaptation of the GBT-based FE formulation to circular cylindrical and conical shells for the following load cases: axial compression without stress concentrations, axial compression with stress concentrations, torsion and bending. The analyses were performed using Matlab [6]. The particularity of each load case is described in detail in the following chapters.

In order to validate the proposed formulations, several Abaqus [7] models were created and analysed using S4 rectangular shell finite elements. The validation of the proposed formulation consisted in a comparison with the results determined by shell finite element analyses (SFEA) in Abaqus. The proposed formulation was considered valid if the differences between the results obtained by the two analysis procedures did not exceed 5%.

1.4. The Structure of the Thesis

The following thesis is structured into 8 chapters. The content of the chapters is summarized below, as follows:

Chapter I: Introduction

The first chapter provides a general presentation of the thesis by including it in the research thematic context. Also, the objectives and the research methodology are stated.

Chapter II: Literature Review

The following chapter briefly presents the important studies from the area of thin walled structures and their buckling analysis methods. In case of the buckling analysis methods the main focus is on GBT by presenting the most related studies which are available up until this moment.

Chapter III: Generalized Beam Theory

The chapter presents general aspects regarding the Generalized Beam Theory for prismatic bars in order to familiarize the reader with the method. Then, the Generalized Beam Theory extension for circular conical shells is described in detail.

Chapter IV: The GBT-based Finite Element Formulation

The following chapter describes the GBT-based Finite Element formulation adapted for circular cylindrical and conical shells. The chapter describes the algorithm of the GBT-based FE formulation for the first order analysis and for the linear buckling analysis of these structures.

Chapter V: Axially Compressed Conical Shells

The chapter presents the case of axially compressed conical shells. The case study was divided into two main categories depending on the pre-buckling stress configurations of the conical shells from the analysed numerical examples: (i) conical shells without stress concentrations and (ii) conical shells with stress concentrations. Also, the numerical examples were also divided in other two cases depending on the wall thickness: (i) conical shells with constant thickness and (ii) conical shells with variable thickness. The chapter presents the differences between the results determined by the two analysis procedures, the buckling modes obtained from SFEA and the graphs of the modal amplitude functions resulted from the proposed GBT formulation. In the case of conical shells with pre-buckling stress concentrations the precision of the GBT-based FE formulation is analysed by meshing the GBT models with finite elements having constant and variable length. Thus, it is shown how to capture more precisely the stress concentrations occurring at the conical shell end sections.

Chapter VI: Conical Shells under Torsion

The chapter describes the case of conical shells under torsion, which is completely different from the case of axially compressed conical shells. The case studies were divided into two main categories depending on the wall thickness: (i) conical shells with constant thickness and (ii) conical

shells with variable thickness. Each case study mentioned previously was also divided into three other cases depending on the length of the analysed structure: (i) short conical shells, (ii) medium conical shells and (iii) long conical shells. As in the previous chapter, the results determined by SFEA are compared to the ones determined by the proposed formulation and the buckling modes resulted from SFEA and the graphs of the modal amplitude functions resulted from the GBT-based FE formulation are illustrated.

Chapter VII: Conical Shells under Bending

Chapter VII presents the case of conical shells under bending, a case study which was approached in a different manner compared to the previous load cases due to the complexity of the buckling process. The numerical examples were divided into two categories depending on the length of the analysed structures: (i) short conical shells and (ii) long conical shells. The chapter describes the first order analysis and, respectively the buckling analysis by presenting the graphs of the stresses that occur in this load case, the buckling modes resulted from SFEA and from the proposed formulation and the graphs of the modal amplitude functions. As in the previous two load cases, the results determined by the two buckling analysis methods were compared.

Chapter VIII: Conclusions

The last chapter presents the conclusions regarding the research developed for the thesis, the personal contributions and the future research projects.

At the end of the thesis, ***Annex I*** presents in detail the analytical expressions of the cross section stiffness matrices and the ***References*** presents all the scientific papers which contributed to the elaboration of the following thesis.

Chapter II
Literature Review

2.1. A Short History of the Research of Thin-walled Structures

Structural elements made of cold-formed steel were first used in civil engineering in 1850s in U.S.A. and U.K., but were only used at large scale starting from the 1940s in U.S.A. [8].

In 1930s, in U.S.A., the development of structural elements made of cold-formed steel was difficult due to the lack of specific codes. The design codes from that period didn't have technical guidelines for thin-walled structures. Because of the necessity of special technical conditions for TWB and due to the lack of previous studies, in 1939, the AISI committee (American Iron and Steel Institute) for research and technology in civil engineering financed a research project at Cornell University to study the behavior of TWB. The research conducted at Cornell University by professor George Winter and his assistants resulted in the development of the following TWB analysis methods: effective width for stiffened compressed members, lateral buckling of beams, bending buckling of columns, bending and twisting buckling of eccentrically and axially loaded columns in elastic and inelastic domain, the deformation of the web of TWB, the assymetrical bending of beams and the design of welded and bolted connections. Also at Cornell University, starting from the 1960s, Teoman Pekoz included the following aspects related to TWB analysis: the effect of residual stresses on columns, the distortional buckling of columns and beams, the design of rack structures, the probabilistic analysis of the bearing capacity of structural members and the design of frames made of TWBs [1].

Weng and Pekoz [9] studied residual stresses in TWBs using experimental methods. The results of the experiments provide the understanding of the distribution and intensity of residual stresses in TWB which are different from the residual stresses found in bars with hot rolled profiles. Based on the experimental results, the idealized distribution of residual stresses in TWB with "C" section was traced. Also, the authors described in [9] the propagation of the yielding plateau in an axially compressed TWB by formulating an equation which describes the degree of extension of the yielding plateau in the respective member.

Mulligan and Pekoz [10] formulated an efficient method to analyse the effects of local buckling in thin-walled columns and beams having one symmetry axis. The post-critical capacity of the cross-section was analysed by the effective width method. The authors developed one formula to determine the effective width which represents the behavior of the cross-section subjected to service loads and to analyse the bearing capacity of stiffened structural members subjected to uniform compression.

Also, the effective width method was proposed for the analysis of stiffened structural members which are eccentrically compressed. The validation of the method was done by comparing the results obtained through calculations with results obtained through experiments on cold-formed steel columns with "C" section.

Miller and Pekoz [11] studied through experimental methods the effects of eccentricity on the bearing capacity of the thin-walled columns subjected to axial forces. The experiments were conducted on 48 long columns with "C" section. The experimental results were compared to the bearing capacities for flexural buckling and flexural-torsional buckling determined using the AISI design code from 1986. Local buckling was analysed using the Effective Width Method. The same paper proposes an analysis method of buckling with respect the minor axis of the cross-section and of the interaction between the force and the lateral displacement of eccentrically loaded columns with initial imperfections.

Kalyanaraman and Pekoz [12] conducted an analytical study on the elastic and inelastic local buckling and on the post-critical behavior of unstiffened TWB subjected to compression. The authors formulated an equation for the elastic local buckling of the compressed unstiffened TWB. The equation starts from the solution of the small displacement equation of plates subjected to membrane stresses which was approximated by a sinusoidal function. In the post-critical study of compressed unstiffened TWB, the Von Karman 4^{th} degree differential equations were solved. These equations describe the small displacements of the plates with out-of-plane imperfections. The differential equations were solved by using the sinusoidal function approximation. The solution of the elastic and inelastic local buckling analysis and of the post-critical behavior analysis obtained by the proposed analytical study were compared with the experimental results.

Schafer et al. [13] provided an overview of computational modeling for elastic buckling and non-linear elastic analysis for cold formed steel elements. The authors focus on recent research and experiences with computational modeling of cold formed steel members conducted with a research group at Johns Hopkins University. The paper describes the use of semi-analytical Finite Strip Method and the collapse modeling using shell finite elements. The authors compared the solutions resulted from Finite Strip Analysis and Shell Finite Element Analysis and emphasized the importance of imperfections, residual stresses, material modeling, boundary conditions, element choice, discretization and solution controls in collapse modeling of cold formed steel structural elements.

Besides the studies conducted at Cornell University, there were other research projects of TWBs made by private companies and other universities in the U.S.A. The results obtained have been presented at national and international conferences and in journals of different engineering organizations. Since 1975, the ASCE (American Society of Civil Engineers) committee for thin-

walled structures had conducted 38 research projects and released 1300 scientific papers entailed in 18 categories. These documents are important sources for researchers and engineers which design thin-walled structures. In 1990, Missouri-Rolla University opened the Center for Thin-walled Structures where 48 research projects were conducted. Researches on the behavior of TWB were also conducted in other parts of the world where there are available design codes for these type of members. Some of these design codes are based on the "Limit States Design" concept. In 1993, the European Commettee for Standardization released Part 1-3 of Eurocode 3 [2] which is designated for the design of thin-walled structures [1].

Hancock et al. [14] proposed strength design curves for thin-walled cross-sections subjected to distortional buckling. The design curves were based on experimental data. Lucas et al. [15] proposed a non-linear elasto-plastic finite element model which is able to predict the behavior of purlin sheeting systems without the need of experimental input or simplifying assumptions. The proposed model incorporates both the sheeting and the purlin. The model takes into account the cross-sectional distortion of the purlin, the flexural and membrane restraining effects of the sheeting and the failure of the purlin by local buckling or yielding. The proposed model was validated by comparing the results with experimental data.

Key and Hancock [16] conducted an experimental programme at the University of Sydney, Australia, where they investigated the behavior of columns with square hollow cross sections. The tests were performed on stub, pinned columns and detailed measurments of the yield stress and residual stress were recorded. After the experimental tests the columns were investigated by large deflection elastic-plastic finite strip analysis including also the measured distribution of the yield stress and residual stress. The analysis took into account the plate geometric imperfections, the variation of yelding stress along the cross section, the stress – strain properties of the material and the patterns of the residual stresses produced by the cold forming process. The influence of the measured residual stress components on the ultimate load and the behavior of the square hollow cross section columns was demonstrated by comparing the analytical results with the experimental results.

Young and Rasmussen [17] investigated the behavior of cold-formed plain and lipped channel columns under compression with fixed and pinned boundary conditions. The authors showed, by means of experiments, that local buckling does not induce general bending in fixed-ended singly symmetric columns as it does in the case of pinned singly symmetric columns. Therefore, the authors demonstrated that local buckling has different effects on fixed ended and pinned singly symmetric columns. The experiments were performed on plain and lipped channel columns made of high strength structural steel which were break-pressed. The samples had four different cross-section geometries and lengths. The experimental tests involved pure local buckling, distortional buckling,

general flexural buckling and torsional-flexural buckling. The effects of local buckling depending on the boundary conditions were investigated by comparing strengths, load shortening, load – deflection curves and longitudinal profiles of buckling deformations.

Blum and Rasmussen [18] carried out an experimental program on a series of portal frame systems composed of back-to-back channels for the columns and rafters. The authors discovered that, by changing the knee brace and knee brace-to-column connection bracket, the buckling capacity of the column was significantly affected. This aspect was not captured in design calculations. The column's buckling capacity must be accurately calculated to predict correctly the frame's behavior and the ultimate buckling loads for design purposes. Therefore, the authors developed an energy method approach to calculate the buckling load of a column with an intermediate elastic torsional restraint. After validating the proposed method by comparing the results with experimental data, the authors observed that the energy method approach estimated the experimental column buckling load by 6%.

Young and Ellobody [19] investigated the behavior and design of cold-formed unequal angle columns using non-linear finite element analysis. The finite element analysis was performed on end fixed columns having different lengths. The measured initial and global imperfections and also the material properties of the specimens were included in the models. The authors showed that the finite element model closely predicted the ultimate experimental loads and the behavior of cold-formed steel unequal angle columns. Using the finite element models the authors performed extensive parametric studies of cross-section geometries. The authors compared the results of the parametric study with the design strengths determined by the North American Specification for cold-formed steel structures and demonstrated that the current design rules were generally unconservative for short and medium length columns with unequal angles. Therefore, the authors proposed design rules for cold-formed steel columns with unequal angles.

Davies et al. [20] conducted a study on the design of perforated cold-formed steel cross-sections under axial load and bending. The purpose of the study was to find analytical methods to design these types of members. The study consisted in experimental tests on columns in which the load position varies along the axis of symmetry. The experimental results were analysed using FEM and a version of GBT. Davies showed that GBT could be modified to take into account perforations such that the lower bound results give a sufficiently accurate design curve for columns. The design curve obtained from the analysis takes into account local, distortional and global buckling. Therefore, extensive testing of perforated cold-formed steel bars is unnecessary.

Ghersi et al. [21] analysed the experimental results of double channel cold-formed beams under local and lateral torsional buckling in order to identify the range definition of the buckling modes

which influence the ultimate behavior of these type of beams. The experimental results were compared to results obtained by Eurocode 3 [2] and AISI [22] design approaches and the agreement was satisfactory. The authors also established the coupled instability range by means of Eurocode 3 formulations. The proposed equations provide useful indications for designers because they relate to the main geometrical parameters of the beam.

Loughlan [23] presented the weakening effects of local buckling on the compressive load carrying capacity of thin-walled cold-formed cross-sections. These effects were studied on pinned compression members with different cross-section shapes. The theoretical results were determined by a differential equation which describes approximatively the overall bending behavior of locally buckled compression members. In the theoretical approach both local and general imperfections were taken into account, showing that the effect of these imperfections was the decrease of the ultimate compressive carrying capacity of cold-formed sections. Experimental tests were carried on concentrically loaded pinned I-section struts and columns and the results were compared to the ones obtained by the theoretical approach. The author showed that the theoretical results were in good agreement with the experimental results. The author also compared the provisions regarding the design of cold-formed compression members of the U.K. Code of Practice with the ones of the American Specification. The author showed that the American design procedure gives more conservatives estimates of collapse loads regarding I-section struts and columns.

Tomà et al. [24] conducted a survey on the fastening possibilities of cold-formed steel structures such as mechanical fasteners, welding and adhesive bonding. The authors emphasized in their study that the selection of the fastening type should not be based only on structural requierments, but also on non-structural requirements such as economic aspects (i.e. total number of necessary fastenings, skill required, the ability to be dismantled, design life and installation costs), durability, watertightness and aesthetics. The study was based on statistical evaluations leading to improved versions of existing design rules and an uniform partial safety factor for bearing capacity.

Madeira et al. [25] developed an optimal design method for cold-formed steel columns. The objectives of the study were to maximize the local buckling capacity and to maximize the distortional buckling capacity. The elastic local, distortional and global buckling loads of the columns were determined using the Finite Strip Method and their bearing capacities were determined by the Direct Strength Method. The main focus of the design problem was the angle of orientation of the cross-section walls. In the numerical examples presented in reference [25], both symmetrical and non-symmetrical cross-sections were considered.

Zagari et al. [26] presented an imperfection sensitivity analysis of thin-walled cold-formed steel members in compression for perforated steel pallet racks having different lengths. The analysis

method applied in this case study is a finite element implementation of the Koiter method coupled with a Monte Carlo simulation. The analysis is also based on an extensive experimental study carried at "Politechnica" University of Timisoara, which showed that there is a strong relation between the buckling mode and a significant reduction of the load bearing capacity. The limit load is evaluated statistically by Koiter's method while thousands of geometrical imperfections are analysed. Thus, the worst combination of geometrical imperfections is determined and the erosion of the critical buckling load due to imperfections and modal interactions is evaluated.

Bertocci et al. [27] conducted an extensive experimental study on centric and eccentric compressive behavior of thin-walled steel uprights of pallet rack systems. The cold-formed steel profiles analysed by the authors are perforated through their whole length and have open, mono-symmetric cross-sections. Besides experimental studies, the pallet rack systems also went through finite element simulations which included geometrical and material non-linearities. The experimental and numerical results were compared to design code prescriptions. The authors remarked that the experimental results show non-symmetrical behavior about the cross-section's weak axis and non-linear, convex bending-bending interaction, unlike the design codes which are safety preserving with an average underestimation of the strength of about 10%.

Tondini and Morbioli [28] determined the flexural bearing capacity of cold-formed laterally restrained steel rectangular hollow flange beams by experimental-numerical methods. The results of the experimental study consisted in material caracterisation and tests on full-scale specimens. The numerical analysis was performed to develop a model capable of reproducing the experimental results. Also, numerical analyses were used to expand the available theory over a wider slenderness range by parametric studies.

Basaglia et al. [29] studied the buckling, post-buckling, collapse and design of cold-formed steel beams under non-uniform bending caused by transverse loadings which act away from the shear centre. This means that the load is applied either at the top or bottom flange. The results of the study consisted in critical load factors determined by Generalized Beam Theory (GBT), plastic collapse load factor determined by ANSYS with first order elastic-plastic Shell Finite Element Analysis (SFEA), ultimate load factors determined by geometrically non-linear elastic-plastic SFEA, also with ANSYS and ultimate load predictions determined with two Direct Strength Method (DSM) design approaches. The values of the ultimate strengths were compared to the values determined using Direct Strength Method (DSM) curves. The authors remarked that the location of the transverse load's point of application influences significantly the beam's buckling and non-linear behavior. Thus, this influence should be taken into account when designing cold-formed beams subjected to transverse loads.

Sadovský and Kriváček [30] studied the ultimate buckling strength of axially loaded cold-formed lipped channel columns. In the numerical examples variations of boundary conditions and eccentricities of the loads were considered. The ultimate strength was determined by geometrical and material non-linear Finite Element (FE) analyses. The geometrical imperfections were approximated as eigenmodes of the linearized buckling problem. For each case study the worst eigenmode imperfection was determined. The authors showed the effects of the boundary conditions and load eccentricities on the ultimate buckling strength of the cold-formed lipped channel columns by determining the lowest collapse loads corresponding to the eigenmode imperfections.

Bonada et al. [31] presented three methodologies to predict the load carrying capacity of cold-formed steel rack columns by using non-linear Finite Element Analysis (FEA). The lengths of the columns were chosen such that the failure occurs due to distortional buckling. The authors showed that, for the chosen range of lengths, the accurate prediction of the ultimate load is more complex than in the case of lengths where failure occurs due to local or global buckling. The columns were analysed using three different methodologies. The first methodology uses the critical buckling mode. The second methodology used for the analysis is iterative and uses the buckling mode that leads to the lowest ultimate load. The first two methodologies use the Finite Element Method. The third methodology uses the GBT-based Finite Element formulation to determine the modal participation of the buckling mode resulted from FEM and to generate a particular combined geometric imperfection. The authors validated the predicted loads by comparing the results determined by the three methodologies mentioned previously with experimental results.

Vraný [32] studied the effect of loading on the rotational restraint of cold-formed steel purlins. The author proposed an analytical model based on the study of redistribution of contact forces. Different case studies of purlins having “Z” and “C” cross-sections were analysed, demonstrating that the effect of loading on the stiffness is different for each case. For example, for C-purlins under gravity loads, the loading does not affect the stiffness, while for C-purlins under uplifting loads, the loading reduces the stiffness. The model results were compared to results determined by numerical simulations.

Kasperska et al. [33] developed an optimal design of selected channel cross-section shapes subjected to bending moment. The problem of optimization was a bicriteria one, in which the cross-section area is the first objective function and the deflection of the beam is the second objective function. The selected design variables were the cross-section geometric parameters. The set of constraints consists in global and local stability conditions, strength condition and technological and constructional requierments in the form of geometric relations. The optimization problem was formulated and solved by the Pareto concept of optimality and preference functions.

Dubina and Zaharia [34] conducted an experimental research for the evaluation of the semi-rigid behavior of bolted connections used in cold-formed steel plane truss joints. The trusses were created in the laboratory of the Department of Steel Construction and Structural Mechanics (CMMC: Construcții Metalice și Mecanica Construcțiilor) of the "Politechnica" University of Timisoara. The semi-rigid character of the joints was established according to Eurocode 3 provisions and from the experimental values of the resistant moment and initial stiffness of the joints. To demonstrate the improvement of the load bearing capacity compared to the classical approach, a numerical analysis was performed on the cold-formed steel truss in which the semi-rigid behavior was taken into account by using the experimental results. The authors proposed a semi-analytical method combined with FEM and calibrated with experimental results for the parametric study of the local behavior of semi-rigid joints.

The same authors [35] had an experimental research on evaluating the real behavior of bolted joints in cold-formed steel trusses. The authors proposed a theoretical model of joint stiffness by performing tests on single lap joints and on truss sub-assemblies. Also the authors developed a formula to evaluate the joint stiffness and from which the buckling length of web members was further determined. The formula was validated through an experimental test performed on a full-scale cold-formed steel truss.

Ungureanu et al. [36] proposed a new solution for cold-formed steel beams of corrugated web and built-up section for flanges in which the beam is composed by a web of trapezoidal cold-formed steel sheet and the flanges of built-up cold-formed steel members such as back-to-back lipped channel cross-sections or angles with turn lips. The flanges and the web can be connected by self-drilling screws or by spot welding. In order to validate and optimize the proposed technical solution, a large experimental program was carried at CEMSIG Research Centre (http://cemsig.ct.upt.ro) of "Politechnica" University of Timișoara, where five beams with corrugated webs having different self-drilling screws and shear panels arrangement patterns were tested.

Dubina [37] showed how test results could be used to solve and validate complex problems of cold-formed steel structures analysis and design. The author presented in [37] the following problems of analysis and/or design of cold-formed steel structures: the calibration of an imperfection factor α for interactive buckling curves, the experimental calibration of stiffness of bolted joins in cold-formed steel trusses, the design assisted by testing of pitched roof cold-formed steel portal frames considering the actual behavior of joints and the design assisted by testing of seismic resistant cold-formed steel framed houses. The author remarked that without experimental tests the solutions of the problems presented in the paper would be difficult to determine.

Dubina and Ungureanu [38] assumed that purlins are semi-continous at the junction between single and lapped sections based on experimental evidence. The authors proposed to take into account the web crippling action at the edge of the lapped section in interaction with the bending moment. Based on that assumption, the authors developed design formulae for strength and stability checking for different types of global and local stress interactions. The formulae were validated by comparing the results with experimental and numerical data.

In the last decades many researchers demonstrated through experimental and numerical analysis that, generally, the design codes for thin-walled structures significantly underestimate their buckling resistance (references needed). Also, the determination of effective widths is a time-consuming task for structural engineers. This motivates the development of new methods of analysis which are more efficient and which are able to provide accurate results regarding the buckling behavior of TWB.

2.2. Studies of Thin-walled Bars with Circular Cross-section

The stability of cylindrical and conical structures has been studied from analytical and experimental point of view since the beginning of the 20th century. First, small displacement theory was used to obtain the solutions of the bifurcation of shell-type structures [39]. However, the experimental results showed that cylindrical structures buckle at loads with values lower than the ones predicted by the small displacement theory. Donnel [40] proposed a non-linear theory for circular cylindrical structures which uses the thin plate hypothesis. Depending on which of the non-linear components of the deformations are taken into account, other large displacement theories were proposed by Sanders [41], Flügge [42] and Novozhilov [43]. *The Love – Timoshenko non-linear theory [44] is used in the numerical studies presented in the following thesis because, compared to Donnel or Sanders theory, it contains additional non-linear components.* Goldfeld summarized the kinematic relationships of the three theories mentioned previously [45].

The following sections present examples of numerical, analytical and experimental studies related to cylindrical and conical shells.

2.2.1. Studies on Cylindrical Shells

Von Karman and Tsien [46] conducted an important study of the stability of circular cylindrical structures under axial loads using Donnel's non-linear theory. In this study the authors showed that the intensity of the load applied to cylindrical structures decreases as the values of the displacement increase. Later, Donnel and Wan [47] showed that the imperfections were the cause of the large differences between the analytical and experimental results of the stability analysis of cylindrical structures.

Arbocz and Hol [48] present a stochastic method which uses first order, second moment ? analysis to evaluate the stability of isotropic, orthotropic and anisotropic nominally? circular cylindrical shells subjected to axial compression, external pressure and/or torsion. The cylindrical shells studied in the paper possess general non-symmetric random initial imperfections. The initial imperfections resulted from measurements and are represented as Fourier series. The Fourier coefficients are then used to construct the second-order statistical properties. The buckling loads were determined by standard computer codes which included a rigorous satisfaction of the specified boundary conditions. The authors showed that the stochastic approach provides a way to combine the latest theoretical findings with the practical experience in an optimal manner by using advanced computational facilities.

Winterstetter and Schmidt [49] conducted a comprehensive experimental and numerical study of cylindrical shells under combined loading. The authors provided rules for the numerical simulation of the realistic buckling behavior of cylindrical shells by means of substitute geometric imperfections.

Rahman and Jansen [50] developed a finite element formulation of Koiter's initial post-buckling theory using a multi-mode approach. The authors illustrated the capability of the implementation for buckling analysis of shell structures including modal interaction. The case study consisted in the post-buckling analysis of a composite cylindrical shell under compression which included the non-linear pre-buckling state. The analysis was carried out using a small number of representative modes.

Singh et al. [51] investigated the influence of meridional curvature on the post-buckling behavior of angle-ply laminated cylindrical shells under axial compression, external pressure, torsion and uniform temperature increase by using a semi-analytical finite element approach. The non-linear governing equations were solved by the iterative method Newton-Raphson coupled with the adaptive displacement control method. The variation of ply angle and ply thickness along the meridional direction were considered in the analysis. According to the results, the imperfection sensitivity of cylindrical shells with negative Gaussian curvature decreases as the height-to-radius ratio increases for all the loading cases considered. In the case of cylindrical shells with positive Gaussian curvature, imperfection sensitivity increases for external pressure, torsion and thermal load, while for axial load it decreases with the increase of height-to-radius ratio.

Alexander [52] developed an approximate theory for the analysis of the collapse of thin cylindrical shells under axial loading. The resulted solution had the following form: $P=Ct^{1.5}\sqrt{D}$, where P is the collapse load, t is the cylindrical shell's thickness, D is the diameter of the cylindrical shell and C is a material constant.

Seide and Weingarten [53] studied the stability of circular cylindrical shells under pure bending by using Bartdorf's modified Donnel's equation and the Galerkin method. The authors showed that the maximum critical bending stress is equal to the critical compressive stress for all practical purposes, which was contrary to the commonly accepted value.

Schenk and Schuëller [54] investigated the effect of random geometric imperfections on the limit loads of isotropic, thin-walled cylindrical shells under deterministic axial compression. The authors introduced a concept for the numerical prediction of the large scatter in the limit load which was observed in experiments using direct Monte Carlo simulation technique in context with the Finite Element Method. The geometric imperfections were modeled as two dimentional, Gaussian stochastic processes with prescribed second moment characteristics which were taken from a database of measured imperfections. The limit loads were determined by geometrically non-linear static analysis using the code STAGS (Structural Analysis of General Shells).

Shen and Chen [55] studied the buckling and post-buckling behavior of perfect and imperfect cylindrical shells having finite length under combined loading of external pressure and axial compression. The authors developed a theoretical analysis for the buckling and post-buckling of circular cylindrical shells under combined loading using a singular perturbation technique. The analysis was based on the boundary layer theory which includes the edge effect in the buckling of shells. The proposed theory was validated by comparing the results with detailed experimental data.

2.2.2. Studies on Conical Shells

Jabareen and Sheinman [56] examined the effect of the pre-buckling non-linearity on the bifurcation point of a conical shell by using Donnel, Sanders and Timoshenko shell theories. The eiegenvalue problem was solved by iterative methods from the non-linear equilibrium state to the bifurcation point. The authors developed a new algorithm for the real buckling behavior which covered the entire non-linear pattern. The proposed algorithm was necessary for structures with a softening process where the pre-buckling non-linearity depresses the buckling level relative to the classical one. The algorithm developed by the authors involves non-linear partial differential equations divided into two sets by the perturbation technique as following: a set of equations for the pre-buckling state and a set of equations for the buckling state. The equations were solved by the following methods: in the circumferential direction the variable was expanded in Fourier series and in the axial direction the finite differences method was used. The procedure was implemented into a general computer code.

Tovstik [57] studied the stability of elastic cylindrical and conical shells assuming that their buckling behavior consisted in the formation of a number of dents which depend on the initial stresses

and on the curvature of the middle surface. The author showed that, in the most simple case, when the initial stresses and the curvature of the middle surface are constant, the dents cover the entire surface of the conical or cylindrical shell. If the initial stresses and the curvature of the middle surface are variable, then the buckling mode is complicated. The dents may occur in the vicinity of the most "vulnerable" lines and points.

Chandrashekhara and Karekar [58] carried out a bending analysis of a truncated conical shell under asymmetrical bending using an approximate theory similar to Donnel's theory for cylindrical shells.

Chryssanthopoulos et al. [59] used a finite element analysis to quantify critical elastic response and imperfection sensitivity in order to validate existing design recommendations for unstiffened cones and to develop a design approach for stringer-stiffened cones under compression. Also, Chryssanthopoulos and Spagnoli [60] studied the non-linear behavior of stringer-stiffened cones under axial compression by using finite elemenet analysis. The authors presented various alternatives of boundary conditions and analysed the sensitivity of the response to the radial edge constraint. The authors showed that the initial stiffness and the limit load can be severily reduced if the radial edge displacements are not constrainted. This means that the linear eiegenvalue results can be misleading.

Kouchakzadeh and Shakouri [61] studied the buckling of two joined conical shells, simply supported and subjected to axial compression by using Donell's thin plate theory and the principle of minimum strain energy. The continuity conditions from the joining section of the two conical shells were expressed by the resultants of the stresses and deformations. The equations were solved in the following manner: for the circumferential direction trigonometric responses were assumed, while for the meridional direction the solutions had the form of series. The paper studies the influence of the cone's vertex angle and of the length of the meridians on the critical buckling load, on the buckling mode and on the number of circumferential half-waves. According to the studies, the critical buckling load of the joined conical shells increases as the slope of the meridians incline to the cylindrical structure. In case of short members, the critical buckling load of joined conical shells decreases rapidly if the values of the angles of their vertices incline to be equal (i.e. there is a lower degree difference between them). In case of long members, the critical buckling load of joined conical shells is equal to the minimum between the critical buckling loads determined separately for each conical shell. Also the bearing capacity of the structure subjected to axial forces increases if two joined conical shells are used instead of one.

Ecsedi [62] derived a formula for the torsional stiffness of a conical membrane shell made of linear elastic homogeneous isotropic material. The torsional stiffness of a truncated conical shell was

defined as the value obtained from the square of the applied torque divided by two times the strain energy in the state of pure torsion.

Maali et al. [63] studied the global longitudinal imperfections created by welding and their effects on external pressure load bearing capacity. The study was carried out using finite element models. The models were modified to include one or two line imperfection with amplitudes of six different magnitudes. According to the study the load-bearing capacity resulted from buckling analysis was double the result from Jaward theory [64] for models without imperfections. Also, the authors remarked that, by increasing the height of the cone, the imperfections' weakening effect also increased.

Sofiyev and Kuruoglu [65] investigated the buckling of homogeneous and non-homogeneous orthotropic thin-walled truncated conical shells under axial load and in large deformation. The authors first derived the governing relations using the large deformation theory with von Karman – Donnel type kinematic non-linearity. The the authors determined the modified Donnel type stability and compatibility equations of non-homogeneous orthotropic thin-walled truncated conical shells in large deformations. The equations were solved analytically. Finally, the authors investigated the influences of the non-homogenity, orthotropy and variation of the conical shell's geometry on the non-linear axial buckling load. The proposed analysis was validated by comparing the results of the study with results from the literature.

Veldman [66] investigated the wrinkling interaction curves of straight and conical inflated beams subjected to torsion and bending. The interaction curve obtained by analytical methods was compered to the one obtained from finite element models. The author showed that the coarseness of the mesh strongly influences the wrinkling load predictions. Thus, a refined mesh is necessary for the analysis. The author also showed that the interaction curve of the conical beam is described by a near straight torque mode path and a quadric bending mode path.

Watts et al. [67] studied the non-linear bending and snap-though instability phenomenon of isotropic composite conical shell panels using the element free Galerkin method (EFG) with moving kriging (MK) shape function. The non-linear equations of equilibrium were developed from Sanders' shell theory along with von Karman's strain-displacement assumptions. The equations were solved by a modified Riks technique in conjunction the Newton-Raphson method. The convergence and accuracy of the EFG method were analysed for the linear and non-linear bending behavior of conical shells. Also, the arc-length control algorithm was used to determine the non-linear equilibrium paths of conical shells under different loading conditions.

Shakouri et al. [68] analysed the simultaneous buckling modes of compressed conical shells. The elastic buckling of shell structures under different loading conditions is described by the

simultaneous presence of several buckling modes corresponding to the same buckling load. In [68] the simultaneous presence of several buckling modes is studied in axially compressed conical shells. For the buckling analysis of these structures Donnel's theory was used, while the presence of the simultaneous buckling modes was determined by the semi-analytical Galerkin method. According to the study, the Galerkin method was successfully applied to axially compressed conical shells, emphasizing, as in the case of cylindrical shells, the presence of simultaneous buckling modes. The results obtained by the Galerkin method were similar to the ones obtained by FEA from the half-wave number distribution's point of view. The distribution of the simultaneous buckling modes of compressed conical shells was described by the Koiter circle [69] for cylindrical shells by using the alternative definitions of the non-dimensional space of wavelengths. Keeping the physical meaning of the half-wavelengths, the buckling modes of conical shells were inserted in the Koiter circle by normalizing the meridional and the circumferential half-waves with respect the middle axis parallel to the linear half-wave from bending given by the average curvature radius of the conical shell. Also the buckling modes of conical shells can be inserted in the Koiter circle by equalizing the half-wave lengths from buckling and the linear half-waves lengths from bending with an ideal cylindrical shell. These optimized values of length and radius of conical shells, determined by simplifying their buckling to the buckling of an equivalent cylindrical shell, may provide an understanding of the distribution of the simultaneous buckling modes and, also, of the sensitivity to imperfections.

Seide [70] studied the buckling of thin circular truncated conical shells under torsion in a manner similar to the buckling under uniform hydrostatic pressure. According to the numerical results, the critical torsional moment of a truncated conical shell is equal to that of an equivalent cylindrical shell whose length and thickness are the axial length and the wall thickness of the analysed conical shell and whose radius is a function of the semi-vertex angle-to-slope ratio of the respective truncated cone.

Shadmehri et al. [71] proposed a semi-analytical buckling analysis method for composite conical shells under axial compression. The buckling analysis of laminated composite conical shells was done taking into consideration the effect of shear strains on the transversal direction because it was demonstrated that the classical plate theory is not precise enough for laminated conical shells with average thickness, where the material anisotropy is severe [72], [73]. The formulation of the method began from the principle of minimum potential energy and, together with the Ritz method, resulted the equation that lead to the determination of the solution of the buckling problem. The authors developed an axial symmetric formulation and, respectively an axial non-symmetric one. The conical shells were analysed with each type of formulation and buckling loads were obtained, with the smallest value being the critical buckling load. According to the analysis, the critical buckling

load of short conical structures with small thickness decreases as the angle of the semi-vertex increases. The decrease of the critical buckling load intensifies when the value of the angle is larger than 20°. This is an important aspect regarding the design of these structures. Also the critical buckling load increases as the angle of the fibers in the short laminated conical shells increases.

2.3. The Analysis and Design Methods of the Thin-walled Structures

The following section briefly presents buckling analysis and design methods for thin walled structures.

2.3.1. The Finite Element Analysis

The Shell Finite Element Analysis (SFEA) is one of the most used for thin-walled structures. This method is able to work easily with complex geometric configurations and with arbitrary loads and supports. The drawbacks of the classical SFEA are as follows: the method is not able to provide the modal participation and the SFEA models require a large number of degrees of freedom in the buckling analysis. Therefore, SFEA was combined with other analysis methods such that less computational effort and time could be achived.

For example, Nedelcu [74] developed a method which combines the GBT with SFEA to perform the buckling analysis of perforated thin-walled members. The proposed method is able to provide the participation of pure buckling modes (i.e. global, local and distortional buckling) in a coupled instability, an aspect which is harder to achieve by using only SFEA. The advantage of the proposed method comes from the fact that only GBT cross-section deformation modes are used in the analysis instead of pure member deformation shapes. Also, there are no restrictions regarding the shape of the member's cross-section, the loading and the boundary conditions.

Also, Nedelcu and Cucu [75] developed a method that combines GBT with SFEA which is able to identify the pure buckling modes from the general buckling of isotropic thin-walled members. The advantage of the method consists in the capacity of using only GBT cross-section deformation modes instead of member mode shapes. Therefore, the participation of each pure buckling mode in a coupled instability can be evaluated accurately and quantitatively. The proposed method doesn't have restrictions regarding the shape of the cross-section, the loading and the boundary conditions.

2.3.2. The Effective Width Method

The Effective Width Method is the most popular buckling design method for thin-walled structures. This method uses an "effective" cross-section, obtained by eliminating areas which are prone to local buckling. Therefore, the determination of the critical local buckling load is avoided.

The critical distortional buckling load is determined using semi-empirical formulae, while the critical global buckling load is determined with the classical Ayrton-Perry formulae. This strategy was adopted by design codes for thin-walled structures such as Eurocode 3 [2], AISI 1996 [22], AISI 2011 [76] and AS/NZS 1996 [77]. The design methods are, generally, similar. The evaluation of the stability consists in the following steps:

(i) The determination of the critical elastic load using the effective cross section;

(ii) Including the weakening caused by imperfections and the possible favorable effects given by the post-critical bearing capacity (for example the significant post-critical strength reserve of the local buckling).

In the last decades, many researchers proved by experimental and numerical methods that, generally, the design codes for thin-walled structures significantilly underestimate their bearing capacity and the determination of the effective cross-section is a time-consuming process for the structural engineer.

2.3.3. The Direct Strength Method

The Direct Strength Method (DSM) was first developed by Hancock and Pekoz. Later, Schafer developed DSM to the current form and introduced it in the design code NAS – Appendix 1 [78] in 2004. This method uses the gross section and is based on the elastic critical loads/moments including cross-section deformation (distortion and local buckling). These critical loads are then used to determine the bearing capacity of the structural member under coupled instability. To evaluate these elastic critical loads, Schafer et al. created the CUFSM [79] program, which is based on a special TWB analysis method called the Constrained Finite Strip Method (cFSM). The authors developed cFSM by inserting some of the hypotheses of the Generalized Beam Theory (described in Section 2.3.5) in the standard Finite Strip Method (FSM, described in the next section). Therefore, the authors forced FSM to determine pure buckling modes used by the DSM for the design of thin-walled structures [80].

2.3.4. The Finite Strip Method

The Finite Strip Method (FSM) is a semi-analytical buckling analysis method developed for thin-walled prismatic plated structures. The FSM is described by the following features: discretization into strips which are in the form of long and narrow rectangular plates, the selection of longitudinal shape functions which represent exact or approximate solutions of the problem and the use of polynomial transverse shape functions similar to Finite Element Method applications. Therefore, FSM involves a significantly smaller number of degrees of freedom than SFEA, requiring less input

data and computational effort. Because it is necessary to pre-define adequate longitudinal shape functions, FSM can only be applied to certain types of regular structures.

In the buckling analysis, the stiffness of each strip results from a combination of small deflection plate bending terms and moderate deflection of membrane terms under plane stress. The adopted shape functions are standard cubic polynomials for the transverse flexural degrees of freedom, linear polynomials for the transverse membrane degrees of freedom and sinusoidal functions along the longitudinal direction. The choice of these longitudinal functions implies that the member's end sections are globally and locally pinned and they are able to warp freely. In this situation, only solutions for the buckling of thin-walled structures with pinned end supports are obtained. However, the FSM is able to analyse more complex boundary conditions.

There are at least two programs based on FSM available to the technical and scientific community, such as THIN-WALL [81] and CUFSM [79].

2.3.5. The Generalized Beam Theory

The Generalized Beam Theory is one of the most evolved methods specialized in the analysis of thin-walled structures. GBT determines the general solution of the linear and non-linear analysis of TWB with prismatic sections using an "enriched" bar theory which is able to describe rigid body displacements and cross-section in-plane and out-of-plane deformation. The method was originally developed by Schardt [5], [82] and it is able to run a variety of structural analyses, the most important being the stability of thin-walled structures [83], [84]. GBT is able to reproduce the buckling shape of the structural member by a linear combination of pure deformation modes which take into account the rigid body displacements (global modes) and the deformations of the transversal plane (local and distortional modes, among others). Therefore, GBT is able to:

(i) Determine the participation of each deformation mode in a coupled instability problem;

(ii) Determine the pure buckling modes (for example, only the global buckling, distortional or local buckling of the analysed member).

Both analyses are necessary for the design of slender TWB, especially for cold-formed steel profiles regardless of the method or the design code applied. Other advantages of GBT are the short computational time and efficiency due to the use of bar elements instead of shell or 3D elements. Therefore, GBT uses less degress of freedom than SFEA or FSM with the same numerical accuracy. The only program based on GBT currently available is GBTUL [85], which is able to perform buckling (bifurcation) and free vibration analyses.

Methods such as SFEM, FSM or spline FSM are able to model any type of thin-walled structure and to perform non-linear analysis in elasto-plastic domain with geometrical imperfections and

residual stresses, but they are not able to determine pure buckling modes without inserting complex kinematic constrains. Also these methods are not able to determine the modal participation in a coupled instability. The specialized methods perform the opposite and this is evident when the analysis is run with GBTUL or CUFSM. Currently, these programs are able to model TWB with prismatic cross-sections and polygonal cross-sections under classical loading and boundary conditions. Also, GBTUL and CUFSM are able to model circular cylindrical shells by approximating the cross-section with a polygon made of at least 30 segments. The programs are not able at the moment to model initial imperfections or residual stresses, to model bars with variable cross-sections and, also, they are limited to buckling and vibration analyses.

2.4. Previous Studies of the Generalized Beam Theory

The following section presents the main numerical and analytical studies regarding the analysis of thin-walled structures using GBT.

2.4.1. Numerical and Analytical Studies of the Generalized Beam Theory

Davies and Leach popularized GBT with the papers „First-Order Generalised Beam Theory" [86] and „Second-Order Generalised Beam Theory" [87].

Bebiano et al. [88] developed a GBT formulation for the elastic linear buckling of thin-walled members with arbitrary flat-walled cross-sections (including closed cells combined with open branches) subjected to general loadings. The general loadings include transverse forces which act away from the member's shear center axis. Also, the general loadings may involve the presence of pre-buckling stress distributions associated with any possible combination of all the stress tensor membrane components and of the cell shear flows. Therefore, all the geometrically non-linear effects need to be taken into consideration. The numerical examples used for the validation of the proposed formulation were as follows: a RHS cantilever subjected to two tip point loads, a simply supported beam with a closed-flange I-section under a uniformly distributed load and a two-cell RHS cantilever subjected to tip transverse forces and couples. For all the numerical examples, the loads were applied both along the shear center axis and along axes parallel to it, located at the beam's top and bottom surfaces. The results were obtained by GBTUL 2.0 and consisted in pre-buckling stress fields, buckling curves and buckling mode shapes. The proposed formulation was validated by comparing the results obtained by GBTUL 2.0 with results obtained by SFEA with ANSYS.

Silvestre and Camotim [89] developed a GBT formulation for the buckling analysis of composite thin-walled members made of laminated plates and which display arbitrary orthotropy. The concepts and procedures of the first order GBT for isotropic materials are adapted to take into account

the member's orthotropy. The same authors developed a second order GBT for the analysis of composite thin-walled members made of laminated plates with arbitrary orthotropy [90]. The proposed second order GBT formulation was validated by investigating the buckling behavior of thin-walled orthotropic columns and beams.

Silvestre and Camotim also present in [91] a GBT formulation for the first order and buckling analysis of composite thin-walled members made of laminated plates which display arbitrary orthotropy, often designated as anisotropic laminates. The proposed formulation includes elastic coupling effects, warping effects, cross-section in-plane deformations and shear deformations. The classic GBT formulation was adapted to take into account the specific aspects associated with shear deformation. The numerical examples analysed and discussed in the paper consisted in a lipped channel column exhibiting non-aligned orthotropy and a lipped channel column with cross-ply orthotropy. For the first numerical example the first order and buckling behavior was assessed, while for the second numerical example the influence of the shear deformations on the buckling behavior was evaluated.

Gonçalves and Camotim [92] studied the local and distortional buckling of TWB with regular convex polygonal sections under axial force, bending and torsion. The authors analysed the influence of the neutral axis of the bar on the critical buckling load and they showed that the lowest values of buckling stresses are obtained when the neutral axis is parallel with the section's wall. The local buckling of the sections where the displacements at the intersection of walls are null becomes critical as the number of walls increases, more exactly the cross-section has at least 10 walls. For bars subjected to torsion, the local and distortional buckling were studied and also the influence of shear strains and coupled deformation modes. Generally, the critical stresses decrease as the length of the bar increases until a certain plateau is reached for long bars, and duplicate buckling modes result.

Also Gonçalves and Camotim [93] determined the deformation modes of the TWB with curved cross-section using GBT by using a polygonal approximation of the middle line. The paper proposes a new cross-section analysis method which discretizates the geometry of the section independentily from its number of degrees of freedom necessary for the determination of the deformation modes. This procedure is more efficient than the cross-section analysis of the polygonal section because a curved section can be analysed with precision without increasing the number of deformation modes. The procedure developed for curved sections may also be applied to sections with rounded corners, because the degrees of freedom obtained from the discretization of the curved sections may be neglected. This possibility does not exist in the cross-section analysis of the classical GBT.

Gonçalves et al. [94] studied the cross-section deformation modes of thin-walled members with arbitrary polygonal cross-section using GBT. The authors focused on the natural shear deformation

modes, more exactly the deformation modes which involve non-null membrane shear strains and which are independent of the cross-section discretization employed. These deformation modes are important in capturing the behavior of thin-walled bars with multi-cell cross-sections under torsion and/or distortion. The authors derivated fundamental properties of the shear modes, proposed an efficient mode extraction procedure and developed analytical results for different particular cases.

Bebiano et al. [95] presented the development and the application of a new procedure to perform GBT cross-section analysis. The proposed procedure is able to analyse arbitrary flat-walled cross-section shapes, it can be numerically implemented in a systematic and straightforward manner and it provides a rational set of deformation modes. The deformation modes determined by the proposed GBT cross-section analysis are hierarchically organized into several families. Each family of deformation modes has well-defined structural and mechanical characteristics.

Silva et al. [96] adapted GBT to TWB made of composite material reinforced with fiber polymers and having arbitrary open section. This GBT extension takes into account the cross-section distortions. The validation of the proposed extension was done by the analysis of an "I" section column. In the paper it is remarked that if the product of the Poisson coefficients is neglected from the elastic properties of the membrane at columns with orthotropic folds, the results of the analyses lead to underestimations of the buckling loads by 300%. Therefore, a new constitutive relationship was proposed based on the hypothesis that the membrane transversal stress resultant is null leading to more precise buckling loads. Also the hypothesis of uniformliy distributed pre-buckling normal stresses in columns with walls having different axial stiffness is incorrect from the theoretical point of view because it leads to errors in results.

De Miranda [97] formulated a GBT which takes into account plate-like (Reissner-like) shear deformations (besides the membrane-like ones already considered in GBT). The shear is introduced through two deformation modes: basic shear and additional shear. For each basic shear there is a bending mode and each one contains a generalized shear deformation such that the classical shear deformation components of Timoshenko's beam theory are recovered. Therefore the out-of-plane rotation doesn't coincide with the derivative of the transversal displacement. The additional shear introduces non-linear variations of the displacements along the section's walls. According to the new kinematic relationships, the cross-section analysis is revised and it is based on an unique method of modal decomposition of both classes of deformation modes. After the modal decomposition the bending displacements can be distinguished from the shear displacements. Also, particularly, the classical degrees of freedom and the beam theories may be recovered.

Peres et al. [98] adapted the first order GBT for TWB with deformable cross-section which have the longitudinal axis as circular arch. This extension makes it possible to keep the classical GBT

hypothesis, more exactly Kirrchhoff's, Vlasov's and the null membrane strain hypotheses. This means that the proposed formulation preserves the general efficiency of GBT for bars with straight longitudinal axis. The equilibrium equations were expressed with respect to GBT modal matrices and also with respect to stress resultants. The proposed formulation is able to recover the classical Winkler equilibrium equations (in case of in-plane deformations) and Vlasov's classical theory (in case of out-of-plane deformations) and the corresponding relationships between stress resultants and strains. The numerical examples were solved using a FE formulation. In all the case studies, the results obtained using only a few deformation modes and a small number of finite elements were precise. Therefore it was demonstrated that the modal decomposition specific to GBT is able to provide a detailed and unique understanding of the first-order behavior of bars with curved longitudinal axis.

Natário et al. [99] developed a GBT formulation to analyse the elastic localized web buckling of thin-walled steel beams under concentrated loads. These could be either cold-formed steel beams subjected to web crippling failure or welded steel beams subjected to patch loading failure. The proposed GBT formulation was validated by comparing the results with values determined by SFEA. The numerical examples consisted in cold-formed steel plain channel beams with web crippling configurations and welded steel "I" section beams with patch loading configurations. The authors found that the pre-buckling longitudinal and shear stresses had to be included in the buckling analysis of External One Flange (EOF), Internal One Flange (IOF) and Patch Loading Test (PLT) configurations. Also, the authors found that the pre-buckling transverse normal stresses had to be included in the buckling analysis of External Two Flange (ETF), Internal Two Flange (ITF) and Opposite Patch Loading Test (OPTL) configurations. In case of beams with EOF, IOF and PLT configurations in the GBT pre-buckling analysis the global and shear modes must be considered, while in the GBT buckling analysis only the local modes may be considered. In case of beams with ETF, ITF and OPTL configurations in the GBT pre-buckling analysis transverse extension modes should be considered, while in the GBT buckling analysis only local modes may be considered.

Davies et al. [100] used two theoretical methods to determine the ultimate load of perforated steel columns and the results obtained by these two methods were compared to the results obtained by experimental studies. Davies showed that the results obtained with GBT are very close with the ones obtained by SFEA and with a shorter computational time.

Jönsson and Andreassen [101] present a new systematic method and a detailed description of the semi-discretization process developed from the kinematic relationships, from strain energy and from the variation of strain energy which lead to the GBT homogeneous differential equation and the complete solution provided by the identification of all the eigenvalues and eigen modes. The proposed method is a considerable theoretical and practical development, because the GBT equations are solved

analytically assuming exponential longitudinal functions and the formulation is validated without giving special attention to simple closed or multi-cell cross-sections.

Piccardo et al. [102] proposed a new method for the evaluation of GBT fundamental deformation modes to analyze the TWB. The proposed method can be applied easily to open, closed or partially closed cross-sections. The main advantage of the method is the capacity to determine an orthogonal set of fundamental deformation modes for any cross-section using a one step numerical procedure. On the other hand, the classical GBT needs two steps for the determination of the same set of deformation modes as follows: in the first step the set of non-orthogonal deformation modes is evaluated and in the second step the set is orthogonalized by solving the eigenproblem. The proposed method was validated through case studies conducted on bars with open "C" section and, respectively for bars with partially closed section. The results showed that the fundamental deformation modes determined using the method proposed by Piccardo et al. were identical with the ones determined by the classical two-step procedure. The deformation modes determined by the proposed method provide similar results even though they aren't exactly identical. The differences occur due to the fact that the dynamic deformation modes may be combined with one or several rigid modes, which is not the case if the deformation modes are determined by the classical procedure. The GBT classical procedure requires a second diagonalization to determine the unlocal deformation modes with physical meaning. Despite this fact, the numerical values which result from the structural analysis are identical and independent from the method used to find the fundamental deformation modes.

Garcea et al. [103] compared the Generalized Eigenvector (GE) method with GBT for determining the cross-section deformation modes of thin-walled members with deformable cross-section. The authors reviewed the two methods by emphasizing their differences and similarities and also their solutions for problems with semi-analytical solutions. Then the GE and GBT deformation modes of four selected cross-sections were determined and analysed in detail. The authors focused on the efficiency and accuracy of the GE and GBT deformation mode sets in the calculation of the global, local, distotsional first-order and buckling behaviors of bars with the previously analysed cross-sections. The authors observed that GE and GBT, which are both based on the method of variable separation, yield accurate results even though the methods use different structural models and mode selection strategies. GE is based on a two-dimensional cross-section discretization which does not rely on simplifying assumptions such as plane stress and Kirrchoff's hypothesis, unlike GBT. The GE deformation modes are separated into independent in-plane and warping components leading to the fact that, for accurate results, more deformation modes are necessary for GE cross-section than for GBT. Moreover, the GBT deformation modes are separated according to strain criteria which makes it easier to discard specific components and avoid locking problems. However, the GE method

requires less computational effort than GBT for the determination of the deformation modes of complex cross-sections and makes it possible to consider plate-like shear deformation and through-thickness deformation. Despite the different assumptioins and mode selection strategies, GE and GBT offer complementary advantages.

Ádány et al. [104] provided the fundamental derivation details and a comparison between GBT and the constrained Finite Strip Method (cFSM) for the buckling analysis of unbranched thin-walled members. The comparison between the two methods included practical aspects and theoretical points on how the displacement fields are decomposed into deformation modes. The numerical examples presented in the paper consisted in the buckling analysis of cold-formed lipped channel members subjected to compresson and bending. The authors showed the power of GBT and cFSM to decompose the buckling mode into pure deformation modes, they illustrated the use of the identified deformation modes to evaluate the modal participation to a buckling mode and demonstrated that GBT and cFSM provide similar capabilities to analyse the stability of thin-walled bars despite their distinct developments.

Nedelcu [3] adapted GBT for the buckling analysis of TWB with variable open cross-section. In this case, the stiffness matrices are no longer constant along the bar's length. Therefore the differential equilibrium equations have a new formulation. In the second order analysis of the bars with variable cross-section, only the effect of pre-buckling longitudinal normal stresses was taken into account. The differentiation of the variable stiffness matrices was done by two methods: analytically, for a particular case of variable cross-section, and numerically, for the general cases of variation. The proposed GBT formulation is only valid with TWB with small variation slopes.

Cai and Moen [105] presented a method for the analysis of TWB with perforations using GBT. The perforated bars are treated as an assembly formed by multiple prismatic sub-bars with compatibility equations for displacements and derivatives of displacements with respect the gross and net cross-section. The GBT system of differential equations was solved using the FEM where the compatibility conditions were expressed in terms of finite element degrees of freedom for the first/order analysis and eiegenbuckling problem. The term which describes the geometric stiffness is changed to take into account the non-linear distribution of the normal stresses in the vicinity of perforations. The normal stresses from the vicinity of perforations require a first/order analysis to determine the initial state of stress before continuing with the buckling analysis.

2.4.2. GBT based Finite Element Formulations

Bebiano et al. **Error! Reference source not found.** used the GBT based FE formulation for the buckling analysis of TWBs subjected to non-uniform bending. The proposed GBT-based

formulation uses beam finite elements which take into account the stiffness reduction associated to applied longitudinal stresses with linear, quadratic and cubic variation. The novelty of the paper is that cubic moments are analytically integrated in the geometric matrices and shear stresses are obtained from equilibrium rather than by a first-order analysis, which makes it unnecessary to use shear modes.

Silvestre and Camotim [107] analysed the stability of TWB with orthotropic "C" section made of a composite material with fiber polymere reinforcement by using a GBT-based FE formulation. The paper is focused on the structural analysis, more exactly on the formulation and validation of the finite elements which lead to a simpler and more efficient analysis for any given orthotropic structural member. The studies showed that a bar divided into *2m* finite elements (where *m* is the number of buckling waves) always leads to precise results with the differences being less than 1%.

Basaglia and Camotim [108] applied the GBT based FE formulation to analyse the buckling behavior of the following thin-walled steel structural systems: beams of storage rack systems, pitched roof industrial frames, portal frames built from cold-formed rectangular hollow section (RHS) profiles and roof supporting trusses. The analysed structural systems exhibit different support conditions and are subjected to various loads. By using GBT, the authors were able to evaluate the effect of different geometries and/or bracing arrangements on the local, distorsional and/or global buckling behavior of the previously mentioned structures. The proposed formulation was validated by comparing the GBT-based results with the results determined by SFEA carried out in ANSYS. The authors remarked that the critical loads and the buckling shapes from the GBT-based FE formulation (which used beam finite elements) and from SFEA with ANSYS (which used shell finite elements) were virtually similar despite the large difference between the numbers of degrees of freedom involved in the analyses.

Basaglia et al. [109] developed a GBT-based FE formulation for the elastic local, distortional and global buckling analysis of frames made of TWB. For the bar finite element used to determine the stiffness matrices, the properties of the frame nodes and the relationships between the modal degrees of freedom of the end sections of the connected members were taken into account. The same paper presents the kinematic models adopted to simulate the transmission of the torsional strains and the compatibility of the local displacements of the frame's nodes.

The same authors applied the GBT based FE formulation for the local, distortional and global buckling analysis of the TWB frames in the post-critical domain [110]. The study of the stability of TWB frames was done by establishing the GBT non-linear system of equilibrium equations and by the discretization method of the bars including the influence of the nodes' behavior. Also constrains were inserted to simulate the compatibility between the deformation of the end sections and the transversal displacement of the walls from bending for two non-aligned bars with full section,

respectively with “C” section connected in the frame’s node. The system of non-linear equations was solved using an incremental-iterative method which combines the Newton-Raphson method with a displacement or load control strategy.

Nedelcu [111] presented a method for the decomposition of elastic buckling modes based on GBT which uses the SFEA. This method is able to decompose any buckling mode in pure deformation modes and determines their quantitative participation. The deformation modes may be determined using FEM or other similar numerical methods. For the formulation of the method of decomposition of the buckling mode, the GBT cross-section analysis was used to obtain the modal components of the deformed section, the end section transversal moments and the stiffness matrices. The GBT modal amplitude functions were determined from the deformations of the finite elements using the modal orthogonality. The modal participation factors were then determined based on these modal amplitude functions. The advantage of the proposed method of decomposition is the fact that there are no restrictions regarding the shape of the cross-section and the loading conditions of the bar. Also the computational speed is large because the eigen problem of the cross-section analysis involves a relatively small number of matrix operations. Therefore a structural analysis which involves complex operations is not necessary anymore. Currently the method was formulated for prismatic TWB with classical boundary conditions.

Camotim et al. [112] developed a GBT-based FE formulation to analyse the local and global buckling behavior of thin-walled bars with arbitrary loading and boundary conditions. The proposed formulation takes into account the longitudinal normal stress gradients and the ensuing pre-buckling shear stresses. The non-standard support conditions illustrated in the paper are full or partial localized displacement or rotation restraints, rigid or elastic intermediate supports and end supports corresponding to angle connections. The numerical examples used for the GBT-based FE analysis consisted in lipped channel beams and lipped “I” section beams under uniformly distributed or mid-span point loads applied at the shear center axis and lipped “I “ section columns under uniform compression. The proposed formulation was validated by comparing the results with values yielded from SFEA with ANSYS.

Basaglia et al. [113] present the GBT-based FE formulation to analyse the global buckling behavior of plane and space thin-walled frames. The proposed formulation includes only the first four rigid body deformation modes and consists in the following aspects: the kinematical models developed to simulate the warping transmission at frame joints which connect at least two non-aligned “U” and “I” section members, the procedures adapted to handle the effects occurring from the non-coincidence of the member’s centroidal and shear center axes, namely cross-sections without double symmetry and the definition of joint elements which provides a relation between the GBT degrees of

freedom of the connected member and the generalized displacements of the joint. The proposed GBT-based FE formulation was validated by comparing the results with values determined by SFEA and beam finite element analysis carried out in ANSYS.

Graça et al. [114] developed a GBT-based FE formulation concerning the local, distortional and global buckling of lipped channel and "Z" section cold-formed steel purlings restrained by steel sheeting and subjected to uplift loads. The proposed formulation is also applied to lapped joints which have the purpose to stop the occurence of local and distortional buckling phenomena. In this case GBT is used to determine the strengthening length of the lapped joint. The authors modeled the steel sheeting by means of elastic translational and rotational springs located at the purlin's upper flange and the lapped joint was modeled by doubling the cross-section's wall thickness. The validation of the formulation consisted in the comparison of the GBT-based results with values determined by SFEA performed with ANSYS.

Henriques et al. [115] adapted the GBT-based FE formulation to calculate the buckling loads of steel-concrete composite beams under hogging bending (i.e. negative bending). In the proposed formulation two types of buckling modes were considered: the local buckling of the web, with the possible occurrence of a torsional rotation of the lower flange, and distortional buckling which combines lateral displacements and rotations of the lower flange with cross-section transverse bending. The buckling loads were determined in two steps: the first step involved the geometrical linear pre-buckling analysis which takes into account shear lag and concrete cracking effects and the second step involves an eigenvalue buckling analysis using the pre-buckling stresses determined at the first step and allowing the cross-section in-plane and out-of-plane deformations. With the proposed GBT formulation, the authors obtained a finite element with a reasonable number of degrees of freedom which is able to fulfill the principles of the inverted "U" frame model prescribed by Eurocode 4 [116].

Also, Henriques et al. [117] developed a GBT-based FE formulation to analyse the materially non-linear behavior of wide-flange steel and steel-concrete composite beams up to collapse. The finite element includes reinforced concrete cracking and/or crushing, shear lag effects and steel beam placticity, including shear deformation of the steel web. The numerical examples presented in [117] showed that the proposed formulation is able to capture all the phenomena specific to steel-concrete composite beams at a very small computational effort.

2.4.3. The Adaptation of the Generalized Beam Theory for Circular Cross-section

Initially GBT was formulated for the buckling analysis of prismatic flat-walled TWBs, but later it was adapted to circular cross-sections. The first studies which adapt GBT for the first order and

buckling analysis of TWB with circular cross-section were conducted by Christof Schardt and Richard Schardt [5], [118], [119]. Further, Silvestre [120] developed the theory by studying the buckling of cylindrical structures under axial compression, bending, compression combined with bending and torsion. Also Silvestre [121] adapted GBT for the buckling analysis of cylindrical structures with elliptical section under compression.

Nedelcu [4] adapted GBT for the buckling analysis of isotropic conical shells. The paper studies only conical shells under axial compression having different boundary conditions. As in the GBT extension to prismatic TWBs with variable cross-section developed by the same author [3], the mechanical and geometrical properties are no longer constant along the bar's length. However, in case of conical shells, these properties can be easily defined. In reference [4], the buckling modes were approximated as a combination of shell-type deformation modes that can be easily determined. The GBT system of equilibrium equations was solved by the the 4^{th} order Runge-Kutta Lobatto IIIA numerical method [122]. This method proved to have limitations in case of structures subjected to arbitrary loading and boundary conditions and it was unstable in the case of coupled instabilities.

2.5. Conclusions

Thin-walled structures, which are frequently used in civil, naval or aerospace engineering, have high bearing capacity despite their small wall thickness. Because of the slenderness of these structural members, TWBs are prone to different types of buckling such as flexural buckling, flexural-torsional buckling, torsional buckling, local buckling or distortional buckling. The design of these structures is complex and often the design codes are based on simplified, approximative and empirical formulae which lead to oversized structures. Experimental and numerical studies have shown that the current design codes for thin-walled structures significantly underestimate their bearing capacity. For this reason it is necessary to develop more efficient buckling analysis methods that provide more accurate results.

For design methods, the Direct Strength Method (DSM) and the Effective Width Method are the most widely accepted. The latter, which eliminates from the cross-section the areas prone to local buckling, has the drawback of being time-consuming for a structural engineer. The buckling analysis methods used for thin-walled structures are generally based on Shell Finite Elements, Finite Strips or Generalized Beam Theory. . Shell elements are able to model any type of thin-walled structures under any loading and boundary conditions and to perform geometrically and physically non-linear analyses, including residual stresses. However, shell models are not able to provide the modal participation in the case of coupled instabilities. It seems arguable that GBT is the most evolved buckling analysis method for TWBs and the most efficient, because the number of degrees of freedom

used in the analysis is much lower than in the case of shell elements and GBT is able to decompose the buckling modes into fundamental deformation modes and to determine their modal participation.

The specialized literature provides different studies related to Generalized Beam Theory. Initially, GBT was developed for the buckling analysis of prismatic TWBs [5], but later this theory was adapted to other types of bars as TWBs with curved longitudinal axis [98], TWBs with circular and elliptical cross-sections [118], [119], [120], [121] and TWB with variable cross-section [3], [4].

Chapter III
Generalized Beam Theory

3.1. Introduction

Thin-walled structures have very slender cross-section walls. Therefore their structural efficiency depends mostly on their sensitivity to local instabilities, such as local buckling and distortional buckling, and global instabilities such as flexural and torsional-flexural buckling. The study of the stability of thin-walled bars begins from the decomposition of the general buckling mode in pure deformation modes such as global modes, where the cross-section has a rigid body behavior, distortional modes, where relative displacements occur in the corners of the section in its own plane, and local modes such as local buckling of walls (see Figure 1.1). Thus, the formulation, validation and calibration of the formulae and of the analysis procedures for TWBs requires advanced knowledge of the buckling phenomenon of these types of members, which means the evaluation of the critical buckling loads and the determination of the corresponding buckling modes. Recently it was proved that Generalized Beam Theory (GBT), formulated by Richard Schardt [5], provides an elegant alternative to the analysis methods mentioned in Chapter II, even though its practical application is not widely spread. Currently GBT is only known to a few members of the scientific community **Error! Reference source not found.**.

GBT, which extends Vlasov's classical beam theory, consists in the decomposition of the buckling mode into a linear combination of cross-section fundamental deformation modes and in the determination of the degree of modal participation in coupled instabilities. These fundamental deformation modes take into account the rigid body displacements (global modes) and the transversal deformations (distortional and local modes) [107]. The efficiency of GBT is given by the use of bar-type elements. Therefore, in the analysis, less degrees of freedom than in shell element models are involved.

GBT was initially developed for prismatic TWBs. Later, this theory was adapted to other types of thin-walled structures such as TWBs with curved longitudinal axis [98], TWBs with variable cross-section [3], [4] and TWBs with circular and elliptic cross-section [118], [119] [120], [121]. The following chapter presents an overview of the GBT for prismatic TWBs and the detailed GBT adaptation for isotropic conical shells with circular cross-section.

3.2. Generalized Beam Theory for Prismatic Cross-sections

The following section presents general aspects of GBT for TWBs with prismatic cross-section. The purpose of the present section is to offer an insight of the GBT procedure in order to better understand the GBT adaptation for conical shells.

First, let us consider the coordinate system and its corresponding displacements from Figure 3.1, where *x*, *s* and *z* are the coordinates with respect the bar's longitudinal axis, the cross-section's middle line andthe wall's thickness, respectively, and *u*, *v* and *w* are their corresponding displacements. GBT is based on the following simplifying assumptions:

(i) The Kirrchoff – Love hypotheses [123] for each cross-section wall:

a) Straight lines perpendicular to the middle plane before deformation remain straight, perpendicular to the middle plane and inextensible after deformation: $\varepsilon_{zz}=0$.

b) The normal stress acting along the direction perpendicular to the middle plane is neglected: $\sigma_{zz}=0$.

(ii) Vlasov's hypothesis [124], which states that the middle plane lines parallel to *x* and *s* axes before deformation remain perpendicular among them after deformation: $\gamma_{xs}=0$.

(iii) The middle plane lines parallel to *s* axis are inextensible: $\varepsilon_{ss}=0$.

The Kirchhoff – Love hypotheses, usually found in thin plates and shells theories, yield plane strain and stress states. Vlasov's hypothesis and hypothesis no. (iii) are valid, in general, for the first order and buckling/vibration analysis of open section elements providing further simplification [125].

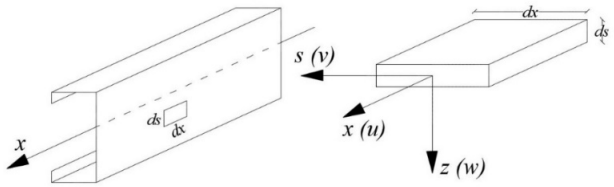

Figure 3.1: The GBT coordinate system and its corresponding displacements.

According to GBT the displacement field is represented such that *x* and *s* middle plane coordinates are separated. Each displacement field component is expressed as a sum of an arbitrary number of products of two functions: one function is defined on the cross-section's middle line domain and the other function is defined along the member's length. Therefore, the displacements *u*, *v* and *w* are expressed as follows:

$$u(x,s) = u_k(s)\phi_{k,x}(x)$$
$$v(x,s) = v_k(s)\phi_k(x) \quad (3.1)$$
$$w(x,s) = w_k(s)\phi_k(x)$$

where: k is the number of the deformation mode;

$u_k(s)$, $v_k(s)$, $w_k(s)$ is the warping, transverse and, respectively flexural components of the middle line displacement profile corresponding to deformation mode k;

$\phi_k(x)$ the modal amplitude function defined with respect the bar's longitudinal axis.

The presence of the derivative of the modal amplitude function $\phi_{k,x}(x)$ in the warping component of the displacement field $u_k(s)$ is a consequence of Vlasov's hypothesis, namely the shear membrane strains are null $\gamma_{xs}^{M}=0$.

GBT is different from other analysis methods because the degrees of freedom consist of cross-section deformation modes which display mechanically meaningful configurations. Each deformation mode is expressed mathematically by a warping, a transverse and a flexural displacement field defined in the cross-section middle line domain (i.e. $u_k(s)$, $v_k(s)$ and $w_k(s)$), (see Eq. (3.1)). Depending on the nature of displacement or deformation involved, the GBT cross-section deformation modes are divided into the following categories:

(i) Conventional deformation modes, which fulfill Vlasov's hypothesis. This category represents accurately the deformation produced by the structural element in different situations and includes the following types of deformation modes:

a) Global modes, represented by the following rigid body deformation modes: axial extension, major and minor axis bending and torsion. These deformation modes involve both in-plane and out-of-plane displacements.

b) Distortional modes, represented by quasi-rigid body displacements of parts of the cross-section. This type includes the flexural deformation of some plates.

c) Local modes, given only by flexural displacements of the cross-section walls without warping or transverse displacements.

(ii) Shear deformation modes, which involve non-null shear strains.

(iii) Transverse extension modes, which involve membrane extension of the walls.

For any given cross-section it is possible to define an infinite number of deformation modes for each category, except for global modes, which are always 4, and distortional modes whose number depends on the cross-section's geometry.

GBT is applied in two steps: (i) the cross-section analysis and (ii) the structural analysis. In the cross-section analysis the deformation modes are identified and the corresponding modal properties are determined. The performance of this step does not depend on the bar's length, on the boundary

conditions or on the applied loads. In the structure analysis the system of differential equilibrium equations is assembled and the solution is determined. In this step the geometric properties of the cross-section, the material properties, the size of the structure, the boundary conditions and the applied loads are known.

3.2.1. The Variation of Strain Energy

The GBT formulation starts from the kinematic relations which have the following expressions:

(i) For the linear terms, by applying hypothesis (ii) and (iii) ($\gamma_{xs}^{M.L}=\varepsilon_{ss}^{M.L}=0$):

$$\begin{aligned}\varepsilon_{xx}^{L} &= \varepsilon_{xx}^{M.L}+\varepsilon_{xx}^{B.L} = u_{,x}-zw_{,xx}\\ \varepsilon_{ss}^{L} &= \varepsilon_{ss}^{M.L}+\varepsilon_{ss}^{B.L} = -zw_{,ss}\\ \gamma_{xs}^{L} &= \gamma_{xs}^{M.L}+\gamma_{xs}^{B.L} = -2zw_{,xs}\end{aligned} \tag{3.2}$$

(ii) For the non-linear terms:

$$\begin{aligned}\varepsilon_{xx}^{NL} &\equiv \varepsilon_{xx}^{M.NL} = \frac{v_{,x}^{2}+w_{,x}^{2}}{2}\\ \gamma_{xs}^{NL} &\equiv \gamma_{xs}^{M.NL} = w_{,s}w_{,x}+v_{,s}v_{,x}\end{aligned} \tag{3.3}$$

The bending terms ($\varepsilon_{xx}^{B.NL}=\gamma_{xs}^{B.NL}=0$) and the terms involving products of warping function derivatives ($u_{,x}$ or $u_{,s}$) from Eq. (3.3) can be neglected for small strains and moderate rotations.

The plane state of stress for the bending terms and the uniaxial stress state for the membrane term, for each cross-section wall, yields the following constitutive relations:

$$\begin{Bmatrix}\sigma_{xx}^{M.L}\\ \sigma_{xx}^{M.B}\\ \sigma_{ss}^{M.B}\\ \tau_{xs}^{M.B}\end{Bmatrix} = \begin{bmatrix}E & 0 & 0 & 0\\ 0 & \dfrac{E}{1-\mu^{2}} & \dfrac{\mu E}{1-\mu^{2}} & 0\\ 0 & \dfrac{\mu E}{1-\mu^{2}} & \dfrac{E}{1-\mu^{2}} & 0\\ 0 & 0 & 0 & G\end{bmatrix}\begin{Bmatrix}\varepsilon_{xx}^{M.L}\\ \varepsilon_{xx}^{M.B}\\ \varepsilon_{ss}^{M.B}\\ \gamma_{xs}^{M.B}\end{Bmatrix} \tag{3.4}$$

where: E is the Young modulus of elasticity;

G is the transversal modulus of elasticity;

μ is Poisson's ratio;

M is the membrane component;

B is the bending component;

$\sigma_{xx}^{M.L}$ is the linear membrane normal stress component along the member's longitudinal axis;

$\varepsilon_{xx}^{M.L}$ is the linear membrane strain component along the member's longitudinal axis;

$\sigma_{xx}^{B.L}$, $\sigma_{ss}^{B.L}$, $\tau_{xs}^{B.L}$ are the linear bending normal stress components along the member's longitudinal axis and, respectively along the cross-section's middle line and the linear bending shear stress component;

$\varepsilon_{xx}^{B.L}$, $\varepsilon_{ss}^{B.L}$, $\gamma_{xs}^{B.L}$ are the linear bendingstrain components along the member's longitudinal axis and, respectively along the cross-section's middle line and the linear bending shear strain component;

According to the linear stability analysis concept, the linearization of the variation of the strain energy along the fundamental path has the following mathematical expression:

$$\partial W = \int_L \int_s \int_t \left(\sigma_{xx}^{M.L} \partial \varepsilon_{xx}^{M.L} + \sigma_{xx}^{B.L} \partial \varepsilon_{xx}^{B.L} + \sigma_{ss}^{B.L} \partial \varepsilon_{ss}^{B.L} + \tau_{xs}^{B.L} \partial \gamma_{xs}^{B.L} + \sigma_{xx}^{0} \partial \varepsilon_{xx}^{M.NL} + \tau_{xs}^{0} \partial \gamma_{xs}^{M.NL} \right) dz ds dx \qquad (3.5)$$

where: σ_{xx}^{0}, τ_{xs}^{0} are the pre-buckling normal stress (along the member's longitudinal axis) and the pre-buckling shear stress, respectively;

$\varepsilon_{xx}^{M.NL}$, $\gamma_{xs}^{M.NL}$ are the non-linear longitudinal membrane strainand the membrane shear strain components, respectively.

By introducing the kinematic relations (i.e. strain – displacement relations) from Eq. (3.3) and the constitutive relations (i.e. stress – strain relations) from Eq. (3.4) into Eq. (3.5) and performing the integrations with respect to the thickness and cross-section's middle line, the variation of strain energy has the following form:

$$\partial W = \int_L \left(\begin{array}{l} C_{ik}^{1} \phi_{k,xx} \partial \phi_{i,xx} + C_{ik}^{2} \phi_{k,xx} \partial \phi_{i,xx} + D_{ik}^{2} \phi_{k} \partial \phi_{i,xx} + D_{ki}^{2} \phi_{k,xx} \partial \phi_{i} + B_{ik} \phi_{k} \partial \phi_{i} + \\ + D_{ik}^{1} \phi_{k,x} \partial \phi_{i,x} - W_j X_{jik}^{\sigma} \phi_{k,x} \partial \phi_{i,x} - W_{j,x} X_{jik}^{\tau} \left(\phi_{k} \partial \phi_{i,x} + \phi_{k,x} \partial \phi_{i} \right) \end{array} \right) dx \qquad (3.6)$$

where: C_{ik}^{1} is the linear stiffness tensor associated with generalized primary warping;

C_{ik}^{2} is the linear stiffness tensor associated with generalized secondary warping;

D_{ik}^{1} is the linear stiffness tensor associated with generalized torsion;

D_{ik}^{2} is the linear stiffness tensor associated with generalized flexural Poisson's effect;

B_{ik} is the linear stiffness tensor associated with generalized transversal bending;

W_j is the resultant of the pre-buckling normal stresses associated with mode *j*.

X_{jik}^{σ} is the geometrical stiffness tensor associated with normal stresses;

$W_{j,x}$ is the resultant of the pre-buckling shear stresses associated with mode *j*.

X_{jik}^{τ} is the geometrical stiffness tensor associated with shear stresses;

j=1…4 is the global deformation mode having the following meanings: *j=1* is axial extension, *j=2* is bending with respect the major axis, *j=3* is bending with respect the minor axis and *j=4* is torsion.

In the classic GBT formulation for bars with prismatic cross-section, matrices C and D are symmetrical. Therefore, the linear stiffness tensors C_{ik} and D_{ik} may be defined as follows:

$$\begin{aligned} C_{ik} &= C_{ik}^{1} + C_{ik}^{2} \\ D_{ik} &= D_{ik}^{1} - \left(D_{ik}^{2} + D_{ki}^{2} \right) \end{aligned} \tag{3.7}$$

The linear and geometrical stiffness tensors are determined by integrating with respect the cross-section's middle line. For members with prismatic cross-section the linear stiffness tensors are determined by the following mathematical expressions [125]:

$$\begin{aligned} C_{ik}^{1} &= Et \int_{s} u_i u_k ds \\ C_{ik}^{2} &= \frac{Et^3}{12\left(1-\mu^2\right)} \int_{s} w_i w_k ds \\ D_{ik}^{1} &= \frac{Gt^3}{3} \int_{s} w_{i,s} w_{k,s} ds \\ D_{ik}^{2} &= \frac{\mu Et^3}{12\left(1-\mu^2\right)} \int_{s} w_i w_{k,ss} ds \\ B_{ik} &= \frac{Et^3}{12\left(1-\mu^2\right)} \int_{s} w_{i,ss} w_{k,ss} ds \end{aligned} \tag{3.8}$$

The geometrical stiffness tensors yield from the following expressions [125]:

$$\begin{aligned} X_{jik}^{\sigma} &= \frac{Et}{C_{jj}} \int_{s} \sigma_{xx}^{0} \left(v_i v_k + w_i w_k \right) ds \\ X_{jik}^{\tau} &= \frac{a_j E}{C_{jj}} \int_{s} \tau_{xs}^{0} w_{i,s} w_k ds \end{aligned} \tag{3.9}$$

where: t is the thickness of the cross-section's wall;

C_{jj} is the cross-section's stiffness associated with deformation mode j;

a_j is a coefficient whose value depends on the deformation mode j. Therefore, $a_j=0$ for $j=1$ and $a_j=1$ for $j=2…4$.

3.2.2. The Cross-section Analysis

The cross-section analysis in the GBT formulation for prismatic bars with open unbranched cross-section begins with the discretization of the bar's cross-section into segments. A cross-section

composed of n segments consists in $n+1$ natural nodes, which are the nodes at the walls ends, and m intermediate nodes plus the two free-end nodes, which are endowed with a flexural degree of freedom.. Figure 3.2 presents an example of discretization for a lipped channel cross-section. According to Figure 3.2 the cross-section has 6 natural nodes (represented by orange circles) and 5 intermediate nodes (represented by magenta rombus).

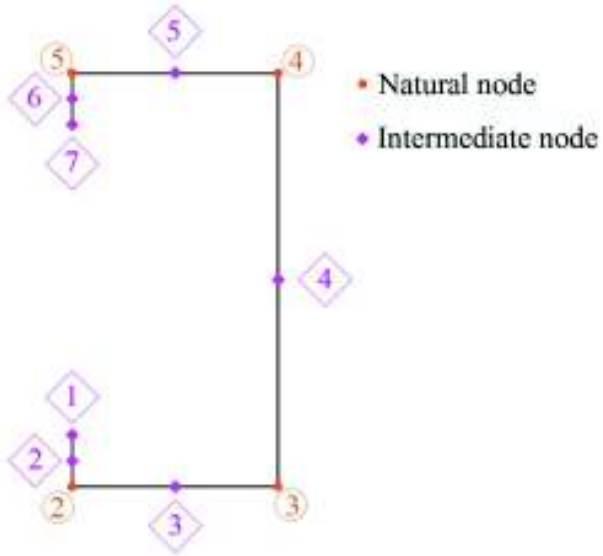

Figure 3.2: The discretization of a lipped channel section.

Generally, each segment should have at least one intermediate node in order to obtain accurate results. . The natural nodes are indispensable in the GBT analysis, while the intermediate nodes are included in case of the local flexural, membrane shear and membrane transverse extension buckling of the walls.

The following step is to determine the cross-section displacement field components represented by the $u_k(s)$, $v_k(s)$ and $w_k(s)$ functions. Firstly, unit warping displacements $u_k=1$, $k=1…n+1$ are imposed at the cross-section's natural nodes, while unit flexural displacements $w_k=1$, $k=n+2…n+m+3$ are inserted at the intermediary nodes and at the free end nodes. Thus, there are $n+1$ elementary warping functions $u_k(s)$ and $m+2$ elementary flexural functions $w_k(s)$. The elementary warping functions have linear variation between consecutive nodes.

The elementary flexural functions $w_k(s)$ fulfill automatically Vlasov's hypothesis because $u=v=0$. The nodal compatibility between the transverse membrane displacements v and the flexural displacements w is achieved by forcing the cross-section to deform in its own plane due to the application of the elementary warping functions $u_k(s)$. By imposing membrane and flexural displacements relative rotations occur between adjacent segments which break the nodal compatibility. Thus, it is necessary to determine the nodal transverse bending moments which ensure rotation compatibility at nodes. The nodal transverse bending moments are obtained by solving the

static indeterminate folded plate problem either by applying the force method or the displacement method.

After the equilibrium and compatibility conditions are ensured, the cross-section displacement field is determined. The components of the cross-section displacement field have the following forms:

(i) $u_k(s)$ are linear functions;

(ii) $v_k(s)$ are constant;

(iii) $w_k(s)$ are cubic functions.

In the following step the GBT system of buckling equations is written in the matrix form as follows:

$$C\phi_{,xxxx} - D\phi_{,xx} + B\phi - \lambda W_j^0 X_j \phi_{,xx} = 0 \tag{3.10}$$

Knowing the cross-section displacement field, the C, D, B stiffness matrices and the X_j geometric matrix are assembled. These matrices are completely populated and their components do not have an obvious physical meaning. Therefore, the GBT matrices must be simplified through simultaneous diagonalization. The assembly and diagonalization of the stiffness and geometric matrices is done in several steps which are detailed in Schardt's reference [5]. The following section presents briefly the diagonalization process of the GBT matrices and the interpretation of the results.

The diagonalization process requires the solution of eigenproblems which lead to the identification of the vectors corresponding to cross-section deformation modes. First the diagonalization of the C and B matrices is performed by solving the eigenproblem with the following matrix equation:

$$\left(B - \lambda_k C\right) \cdot d_k = 0 \tag{3.11}$$

where: λ_k is the eigenvalue corresponding to deformation mode k;

d_k is the eigen vector corresponding to the eigenvalue λ_k associated with deformation mode k.

By solving the eigen value problem from Eq. (3.11), $n+m+3$ eigenvalues result with the first four being null. The eigenvectors d_k are assembled in a matrix U_I. The eigenvalues are sorted in ascending order, while the eigenvectors d_k of the matrix U_I are permuted according to their corresponding eigenvalue. Figure 3.3 presents the patterns of the first diagonalization of B and C matrices and the transformation of the matrix U_I.

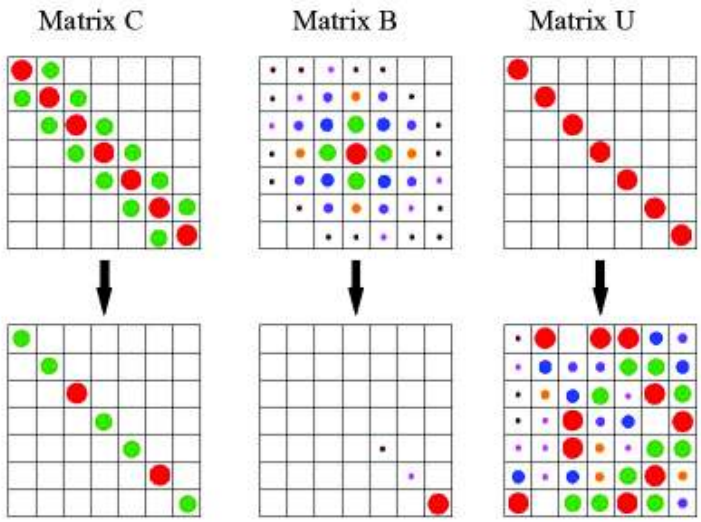

Figure 3.3: The diagonalization patterns of *B* and *C* matrices and the transformation of the modal matrix U_I.

The eigenvalues resulted from Eq. (3.11) have the following physical meaning [104]:

(i) $\lambda_k=0$, $k=1\ldots4$ (4 eigenvectors d_k) are associated with cross-section rigid body deformations, namely axial extension, bending with respect to the major axis, bending with respect to the minor axis and torsion;

(ii) $\lambda_k>0$, $k=5\ldots n+1$ ($n-3$ eigenvectors d_k) are associated with cross-section deformation described by warping and fold-line displacements. These are also known as distortional modes.

(iii) $\lambda_k>0$, $k=n+2\ldots n+m+3$ ($m+2$ eigenvectors d_k) are associated with cross-section in-plane deformation without warping and fold-line displacements, but with significant wall bending, the so-called local modes.

The second diagonalization involves the determination of the four rigid body deformation modes. Therefore, the stiffness matrices *C* and *D* are transformed such that their size is 4x4 resulting the matrices C_{4x4} and D_{4x4}. The eigenproblem is solved with the following equation:

$$\left(D_{4x4}-\lambda_k C_{4x4}\right)\cdot d_k=0 \tag{3.12}$$

By solving Eq. (3.12) four eigenvalues result. Three out of the four determined eigenvalues are null. The first four eigenvectors d_k of the matrix U_{II} are sorted according to their corresponding eigenvalue λ_k. Figure 3.4 presents the diagonalization pattern of matrix D_{4x4} and the transformation of the matrices C_{4x4} and U_{II}.

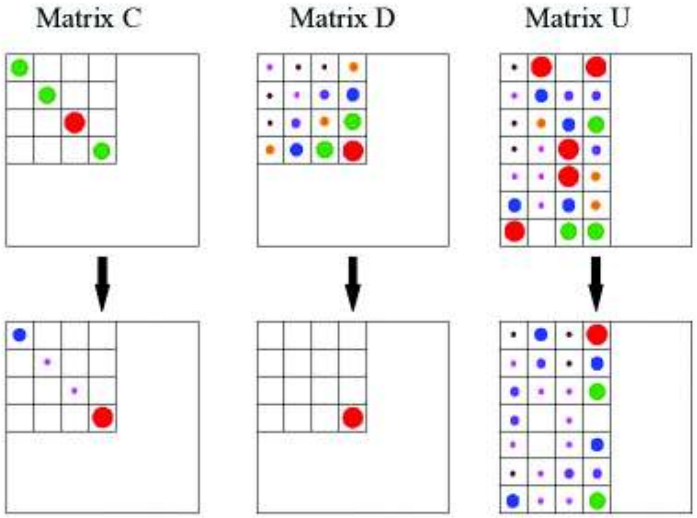

Figure 3.4: The diagonalization pattern of D_{4x4} matrix and the transformation of C_{4x4} and U_{II} matrices.

The eigenvalues determined by Eq. (3.12) are interpreted in the following manner [104]:

(i) $\lambda_k=0$, $k=1\ldots3$ (3 eigenvectors d_k) is associated with cross-section rigid body displacements without twisting rotation, namely extension, bending with respect to the major axis and bending with respect to the minor axis deformation modes.

(ii) $\lambda_4>0$ corresponding to eigenvector d_4 is associated with the cross-section rigid body displacement with twisting rotation, namely the torsion mode.

In the last diagonalization process the bending and the axial extension modes are determined. The stiffness matrix C is transformed such that its size is 3x3 and the stiffness matrix K ($K\equiv X$), with the same size, is assembled. The last eigenproblem is solved using the matrices C_{3x3} and K_{3x3} as follows:

$$\left(K_{3x3}-\lambda_k C_{3x3}\right)\cdot d_k=0 \tag{3.13}$$

Therefore, by solving Eq. (3.13) three eigenvalues λ_k result. One of the determined eigenvalues is null. The first three eigenvectors d_k are sorted according to their corresponding eigenvalue into the matrix U_{III}. Figure 3.5 shows the diagonalization pattern of matrix K_{3x3} and the transformation of the matrices U_{III} and C_{3x3}.

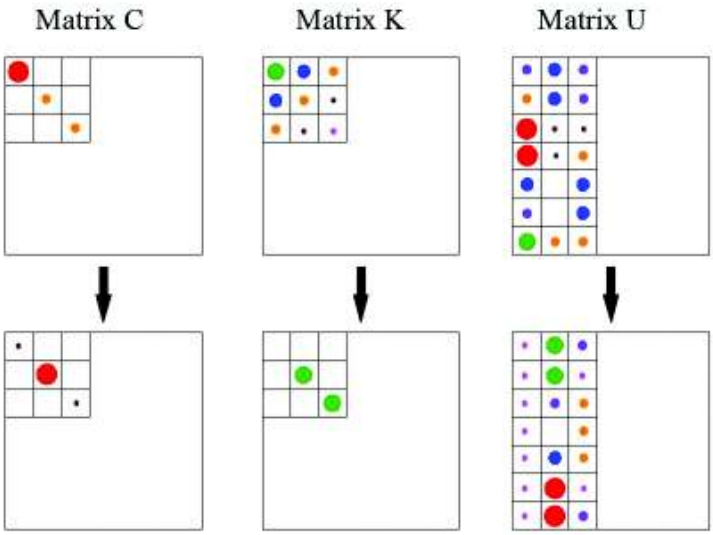

Figure 3.5: The diagonalization pattern of K_{3x3} matrix and the transformation of U_{III} and C_{3x3} matrices.

The eigenvalues yielded from Eq. (3.13) have the following meaning [104]:

(i) $\lambda_1=0$ corresponding to eigenvector d_1 is associated with cross-section rigid body displacement without in-plane deformations, namely the axial extension mode.

(ii) $\lambda_k>0$, $k=2, 3$ (eigen vectors d_2, respectively d_3) is associated with cross-section rigidy body displacement with in-plane deformations, namely the bending modes about central principal axes.

3.2.3. The Structural Analysis

The GBT structural analysis is simpler, because it involves procedures known in structural analysis problems. The structure analysis begins with the assembly of the matrices U_I, U_{II} and U_{III} into the global transformation matrix $\tilde{U}$ having the size $(n+m+3)$x$(n+m+3)$. Each column of the matrix $\tilde{U}$ corresponds to one of the $n+m+3$ orthogonal deformation modes. After the global transformation matrix $\tilde{U}$ is assembled, the stiffness matrices C, B, D and the geometric matrix X_j, all of them fully populated are transformed as following:

$$\begin{aligned}\tilde{C} &= \tilde{U}^T C \tilde{U} \\ \tilde{D} &= \tilde{U}^T D \tilde{U} \\ \tilde{B} &= \tilde{U}^T B \tilde{U} \\ \tilde{X}_j &= \tilde{U}^T X_j \tilde{U}\end{aligned} \tag{3.14}$$

The elements of the transformed matrices $\tilde{C}$, $\tilde{D}$, $\tilde{B}$ and $\tilde{X}_j$ are the cross-section modal mechanical properties as following: the global deformation modes represented by axial extenstion, bending and torsion, the distorsional deformation modes and the local deformation modes. After the transformation

of the stiffness and geometric matrices, the GBT system of equilibrium equations has the following modal form:

$$\tilde{C}\tilde{\phi}_{,xxxx} - \tilde{D}\tilde{\phi}_{,xx} + \tilde{B}\tilde{\phi} - \lambda\tilde{W}_j^0\tilde{X}_j\tilde{\phi}_{,xx} = \tilde{0} \tag{3.15}$$

In case of the geometric matrix $\widetilde{X}_j$ there are two situations:

(i) If the elements of matrix $\widetilde{X}_j$ outside the main diagonal are null, then the GBT system of equilibrium equations is uncoupled. This case is specific to axially compressed structures. This is not true, matrix D is not diagonal. Only for rigid-body modes this holds.

(ii) If the elements of matrix $\widetilde{X}_j$ outside the main diagonal are non-null, then the GBT system of equilibrium equations is coupled. This situation occurs in structures subjected to torsion or bending.

One of the advantages of GBT is that an arbitrary number of deformation modes can be considered. The number of selected deformation modes is necessary to solve the system of equilibrium equations associated with them. The resulted buckling mode is expressed as a linear combination of the respective deformation modes. The solution of the GBT differential system of equations may be solved as follows:

(i) By exact methods, where analytical expressions are obtained. These analytical expressions are solutions of the homogeneous differential equations. The exact solutions may only be determined in case of simply supported bars and they are expressed as sinusoidal functions. In case of bars with other types of boundary conditions (other than simple supports), to determine exact solutions no more than 2 deformation modes can be inserted in the analysis.

(ii) By aproximative methods, which involve numerical discretization methods as Finite Difference Method (FDM) or Finite Element Method (FEM). Therefore aproximative solutions are determined for bars with any type of boundary conditions.

3.3. Generalized Beam Theory for Conical Shells

The following section presents the GBT adapted for isotropic conical shells with circular cross-section. Let us consider the conical shell from Figure 3.6 with length L, thickness t and angle of the semi-vertex α. Also, the x_g, y_g, z_g global coordinate system and the x, θ, z local coordinate system are considered, where $x \in [0, L/\cos\alpha]$ is the meridional coordinate, $\theta \in [0, 2\pi]$ is the circumferential coordinate and $z \in [-t/2, t/2]$ is the normal coordinate. The structure's displacements with respect the local coordinate system are the following: u is the displacement on meridional direction, v is the displacement on circumferential direction and w is the displacement on normal direction.

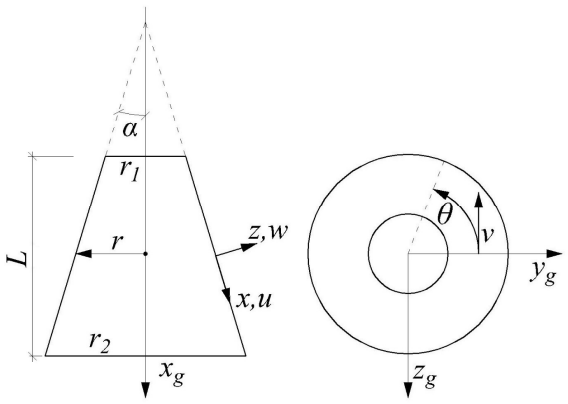

Figure 3.6: The geometry of the conical shell.

3.3.1. Past Research

3.3.1.1. The Kinematic Relations

As in the case of TWBs with prismatic cross-section, the GBT formulation for circular conical shells begins from the kinematic relations which, in this case, have the following pattern:

$$\{\varepsilon\}=\{\varepsilon^M\}+\{\varepsilon^B\}=\{\varepsilon^M\}+z\{\chi\} \tag{3.16}$$

where: $\{\varepsilon^M\}$, $\{\varepsilon^B\}$ are membrane, respectively bending strains;

$\{\chi\}$ is the vector of curvature variation with respect the middle surface.

According to Love – Timoshenko theory [44], the kinematic relations have the following mathematical expressions in case of conical shells, with the following linear and non-linear components:

$$\begin{aligned}
\varepsilon_{xx}^M &= \varepsilon_{xx}^{M.L}+\varepsilon_{xx}^{M.NL}=u_{,x}+\left(\frac{w_{,x}^2}{2}+\frac{v_{,x}^2}{2}\right)\\
\varepsilon_{\theta\theta}^M &= \varepsilon_{\theta\theta}^{M.L}+\varepsilon_{\theta\theta}^{M.NL}=\left(\frac{v_{,\theta}}{r}+\frac{wc}{r}+\frac{us}{r}\right)+\left[\frac{1}{2}\left(\frac{vc-w_{,\theta}}{r}\right)^2+\frac{1}{2}\left(\frac{v_{,\theta}+wc}{r}\right)^2\right]\\
\gamma_{x\theta}^M &= \gamma_{x\theta}^{M.L}+\gamma_{x\theta}^{M.NL}=\left(\frac{u_{,\theta}}{r}+v_{,x}-\frac{vs}{r}\right)+\left(\frac{w_{,x}w_{,\theta}}{r}-\frac{vw_{,x}c}{r}+\frac{v_{,x}v_{,\theta}}{r}\right)\\
\chi_{xx} &= -w_{,xx}\\
\chi_{\theta\theta} &= -\frac{w_{,\theta\theta}}{r^2}-\frac{w_{,x}s}{r}+\frac{v_{,\theta}c}{r^2}
\end{aligned} \tag{3.17}$$

$$\chi_{x\theta} = 2\left[-\frac{w_{,\theta x}}{r} + \frac{w_{,\theta}s}{r^2} + \frac{c}{r}\left(\frac{v_{,x}}{2} - \frac{vs}{r}\right)\right]$$

where: $s=sin\alpha$ and $c=cos\alpha$.

The last term of the non-linear shear strain $\gamma_{x\theta}^{M.NL}$ is often neglected depending on the nature of the applied load, while the last term of the non-linear hoop strain $\varepsilon_{\theta\theta}^{M.NL}$ is always neglected [45]. In the case studies presented in [4] both terms were neglected. The last terms *us/r* and *–vs/r* of the linear membrane hoop strain $\varepsilon_{\theta\theta}^{M.L}$ and, respectively, of the linear membrane shear strain $\gamma_{x\theta}^{M.L}$, were taken into account, but it was noticed that there were no significant effects in any of the analysed numerical examples. Therefore it is recommened to neglect them. According to GBT, the *u*, *v* and *w* displacements of the middle surface are expressed as summation of products between orthogonal functions:

$$u = \sum_{k=1}^{n} \overline{u}_k(x,\theta), \quad v = \sum_{k=1}^{n} \overline{v}_k(x,\theta), \quad w = \sum_{k=1}^{n} \overline{w}_k(x,\theta) \tag{3.18}$$

where: *n* is the number of cross section deformation modes.

The terms of Eq. (3.18) are then expressed, according to GBT, as products of orthogonal functions:

$$\begin{aligned} \overline{u}_k(x,\theta) &= u_k(\theta) r(x) \phi_{k,x}(x) \\ \overline{v}_k(x,\theta) &= v_k(\theta) \phi_k(x) \\ \overline{w}_k(x,\theta) &= w_k(\theta) \phi_k(x) \end{aligned} \tag{3.19}$$

where: $u_k(\theta)$, $v_k(\theta)$, $w_k(\theta)$ are the cross-section warping, transverse and, respectively, normal displacement componets of the conical shell's mid-line cross-section corresponding to deformation mode *k*;

$\phi_k(x)$ are the modal amplitude functions defined with respect to the longitudinal axis.

3.3.1.2. The Shell-Type Deformation Modes

The classical GBT assumes that the linear membrane transverse strains $\varepsilon_{\theta\theta}^{ML}$ and the linear membrane shear strains $\gamma_{x\theta}^{ML}$ are null. In the case of conical shells, if the terms *us/r* and *–vs/r* are neglected, then the v_k and w_k cross-section displacements may be expressed with respect to the meridional displacement u_k as follows:

$$v_k = -u_{k,\theta} \qquad w_k = -\frac{v_{k,\theta}}{c} = \frac{u_{k,\theta\theta}}{c} \tag{3.20}$$

In the case of circular closed sections there are two sets of trigonometric functions used also in references [45], [118], [119] and [120]:

$$u_k = \begin{cases} \sin(m\theta), & m = k/2, \quad k = 2,4,6,...,n \\ \cos(m\theta), & m = (k-1)/2, \quad k = 3,5,7,...,n+1 \end{cases} \tag{3.21}$$

where: n is the number of deformation modes considered.

In case of cylindrical bars with elliptical cross-section, the sets of trigonometric functions used in reference [121] were different from the ones in Eq. (3.21) and they may be applied to conical shells with elliptical cross-section in other case studies.

For a given number of m circumferential waves there are two similar deformation modes having a different order k. Therefore, in the buckling analysis of uniformly compressed structures, there is always a set of two buckling modes with equal critical buckling loads. The independent trigonometric functions from Eq. (3.21) define the shell-type deformation modes. Figure 3.7 shows the cross-section in-plane configurations of the first 12 shell-type deformation modes.

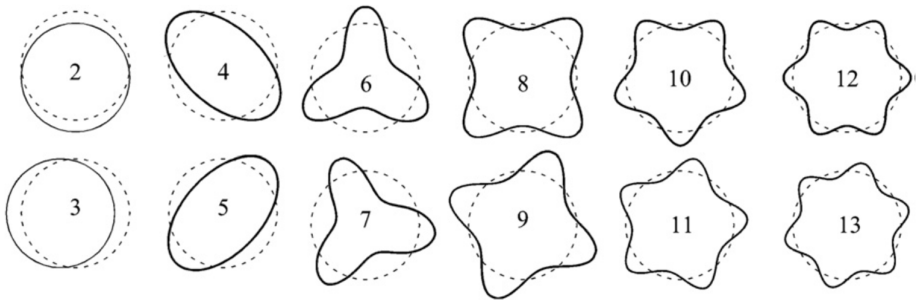

Figure 3.7: The shell-type deformation modes.

3.3.2. Personal Contributions

3.3.2.1. The Shear Deformation Modes

Initially it was assumed that the shell-type deformation modes can describe with enough accuracy the buckling modes of structures with circular cross-section. In the numerical examples presented in the thesis there were situations when Vlasov's hypothesis $\gamma_{x\theta}^{ML}=0$ led to results with significant errors. Therefore two **new** deformation mode types were introduced as follows:

(i) "u" shear deformation modes, where the warping displacement u_k is identical to the one described by the shell-type deformation modes (see Eq. (3.21)), while the rest of the cross-section displacements are null $v_k=w_k=0$. Figure 3.8 shows the "u" shear deformation mode of order $k=4$.

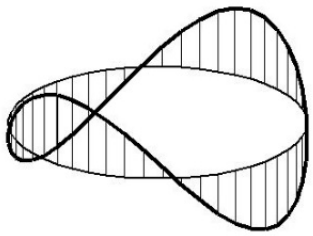

Figure 3.8: "u" shear deformation mode ($k=4$).

(ii) "v" shear deformation modes, where the hoop displacement v_k is identical with the one described by the shell-type deformation modes (see Eq. (3.20) and (3.21)), while the rest of the cross-section displacements are null $u_k=w_k=0$.

3.3.2.2. The Additional Deformation Modes

In most cases the shell-type deformation modes, along with the shear deformation modes, can describe quite accurately the buckling modes of TWBs with circular cross-section and conical shells. However, for performing a first order analysis capable of determining rigorously the pre-buckling stresses and of taking into account the deformation of the structural member on the circumferential direction, additional deformation modes must be inserted as well.

a. The Additional Deformation Modes of Conical Shells under Axial Compression

In the case of axial compression, the additional deformation modes are the axial extension, the axisymmetric extension and the torsion and they are illustrated in Figure 3.9. Vlasov's and the null membrane transverse extension hypotheses ($\gamma_{x\theta}^{ML}=\varepsilon_{\theta\theta}^{ML}=0$) used to determine the shell-type deformation modes are no longer valid. In case of each additional deformation mode, the cross-section displacements are constant. In the case of circular cylindrical bars, the cross-section displacements have the following values according to Silvestre [120]:

(i) The axial extension mode:

$$u_e = 1, \quad v_e = 0, \quad w_e = 0 \tag{3.22}$$

(ii) The axisymmetric extension mode:

$$u_a = 0, \quad v_a = 0, \quad w_a = 1 \tag{3.23}$$

(iii) The torsion mode:

$$u_t = 0, \quad v_t = r, \quad w_t = 0 \tag{3.24}$$

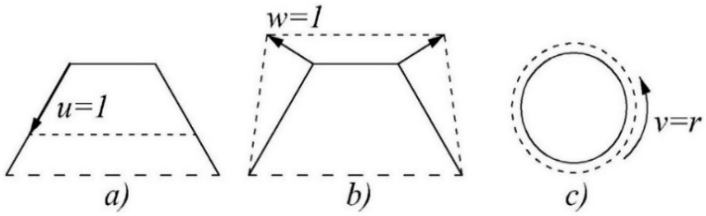

Figure 3.9: The additional deformation modes: a) axial extension, b) axisymmetric extension and c) torsion.

b. The Additional Deformation Modes of Conical Shells under Bending

In the case of conical shells under bending, the following deformation modes are used in the first order analysis:

(i) Mode 1, where the cross-section displacements have the following values:

$$u_1 = \sin(\theta) \quad v_1 = 0 \quad w_1 = 0 \tag{3.25}$$

(ii) Mode 2, where the cross-section displacements are as follows:

$$u_2 = 0 \quad v_2 = -\cos(\theta) \quad w_2 = 0 \tag{3.26}$$

(iii) Mode 3, with the following cross-section displacements:

$$u_3 = 0 \quad v_3 = 0 \quad w_3 = -\sin(\theta) \tag{3.27}$$

3.3.2.3. The Variation of Strain Energy

Let us consider the following expression of the linearization of the strain energy variation:

$$\delta W = \int_L \iint_t \left(\sigma_{xx}^L \delta\varepsilon_{xx}^L + \sigma_{\theta\theta}^L \delta\varepsilon_{\theta\theta}^L + \tau_{x\theta}^L \delta\gamma_{x\theta}^L + \sigma_{xx}^0 \delta\varepsilon_{xx}^{NL} + \sigma_{\theta\theta}^0 \delta\varepsilon_{\theta\theta}^{NL} + \tau_{x\theta}^0 \delta\gamma_{x\theta}^{NL} \right) dz r d\theta dx = 0 \tag{3.28}$$

where: σ_{xx}^0, $\sigma_{\theta\theta}^0$, $\tau_{x\theta}^0$ are the pre-buckling normal meridional stresses, normal hoop stresses and, respectively shear stresses.

The constitutive relations are the following:

$$\begin{aligned} \sigma_{xx} &= Q_{11}\varepsilon_{xx} + Q_{12}\varepsilon_{\theta\theta} \\ \sigma_{\theta\theta} &= Q_{21}\varepsilon_{xx} + Q_{22}\varepsilon_{\theta\theta} \\ \tau_{x\theta} &= Q_{33}\gamma_{x\theta} \end{aligned} \tag{3.29}$$

where: $Q_{11}=Q_{22}=E/(1-\mu^2)$, $Q_{12}=Q_{21}=\mu Q_{11}$ and $Q_{33}=G$;

E, G is the Young elasticity module, respectively the transverse module;

μ is Poisson's coefficient.

By using the kinematic relations from Eq. (3.17) and the constitutive relations from Eq. (3.29) and performing the integrations with respect the thickness and the cross-section's circumference, the following expression of the variation of the strain energy results:

$$\delta W = \int_L \left(\begin{array}{l} C_{ik}\phi_{k,xx}\delta\phi_{i,xx} + D^1_{ik}\phi_k\delta\phi_{i,xx} + D^2_{ik}\phi_k\delta\phi_{i,xx} + D^2_{ki}\phi_{k,xx}\delta\phi_i + B_{ik}\phi_k\delta\phi_i + G_{ik}\phi_k\delta\phi_{i,x} + G_{ki}\phi_{k,x}\delta\phi_i + \\ H_{ik}\phi_{k,x}\delta\phi_{i,xx} + H_{ki}\phi_{k,xx}\delta\phi_{i,x} + X^{\sigma x}_{jik}\phi_{k,x}\delta\phi_{i,x} + X^{\sigma\theta}_{jik}\phi_k\delta\phi_i + X^{\tau}_{jik}\left(\phi_k\delta\phi_{i,x} + \phi_{k,x}\delta\phi_i\right) \end{array} \right) dx \quad (3.30)$$

where: C_{ik}, D^1_{ik}, D^2_{ik}, B_{ik}, G_{ik}, H_{ik} are the linear stiffness tensors which describe the general warping, twisting and the cross section distorsion;

$X^{\sigma x}_{jik}$, $X^{\sigma\theta}_{jik}$, X^{τ}_{jik} are geometrical stiffness tensors which take into account the second order effects of the pre-buckling meridional, hoop and, respectively shear stresses associated to deformation mode j.

The mathematical expressions of these matrices are as follows:

$$C_{ik} = \oint \left(A_{11}u_iu_kr^2 + D_{11}w_iw_k \right) rd\theta \quad (3.31)$$

$$D^1_{ik} = \oint \left(\begin{array}{l} \left(A_{11} + 2\tilde{A}_{12} + \tilde{A}_{22}\right)u_iu_ks^2 + A_{33}\left(u_{i,\theta} + v_i\right)\left(u_{k,\theta} + v_k\right) + \\ + D_{22}\dfrac{w_iw_ks^2}{r^2} + D_{33}\dfrac{2w_{i,\theta} - v_ic}{r}\dfrac{2w_{k,\theta} - v_kc}{r} \end{array} \right) rd\theta \quad (3.32)$$

$$D^2_{ik} = \oint \left(A_{12}\left(v_{i,\theta} + w_ic\right)u_k + D_{12}\frac{w_{i,\theta\theta} - v_{i,\theta}}{r^2}w_k \right) rd\theta \quad (3.33)$$

$$B_{ik} = \oint \left(\begin{array}{l} A_{22}\dfrac{\left(v_{i,\theta} + w_ic\right)}{r}\dfrac{\left(v_{k,\theta} + w_kc\right)}{r} + \tilde{A}_{33}\dfrac{v_iv_ks^2}{r^2} + \\ D_{22}\dfrac{w_{i,\theta\theta} - v_{i,\theta}c}{r^2}\dfrac{w_{k,\theta\theta} - v_{k,\theta}c}{r^2} + 4D_{33}\dfrac{w_{i,\theta}s - v_isc}{r^2}\dfrac{w_{k,\theta}s - v_ksc}{r^2} \end{array} \right) rd\theta \quad (3.34)$$

$$G_{ik} = \oint \left(\begin{array}{l} \left(A_{12} + \tilde{A}_{22}\right)\dfrac{\left(v_{i,\theta} + w_ic\right)u_ks}{r} - \tilde{A}_{33}\dfrac{v_i\left(u_{k,\theta} + v_k\right)s}{r} + \\ D_{22}\dfrac{w_{i,\theta\theta} - v_{i,\theta}c}{r^2}\dfrac{w_ks}{r} - D_{33}\dfrac{2\left(w_{i,\theta} - v_ic\right)}{r^2}\dfrac{\left(2w_{k,\theta} - v_k\,\mathrm{c}\right)s}{r} \end{array} \right) rd\theta \quad (3.35)$$

$$H_{ik} = \oint \left(\left(\tilde{A}_{11} + A_{12}\right)u_iu_ks + D_{12}\frac{w_iw_ks}{r} \right) rd\theta \quad (3.36)$$

$$X_{jik}^{\sigma x} = \int_{\Omega} \sigma_{xx}^{0} \left(w_i w_k + v_i v_k \right) t r d\theta \tag{3.37}$$

$$X_{jik}^{\sigma\theta} = \int_{\Omega} \left(\sigma_{\theta\theta}^{0} \frac{w_{i,\theta} - v_i c}{r} \frac{w_{k,\theta} - v_k c}{r} \right) t r d\theta \tag{3.38}$$

$$X_{jik}^{\tau} = \int_{\Omega} \tau_{x\theta}^{0} \left(w_i \frac{w_{k,\theta} - v_k c}{r} \right) t r d\theta \tag{3.39}$$

where: $A_{ij}=Q_{ij}t$, $D_{ij}=Q_{ij}t^3/12$.

If the terms $-vs/r$ and us/r of the kinematic relationships from Eq. (3.17) are taken into account, then $\widetilde{A}_{ij}=A_{ij}$, else $\widetilde{A}_{ij}=0$.

In case of the shell-type deformation modes and shear deformation modes, Eq. (3.20) may be used to determine the tensors mentioned previously by using only the warping displacement u_k. The trigonometric functions which describe the warping displacements u_k (see Eq. (3.21)) fulfill simultaneously the orthogonality conditions which appear in the mathematical expressions of the tensors in the C, D^1, D^2, B, G, H and X stiffness matrices:

$$\int_{\Omega} u_k u_i d\theta = 0, \quad \int_{\Omega} u_{k,\theta\theta} u_{i,\theta\theta} d\theta = 0, \quad \int_{\Omega} u_{k,\theta\theta\theta\theta} u_{i,\theta} d\theta = 0, \ etc. \tag{3.40}$$

Thus, diagonal tensors result for the shell-type deformation modes and, respectively for shear deformation modes (i.e. “u” and “v” shear modes). However, between these two categories of deformation modes there is coupling, but only for the deformation modes with the same order k. For example, if for the stiffness matrix C there are n shell-type deformation modes with index k and, also, n shear deformation modes, by introducing equations (3.20) and (3.21) in Eq. (3.31), the following mathematical expressions result:

$$\begin{aligned} C_{kk} &= \int_{\Omega} \left(A_{11} u_k u_k r^3 + D_{11} \frac{u_{k,\theta\theta} u_{k,\theta\theta}}{c^2} r \right) d\theta \qquad for\ k = 2...n+1 \\ C_{ks} &= C_{ss} = \int_{\Omega} A_{11} u_k u_k r^3 d\theta \qquad where\ s = k+n \end{aligned} \tag{3.41}$$

where the warping displacement u_s of “u” a shear deformation mode is identical to the warping displacement u_k of the shell-type deformation mode. In C matrix from Eq. (3.41) it can be remarked that there is a coupling between shell-type deformation modes and “u” shear deformation modes. Similar couplings exist for all the stiffness matrices. These couplings are presented in detail in Annex III. However, the shell-type deformation modes and the shear deformation modes are not coupled with the additional deformation modes presented in Section 3.3.2.3.

The only practical case where the buckling modes are completely uncoupled is in the case of axially compressed conical shells, when only the shell-type deformation modes are considered. This is due to the fact that the only non-null geometric matrices $X_1^{\sigma x}$ and $X_1^{\sigma \theta}$ are diagonal. Also, the pre-buckling normal stresses σ_{xx}^0 and $\sigma_{\theta\theta}^0$ are constant along the cross-section, while the pre-buckling shear stresses $\tau_{x\theta}^0$ are null.

By introducing equations (3.20) and (3.21) in equations (3.32) – (3.39) for each stiffness matrix result analytical expressions similar to the ones from reference [4] in case of shell-type deformation modes. The complete list of the analytical expressions is given in Annex I. Because the radius r is variable along the member's length, the elements of the stiffness matrices are no longer constant with respect to the longitudinal axis. Therefore, the elements of the stiffness matrices from the expression of variation of strain energy need to be integrated with respect to the longitudinal axis.

In the case of axially compressed conical shells, presented in this thesis, the deformations resulting from first order analyses are described by the coupling of the first two additional deformation modes: the axial extension (e) and the axisymmetric extension (a). Because there are no shear stresses in this case, the variation of the strain energy for the first order analysis has the following expression:

$$\delta W = \int_L \iint_t \left(\sigma_{xx,i}^L \delta \varepsilon_{xx,k}^L + \sigma_{\theta\theta,i}^L \delta \varepsilon_{\theta\theta,k}^L \right) dz r d\theta dx \tag{3.42}$$

where i, k may be any of the deformation modes e or a.

By introducing equations (3.22) and (3.23) together with the kinematic and constitutive relationships from equations (3.17) and (3.29), the variation of the strain energy has the following form:

$$\delta W = \int_L \begin{pmatrix} C_{ik}\phi_{k,xx}\delta\phi_{i,xx} + D_{ik}^1\phi_{k,x}\delta\phi_{i,x} + D_{ik}^2\phi_k\delta\phi_{i,xx} + D_{ki}^2\phi_{k,xx}\delta\phi_i + B_{ik}\phi_k\delta\phi_i + \\ H_{ik}\phi_{k,x}\delta\phi_{i,xx} + H_{ki}\phi_{k,xx}\delta\phi_{i,x} + F_{ik}\phi_{k,x}\delta\phi_i \end{pmatrix} dx \tag{3.43}$$

where: F_{ik} is the linear stiffness tensor which describes the coupling between the axial extension and axisymmetric extension modes. The mathematical expression is as follows:

$$F_{ik} = \int A_{11} \frac{sc}{r^2} r d\theta \tag{3.44}$$

The stiffness matrices, having the size 2x2, are determined by integration with respect to the cross-section thickness and circumference directions and they have the following mathematical expressions:

(i) For axial extension mode:

$$C_{ee} = 2\pi A_{11} r, \quad D_{ee}^{1} = \frac{2\pi A_{11} s^2}{r}, \quad D_{ee}^{2} = 0$$
$$B_{ee} = 0, \qquad H_{ee} = 2\pi A_{12} s, \qquad F_{ee} = 0 \tag{3.45}$$

(ii) For axisymmetric extension mode:

$$C_{aa} = 2\pi D_{11} r, \qquad D_{aa}^{1} = \frac{2\pi A_{11} s^2}{r}, \qquad D_{aa}^{2} = 0$$
$$B_{aa} = \frac{2\pi A_{11} c^2}{r}, \quad H_{aa} = 2\pi D_{12} s, \qquad F_{aa} = 0 \tag{3.46}$$

(iii) For the coupling between the axial extension and axisymmetric modes:

$$C_{ea} = 0, \qquad D_{ea}^{1} = 0, \qquad D_{ea}^{2} = 2\pi A_{12} c$$
$$B_{ea} = 0, \qquad H_{ea} = 0, \qquad F_{ea} = \frac{2\pi A_{11} sc}{r} \tag{3.47}$$

3.4. Conclusions

The GBT analysis is performed in two steps: (i) the cross-section analysis, which establishes the fundamental deformation modes and the modal properties and (ii) the structural analysis, which determines the buckling modes and the critical buckling loads. The cross-section analysis has several steps which consist in the diagonalization of the cross-section stiffness matrices. These steps are described in detail in the literature. The structural analysis, where the geometrical and material properties of the analysed structure are known, consists in the determination of the solution of the GBT system of equilibrium equations (4^{th} order differential equations) by exact methods or by approximative methods.

Chapter III presented the GBT formulation for isotropic conical shells. The formulation begins from the kinematic relations of Love – Timoshenko theory [44] (see Eq. (3.17)). In the case of conical shells three types of deformation modes were identified: (i) shell-type deformation modes, described by two sets of independent trigonometric functions (see Eq. (3.21)), where for a number of *m* circumferential waves there are two similar deformation modes with distinct *k* order, (ii) shear deformation modes entailed in two categories: "u" shear deformation modes ($u_k \neq 0$, $v_k = w_k = 0$) and "v" shear deformation modes ($v_k \neq 0$, $u_k = w_k = 0$) and (iii) additional deformation modes: axial extension, axisymmetric extension and torsion, which are necessary in a first order analysis.

As in the case of GBT for prismatic bars, in the GBT for conical shells the variation of the strain energy is formulated. After the integration with respect to the cross-section thickness and circumference, the stiffness and geometric matrices are obtained. Because conical shells have variable

cross-section, the stiffness and geometric matrices are also integrated with respect the longitudinal axis (see Eq.

(3.30)). In the case of axially compressed conical shells, the deformation of the structure is described in the first order analysis by a coupling between the axial extension and axisymmetric extension deformation modes. Thus, by integrating the variation of the strain energy with respect to the cross-section thickness and circumference result stiffness matrices having a size 2x2 size (see Eq. (3.43)).

Chapter IV
The GBT-based Finite Element Formulation

4.1. Introduction

The GBT buckling analysis method for thin walled structures decomposes the buckling mode into a linear combination of fundamental deformation modes and therefore the degree of modal participation is easily assessd in coupled instabilities. A GBT analysis consist in two steps: the cross section analysis, where the deformation modes and the modal properties are established, and the structural analysis.

The GBT structural analysis corresponds solving a system of 4th order differential equations having the unknowns funcitons $\phi_k(x)$ which correspond to the modal amplitude functions (see Eq. (3.1)). By solving the GBT system of differential equations the buckling modes and the associated buckling loads are obtained.

In case of cylindrical bars, Silvestre [120] determined the solution of the GBT system of differential equations using the Galerkin method. According to the results in case of pinned bars, both globally and locally, with end sections free to warp, the Galerkin method is extremely advantageous. The modal amplitude functions $\phi_k(x)$ have sinusoidal form. In case of conical shells with circular cross section, Nedelcu [4] solved the GBT system of differential equations by the numerical method Runge-Kutta, namely the 4^{th} order Lobatto IIIA colocation method [122]. The method proved to be unstable when the number of deformation modes included in the analysis was large and it has limits regarding structures with arbitrary loads and boundary conditions.

The following chapter presents the GBT-based Finite Element (FE) formulation implemented to determine the solution of the GBT system of differential equations for isotropic conical shells. The Finite Element Method (FEM) was chosen because structures with different loads and boundary conditions may be easily analysed. The GBT based FE formulation was used in other papers such as [109], [110] or [107], presented in Section 2.5.2.

4.2. General Aspects of the Finite Element Formulation

The GBT system of differential equations may be solved by analytical methods for simple loading and boundary conditions and by approximate methods such as the Finite Element Method (FEM). The Finite Element Method consists in the approximation of any continuous domain into a discrete model. This discrete model is made of a finite number of sub-domains called finite elements.

In the FEM the problem may be formulated in terms of displacements, strains, stresses or as combination of these three. The most used FEM formulation is the one in displacements [126].

For conical shells, the GBT system of differential equations was initially solved, in reference [4], by the numerical method Runge-Kutta, namely the 4th order Lobatto IIIA colocation method [122], which was implemented as Matlab function *bvp4c* [6]. The 4th order Lobatto IIIA colocation method uses a finite space of solutions of the modal amplitude function $\phi_k(x)$ having the form of *n*-degree polynomials and a mesh of points in the range [*0*, *L*] named colocation points. From these colocation points the solution which fulfills the respective differential equation is selected.

The initial method had satisfactory results for buckling analyses where the solution was determined by a single deformation mode, more exactly in case of axially compressed structures. However, the method has a major drawback: the solution, which in this case is the shape of the modal amplitude function $\phi_k(x)$, must be guessed initially. In case of axially compressed structures with simple boundary conditions this may be done easily by introducting combinations of trigonometric functions compatible with the boundary conditions. However, in case of sudden variations of the modal amplitude function, if the guessed solution is wrong, then the first eiegenvalue may be lost or it could result in non-convergence. This problem occurs in case of coupled instabilities where the shear deformation modes may have an unpredictable behavior as it is illustrated in the numerical examples in the following chapters. Another difficulty of the Runge-Kutta method is the insertion of the boundary conditions, more exactly 4x*n* boundary conditions, where 4 is the order of the differential equations and *n* is the number of deformation modes.

Because of the drawbacks of the Runge-Kutta numerical method, a GBT-based FE formulation was preferred to solve the GBT system of differential equations in case of conical shells. The GBT-based FE formulation was applied in other studies such as [109], [110], [107] and **Error! Reference source not found.**. Basaglia [109] used the GBT-based FE formulation for calculating the elastic local, distortional and global buckling of TWB frames. The bar finite element used in the analysis takes into account the caracteristics of the frame's nodes and the relationships between the modal degrees of freedom of the end section of the connected member and the modal degrees of freedom of the respective connection. In reference [110], the GBT-based FE formulation was used for the local, distortional and global buckling analysis of the TWB frames in the post-critical domain. Silvestre and Camotim [107] used a GBT-based FE formulation for the stability analysis of TWBs with orthotropic "C" section made of a composite material reinforced with fiber carbon polymers. Bebiano et al. **Error! Reference source not found.** used a GBT-based FE formulation for the buckling analysis of TWBs subjected to non-uniform bending.

In FEM the insertion of any type of boundary conditions is a simple procedure. Regarding computational efficiency, unlike FEM, the Runge-Kutta numerical method doesn't operate with classical degrees of freedom. The approximate solution is a continuous function having the form of a cubic polynomial for each sub-range of the mesh along the length of the structure. The number of points of the mesh may be approximated as FEM degrees of freedom. In the following case studies, the number of points of the mesh has the same magnitude order as the number of FEM degrees of freedom. To obtain convergence, the size of the mesh had to be iteratively adapted. This is the reason why FEM is a faster analysis method.

In this thesis the GBT-based FE formulation initially developed for prismatic bars ([109], [110], [107] and **Error! Reference source not found.**) was adapted for structures with circular cross section and, at the same time, with variable cross section along the longitudinal axis. This formulation was applied for both the first order analysis and the buckling analysis.

4.3. The Algorythm of the Finite Element Formulation

In the case of conical shells, the GBT-based FE formulation, initially applied for TWBs with prismatic cross-section ([109], [110], [107] and **Error! Reference source not found.**), was adapted for structures with circular cross section and, at the same time, with variable cross section with respect to the member's longitudinal axis. The GBT-based FE formulation starts from the variation of the strain energy, given by Eq. (3.43), in the first order analysis and, respectively by Eq.

(3.30), for the buckling analysis. Also, the formulation in displacements is used which means that the problem's unkwowns are the amplitudes of the deformation modes at the element nodes. The finite elements used in the formulation are bar FE with two nodes and 4 degrees of freedom (DOFs) for each deformation mode, i.e. 2 degrees of freedom for each node, for each deformation mode. In case there are n deformation modes, then one finite element has $4n$ DOFs, i.e. $2n$ DOFs for each node.

The shape functions used to approximate the modal amplitude function $\phi_k(x)$ are the cubic Hermite polynomials, which have the following expresions:

$$\begin{aligned} \psi_1 &= L_e\left(\xi^3 - 2\xi^2 + \xi\right), \quad \psi_2 = 2\xi^3 - 3\xi^2 + 1 \\ \psi_3 &= L_e\left(\xi^3 - \xi^2\right), \qquad \psi_4 = -2\xi^3 + 3\xi^2 \end{aligned} \tag{4.1}$$

where L_e is the length of the finite element and $\xi = x/L_e$.

Figure 4.1 presents the shape functions in the range $\xi \in [0,1]$.

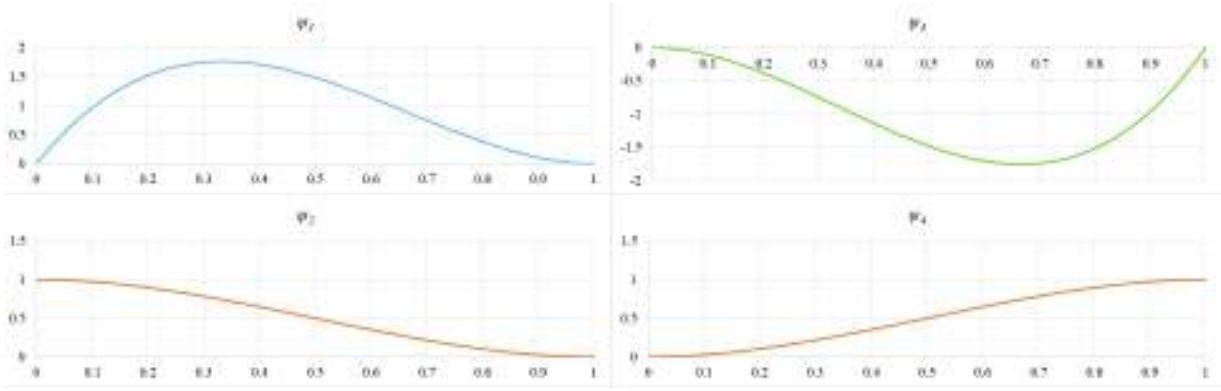

Figure 4.1: The shape functions.

Each modal amplitude function $\phi_k(x)$ is approximated as follows:

$$\phi_k(x) = d_1\psi_1 + d_2\psi_2 + d_3\psi_3 + d_4\psi_4 \tag{4.2}$$

where: $d_1=\phi_{k,x}(0)$, $d_2=\phi_k(0)$, $d_3=\phi_{k,x}(L_e)$ and $d_4=\phi_k(L_e)$ are the finite element's degrees of freedom (DOFs).

4.3.1. The GBT-based FE Formulation for the First Order Analysis

In the first order analysis the the variation of strain energy leads to the following standard matrix equation:

$$\left[K^{(e)}\right]\left\{d^{(e)}\right\} = \left\{f^{(e)}\right\} \tag{4.3}$$

where $[K^{(e)}]$ is the finite element stiffness matrix;

$\{d^{(e)}\}$ is the displacement vector;

$\{f^{(e)}\}$ is the vector of equivalent nodal forces.

In the case of axially compressed conical shells, the elements of the finite element stiffness matrix are determined as follows:

$$K_{pr}^{ik} = \int_{L_e} \begin{pmatrix} C_{ik}\psi_{p,xx}\psi_{r,xx} + D_{ik}^1\psi_{p,x}\psi_{r,x} + D_{ik}^2\psi_p\psi_{r,xx} + D_{ki}^2\psi_{p,xx}\psi_r + B_{ik}\psi_p\psi_r + \\ +H_{ik}\psi_{p,x}\psi_{r,xx} + H_{ki}\psi_{p,xx}\psi_{r,x} + F_{ik}\psi_{p,x}\psi_r \end{pmatrix} dx \tag{4.4}$$

The elements of the $[K^{(e)}]$ stiffness matrix are determined with the following formula in case of conical shells under bending:

$$K_{pr}^{ik} = \int_{L_e} \begin{pmatrix} C_{ik}\psi_{p,xx}\psi_{r,xx} + D_{ik}^1\psi_{p,x}\psi_{r,x} + D_{ik}^2\psi_p\psi_{r,xx} + D_{ki}^2\psi_{p,xx}\psi_r + B_{ik}\psi_p\psi_r + \\ +G_{ik}\psi_p\psi_{r,x} + G_{ki}\psi_{p,x}\psi_r + H_{ik}\psi_{p,x}\psi_{r,xx} + H_{ki}\psi_{p,xx}\psi_{r,x} \end{pmatrix} dx \tag{4.5}$$

where i, k may be any of the following deformation modes: (i) axial extension or axisymmetrical extension for axially compressed conical shells (see Section 3.3.2.2., a.) and (ii) mode 1, mode 2 or mode 3 for conical shells under bending (see Section 3.3.2.2., b.);

p, r are the finite element's degrees of freedom (p, $r=1...4$).

The difference between Eq. (4.4) and Eq. (4.5) is the presence of the linear stiffness matrix tensor F_{ik} which describes the coupling between the axial extension and axisymmetric extension modes, a phenomenon only specific to conical shells under axial compression with stress concentrations.

The arbitrary exterior loads that are applied to the conical shell are replaced by equivalent nodal forces applied at the finite element's end sections. The vector of equivalent nodal forces of one finite element is obtained with the following expression:

$$f_i = \int \left(\begin{bmatrix} f_{0\_x} & 0 & 0 \\ 0 & f_{0\_y} & f_{0\_z} \\ f_{Le\_x} & 0 & 0 \\ 0 & f_{Le\_y} & f_{Le\_z} \end{bmatrix} \begin{Bmatrix} u_i \\ v_i \\ w_i \end{Bmatrix} \right) r d\theta \tag{4.6}$$

where f_0 and f_{Le} are the equivalent nodal forces distributed at the finite element's end sections;

x, y, z are the projections of the equivalent nodal forces on the corresponding local axis.

Figure 4.2 presents the algorithm of the GBT-based FE formulation for the first order analysis as a flow chart. According to Figure 4.2 the variables in the flow chart are as follows:

$K^{(e)}$ is the finite element mechanical stiffness matrix;

$f^{(e)}$ is the finite element vector of equivalent nodal forces;

K is the global stiffness matrix;

f is the global vector of equivalent nodal forces;

K_{red} is the reduced global stiffness matrix after the elimination of the lines and columns corresponding to blocked degrees of freedom;

f_{red} is the reduced global vector of equivalent nodal forces after the elimination of the columns corresponding to blocked degrees of freedom;

d_{free} is the vector of free displacements;

d_{total} is the vector of total displacements (i.e. of all the finite elements);

L is the matrix of localization which is used to transfer the degrees of freedom from finite element level to global level.

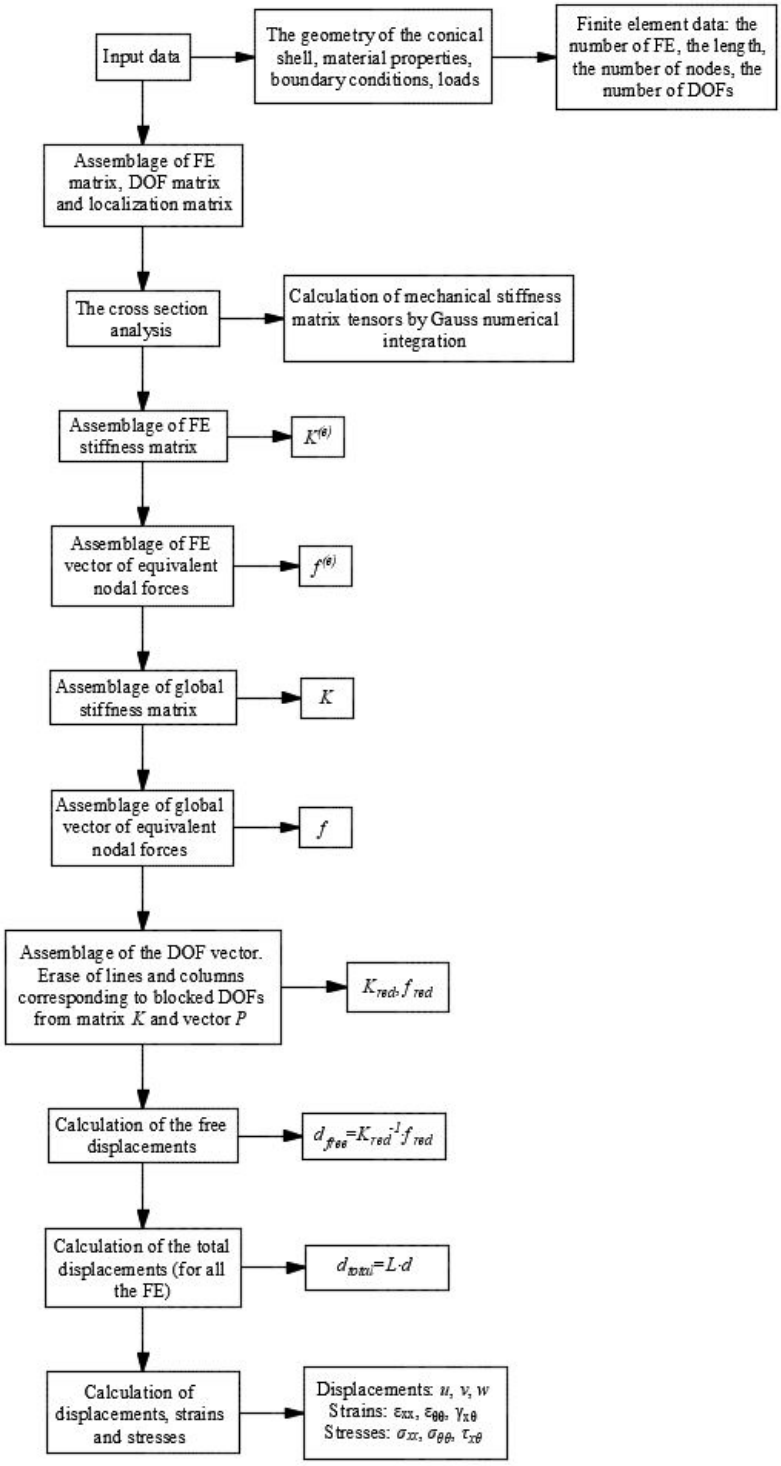

Figure 4.2: The flowchart of the GBT-based FE formulation for the first order analysis.

4.3.2. The GBT-based FE Formulation for the Buckling Analysis

By introducing Eq. (4.2) in Eq.

(3.30) and operating the integrations the matrix eigenvalue equation for buckling analysis is obtained:

$$\left(\left[K^{(e)}\right]+\lambda\left[G^{(e)}\right]\right)\left\{d^{(e)}\right\}=\{0\} \tag{4.7}$$

where $[K^{(e)}]$, $[G^{(e)}]$ is the finite element linear stiffness and geometric stiffness matrices, respectively;

$\{d^{(e)}\}$ is the displacement vector;

λ is the loading parameter and eigenvalue corresponding to the displacement vector $\{d^{(e)}\}$. λ_c is the lowest eigenvalue and it is called critical buckling parameter.

The elements of the $[K^{(e)}]$ and $[G^{(e)}]$ matrices are determined with the following expressions:

$$K_{pr}^{ik}=\int_{L_e}\left(\begin{array}{l} C_{ik}\psi_{p,xx}\psi_{r,xx}+D_{ik}^{1}\psi_{p,x}\psi_{r,x}+D_{ik}^{2}\psi_{p}\psi_{r,xx}+D_{ki}^{2}\psi_{p,xx}\psi_{r}+B_{ik}\psi_{p}\psi_{r}+ \\ +G_{ik}\psi_{p}\psi_{r,x}+G_{ki}\psi_{p,x}\psi_{r}+H_{ik}\psi_{p,x}\psi_{r,xx}+H_{ki}\psi_{p,xx}\psi_{r,x} \end{array}\right)dx \tag{4.8}$$

$$G_{pr}^{ik}=-\int_{L_e}\left(X_{jik}^{\sigma x}\psi_{p,x}\psi_{r,x}+X_{jik}^{\sigma\theta}\psi_{p}\psi_{r}+X_{jik}^{\tau}\left(\psi_{p}\psi_{r,x}+\psi_{p,x}\psi_{r}\right)\right)dx \tag{4.9}$$

where i, k=2...n;

p, r are the finite element's degrees of freedom (p, r=1...4).

In Figure 4.3 is the algorithm of the GBT-based FE formulation for the buckling analysis as flow chart. According to Figure 4.3 the variables in the flow chart are as following:

$K^{(e)}$, $G^{(e)}$ are the finite element linear stiffness and geometric stiffness matrices;

K, G are the global linear stiffness and global geometric stiffness matrices, respectively;

K_{red}, G_{red} are reduced matrices, after the elimination of the lines and columns corresponding to blocked degrees of freedom;

λ_b is the eigenvalue;

$\{d_b\}$ is the eigen vector corresponding to the eigenvalue λ_b;

λ_c is the critical buckling coefficient which is the smallest eigenvalue;

σ_c, τ_c are critical stresses.

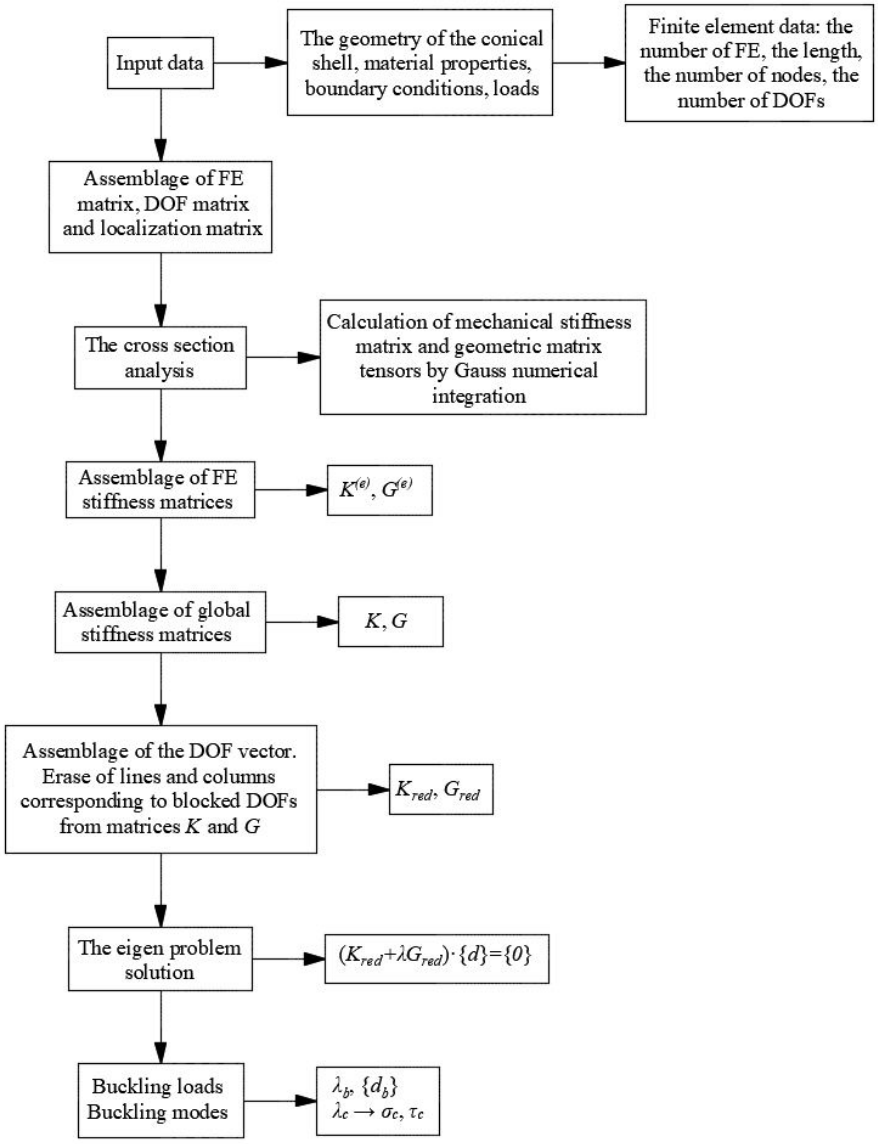

Figure 4.3: The flow chart of the GBT-based FE formulation for the buckling analysis.

Because conical shells have variable cross section, the linear and geometrical stiffness matrices are also variable with respect to the member's longitudinal axis. Therefore, the stiffness matrices from equations (4.4), (4.8) and (4.9) are also integrated with respect to the finite element's length. This is an important aspect which distinguishes the proposed FE formulation from the FE formulations for prismatic bars. The integration with respect to the finite element's length was performed by Gauss numerical integration. In all the numerical examples presented in the following chapters 4 integration points were used. Using a larger number of integration points did not improved the accuracy of the solution.

The first step of this procedure was dividing the analysed structure into a certain number of finite elements. The nodal degrees of freedom are identified and are grouped in the vector $\{d\}$. The

finite element stiffness matrices are assembled to form the global linear stiffness matrix [K] and the global geometric stiffness matrix [G]. The same procedure is applied to the vector of equivalent nodal forces {f} and to the vector of displacements {d}. In the case of first order analyses, the solution of the system of matrix equations $[K]\cdot\{d\}=\{f\}$ is the displacement vector {d} from which the pre-buckling strains and stresses are found. The buckling analysis is performed by using the stresses determined in the first order analysis and by determining the solutions of the eigenproblem $[K+\lambda G]\cdot\{d\}=\{0\}$, from which the eigenvalues λ and the eigenvectors $\{d_b\}$ are found. The lowest eigenvalue λ_c is the critical buckling coefficient.

To find the deformed configuration of the analysed conical shell, the modal amplitude functions $\phi_k(x)$ are determined by the superposition of the shape functions $\psi_i(\xi)$ using Eq. (4.2). Then the displacements are found by using Eq. (3.19).

4.4. Conclusions

The GBT structural analysis leads to a system of 4th order differential equations with the unknowns $\phi_k(x)$, which are the modal amplitude functions expressed by Eq. (3.1). The GBT system of differential equations may be solved by exact methods or by approximate methods. Exact methods are possible in some cases, namely when then analytical solutions are in the form of sinusoidal functions. The exact methods have limited practical application and they are recommended only for simple loads and boundary conditions.

In the case of conical shells, the GBT system of differential equations is solved in this work by approximate methods, more exactly by the Finite Element Method. Thus, the GBT-based FE formulation, initially used for prismatic bars ([109], [110], [107], **Error! Reference source not found.**), was adapted for structures with circular sections and variable section with respect the longitudinal axis. In the procedure presented in Chapter IV, the displacement formulation (i.e. the unknowns of the problem are the nodal values and derivatives of the mode amplitude functions) was used. The finite elements used in the analysis are bar-type elements, with two nodes and 4 degrees of freedom (2 degrees of freedom for each node). One important aspect which distinguishes the proposed FE formulation from the FE formulations for prismatic bars is the fact that the elements of the linear and geometric stiffness matrices vary with respect to the member's longitudinal axis because conical shells have variable cross section.

For the validation of the proposed formulation, the following chapters present numerical examples of first order analysis and buckling analysis of conical shells under different loads and boundary conditions.

Chapter V
Axially Compressed Conical Shells

5.1. Introduction

In the case of conical shells, the GBT system of differential equations is solved by the Finite Element Method (FEM). Therefore, the GBT-based FE formulation, initially applied to prismatic bars ([109], [110], [107], **Error! Reference source not found.**), was adapted for structures with circular cross section and variabile cross section with respect the longitudinal axis. To validate the proposed formulation several case studies were performed. The case studies involved conical shells under different loads and boundary conditions. The proposed procedure was implemented in a Matlab code [6] and the results were compared to the results determined by Shell Finite Element Analysis (SFEA). The SFEA analyses were performed in Abaqus [7] with S4 rectangular shell finite elements. The Abaqus models for conical shells have a regular mesh along the cross section, while along the length of the structure the size of the mesh varies from *5 mm* at the top radius to *50 mm* at the bottom radius.

This chapter presents the case of axially compressed conical shells. Therefore, let us consider the conical shell from Figure 5.1. The conical shell is made of steel: $E=210\ GPa$, $\mu=0.3$. In the case of axially compressed conical shells two situations were considered: conical shells with constant thickness and conical shells with variable thickness. In the first situation, the conical shells have a thickness $t=1\ mm$. In the case of conical shells with variable thickness the following configuration was considered: in the first half of the structure the thickness is $t_1=1\ mm$, while in the second half of the structure the thickness is $t_2=2\ mm$. In case of conical shells with constant thickness, the length was considered $L=48\ mm$ and $L=1200\ mm$. In the case of conical shells with variable thickness the length is $L=1000\ mm$. The top radius is $r_1=50\ mm$, while the value of the bottom radius r_2 ranges between *50* and *1000 mm*. The analysed conical shells have different boundary conditions which will be presented in the following sections.

The axial load was introduced as $P=\lambda \cdot P_0$, where λ is the loading coefficient and P_0 is the pre-buckling axial load used in the first-order analysis. In all the numerical examples presented in the following sections the value of the pre-buckling axial load is $P_0=1\ kN$.

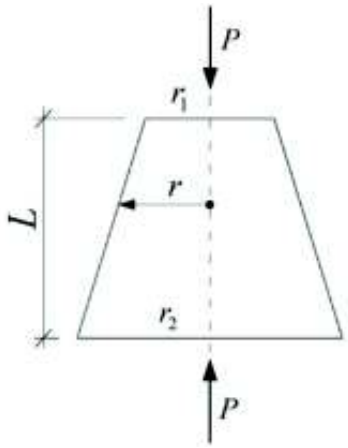

Figure 5.1: The geometry of the axially compressed conical shell.

In case of axially compressed conical shells, the deformed configuration resulting from a first-order analysis is described by a coupling between the axial extension and axisymmetric extension modes. The buckling modes are described by one shell-type deformation mode. It must be remarked that since there is no coupled instability (i.e. coupled deformation modes) the computational time and effort is low, which is an advantage impossible to achieve using SFEA. In case of axial compression, all the GBT matrices are diagonal having a size nxn, where n is the number of deformation modes. The finite element matrices $[K^{(e)}]$ and $[G^{(e)}]$ have a size 4nx4n and they are assembled by adding 4x4 matrices (i.e. there are 4 DOFs for each deformation mode) on the diagonal.

The axially compressed conical shells were divided in two main case studies according to their boundary conditions as following:

(i) Conical shells without stress concentrations;

(ii) Conical shells with stress concentrations.

These case studies are presented in detail in the following sections.

5.2. Conical Shells without Stress Concentrations

Conical shells without stress concentrations have boundary conditions of simply supported and/or fixed end type. The v and w displacements are always blocked in this type of boundary conditions such that the pre-buckling hoop normal stresses $\sigma^0_{\theta\theta}$ have very low values on the entire structure as it was remarked from the results obtained in first-order analysis. Therefore the effect of the hoop stresses $\sigma^0_{\theta\theta}$ on the buckling behavior is neglected. The meridional normal stresses σ^0_{xx} don't have significant local variations in this case so they may be approximated on the entire structure by a simple mathematical expression [4]:

$$\sigma^0_{xx} = \frac{P}{2\pi rtc} \tag{5.1}$$

5.2.1. Conical Shells with Constant Thickness

The following section presents numerical examples of conical shells without stress concentrations having constant thickness. These numerical examples are divided in two categories: (i) long conical shells, with the length *L=1200 mm* and (ii) short conical shells, with the length *L=48 mm*.

5.2.1.1. Long Conical Shells

a) Simply Supported Conical Shells

The simply supported conical shells are free to warp (i.e. the *u* displacement is free), while the *v* and *w* displacements are blocked at both end sections. The buckling mode of the structure is described by a single cross section deformation mode *k* (see Figure 5.2) and by the number of longitudinal half-waves n_{hw}. Figure 5.2 shows the critical buckling modes of the long simply supported conical shells for different values of the bottom radius r_2 and the corresponding critical buckling coefficients λ_c. The same cases were studied in reference [4] using numerical integration instead of FEM and there are no significant differences between the final results as seen in Table 5.1. In Figure 5.3 are the normalized graphs of the modal amplitude function $\phi_k(x)$.

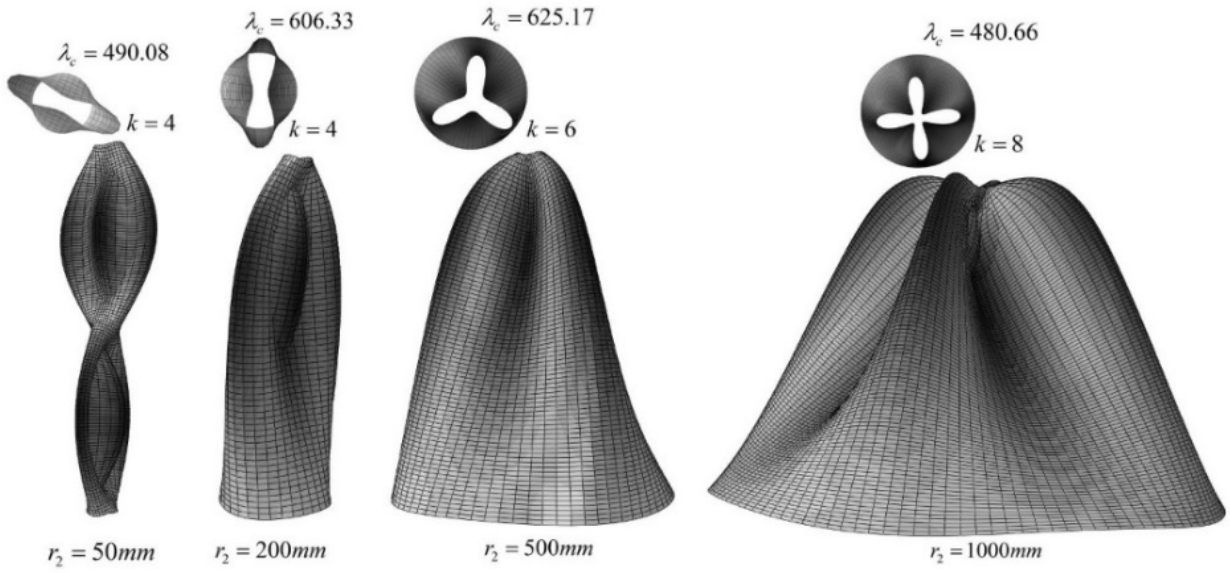

Figure 5.2: The critical buckling modes of long simply supported conical shells resulting from SFEA.

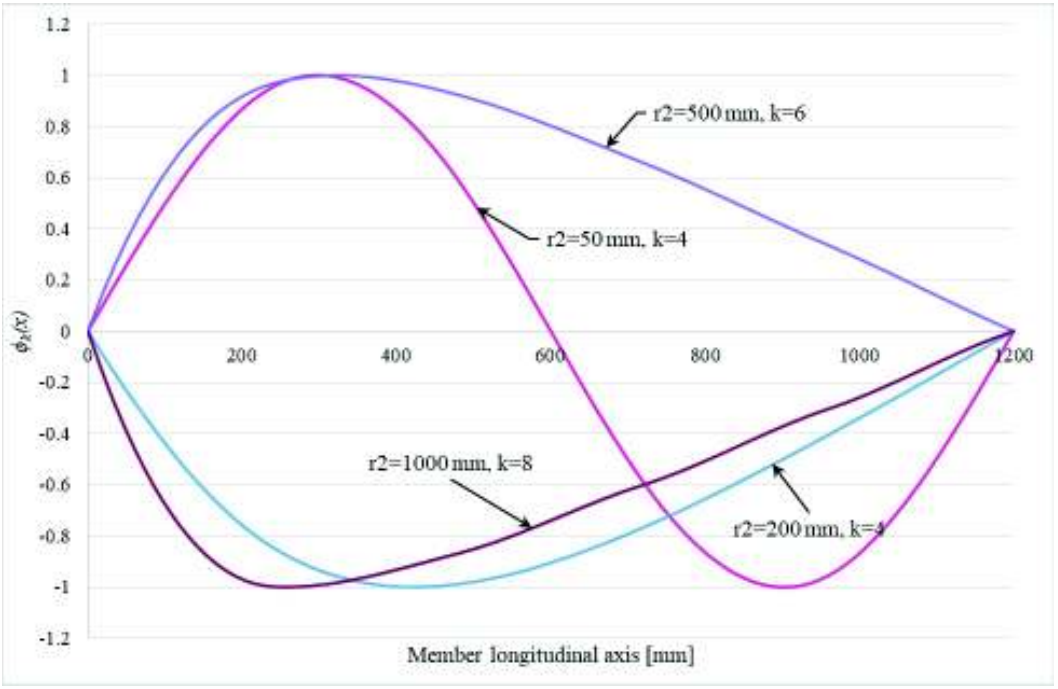

Figure 5.3: Long simply supported conical shells: the graphs of the modal amplitude functions $\phi_k(x)$.

Table 5.1 presents the cri\tical buckling coefficients resulted from SFEA, the ones resulted from the GBT-based FE formulation (i.e. GBT-FEM) and, respectively from the Runge-Kutta numerical method (i.e. GBT-Runge Kutta) [4]. The table also shows the differences in percentage between the results obtained from the GBT-based FE formulation and the ones obtained from SFEA. According to the table both GBT-based formulations provide similar results, but, as previously mentioned, the GBT-based FE formulation is superior in terms of convergence speed, of versatility of load and boundary condition cases and, the most important, of the possibility of coupled instabilities analysis. Table 5.1 also shows the order of the cross section deformation mode *k* and the corresponding number of longitudinal half-waves n_{hw}. The values from the table were determined for 5 FE in the GBT-based FE formulation resulting 6 nodes and 12 DOFs for all the cases. In SFEA, for the cylindrical shell 22,506 DOFs were used. The number of DOFs used in SFEA reached 52,974 for the conical shell with the bottom radius r_2=*1000 mm*. The large ratio between the number of DOFs used in SFEA and the number of DOFs used in the GBT-based FE formulation is also preserved in the rest of the numerical examples.

Table 5.1: SFEA vs GBT-FEM results for long simply supported conical shells.

r_2[mm]	λ_c SFEA	λ_c GBT-FEM	Differences (2) vs. (3)	λ_c GBT-Runge Kutta	Differences (2) vs. (5)	k	n_{hw}
(1)	*(2)*	*(3)*	*(4)*	*(5)*	*(6)*	*(7)*	*(8)*
50	490.40	492.54	0.43%	491.35	0.19%	4	2
60	493.85	502.45	1.71%	501.40	1.53%	4	2
70	525.27	541.11	2.93%	540.36	2.87%	4	2
90	563.92	558.34	1.00%	557.95	1.06%	4	1
100	522.76	520.14	0.50%	519.93	0.54%	4	1
120	490.72	487.74	0.61%	486.95	0.77%	4	1
150	498.57	505.56	1.38%	504.23	1.13%	4	1
200	606.33	629.77	3.72%	625.18	3.11%	4	1
300	672.62	675.82	0.47%	673.24	0.09%	6	1
400	610.41	617.72	1.18%	612.61	0.36%	6	1
500	627.06	640.83	2.15%	633.97	1.10%	6	1
1000	480.97	471.42	2.03%	466.53	3.00%	8	1

Figure 5.4 ilustrates the finite element convergence of the GBT for long simply supported conical shells. The results presented in the figure were determined for a conical shell with the bottom radius r_2=*500 mm*. According to the figure the minimum number of FE for which the difference between the SFEA results and the GBT-FEM results is less than 5% is 3.

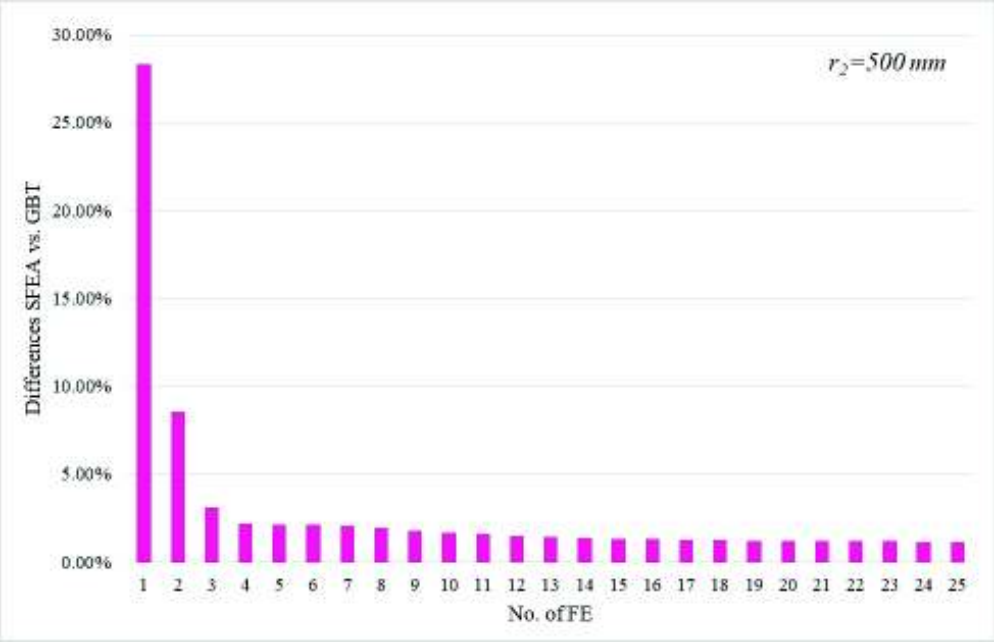

Figure 5.4: The finite element convergence of the long simply supported conical shells.

b) Fixed End Conical Shells

In the following case study, the conical shells have both end sections fixed which means that all the displacements are blocked. Figure 5.5 presents the critical buckling modes resulted from SFEA for different values of the bottom radius r_2 and Figure 5.6 shows the normalized graphs of the modal amplitude functions. Table 5.2 presents the differences between the results determined by SFEA and the ones determined by GBT-based FE formulation. Also the table shows the corresponding cross section deformation mode k. The values from Table 5.2 were determined using 15 FE in the GBT model. Because the number of longitudinal half-waves n_{hw} is not an integer and their amplitude varies with respect to the structure's lenght, the parameter was not included in the table.

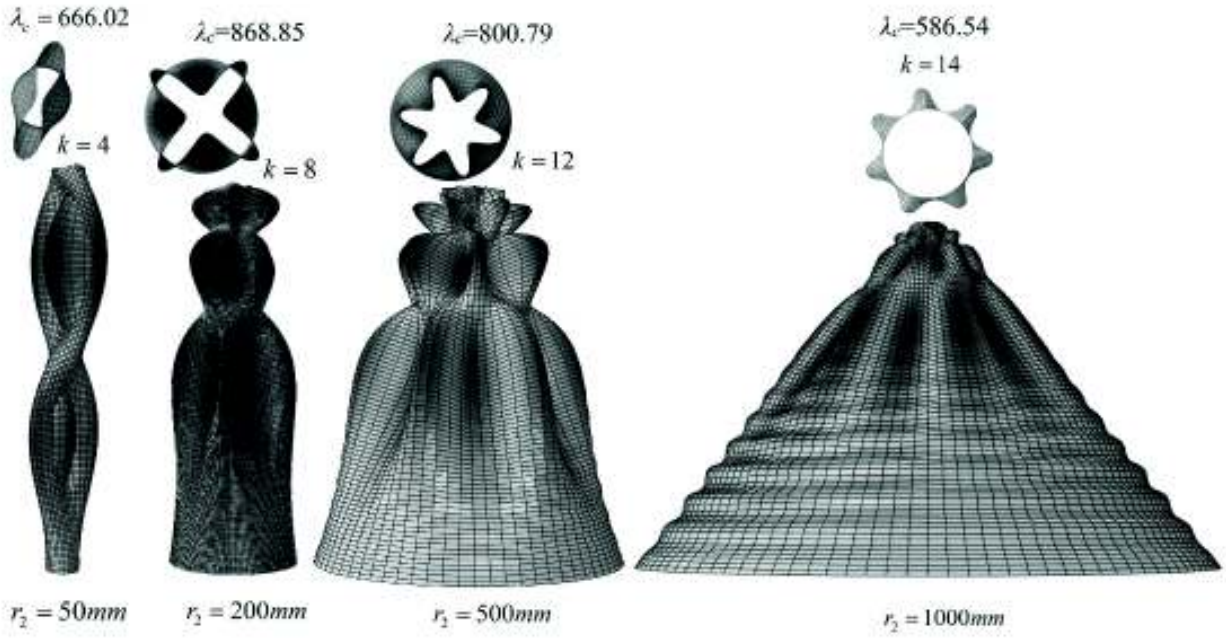

Figure 5.5: The critical buckling modes of long fixed end conical shells resulting from SFEA.

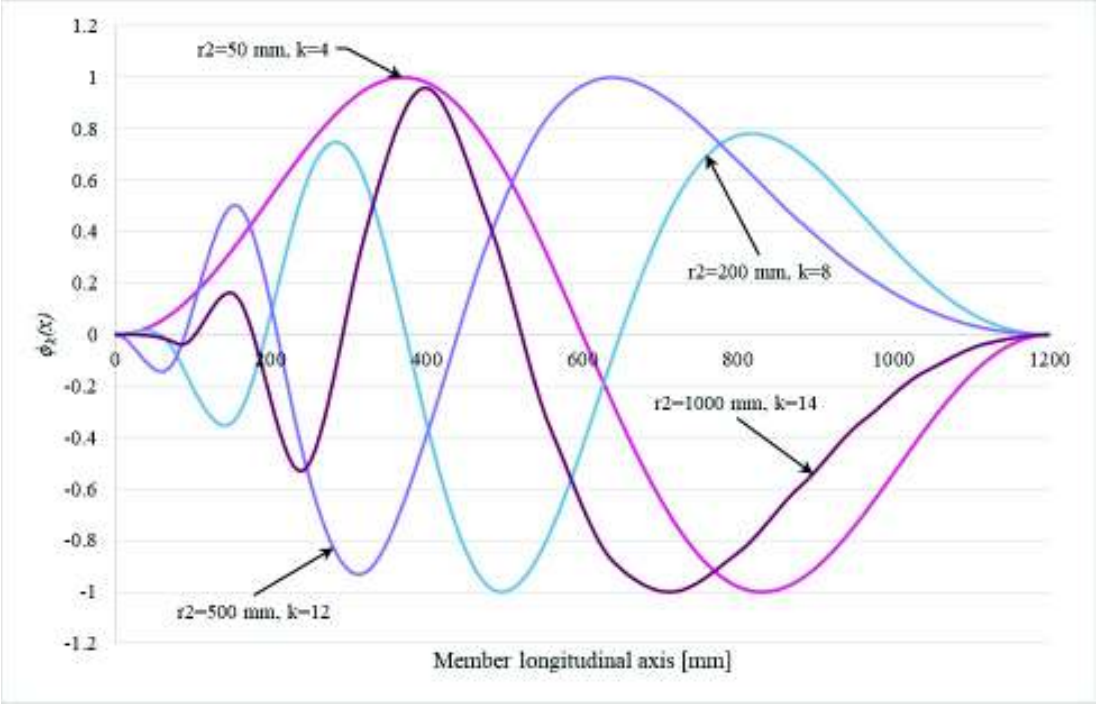

Figure 5.6: Long fixed end conical shells: the graphs of the modal amplitude functions $\phi_k(x)$.

Table 5.2: SFEA vs GBT-FEM results for long fixed end conical shells.

r_2 [mm]	λ_c SFEA	λ_c GBT-FEM	Differences	k
50	666.02	677.63	1.71%	4
60	760.26	729.93	4.16%	4
70	728.22	752.46	3.22%	6
90	756.49	771.13	1.90%	6
100	783.20	799.99	2.10%	6
120	822.78	810.65	1.50%	6
150	827.81	834.82	0.84%	8
200	868.85	853.52	1.77%	8
300	839.65	863.44	2.74%	10
400	873.67	856.76	1.97%	10
500	800.79	826.75	3.14%	12
1000	586.54	590.90	0.74%	14

c) Conical shells simply supported at both ends and at the middle of the span

In the following case study conical shells simply supported at both ends and at the middle of the span are analysed. Therefore, the proposed formulation's capacity to analyse different boundary conditions is demonstrated. All the structure's supports are free to warp, while the v and w displacements are blocked. The buckling mode of the structure is described by the number of circumferential half-waves k and by the number of longitudinal half-waves n_{hw}. Figure 5.7 shows the

critical buckling modes resulting from SFEA for different values of the bottom radius r_2 and Figure 5.8 shows the normalized graphs of the modal amplitude functions. Table 5.3 shows the differences between the critical bucklng coefficients λ_c resulted from SFEA and the ones resulted from the GBT-based FE formulation. As in the previous cases, the differences between the sets of results do not exceed 5%.

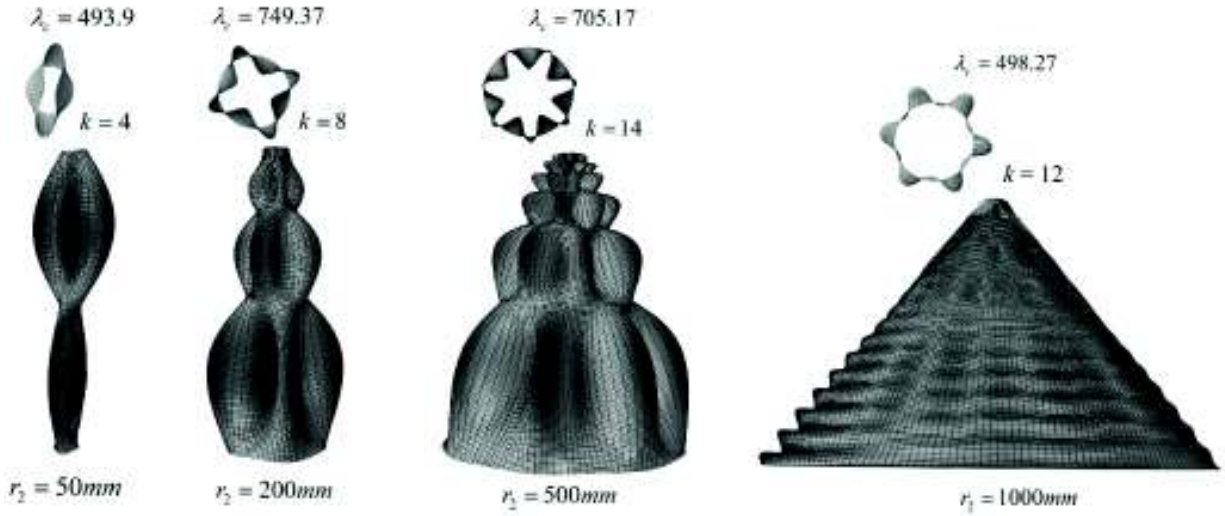

Figure 5.7: The critical buckling modes of long conical shells simply supported at both end and at the middle of the span resulting from SFEA.

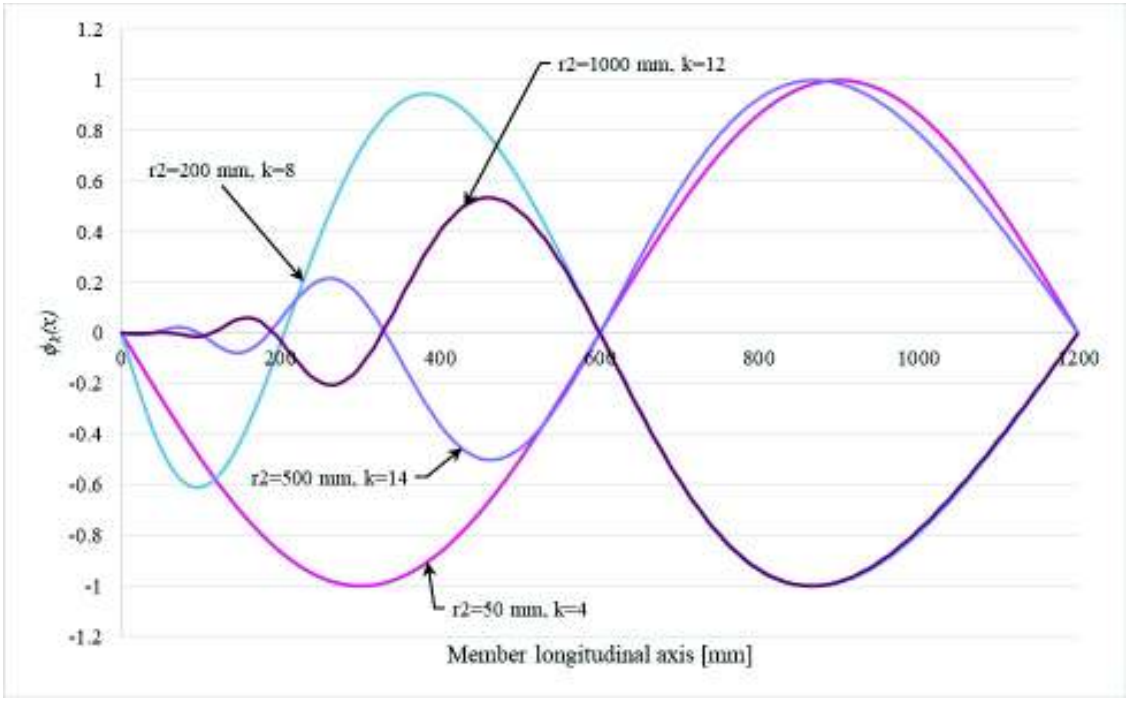

Figure 5.8: Long conical shells simply supported at both ends and at the middle of the span: the graphs of the modal amplitude functions $\phi_k(x)$.

Table 5.3: SFEA vs GBT-FEM results for long conical shells simply supported at both ends and at the middle of the span.

r_2 [mm]	λ_c SFEA	λ_c GBT-FEM	Differences	k
50	493.90	491.84	0.42%	4
60	499.10	504.95	1.16%	4
70	533.50	545.80	2.25%	4
90	631.46	658.83	4.15%	4
100	665.41	673.34	1.18%	6
120	669.51	693.54	3.47%	6
150	737.43	769.23	4.13%	8
200	749.37	766.30	2.21%	8
300	741.76	776.83	4.51%	10
400	729.33	747.31	2.41%	12
500	705.17	708.69	0.50%	14
1000	498.27	500.08	0.36%	12

d) Conical shells simply supported at one end and fixed at the other

In the following case study the buckling behavior of conical shells simply supported at the top end (radius r_1) and fixed at the bottom (radius r_2) is presented. Figure 5.9 shows the critical buckling modes of the conical shells having different values of the bottom radius r_2, the cross section deformation mode k and the corresponding critical buckling coefficient λ_c. Figure 5.10 presents the normalized graphs of the modal amplitude functions $\phi_k(x)$ for different values of the bottom radius r_2 obtained by the GBT-based FE procedure. The distribution pattern of the half-waves in the graphs of the modal amplitude functions $\phi_k(x)$ of conical shells simply supported at one end and fixed at the other one is similar to the graphs determined for fixed end conical shells. The difference between the graphs of the modal amplitude functions from the current case (see Figure 5.10) and the graphs of the fixed end conical shells (see Figure 5.6) is that they start directly from zero, corresponding to the simply supported section (at the left side of Figure 5.10).

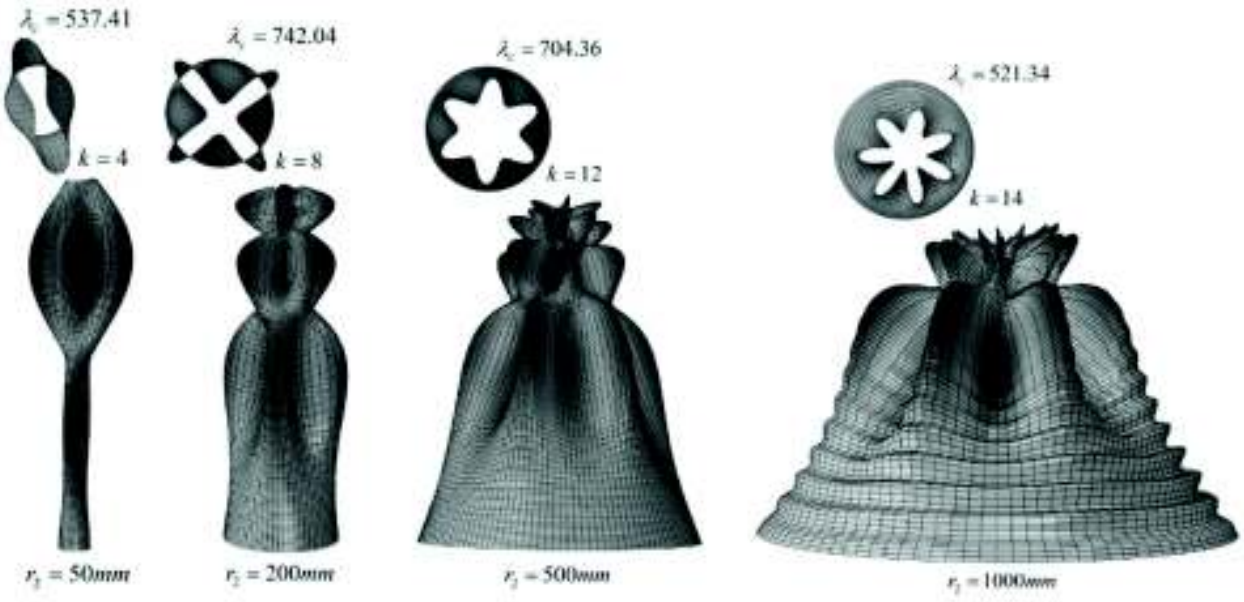

Figure 5.9: The critical buckling modes of long conical shells simply supported at one end at fixed at the other one resulting from SFEA.

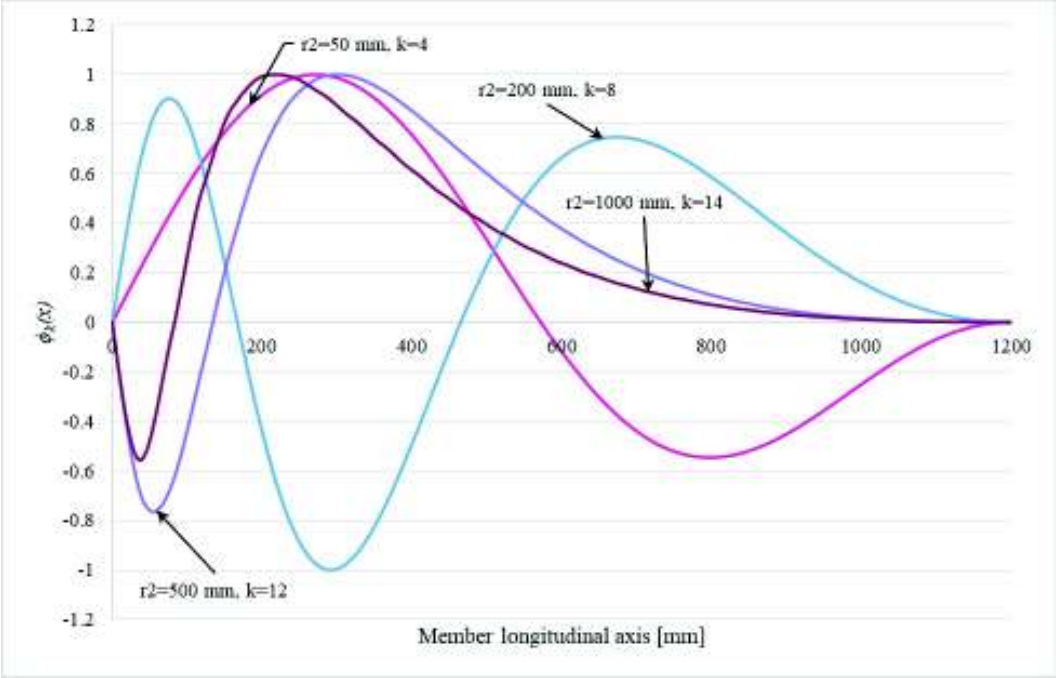

Figure 5.10: Long conical shells simply supported at an end and fixed at the other one: the graphs of the modal amplitude functions $\phi_k(x)$.

Table 5.4 presents the differences between the two modeling techniques. In the GBT-based FE procedure the values were determined using 30 FE. As in the previous numerical examples, there were no significant differences between the results.

Table 5.4: SFEA vs GBT-FEM results for long conical shells simply supported at one end and fixed at the other one.

r_2 [mm]	λ_c SFEA	λ_c GBT-FEM	Differences	k	n_{hw}
50	537.41	542.41	0.92%	4	2
60	562.51	574.23	2.04%	4	2
70	590.04	601.59	1.92%	4	2
90	600.33	606.86	1.08%	4	1
100	606.58	615.23	1.41%	4	1
120	645.44	662.05	2.51%	4	1
150	699.40	713.38	1.96%	6	2
200	742.04	757.93	2.10%	8	3
300	740.89	759.75	2.48%	8	2
400	726.00	759.45	4.41%	10	3
500	704.36	731.96	3.77%	12	4
1000	521.34	499.18	4.44%	14	3

5.2.1.2. Short Conical Shells

a) Simply Supported Conical Shells

As in the case of long conical shells, the short simply supported conical shells are free to warp while the v and w displacements are blocked. Figure 5.11 illustrates the critical buckling loads of short simply supported conical shells for different values of the bottom radius r_2 resulting from SFEA. Figure 5.13 presents the normalized graphs of the modal amplitude functions $\phi_k(x)$ and Figure 5.12 the critical buckling modes, both resulted from the GBT-based FE formulation performed with Matlab. According to Figure 5.13, unlike long conical shells, in case of axially compressed short conical shells the shear deformation modes also play a significant role, besides the shell-type deformation modes.

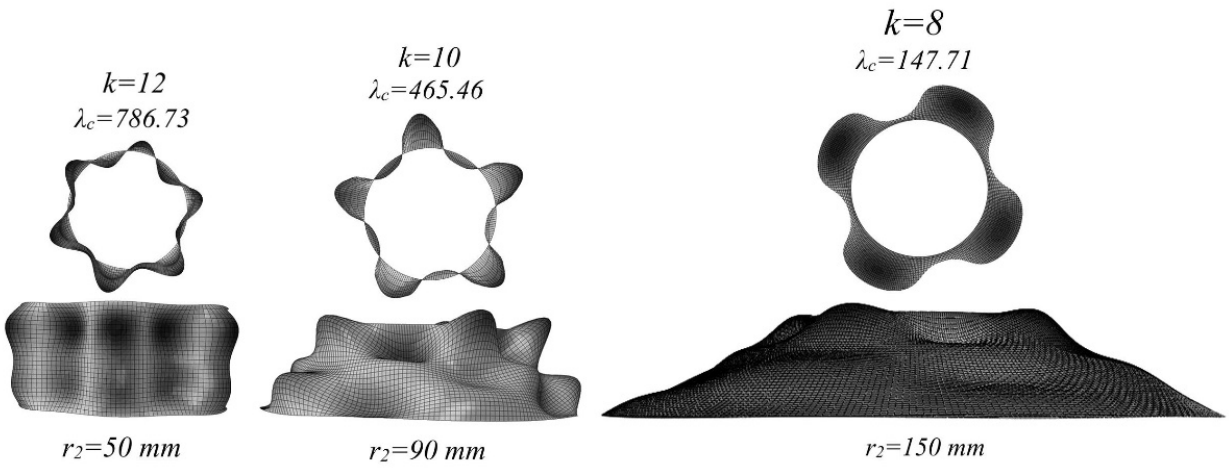

Figure 5.11: The critical buckling modes of short simply supported conical shells resulting from SFEA.

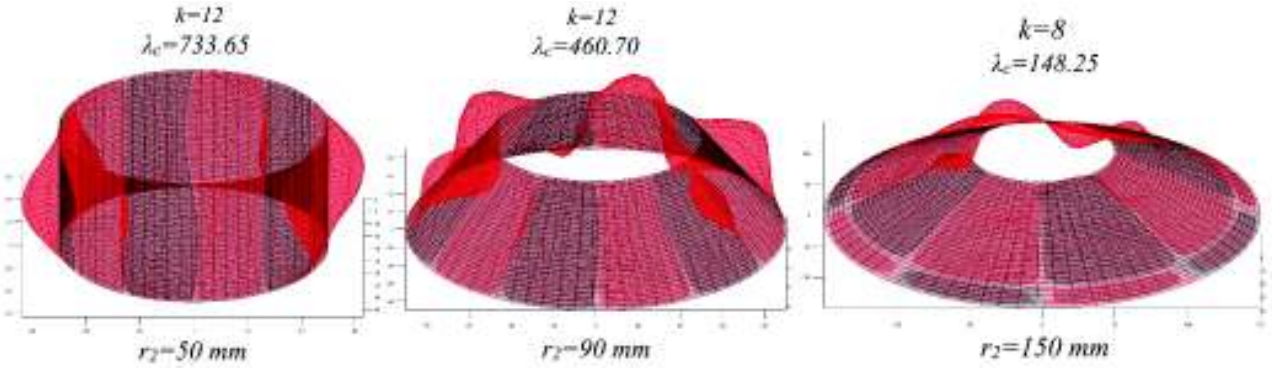

Figure 5.12: Short simply supported conical shells: the critical buckling modes resulting from the GBT-based FE formulation in Matlab.

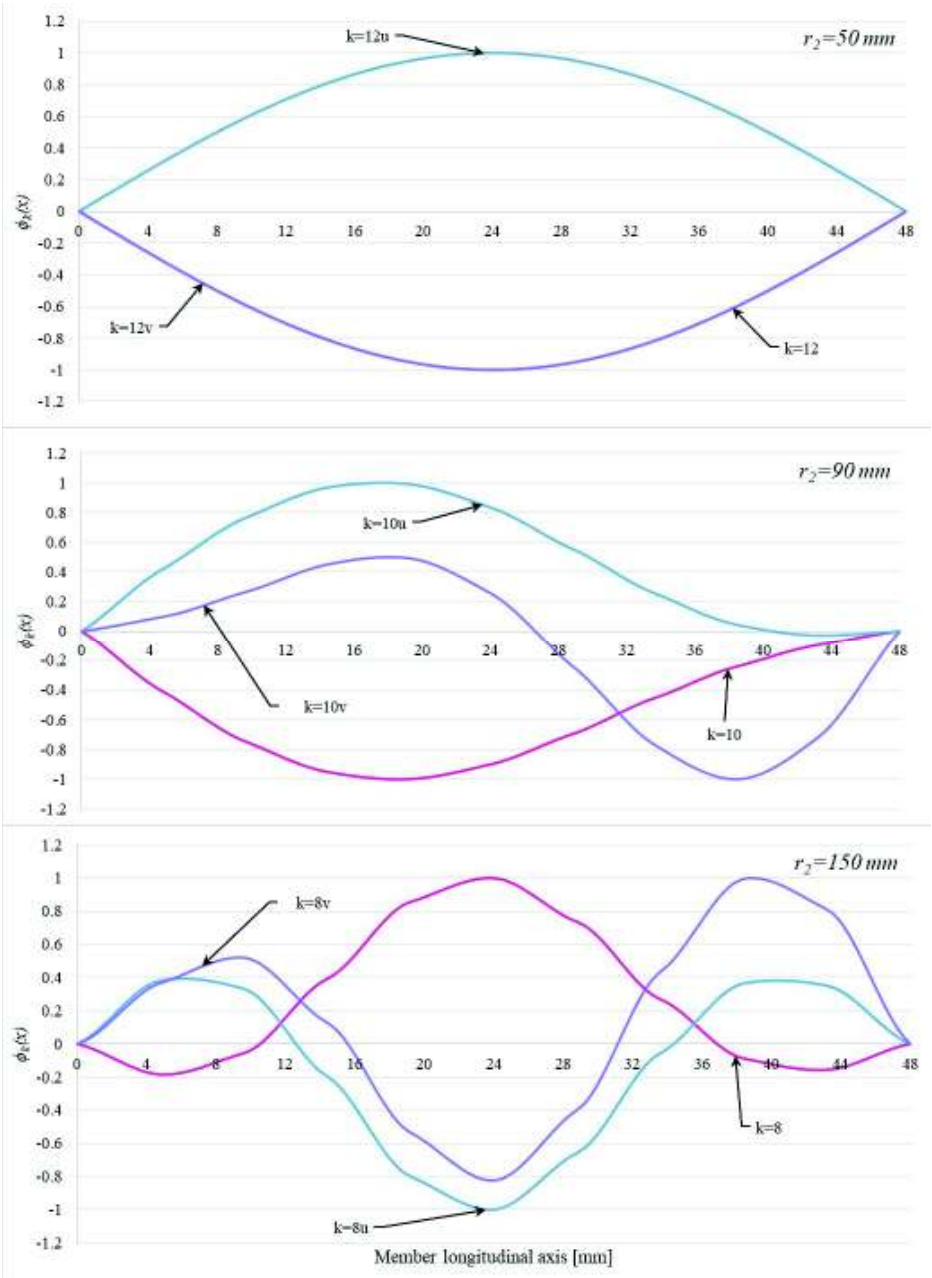

Figure 5.13: Short simply supported conical shells: the graphs of the modal amplitude functions $\phi_k(x)$.

Table 5.5 presents the differences between the critical buckling coefficients λ_c determined by SFEA and the GBT-based FE formulation. According to the table the differences between the results do not exceed 5%.

Table 5.5: SFEA vs GBT-FEM results for short simply supported conical shells.

r_2 [mm]	λ_c SFEA	λ_c GBT-FEM	Differences	k
50	786.73	773.65	1.69%	12
60	746.55	731.67	2.03%	12
70	664.63	652.68	1.83%	12
90	465.46	460.70	1.03%	10
100	376.58	376.96	0.10%	10
120	249.74	247.90	0.74%	10
150	147.71	148.25	0.37%	8
200	72.73	72.23	0.69%	8
300	27.74	27.64	0.38%	6

b) Fixed End Conical Shells

The short fixed end conical shells have all the displacements and rotations blocked at both end sections as in the case of long fixed end conical shells. Figure 5.14 shows the critical buckling modes, the critical buckling coefficients and the corresponding cross section deformation modes k determined by SFEA with Abaqus and in Figure 5.16 are the normalized graphs of the modal amplitude functions. Also Figure 5.15 illustrates the critical buckling modes resulted from the GBT-based FE formulation performed with Matlab. As in the previous case, the shear deformation modes appear along with the shell-type deformation modes.

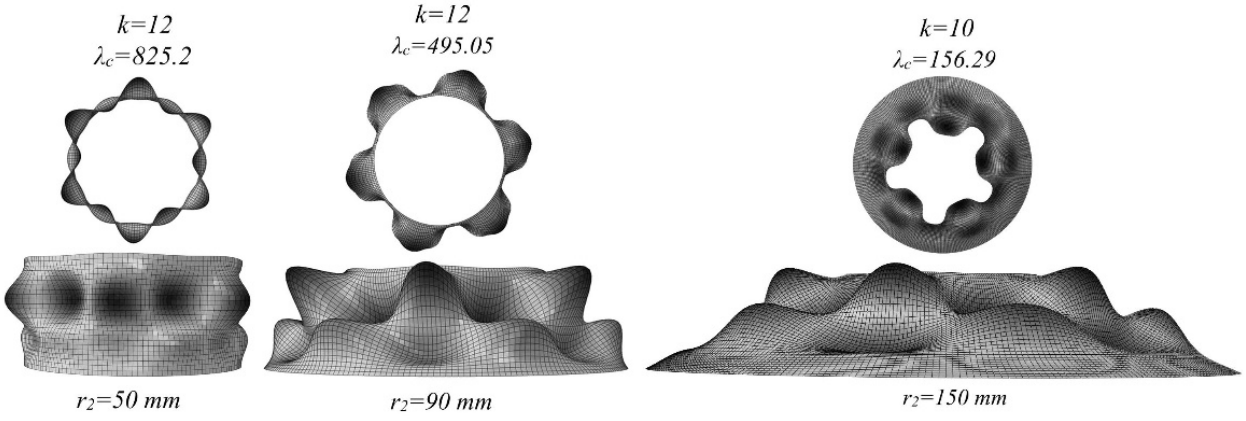

Figure 5.14: The critical buckling modes of short fixed end conical shells resulting from SFEA.

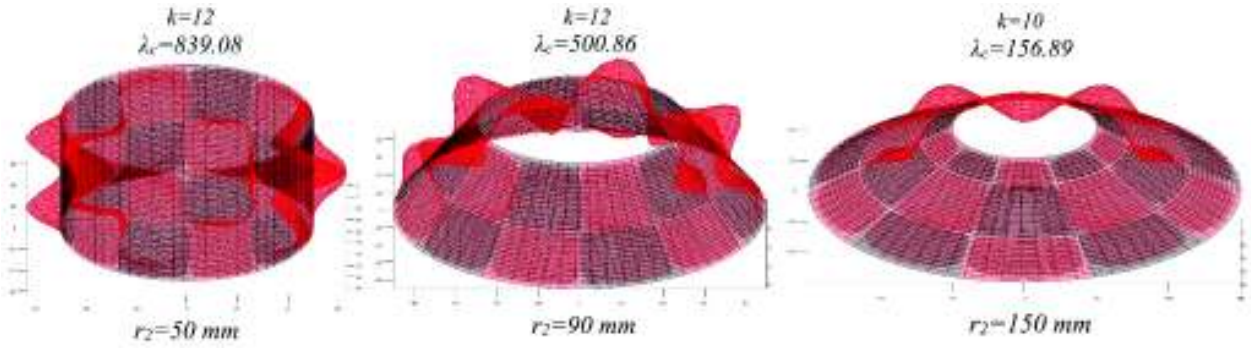

Figure 5.15: Short fixed end conical shells: the critical buckling modes resulting from the GBT-based FE formulation in Matlab.

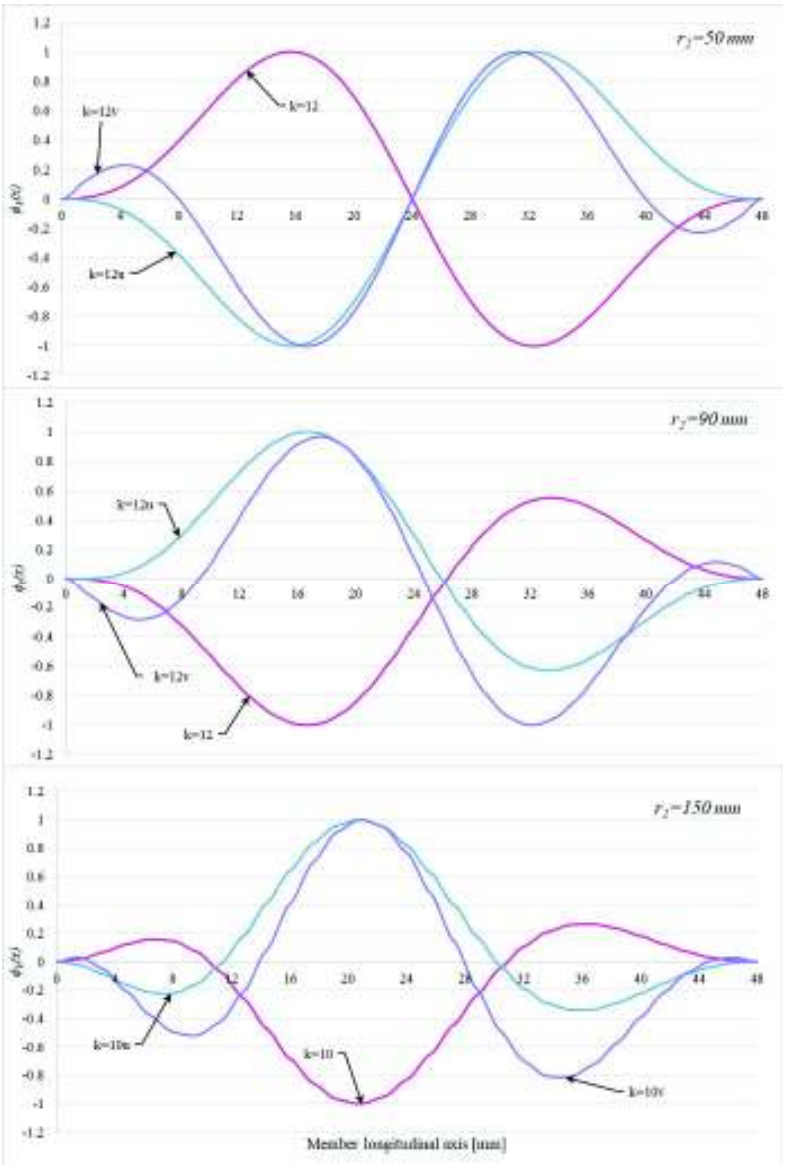

Figure 5.16: Short fixed end conical shells: the graphs of the modal amplitude functions $\phi_k(x)$.

Table 5.6 shows the differences between the results determined by SFEA and the ones determined by the GBT-based FE procedure. As in the previous cases the differences do not exceed 5%.

Table 5.6: SFEA vs GBT-FEM results for short fixed end conical shells.

r_2 [mm]	λ_c SFEA	λ_c GBT-FEM	Differences	k
50	825.2	839.08	1.65%	12
60	798.34	810.65	1.52%	12
70	713.77	723.31	1.32%	12
90	495.05	500.86	1.16%	12
100	402.28	406.79	1.11%	12
120	269.34	270.72	0.51%	10
150	156.29	156.89	0.39%	10
200	77.42	77.33	0.13%	8
300	29.56	29.39	0.60%	8

5.2.2. Conical Shells with Variable Thickness

In the following sections, conical shells without stress concentrations have variable thickness as illustrated in Figure 5.17: in the first half of the structure the thickness is $t_1=1$ *mm*, while in the second half of the structure the thickness is $t_2=2$ *mm*. The length of the conical shells with variable thickness is $L=1000$ *mm*. The Abaqus models were analysed using a mesh with 5 mm size and S4 shell finite elements. The following sections present simply supported and fixed end conical shells with variable thickness.

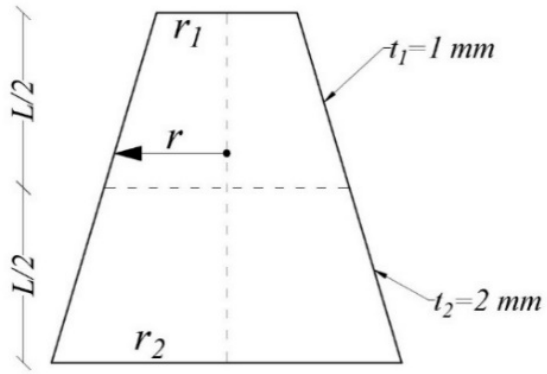

Figure 5.17: The geometry of the axially compressed conical shell with variable thickness.

5.2.2.1. Simply Supported Conical Shells

As in the case of simply supported conical shells with constant thickness, the conical shells with variable thickness are free to warp, while the *v* and *w* displacements are blocked. In Figure 5.18 the critical buckling modes of the simply supported conical shells with variable thickness resulting from SFEA are illustrated. Figure 5.19 presents the critical buckling modes of the same conical shells from the GBT-based FE procedure performed with Matlab. Figure 5.20 shows the normalized graphs of the modal amplitude functions $\phi_k(x)$ obtained from the GBT-based FE procedure.

According to Figure 5.20, unlike in the case of conical shells with constant thickness, in this case the shear deformation modes occur along with the shell-type deformation modes. It can also be remarked that the graphs of the modal amplitude functions $\phi_k(x)$ of the "v" shear modes have a jump at $x=500\ mm$ (i.e. the section corresponding to the middle of the span) which emphasizes the change from $t_1=1\ mm$ to $t_2=2\ mm$. This jump is very strong for conical shells with a bottom radius of $r_2=50\ mm$ and $r_2=200\ mm$. Also, in the zone with $t_1=1\ mm$, on the left side of the graphs, the modal amplitude functions have more half-waves than for $t_2=2\ mm$ (on the right side of the graphs). This obviously is a consequence of the fact that the stiffness of the zone with *2 mm* thickness is higher than that of the *1 mm* thickness zone.

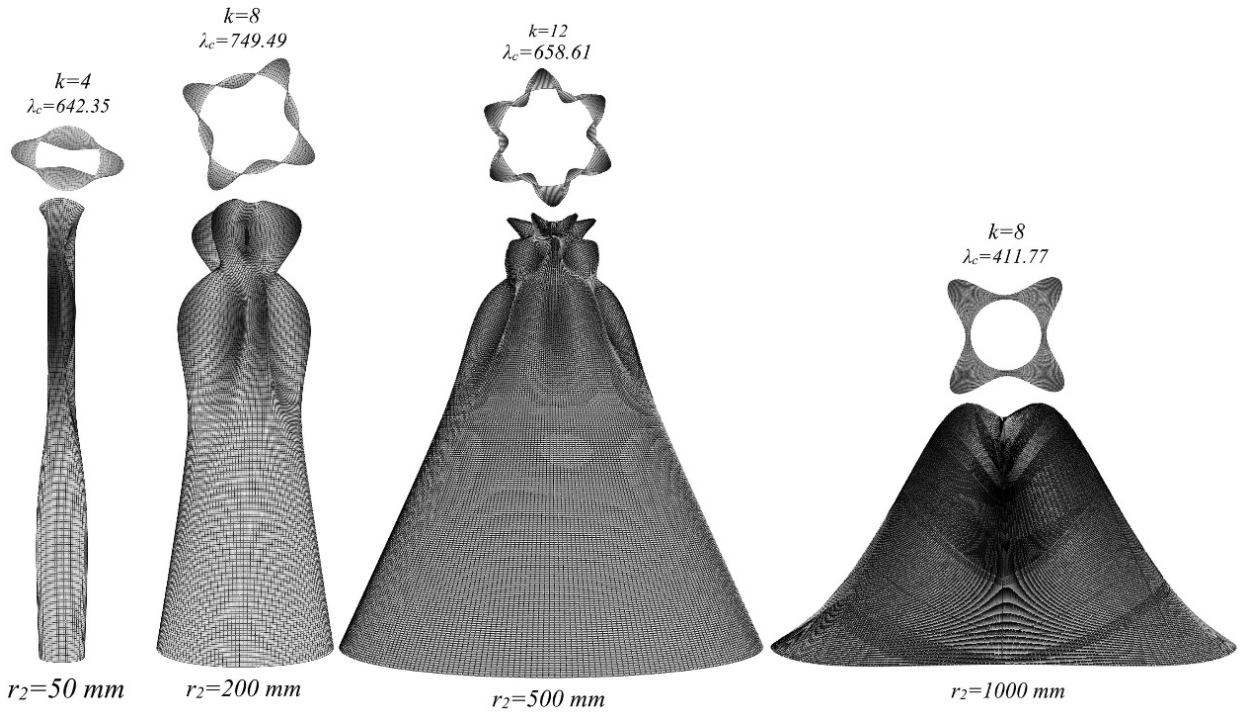

Figure 5.18: The critical buckling modes of simply supported conical shells with variable thickness resulting from SFEA.

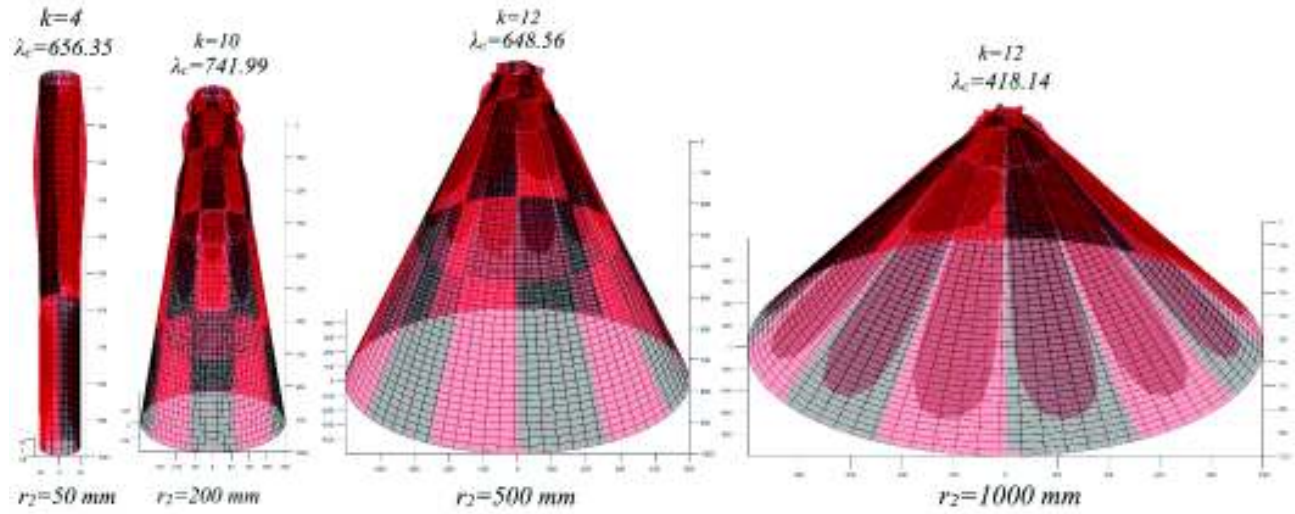

Figure 5.19: Simply supported conical shells with variable thickness: the critical buckling modes resulting from the GBT-based FE formulation in Matlab.

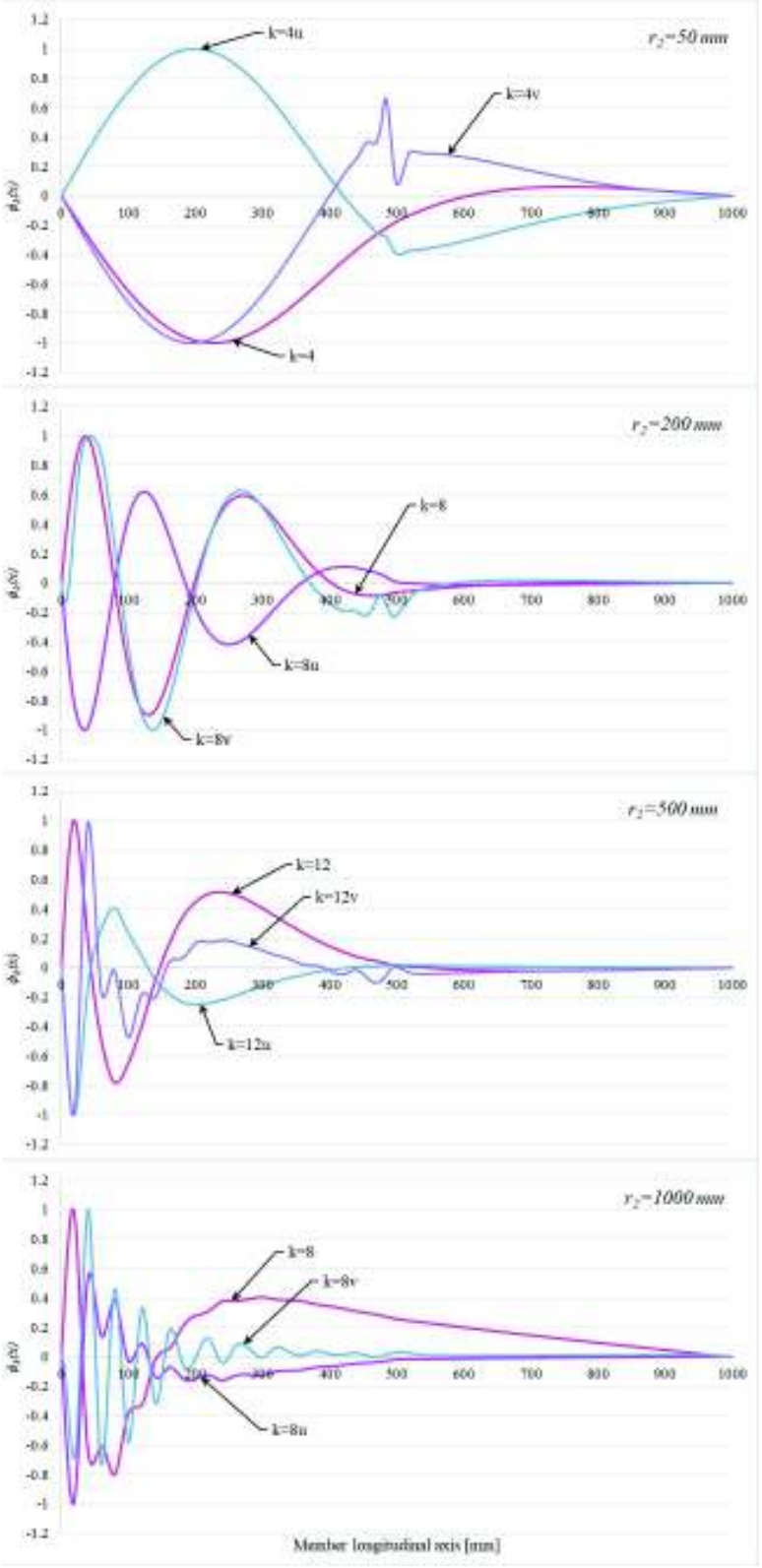

Figure 5.20: Simply supported conical shells with variable thickness: the graphs of the modal amplitude functions $\phi_k(x)$.

Table 5.7 presents the differences between the results determined by SFEA and the ones determined by the proposed formulation. These differences do not exceed 5% if the shear deformation

modes are included in the analysis. If the shear deformation modes are not taken into account, the differences between the results may reach up to 8.05% for the conical shell with the radius r_2=*200 mm*.

Table 5.7: SFEA vs GBT-FEM results for simply supported conical shells with variable thickness.

r_2 [mm]	λ_c SFEA	λ_c GBT-FEM with shear modes	λ_c GBT-FEM without shear modes	Differences with shear modes	Differences without shear modes	k
50	642.35	656.35	673.16	2.13%	4.58%	4
60	669.01	688.59	704.70	2.84%	5.06%	4
70	702.76	696.08	744.053	0.96%	5.55%	6
90	719.37	716.90	770.07	0.34%	6.58%	6
100	729.26	727.56	772.63	0.23%	5.61%	6
120	708.71	732.50	734.83	3.25%	3.55%	4
150	714.37	739.94	741.85	3.46%	3.71%	4
200	749.49	741.99	815.14	1.01%	8.05%	8
300	715.45	725.37	738.23	1.37%	3.09%	6
400	675.13	691.36	701.36	2.35%	3.74%	6
500	658.61	648.56	675.91	1.55%	2.56%	12
1000	411.77	418.14	419.28	1.52%	1.79%	8

5.2.2.2. Fixed End Conical Shells

In this case the conical shells have all the end section displacements blocked as in the previous cases. Figure 5.21 shows the critical buckling modes obtained from SFEA and also the critical buckling coefficients λ_c and the corresponding cross section deformation modes k. Figure 5.22 also shows the critical buckling modes of the fixed end conical shells with variable thickness, but this time the buckling modes result from the GBT-based FE procedure performed with Matlab. Figure 5.23 shows the normalized graphs of the modal amplitude functions. As in the previous case, the graphs of the modal amplitude functions for the "v" shear modes have a jump at x=*500 mm*, in the middle of the span more exactly, which shows the jump from t_1=*1 mm* to t_2=*2 mm*. Also the zone with t_1=*1 mm* thickness (the left side of the graph) has more half-waves than the zone with t_2=*2 mm* thickness t_2=*2 mm* (the right side of the graph) which means that, as in the previous case, the stiffness of the zone with a *2 mm* thickness is higher than that of the *1 mm* thickness.

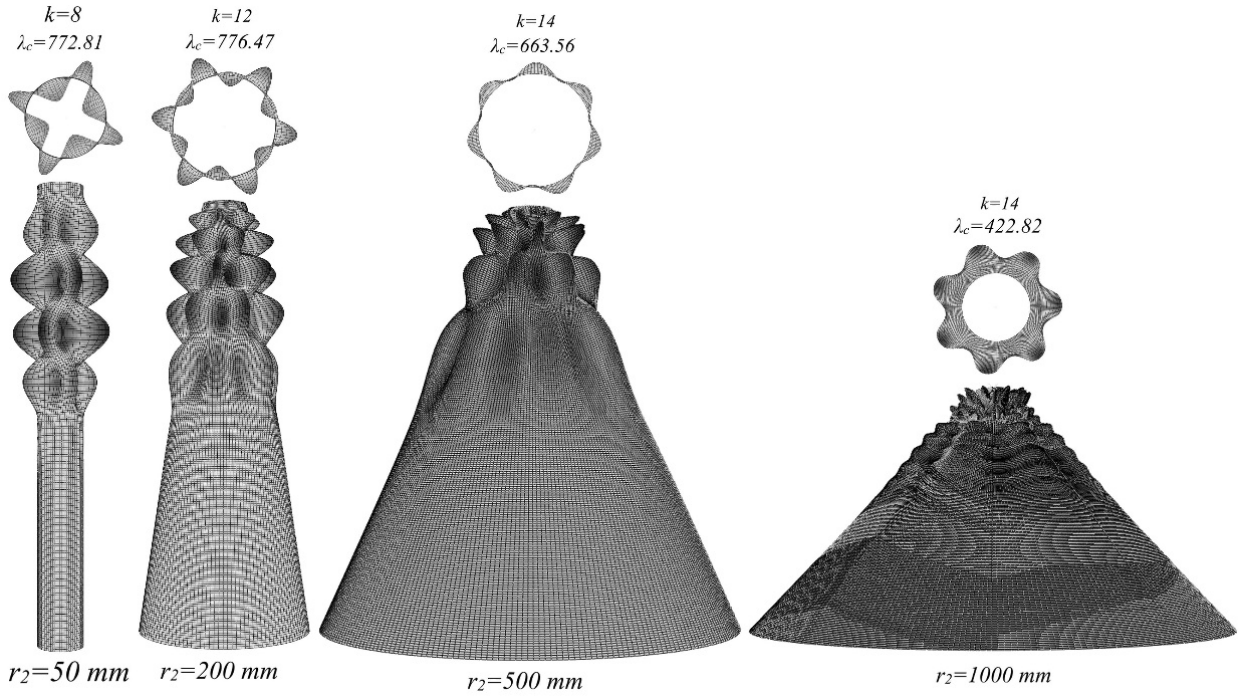

Figure 5.21: The critical buckling modes of fixed end conical shells with variable thickness resulting from SFEA.

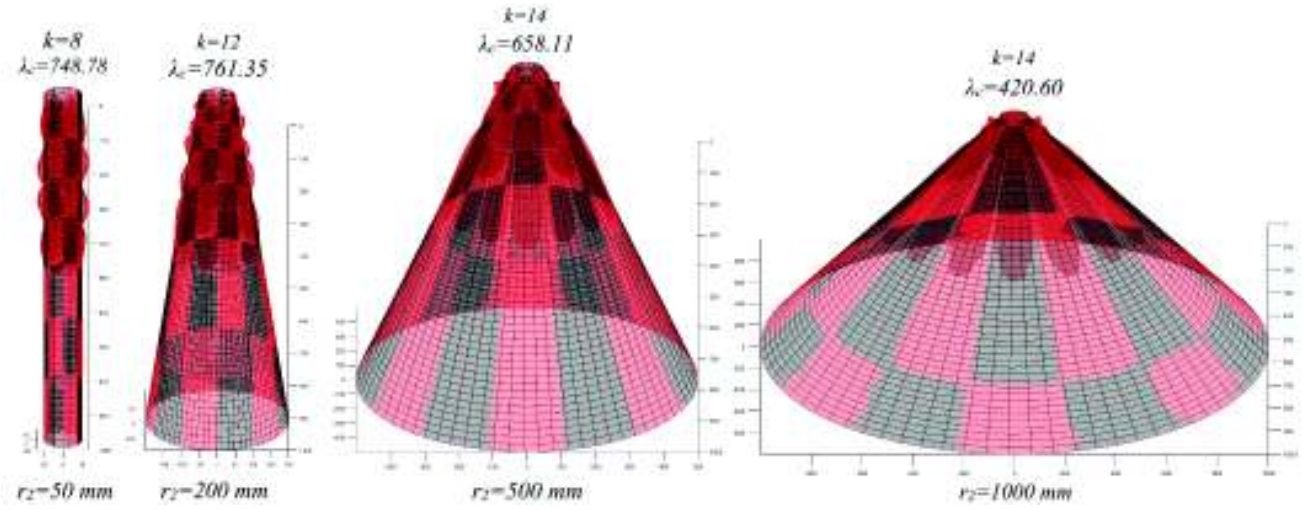

Figure 5.22: Fixed end conical shells with variable thickness: the critical buckling modes resulting from the GBT-based FE formulation in Matlab.

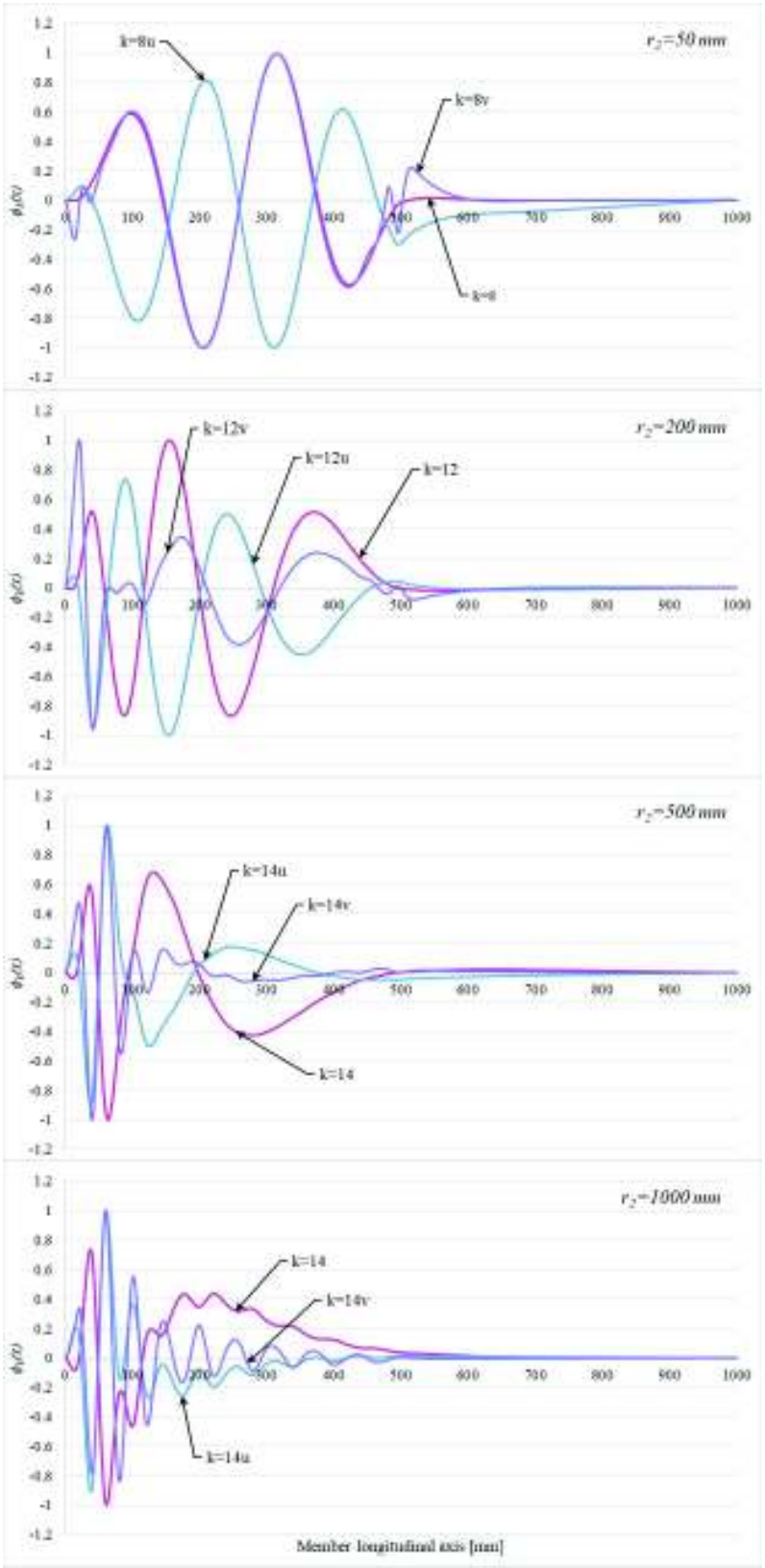

Figure 5.23: Fixed end conical shells with variable thickness: the graphs of the modal amplitude functions $\phi_k(x)$.

Table 5.8 shows the differences between the results determined by SFEA and the results determined by the GBT-based FE procedure. The differences do not exceed 5% if the shear

deformation modes are included in the buckling analysis. If the shear deformation modes are ignored in the buckling analysis, then the smallest difference between results is 1.13% for the conical shell with the radius r_2=*1000 mm* and the largest difference between results is 12.32% for the conical shell with the radius r_2=*100 mm*.

Table 5.8: SFEA vs GBT-FEM results for fixed end conical shells with variable thickness.

r_2 [mm]	λ_c SFEA	λ_c GBT-FEM with shear modes	λ_c GBT-FEM without shear modes	Differences with shear modes	Differences without shear modes	k
50	772.81	748.78	859.44	3.21%	10.08%	8
60	776.52	754.62	865.67	2.90%	10.30%	8
70	783.23	756.65	869.36	3.51%	9.91%	10
90	781.87	761.53	889.26	2.67%	12.08%	10
100	781.03	763.28	890.73	2.32%	12.32%	10
120	785.68	765.19	878.37	2.68%	10.55%	10
150	782.08	764.58	855.35	2.29%	8.57%	12
200	776.47	761.35	815.14	1.99%	4.74%	12
300	750.88	736.89	764.38	1.90%	1.77%	14
400	707.57	701.56	723.45	0.86%	2.19%	14
500	663.56	658.11	675.91	0.83%	1.83%	14
1000	422.82	420.60	427.64	0.53%	1.13%	14

5.3. Conical Shells with Stress Concentrations

The conical shells with stress concentrations considered are cantilevered (only one end fixed, where all the displacements are blocked, and the other end is free). The axial load is introduced at the free end section of the cantilever conical shell and produces significant end local effects. These local effects produce local deformations (see Figure 5.24) and large local variations of the (pre-buckling) normal hoop stresses first-order (see Figure 5.25 and Figure 5.26 – the free end is on the left side of the graphs). In these figures, the bottom radius of the conical shell is r_2=*1000 mm*. These pre-buckling stress concentrations cannot be neglected anymore or approximated by simplified formulae, as Eq. (5.1).

In [4], the normal hoop stress $\sigma^0_{\theta\theta}$ on a cross section strip with unitary width measured from the free end was determined with the mathematical expression of the normal hoop stress of cylindrical shells under exterior pressure (Eq. (24) in reference [4]). The new component of the variation of strain energy given by the local effect of the hoop stresses $\sigma^0_{\theta\theta}$ was added to the existent boundary conditions. Even though satisfactory results were obtained, this approach is a simplification and its success is

mostly due to the very high hoop stress $\sigma^0_{\theta\theta}$ concentrations in the free end of the structural configuration, as can be observed in Figure 5.26. Figure 5.25 and Figure 5.26 show that the GBT formulation yields very accurate first-order results when compared with a shell model. The new proposed GBT-based FE formulation is capable to take into account the pre-buckling stresses accurately, which influence the buckling forces.

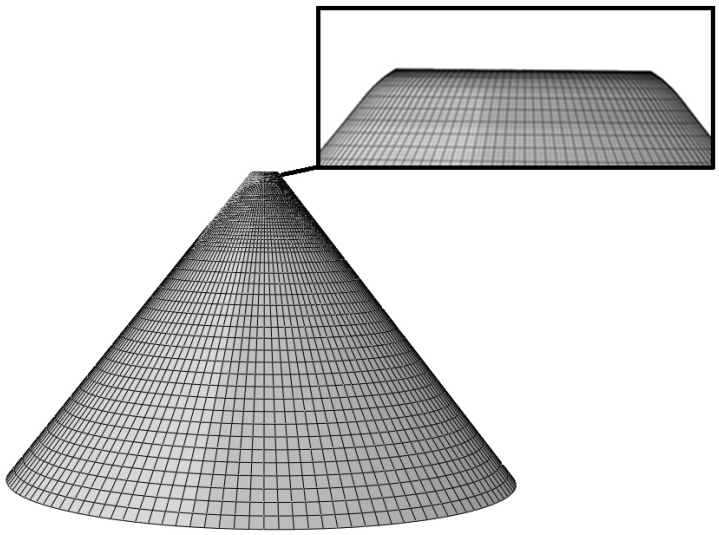

Figure 5.24: The displacements at the free end of an axially compressed cantilever conical shell resulting from SFEA. The scaling factor is 200.

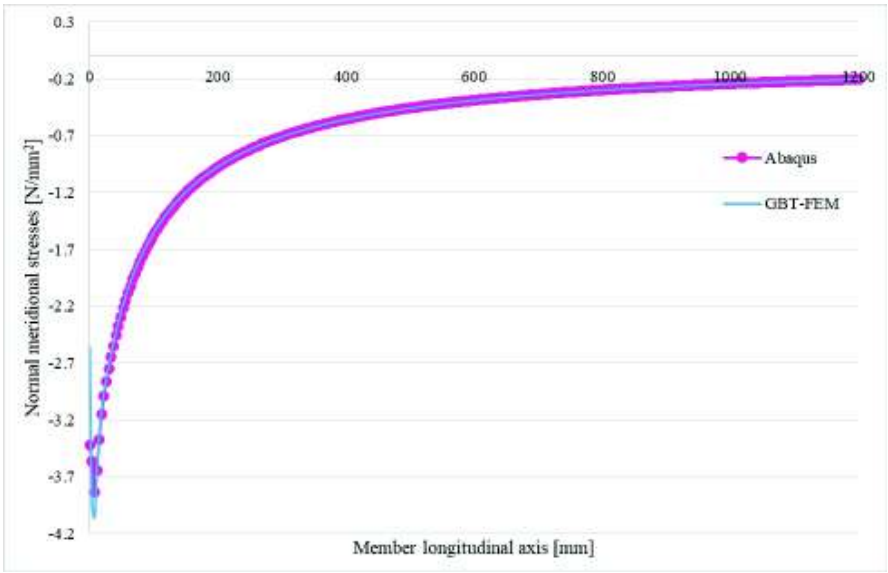

Figure 5.25: The pre-buckling normal meridional stresses σ^0_{xx} of an axially compressed cantilever conical shell with the radius r_2=*1000 mm*.

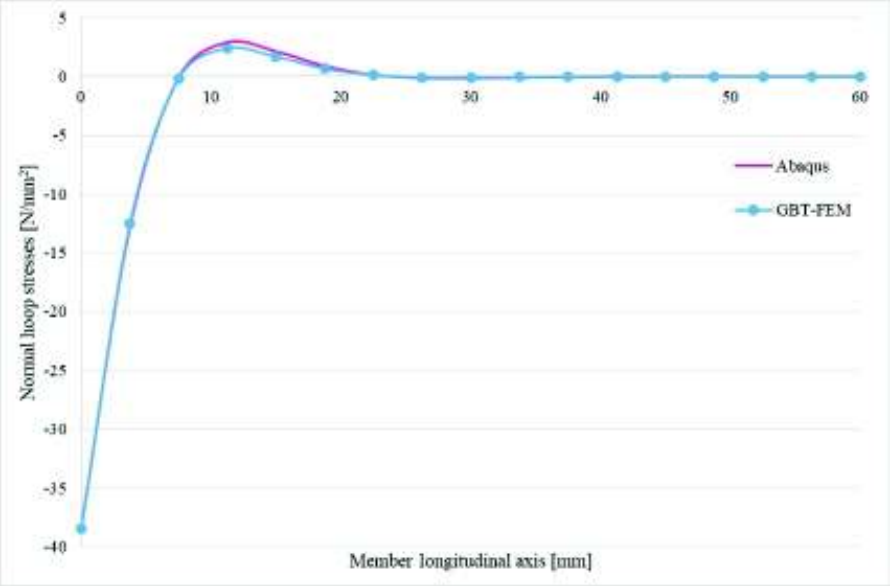

Figure 5.26: The pre-buckling normal hoop stresses $\sigma_{\theta\theta}^{0}$ of an axially compressed cantilever conical shell with the radius r_2=*1000 mm*.

The first-order analysis of conical shells with stress concentrations followed the algorithm presented in Section 4.3.1 (see Figure 4.2). In the case of axially compressed conical shells loaded with an axial force P_0 at the end section x=*0*, the vector of equivalent nodal forces is the following:

$$f^{(e)} = \{P_0 \cos\alpha \;\; 0 \;\; 0 \;\; 0 \;\; 0 \;\; -P_0 \sin\alpha \;\; 0 \;\; 0\}^T \tag{5.2}$$

where the first 4 components correspond to the axial extension mode and the remaining 4 components correspond to the axisymmetric extension mode.

The normal hoop stresses $\sigma_{\theta\theta}^{0}$ resulting from the first-order analysis are then used in the buckling analysis to determine the geometric tensors $X_{1ik}^{\sigma\theta}$ (see Eq. (3.38)) which take into account the second-order effects. The geometric tensors $X_{1ik}^{\sigma\theta}$ are then used to determine the elements of the finite element geometric stiffness matrix (see Eq. (4.8)).

5.3.1. Conical Shells with Constant Thickness

The following section presents numerical examples of conical shells with stress concentrations which have constant thickness. As in the previous section, these numerical examples are entailed in two categories: (i) long conical shells, having a length *L=1200 mm* and (ii) short conical shells, with length *L=48 mm*.

5.3.1.1. Long Conical Shells

a) Cantilever Conical Shells

Figure 5.27 and Figure 5.28 show the critical buckling modes resulting from SFEA and the GBT-based FE procedure performed with Matlab, while Figure 5.29 shows the normalized graphs of the modal amplitude functions.

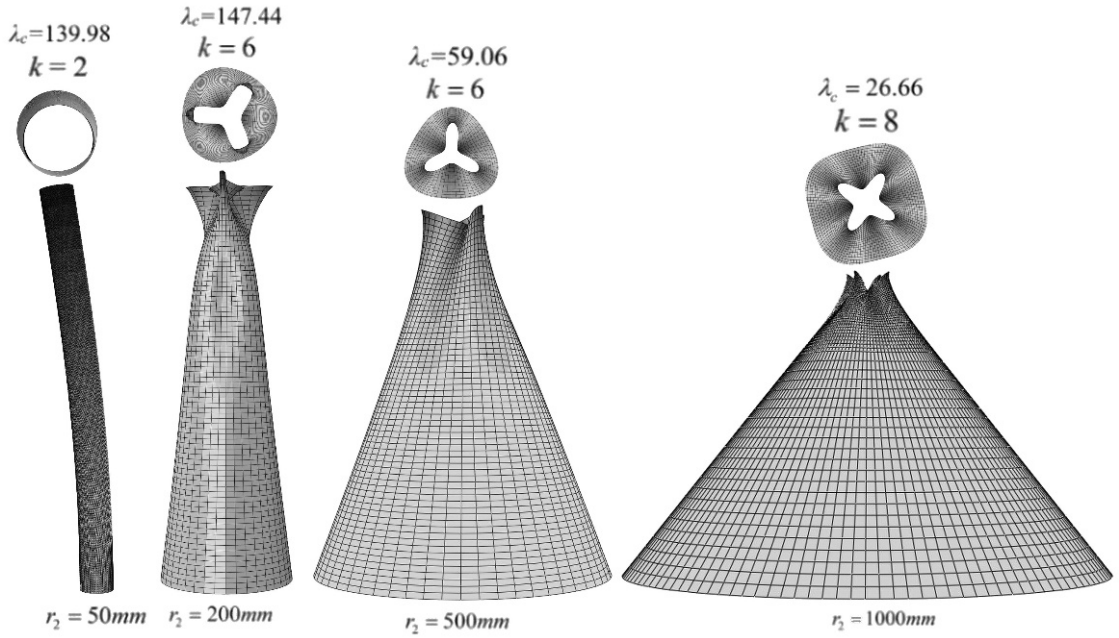

Figure 5.27: The critical buckling modes of long cantilever conical shells resulting from SFEA.

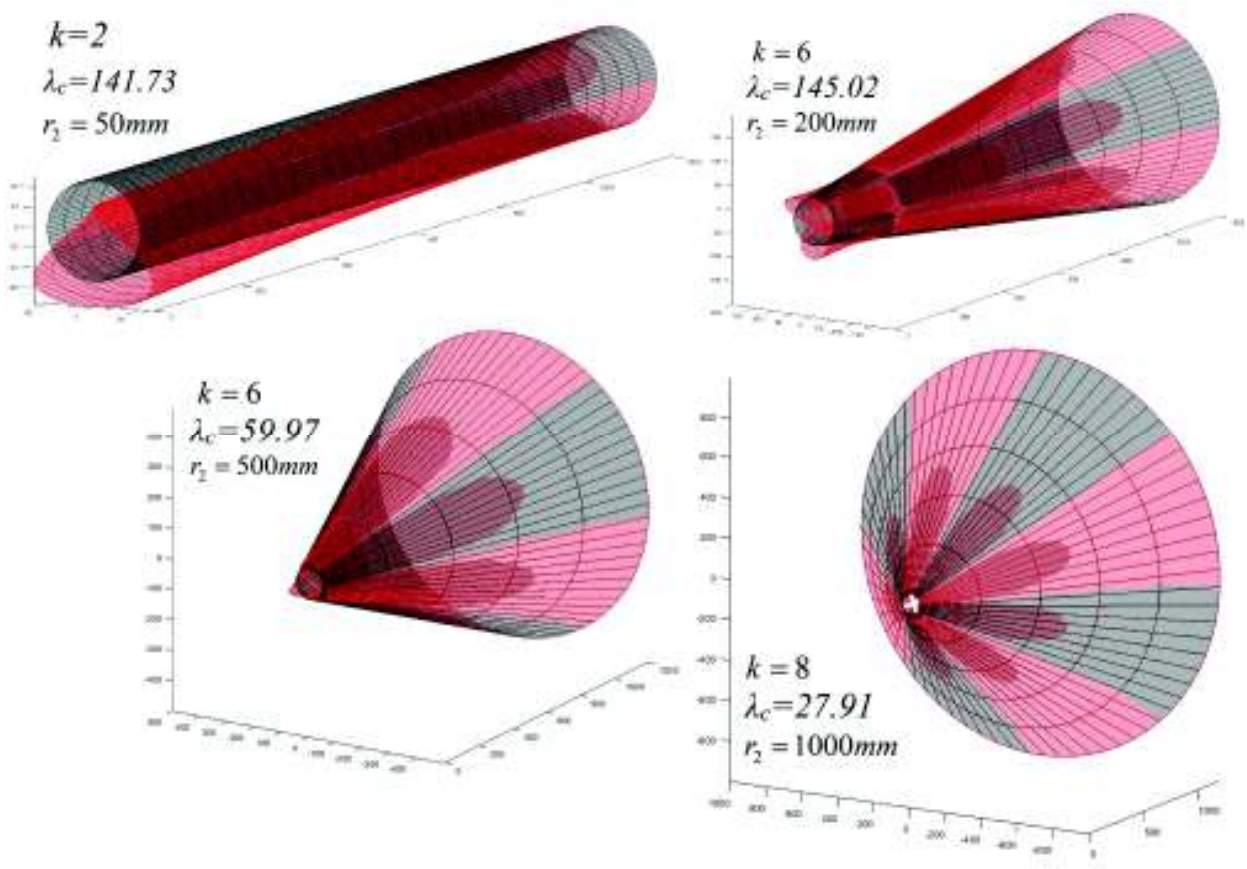

Figure 5.28: Cantilever conical shells: the critical buckling modes resulting from the GBT-based FE formulation in Matlab.

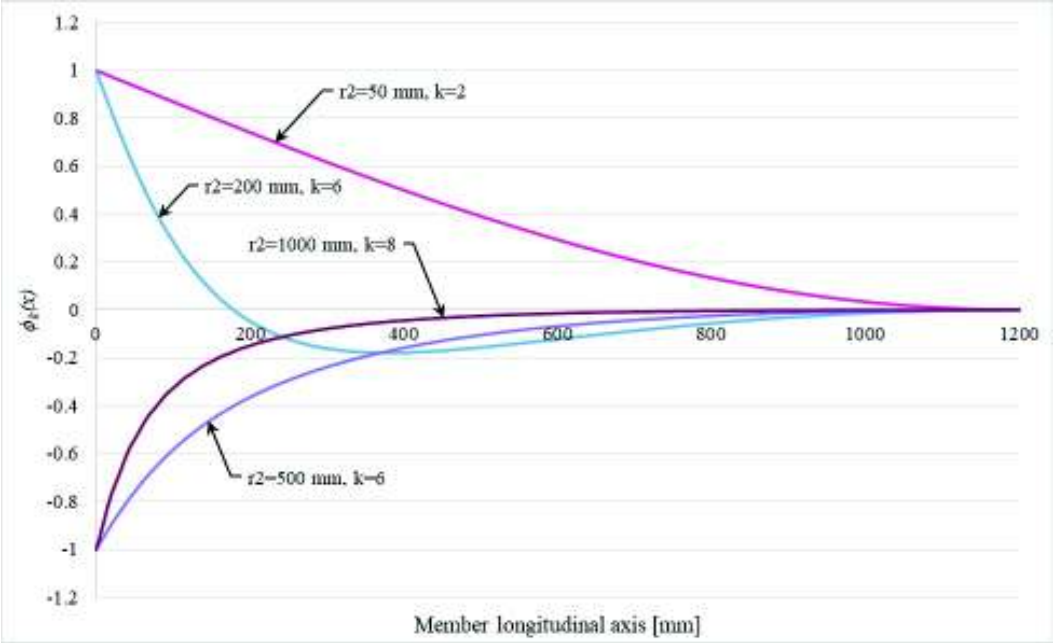

Figure 5.29: Long cantilever conical shells: the graphs of the modal amplitude functions $\phi_k(x)$.

To demonstrate the importance of first-order local end effects a simplified analysis was run in which the normal hoop stresses $\sigma^0_{\theta\theta}$ were neglected and the normal meridional stresses σ^0_{xx} were approximated by Eq. (5.1). Table 5.9 shows the differences between the rigorous procedure and the simplified procedure. The results were compared to the critical buckling coefficient determined by SFEA. By the simplified procedure resulted errors up to 90% for large values of the bottom radius r_2, proving the fact that local end effects must be taken into account in the buckling analysis of the cantilever conical shells with the free end loaded.

Table 5.9: SFEA vs GBT-FEM results when local effects are taken/not taken into account.

r_2 [mm]	λ_c SFEA	λ_c GBT-FEM with local effects	λ_c GBT-FEM without local effects	Differences SFEA vs. GBT with local effects	Differences SFEA vs. GBT without local effects	k
50	139.98	141.73	141.73	1.24%	1.24%	2
60	204.9	207.98	207.98	1.48%	1.48%	2
70	233.62	234.61	262.55	0.42%	11.02%	4
90	230.53	229.20	288.55	0.58%	20.11%	4
100	226.82	227.64	307.15	0.36%	26.15%	4
120	218.06	215.80	351.75	1.05%	38.01%	6
150	182.8	182.89	377.65	0.05%	51.60%	6
200	147.44	145.02	392.85	1.67%	62.47%	6
300	100.6	101.13	423.02	0.53%	76.22%	6
400	74.551	76.09	406.42	2.03%	81.66%	6
500	59.068	59.97	386.48	1.50%	84.72%	6
1000	26.66	27.91	272.91	4.48%	90.23%	8

b) Cantilever Conical Shells with Simple Support at the Middle of the Length

In the following case study a cantilever conical shell with a simple support at the middle of the length is analysed. As it was previously mentioned, the cantilever conical shells have the end corresponding to the top radius free and the end corresponding to the bottom radius fixed. At the middle of the length, the cantilever has a simple support which allows warping, while the v and w displacements are blocked. Figure 5.30 and Figure 5.31 show the buckling modes resulting from SFEA and the GBT-based FE formulation, respectively, and Figure 5.32 shows the normalized graphs of the modal amplitude functions $\phi_k(x)$. Table 5.10 shows the differences between the SFEA and GBT and also the corresponding cross section deformation mode k. As in the previous case the local end effects are present and they must not be neglected. By comparing the critical buckling coefficients from Table 5.9 and Table 5.10 one can observe that the intermediary simple support enhances the stiffness of the conical shell, but only for small values of the bottom radius r_2. This is due to localized buckling occurring at the free end, for large values of the conical shell's bottom radius with respect the longitudinal axis, a phenomenon which can be easily observed from Figure 5.32.

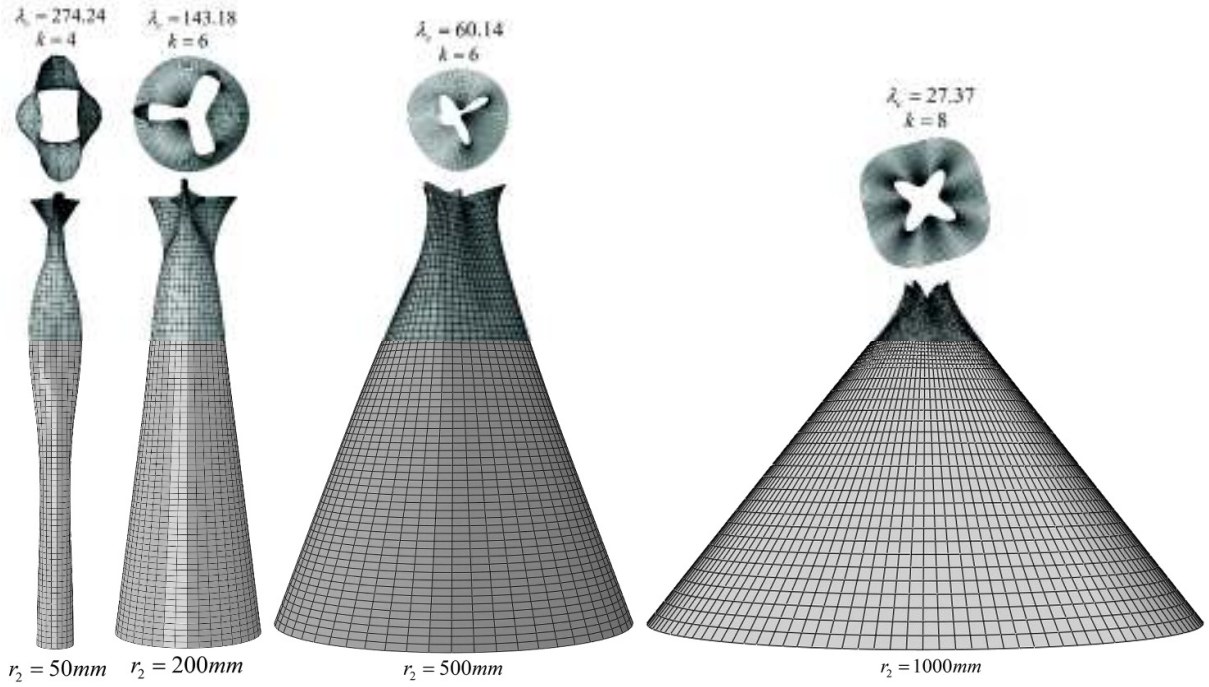

Figure 5.30: The critical buckling modes of cantilever conical shells with simple support at the middle of the length resulting from SFEA

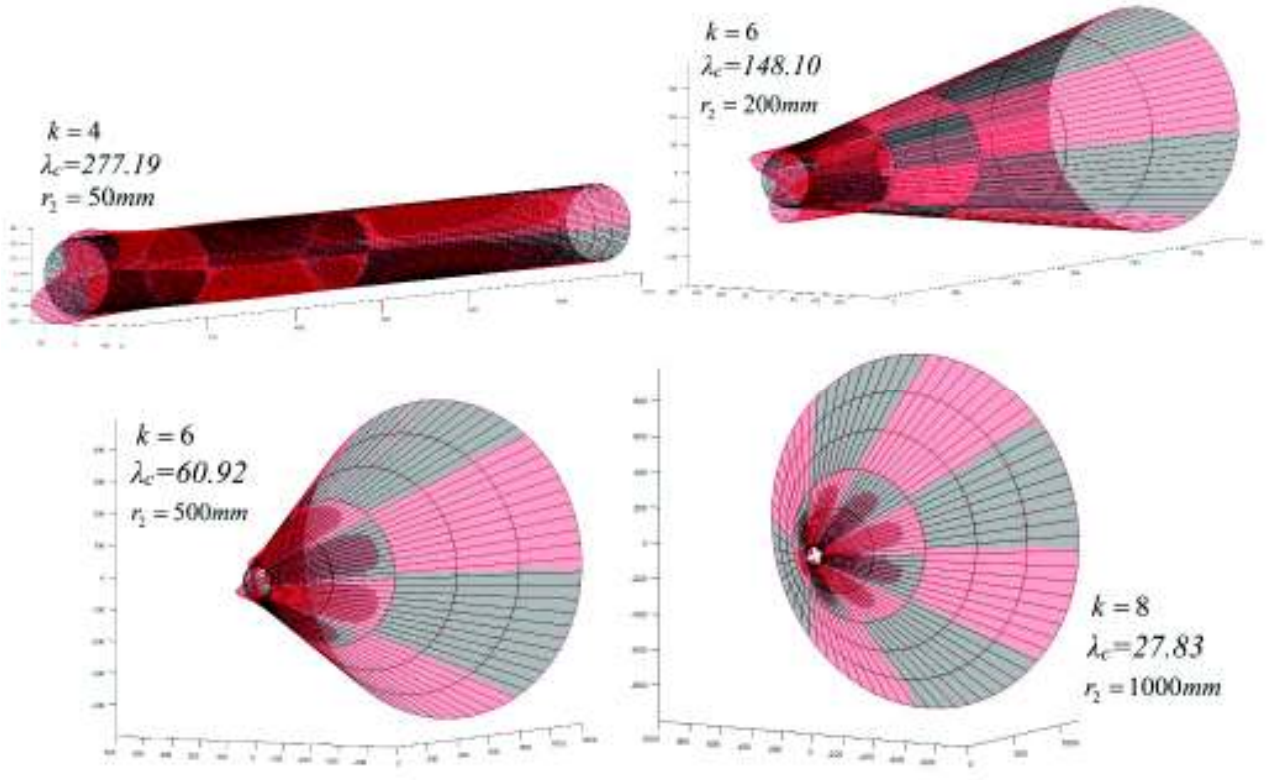

Figure 5.31: Cantilever conical shells with a simple support at the middle of the length: the critical buckling modes resulting from the GBT-based FE formulation in Matlab.

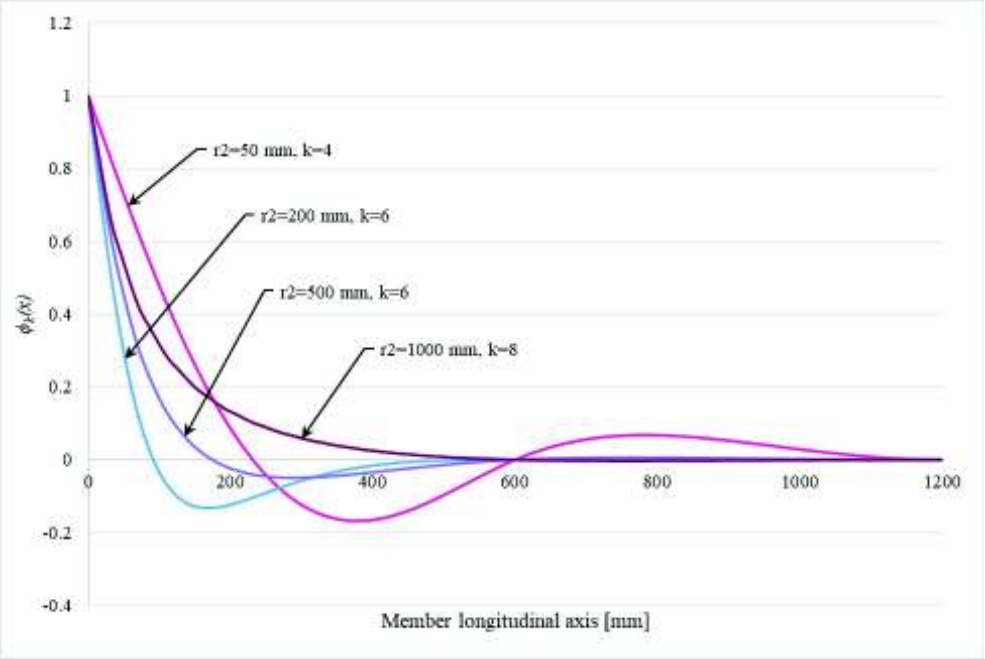

Figure 5.32: Cantilever conical shells with simple support at the middle of the length: the graphs of the modal amplitude functions $\phi_k(x)$.

Table 5.10: SFEA vs GBT-FEM results for cantilever conical shells with simple support at the middle of the length.

r_2 [mm]	λ_c SFEA	λ_c GBT-FEM	Differences	k
50	274.24	277.19	1.06%	4
60	272.15	277.53	1.94%	4
70	267.67	274.05	2.33%	4
90	257.23	256.12	0.43%	4
100	244.72	243.87	0.35%	4
120	219.45	215.76	1.71%	6
150	183.06	184.08	0.55%	6
200	143.18	148.10	3.32%	6
300	101.03	100.98	0.04%	8
400	74.81	76.32	1.97%	6
500	60.14	60.92	1.27%	6
1000	27.37	27.83	1.62%	8

5.3.1.2. Short Conical Shells

The following section presents the buckling analysis of short cantilever conical shells. As in the case of long cantilever conical shells, the local end effects, which occur at the loaded free end, must be taken into account. Figure 5.33 and Figure 5.34 show the critical buckling modes resulting from SFEAand the GBT-based FE procedure performed with Matlab, respectively, and in Figure 5.35 the

normalized graphs of the modal amplitude functions are displayed. Unlike in the previous case (i.e. long cantilever conical shells), along with the shell-type deformation modes the shear deformation modes also participate in the results. Also in Figure 5.35 one can observe the areas with stress concentrations.

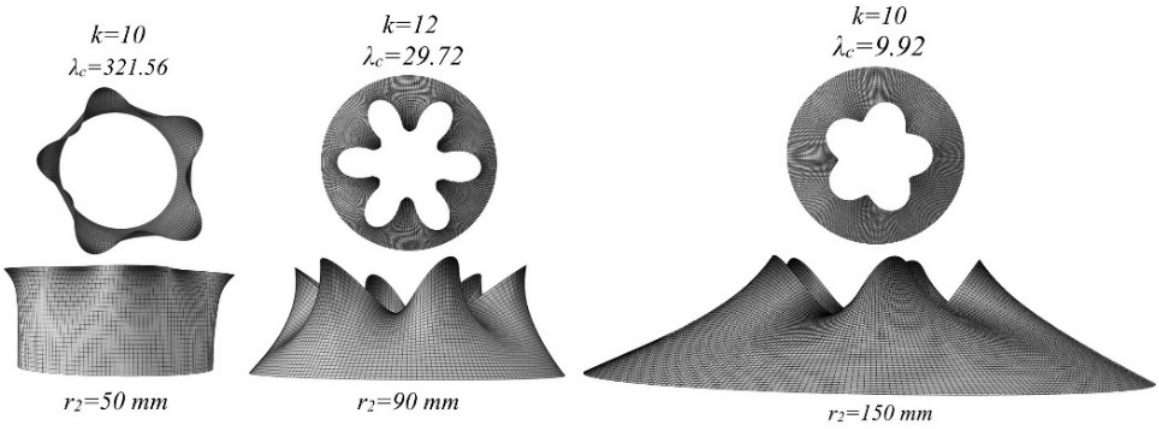

Figure 5.33: The critical buckling modes of short cantilever conical shells resulting from SFEA.

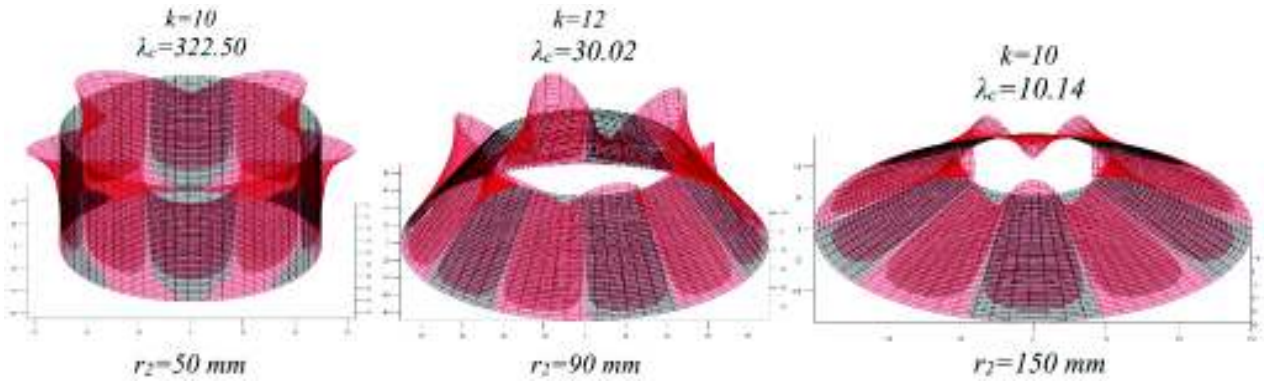

Figure 5.34: Short cantilever conical shells: the critical buckling modes resulting from the GBT-based FE formulation in Matlab.

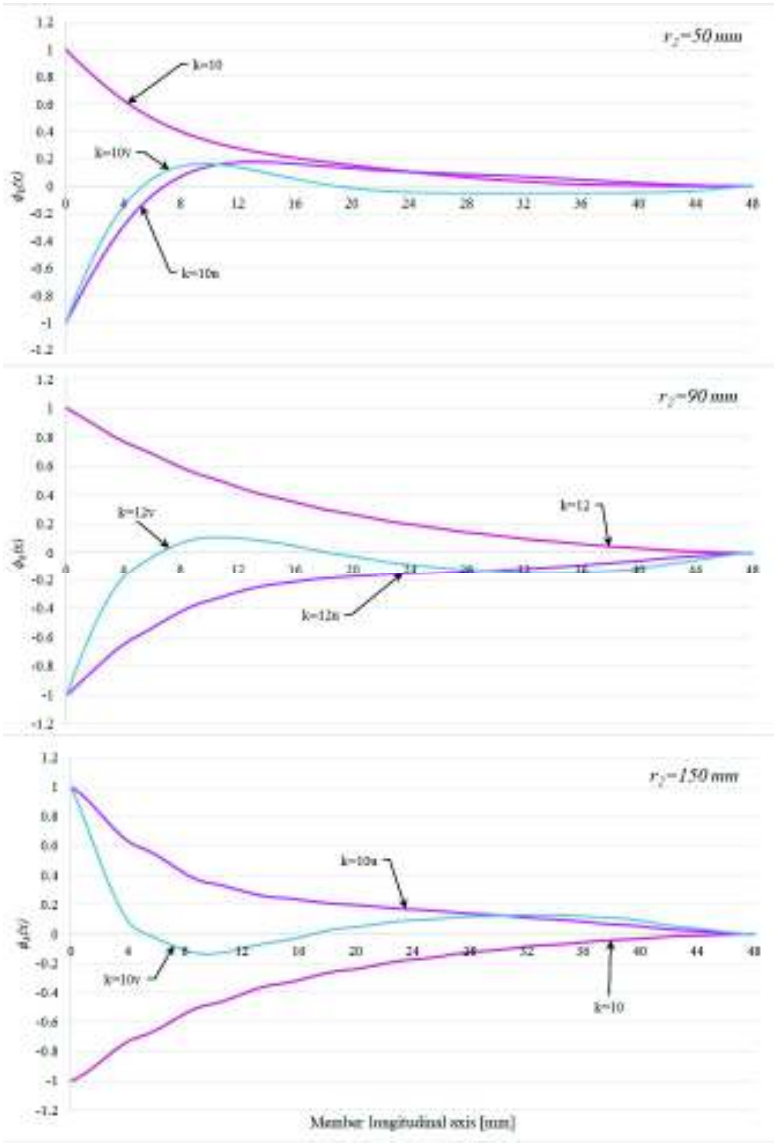

Figure 5.35: Short cantilever conical shells: the graphs of the modal amplitude functions $\phi_k(x)$.

Table 5.11 shows the differences between the results determined by SFEA and the GBT-based FE formulation. As in the previous case, the stress concentrations must be taken into account in the buckling analysis in order to keep the differences between the results below 5%. Besides the stress concentrations at the free end, the shear deformation modes must also be included in the analyses.

Table 5.11: SFEA vs GBT-FEM results for short cantilever conical shells.

r_2 [mm]	λ_c SFEA	λ_c GBT-FEM	Differences	k
50	321.56	322.50	0.29%	10
60	103.36	104.22	0.82%	12
70	58.60	58.98	0.65%	12
90	29.71	30.02	1.01%	12
100	23.38	23.73	1.47%	12
120	15.59	15.52	0.43%	10
150	9.92	10.14	2.15%	10
200	5.70	5.74	0.70%	8
300	3.03	2.88	5.00%	6

5.3.2. Conical Shells with Variable Thickness

In the following section conical shells with stress concentrations and variable thickness are considered, as illustrated in Figure 5.36: the first half of the structure has a thickness $t_1=1\ mm$, while the second half of the structure has a thickness $t_2=2\ mm$. The length of the conical shells with variable thickness is $L=1000\ mm$. The models created in Abaqus were analysed using a mesh size of 5 mm and S4 shell finite elements. As in the case of conical shells with constant thickness, the pre-buckling stresses are determined by first-order analysis. Figure 5.36 and Figure 5.37 show the critical buckling modes of the cantilever conical shells with variable thickness resulting from SFEA and the GBT-based FE procedure performed with Matlab, respectively, and in Figure 5.38 the normalized graphs of the modal amplitude functions are provided.

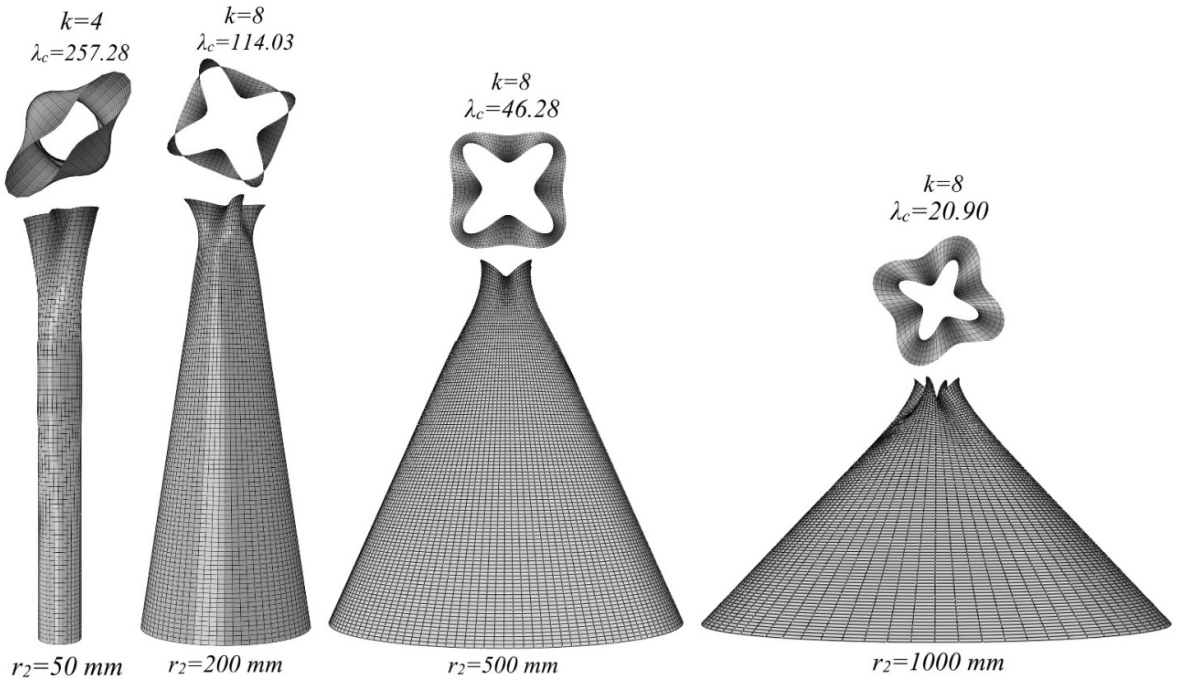

Figure 5.36: The critical buckling modes of cantilever conical shells with variable thickness resulting from SFEA.

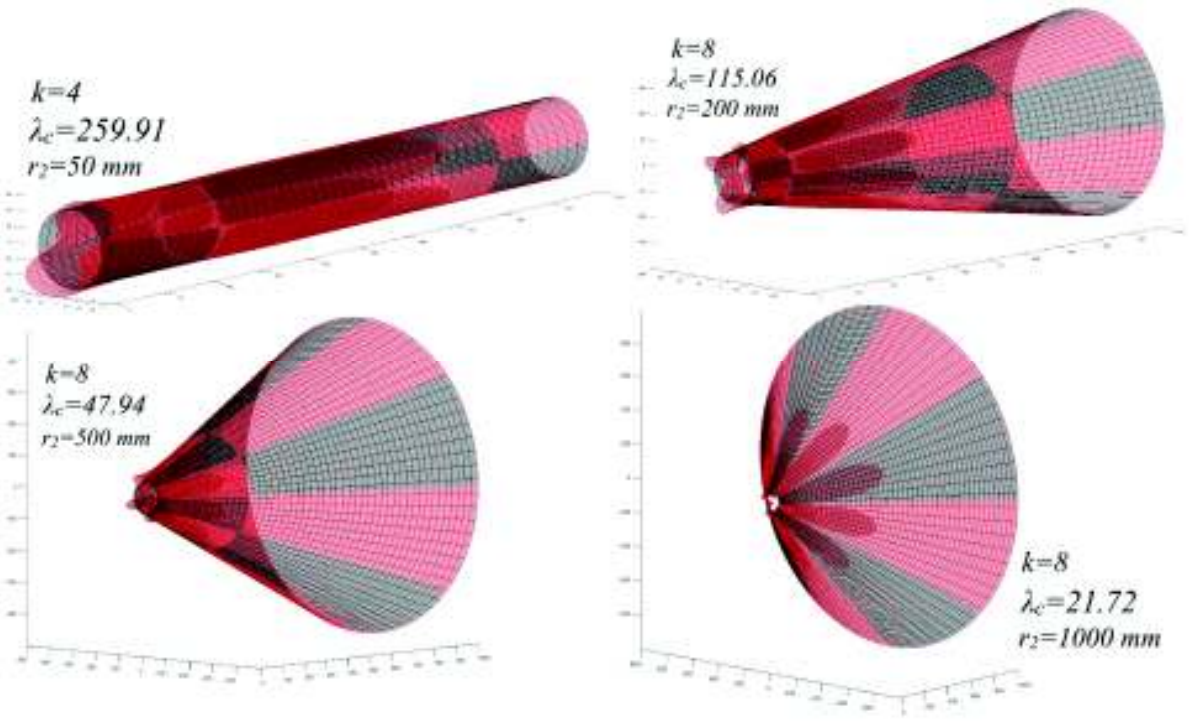

Figure 5.37: Cantilever conical shells: the critical buckling modes resulting from the GBT-based FE formulation in Matlab.

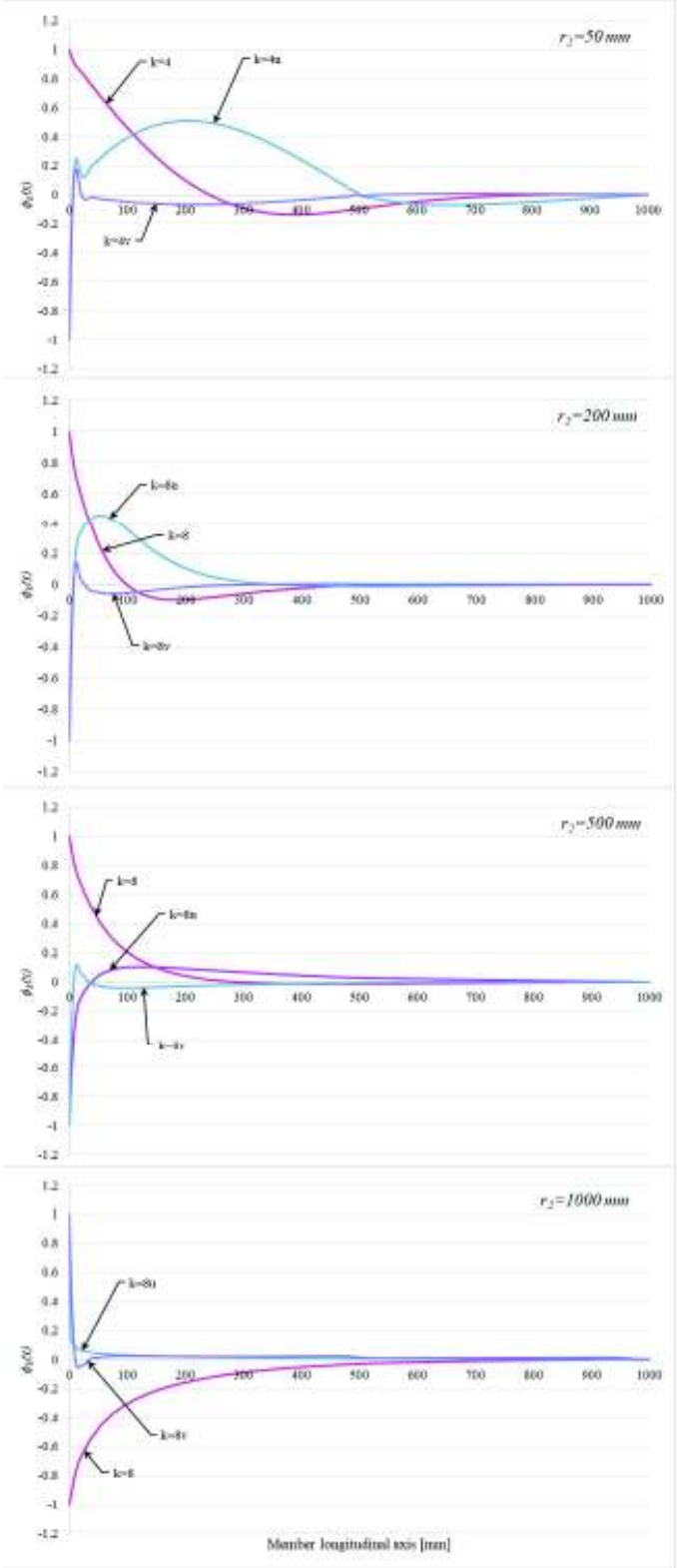

Figure 5.38: Cantilever conical shells with variable thickness: the graphs of the modal amplitude functions $\phi_k(x)$.

According to Figure 5.38, the "u" and "v" shear modes are also present along with the shell-type deformation modes. The graphs of the modal amplitude functions $\phi_k(x)$ corresponding to shear

deformation modes show as well the effects of the stress concentrations at the free end, where the axial compression is applied.

Table 5.12 shows the differences between the results determined by SFEA and the ones determined using GBT for different values of the bottom radius r_2. The results were obtained with 30 FE in the GBT-based model. To demonstrate the importance of taking into account the shear deformation modes a separate analysis was run in which the GBT-based FE formulation was applied using only the shell-type deformation modes. According to Table 5.12 the differences between the results determined by SFEA and the ones determined by the GBT-based FE formulation with shear deformation modes do not exceed 5%. When the shear deformation modes are neglected, the differences between the results are larger, demonstrating the influence of this type of deformation modes.

Table 5.12: SFEA vs GBT-FEM results for cantilever conical shells with variable thickness when shear deformation modes are taken/not taken into account.

r_2 [mm]	λ_c SFEA	λ_c GBT-FEM with shear modes	λ_c GBT-FEM without shear modes	Differences with shear modes	Differences without shear modes	k
50	257.28	259.91	293.08	1.01%	12.22%	4
60	249.79	253.10	283.84	1.31%	12.00%	4
70	241.96	246.30	275.07	1.76%	12.04%	4
90	216.57	218.80	257.59	1.02%	15.93%	6
100	202.33	204.71	239.36	1.16%	15.47%	6
120	178.03	178.21	209.49	0.10%	15.02%	8
150	147.68	148.15	176.18	0.32%	16.18%	8
200	114.03	115.06	134.78	0.90%	15.40%	8
300	77.56	79.22	91.10	2.09%	14.86%	8
400	58.32	60.12	68.66	2.99%	15.06%	8
500	46.28	47.94	54.52	3.45%	15.10%	8
1000	20.90	21.72	24.61	3.79%	15.08%	8

5.3.3. The Accuracy of the GBT-based FE Formulation

In the previous example, the high variation of the pre-buckling normal stresses occur on a limited zone near the free end where the finite element mesh should be sufficiently refined to capture them. To verifiy the precision and stability of the GBT-based FE formulation two case studies were considered for the analysed numerical examples: (i) finite elements with constant length and (ii) finite

elements with variable length. In Abaqus the size of the shell finite elements ranges linearly from aproximately *5 mm* at the free end to *50 mm* at the fixed end.

5.3.3.1. Finite Elements with Constant Length

In this case study the cantilever conical shells were modeled with shell finite elements having constant length. Figure 5.40 shows the differences between the results determined by SFEA and the ones determined by the GBT-based FE formulation for a cantilever conical shell having the bottom radius r_2=*500 mm*. In the GBT-based FE formulation the number of finite elements ranges from 1 to 15. According to Figure 5.40 the minimum number of finite elements where the difference between the results is under 5% is 6.

5.3.3.2. Finite Elements with Variable Length

In this case, the previous numerical example (i.e. the conical shell with the bottom radius r_2=*500 mm*) was analysed using a mesh made of finite elements with variable length. Figure 5.39 describes the discretization of cantilever conical shells using finite elements with variable length. At the free end of the conical shell, in the area with local effects, the finite elements have constant length on a distance equal to $r_1/\cos\alpha$, where r_1 is the top radius and α is the angle of the conical shell's semi-vertex. Therefore the area with local effects has a refined mesh. On the rest of the conical shell's length, in the area without local effects, the length of the finite elements increases linearly, therefore resulting in a coarser mesh in this zone.

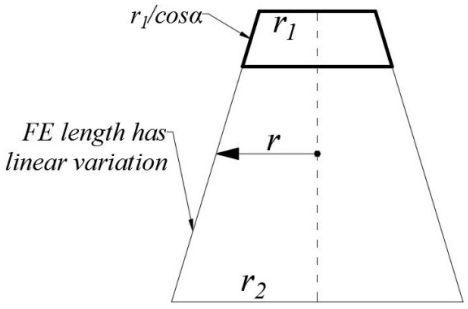

Figure 5.39: The discretization of the cantilever conical shell with finite elements having variable length.

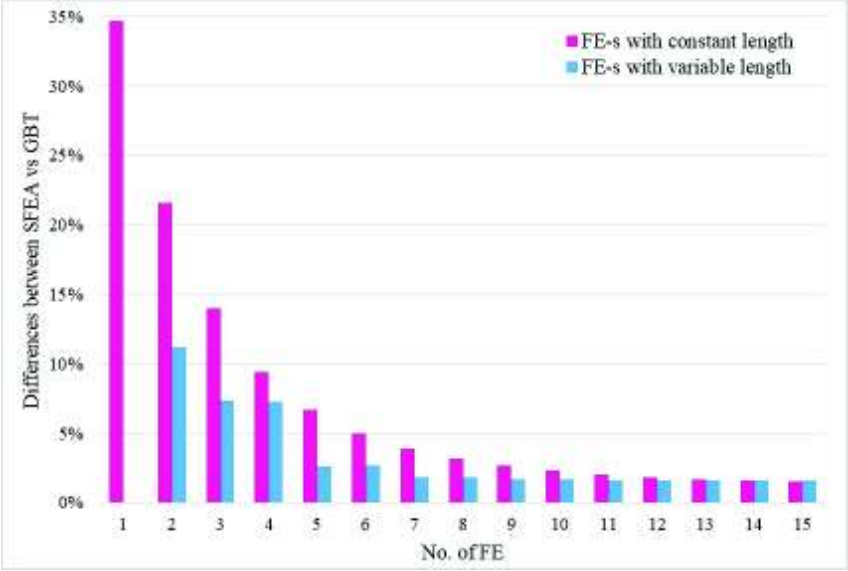

Figure 5.40: The differences between SFEA vs GBT results for different numbers of finite elements of the GBT model.

Table 5.13 presents the results determined for the different types of meshing and also the results determined by SFEA. These results are compared in Figure 5.40 to the values determined using shell? FE with constant length. According to Figure 5.40 the differences between the SFEA results and the GBT results are now under 3% for only 5 FE, meaning that 2 FE in the area with local effects and 3 FE in the area without local effects suffice.

Table 5.13: The differences between SFEA vs GBT results for different sizes of the FE mesh.

No. of FE in the area with local effects	No. of FE in the area without local effects	λ_c SFEA	λ_c GBT	Differences
1	1	59.06	66.53	11.23%
1	2		63.76	7.37%
2	2		63.68	7.26%
2	3		60.65	2.62%
3	3		60.70	2.70%
3	4		60.14	1.80%
4	4		60.15	1.81%
4	5		60.05	1.65%
5	5		60.05	1.65%
5	6		60.02	1.60%
6	6		60.02	1.61%
6	7		60.01	1.58%
7	7		60.01	1.59%
7	8		60.01	1.57%

5.4. Conclusions

This chapter presented the case of axially compressed conical shells. The numerical examples studied in this loading case were divided into two main categories: (i) axially compressed conical shells without stress concentrations and (ii) axially compressed conical shells with stress concentrations. The conical shells without stress concentrations are supported at both end sections. These are simply supported structures, fixed end structures or combinations between these types of boundary conditions. In this case, the stress concentrations which occur at the supports are so small that they can be neglected (note: I think the stress concentrations are not small, but the supports make them less relevant for buckling). The axially compressed conical shells with stress concentrations are cantilever conical shells where the load is applied at the free end. For both categories mentioned previously the following case studies were considered: long andshort conical shells with constant thickness, and conical shells with variable thickness.

According to the numerical examples presented in this chapter a few remarks can be highlighted. The first remark is the fact that in all the case studies the differences between the results

determined by SFEA and the ones determined by the GBT-based FE procedure do not exceed 5%. Unlike in SFEA, in order to achieve results with similar precision using GBT, a small number of finite elements suffices. For example, according to Figure 5.4 the minimum number of necessary finite elements for which the differences between the two analysis and modeling procedures is under 5% is only 3. The fact that for all the boundary conditions and geometric configurations analysed in this chapter the differences between the two analysis methods did not exceed 5% shows that the GBT-based FE formulation is both accurate and versatile.

The second remark is related to short conical shells and conical shells with variable thickness. In this case, in order to have good results with differences less than 5% with respect to a SFEA, the "u" and "v" shear modes must be inserted in the analysis, besides the shell-type deformation modes. It was proved according to Table 5.12 that the differences between the results determined by SFEA and the ones determined by the proposed formulation exceed 5% if the shear deformation modes are neglected from the buckling analysis.

The last remark is about conical shells with stress concentrations. In this case the analysis had two steps. In the first step a first-order analysis is performed, from which the pre-buckling normal meridional and hoop stresses are obtained. In the second step, a buckling analysis is performed using the pre-buckling normal stresses determined by the first-order analysis. To demonstrate the importance of including stress concentrations in the buckling analysis of cantilever conical shells, a separate analysis was run in which the normal hoop stresses were neglected, while the normal meridional stresses were approximated by Eq. (5.1). According to Table 5.9, the differences between the SFEA results and the GBT-based FE results exceed 5% when the stress concentrations are neglected, reaching up to 90% in case of large values of the bottom radius r_2.

Also in the case of conical shells with stress concentrations, the influence of the meshing procedure on the final results was analysed. Two situations were considered: in the first situation the shells were meshed with finite elements having constant length, while in the second situation the shells were meshed with finite elements having variable length. In the second case, the models were meshed as following: at the free end, on a distance equal to $r_1/\cos\alpha$, finite elements with constant length were used resulting in a refined mesh, while on the rest of the structure the length of the finite elements increases linearly resulting in a coarser mesh (see Figure 5.39). At the free end the refined mesh is able to capture more accurately the stress concentrations that occur due to the axial compression applied in that area. Figure 5.40 shows that the mesh with finite elements having variable length is more efficient than the mesh with finite elements having constant length. Therefore, the minimum number of finite elements necessary to have differences under 5% between the two modeling procedures is 5 in the case of finite elements with variable length (i.e. 2 FE in the area with

stress concentrations and 3 FE for the rest of the structure). In the of case finite elements with constant length, the minimum number necessary to have differences between results under 5% is 7.

Chapter VI
Conical Shells under Torsion

6.1. Introduction

Chapter V presented axially compressed conical shells. That study was divided into two main categories: conical shells without stress concentrations and conical shells with stress concentrations. In all the boundary conditions and geometrical configuration cases presented in Chapter V, the differences between the results determined by SFEA and the ones determined by the GBT-based FE procedure did not exceed 5%. This showed that the developed GBT-based FE formulation is both versatile and accurate. The case of axially compressed conical shells is, generally, a rather simple case because the solution of the GBT system of differential equations can be sought using only one shell-type deformation mode (where only these deformation modes need to be taken into account). This is due to the fact that the GBT system of differential equations is not coupled for axially compressed conical shells. Therefore, the unknowns can be determined by solving each equation of the system separately.

In this chapter the buckling analysis of conical shells under torsion is presented. Unlike for axially compressed conical shells, where the geometric matrix $X_{1ik}^{\sigma x}$ (see Eq. (3.37), where *j=1* is the axial compresson) is diagonal if only the shell-type deformation modes are taken into account, in the case of conical shells under torsion the GBT system of differential equations is coupled. This means that the system's equations cannot be solved separately. The geometric matrix X_{4ik}^{τ} (see Eq. (3.39), where *j=4* corresponds to torsion) is not diagonal. The critical buckling mode resulting from the analysis is always a combination between two similar shell-type deformation modes with the same order *m*. This buckling behavior was initially observed in cylindrical shells [120]. In case of conical shells under torsion, besides the shell-type deformation modes, shear deformation modes need to be introduced, because their absence leads to non-negligible errors.

For the numerical examples presented in the following sections the conical shell from Figure 6.1 was considered. The analysed conical shells are made of steel ($E=210\ GPa$, $\mu=0.3$), the top radius is $r_1=50\ mm$, while the bottom radius r_2 ranges between *50* and *1000 mm*. As in the case of axially compressed conical shells presented in Chapter V, two situations were considered: (i) conical shells with constant thickness and (ii) conical shells with variable thickness. The length of the analysed structures also ranges between *200* and *5000 mm*. Therefore the case studies were divided into three categories: (i) short conical shells, (ii) medium conical shells and (iii) long conical shells.

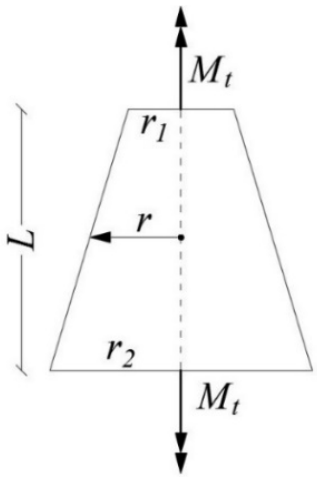

Figure 6.1: The geometry of the conical shell under torsion.

The analysed conical shells are fixed at both ends. The initial torsional moment M_t, introduced at the ends of the structure, produces a shear stress $\tau_0=1000\ N/mm^2$ at the top end (with radius r_1). The initial state of stress was determined by a first order analysis using the torsion mode described by Eq. (3.24). However, the state of stress of conical shells under torsion is described only by shear stresses which can also be determined with Bredt's classical expression:

$$\tau_{x\theta}^{0} = \frac{M_t}{2t\pi r^2} \tag{6.1}$$

The proposed procedure implemented in Matlab [6] was adapted to conical shells under torsion where the deformation modes are coupled. The final results were compared to the results determined by SFEA which was run in Abaqus [7] with S4 rectangular shell finite elements. The size of the mesh ranges between *5* and *20 mm* depending on the size of the bottom radius r_2 and on the length of the analysed structure. For example, for the conical shells with $r_2=50\ mm$ a mesh with *5 mm* was used, while for $r_2=1000\ mm$ the element size was *20 mm*.

In the following sections several numerical examples of conical shells under torsion are presented. These numerical examples were divided into two main categories: (i) conical shells with constant thickness and (ii) conical shells with variable thickness. The two main categories were also each divided into three cases depending on the length of the structure as follows: (i) short conical shells ($L<1000\ mm$), (ii) medium conical shells (L ranges *1000 between 2000 mm*) and (iii) long conical shells ($L\geq2000\ mm$).

6.2. Conical Shells with Constant Thickness

The following section presents conical shells under torsion with constant thickness. In the numerical examples presented in the next sections the thickness of the wall is $t=1\ mm$.

6.2.1. Short Conical Shells

The following case study concerns short conical shells under torsion. The short conical shells are structures having a length $L<1000\ mm$. For the numerical examples in this category the following lengths were considered: $L=200\ mm$, $L=400\ mm$ and $L=800\ mm$.

Figure 6.2 shows the critical buckling modes of short conical shells with $L=800\ mm$ resulting from SFEA. Figure 6.3 presents the corresponding buckling modes resulting from the GBT-based FE formulation performed with Matlab. Besides the critical buckling modes, the figures also show the corresponding critical buckling coefficients λ_c and cross section deformation modes k.

In Figure 6.4 are illustrated the normalized graphs of the modal amplitude functions $\phi_k(x)$ for short conical shells with $L=800\ mm$ resulting from the GBT-based FE procedure. According to Figure 6.4, besides the shell-type deformation modes, the "u" and "v" shear modes also appear. It can also be remarked that, for the conical shell with $r_2=500\ mm$, the longitudinal half-waves are concentrated near the top (at the left side of the graph), which means that the bottom area is stiffer. For $r_2=50\ mm$ and$r_2=100\ mm$, the graphs of the modal amplitude functions for the "v" shear modes reveal concentrations near the end sections (i.e. in the fixed ends). This might show possible stress concentrations.

Table 6.1 shows the differences between the results determined by SFEA and the ones determined by the GBT-based FE formulation. The differences do not exceed 5%. According to Table 6.1, as the length of the conical shell increases, the value of the critical buckling coefficient and the order of the cross section deformation mode k decrease. Also, the length of the longitudinal half-waves decreases as the number of circumferential half-waves k increases. This means that, as the length increases, the conical shell becomes more flexible and more sensitive to buckling.

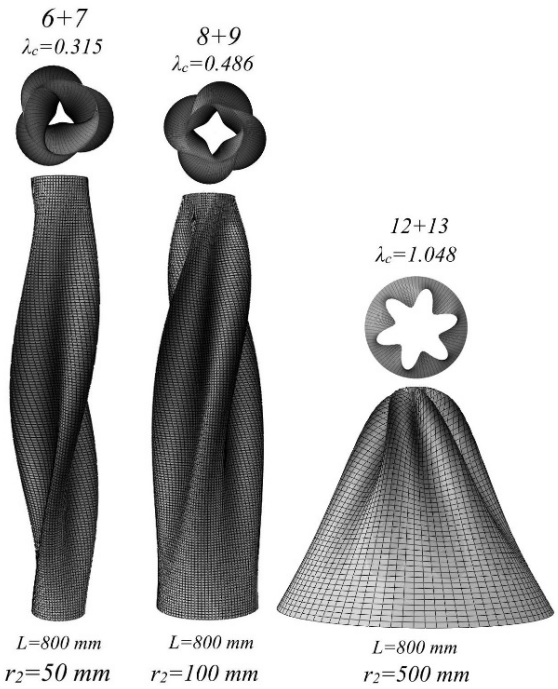

Figure 6.2: The critical buckling modes of short conical shells under torsion having the length *L=800 mm* resulting from SFEA.

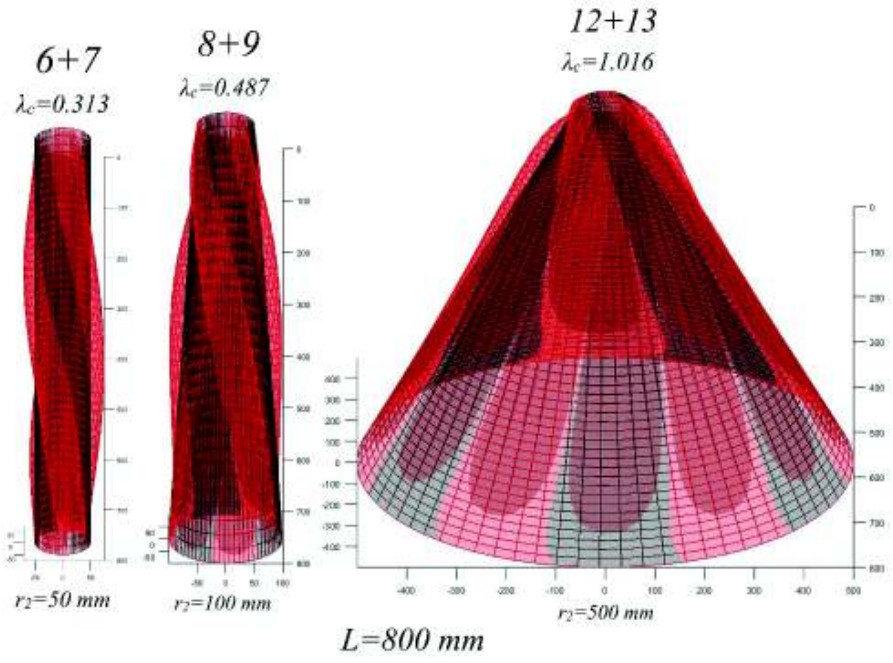

Figure 6.3: The critical buckling modes of short conical shells under torsion having the length *L=800 mm* resulting from the GBT-based FE formulation performed with Matlab code.

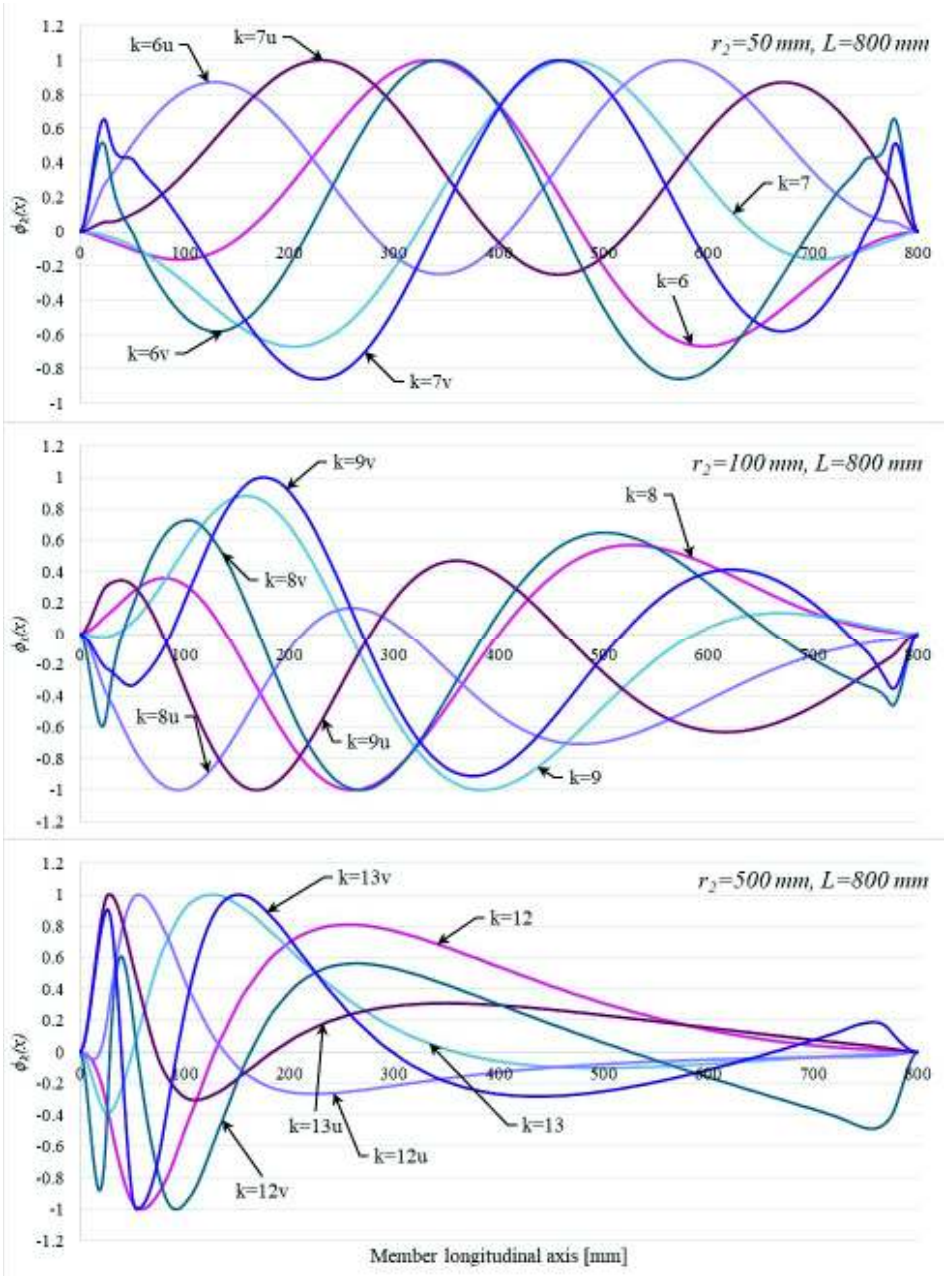

Figure 6.4: Short conical shells under torsion: the graphs of the modal amplitude functions $\phi_k(x)$.

Table 6.1: SFEA vs GBT-FEM results for short conical shells under torsion.

r_2=50 mm				
L [mm]	**λ_c SFEA**	**λ_c GBT-FEM**	**Differences**	**k**
200	0.64994	0.6279	3.51%	10+11
400	0.45344	0.4443	2.06%	8+9
800	0.31477	0.313	0.57%	6+7
r_2=100 mm				
L [mm]	**λ_c SFEA**	**λ_c GBT-FEM**	**Differences**	**k**
200	0.93626	0.9354	0.09%	12+13
400	0.67276	0.6732	0.07%	10+11
800	0.4862	0.4877	0.31%	8+9
r_2=500 mm				
L [mm]	**λ_c SFEA**	**λ_c GBT-FEM**	**Differences**	**k**
800	1.0484	1.0165	3.14%	12+13

6.2.2. Medium Conical Shells

The following section studies numerical examples of medium conical shells under torsion. The medium conical shells are structures having a length ranging between *1000 mm* and *2000 mm*. In this case the analysed numerical examples have *L=1000 mm* and *L=1500 mm*.

Figure 6.5 illustrates the critical buckling modes of conical shells with *L=1500 mm* resulting from SFEA. The critical buckling modes of the same conical shells resulting from the GBT-based FE procedure performed with Matlab are presented in Figure 6.6.

Figure 6.7 shows the normalized graphs of the modal amplitude functions for *L=1500 mm* resulting from the proposed formulation. As in the previous case, for conical shells with r_2=*500 mm* and r_2=*1000 mm*, the half-waves concentrate at the top end. This means that the cross sections near the bottom are stiffer.

Table 6.2 shows the differences between the results determined by SFEA and the ones determined by the proposed formulation which, like in the previous case, do not exceed 5%. According to Table 6.2, in the case of conical shells with r_2=*50 mm* and r_2=*500 mm*, the order of the cross section deformation mode k decreases, while in the case of conical shells with r_2=*100 mm* and r_2=*1000 mm*, the order of the cross section deformation mode k remains unchanged. As in the previous case, the value of the critical buckling coefficient decreases as the length of the conical shell increases.

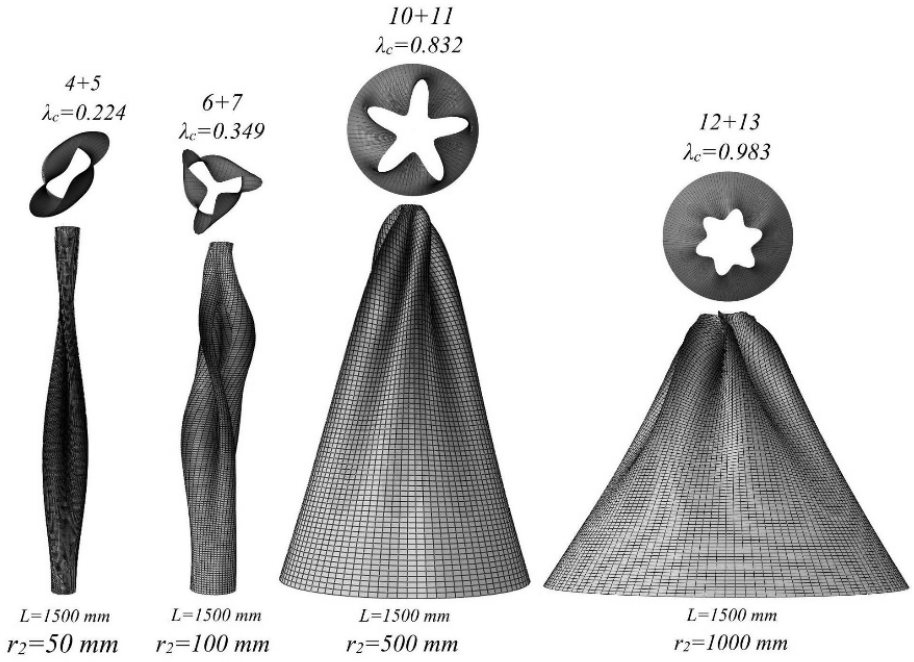

Figure 6.5: The critical buckling modes of medium conical shells under torsion having the length *L=1500 mm* resulting from SFEA.

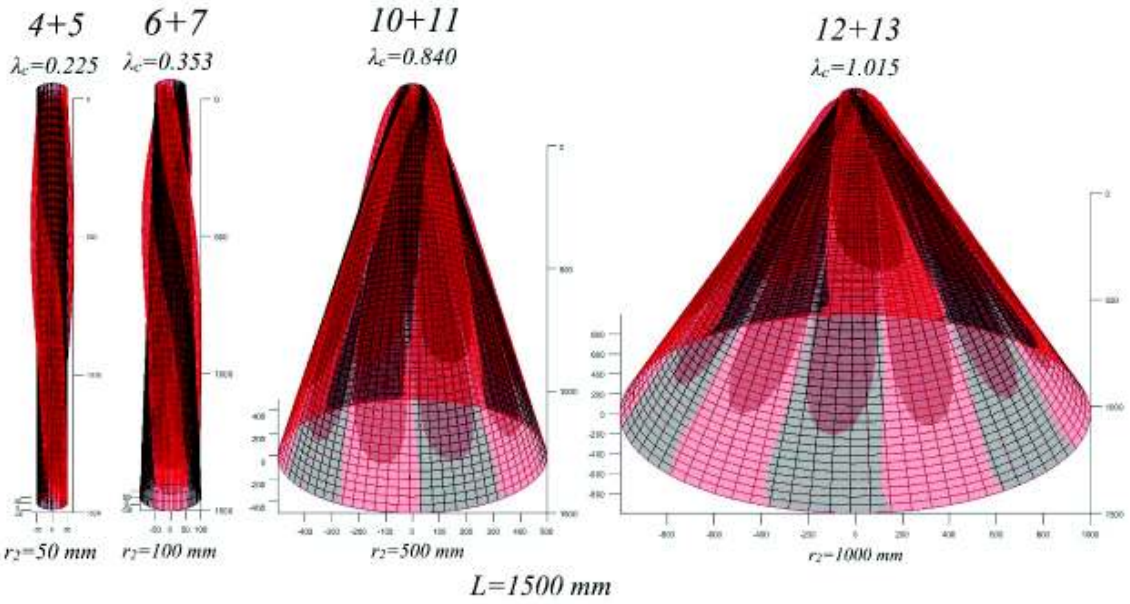

Figure 6.6: The critical buckling modes of medium conical shells under torsion having the length *L=1500 mm* resulting from the GBT-based FE formulation performed with Matlab code.

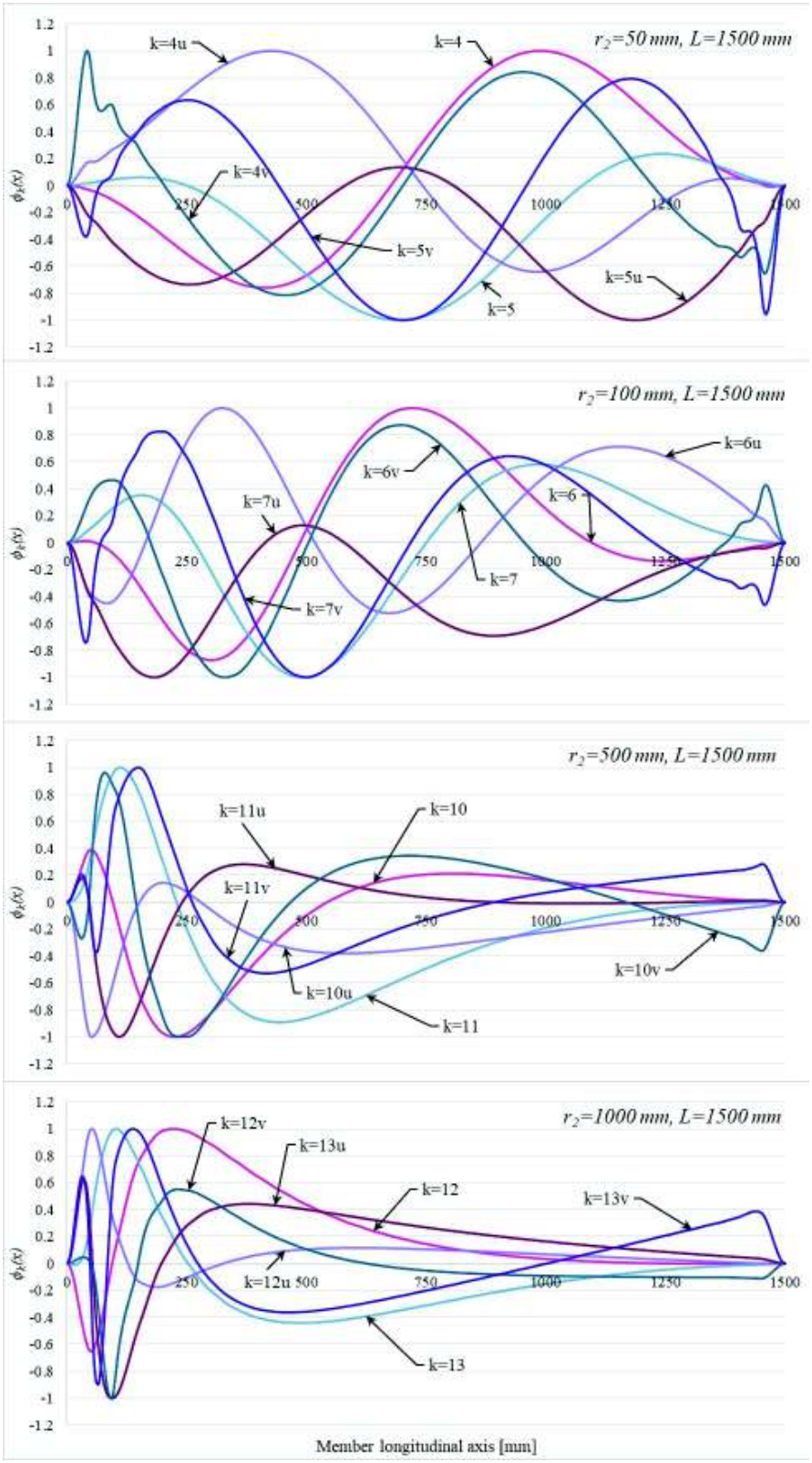

Figure 6.7: Medium conical shells under torsion: the graphs of the modal amplitude functions $\phi_k(x)$.

Table 6.2: SFEA vs GBT-FEM results for medium conical shells under torsion.

r_2=50 mm				
L [mm]	**λ_c SFEA**	**λ_c GBT-FEM**	**Differences**	**k**
1000	0.29272	0.2908	0.66%	6+7
1500	0.22366	0.2257	0.90%	4+5
r_2=100 mm				
L [mm]	**λ_c SFEA**	**λ_c GBT-FEM**	**Differences**	**k**
1000	0.43306	0.4411	1.82%	6+7
1500	0.34991	0.3534	0.99%	6+7
r_2=500 mm				
L [mm]	**λ_c SFEA**	**λ_c GBT-FEM**	**Differences**	**k**
1000	1.0075	0.9604	4.90%	12+13
1500	0.8318	0.8404	1.02%	10+11
r_2=1000 mm				
L [mm]	**λ_c SFEA**	**λ_c GBT-FEM**	**Differences**	**k**
1000	1.0121	1.0484	3.46%	12+13
1500	0.98308	1.0158	3.22%	12+13

6.2.3. Long Conical Shells

The following numerical examples illustrate long conical shells under torsion. The long conical shells are structures having the length $L \geq 2000$ *mm*.

Figure 6.8 illustrates the critical buckling modes of long conical shells under torsion with length $L=5000$ *mm* resulting from SFEA. Figure 6.9 presents the critical buckling modes resulting from the GBT-based FE procedure performed with Matlab for the same conical shells.

Figure 6.10 presents the normalized graphs of the modal amplitude functions $\phi_k(x)$ for conical shells with $L=5000$ *mm* resulting from the proposed formulation. As in the cases mentioned previously, for conical shells with large values of the bottom radius r_2, the half-waves concentrate at the top end, because in the bottom the cross sections are stiffer.

Table 6.3 shows the differences between the results determined by the two analysis methods which, as in the previous sections, do not exceed 5%. According to Table 6.3, in the case of conical shells with $r_2=50$ *mm*, the order of the cross section deformation mode k remains unchanged as the length increases, while in the rest of the cases, the order of the cross section deformation mode k decreases.

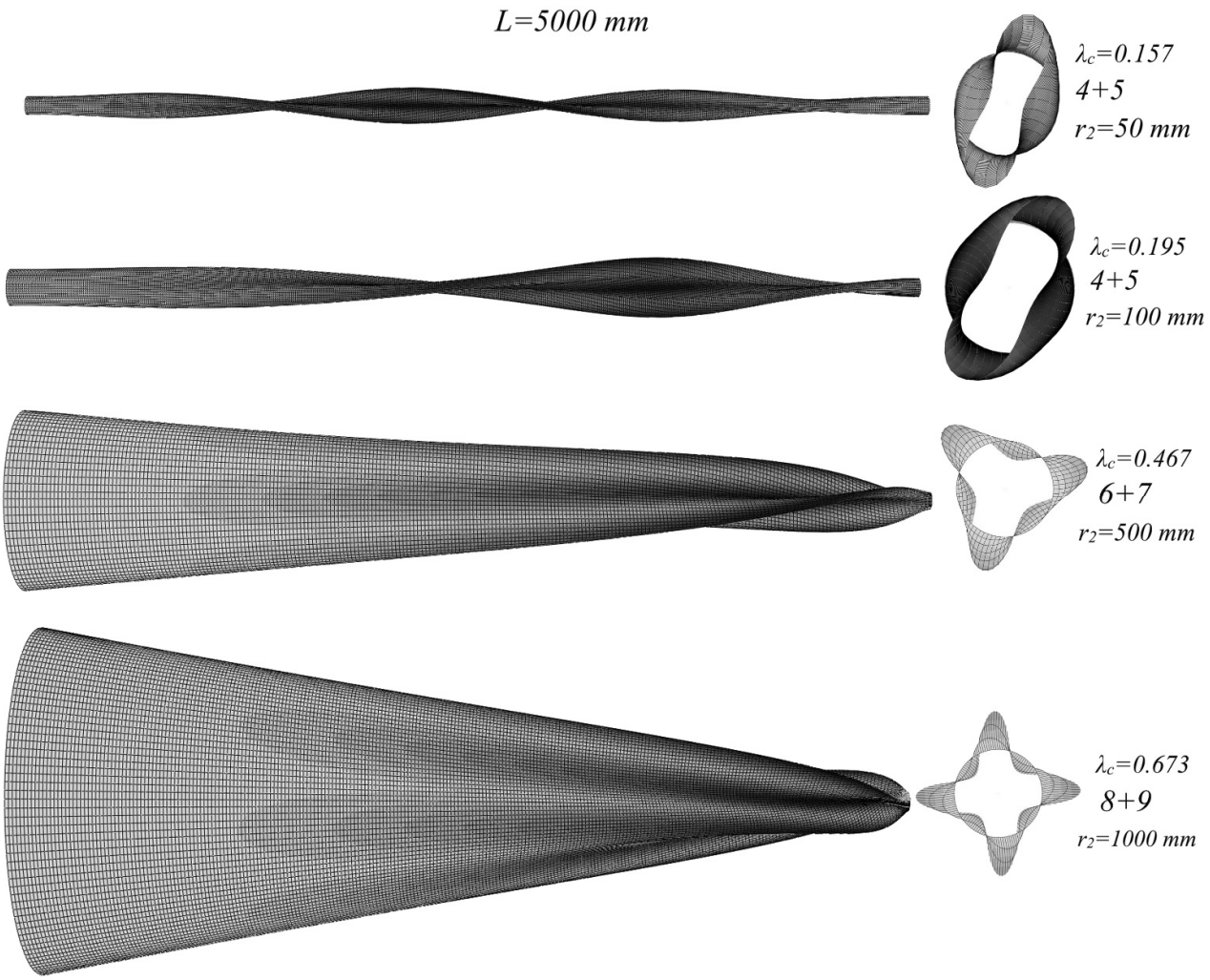

Figure 6.8: The critical buckling modes of long conical shells under torsion having the length *L=5000 mm* resulting from SFEA.

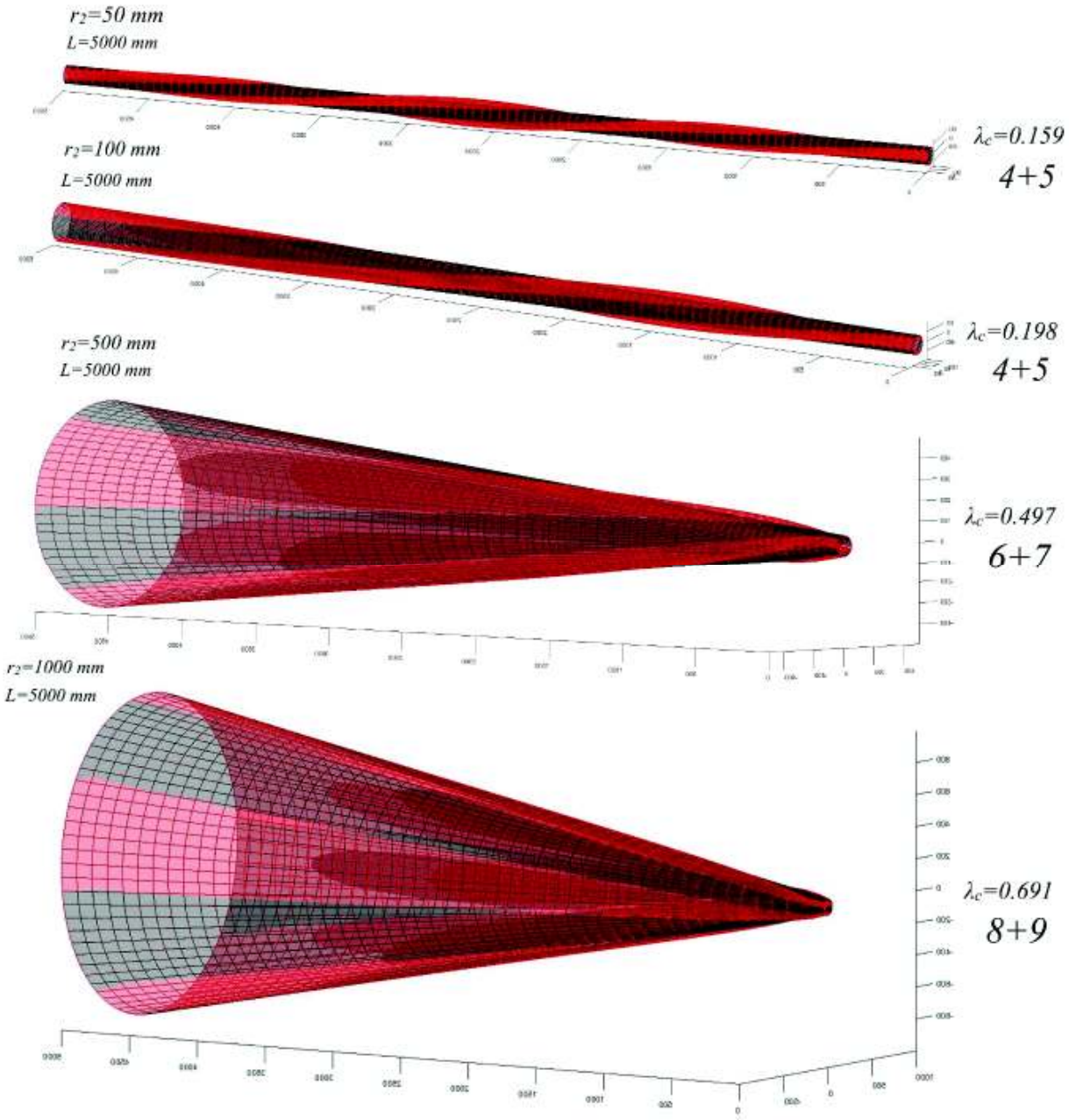

Figure 6.9: The critical buckling modes of long conical shells under torsion having the length *L=5000 mm* resulting from the GBT-based FE formulation performed with Matlab code.

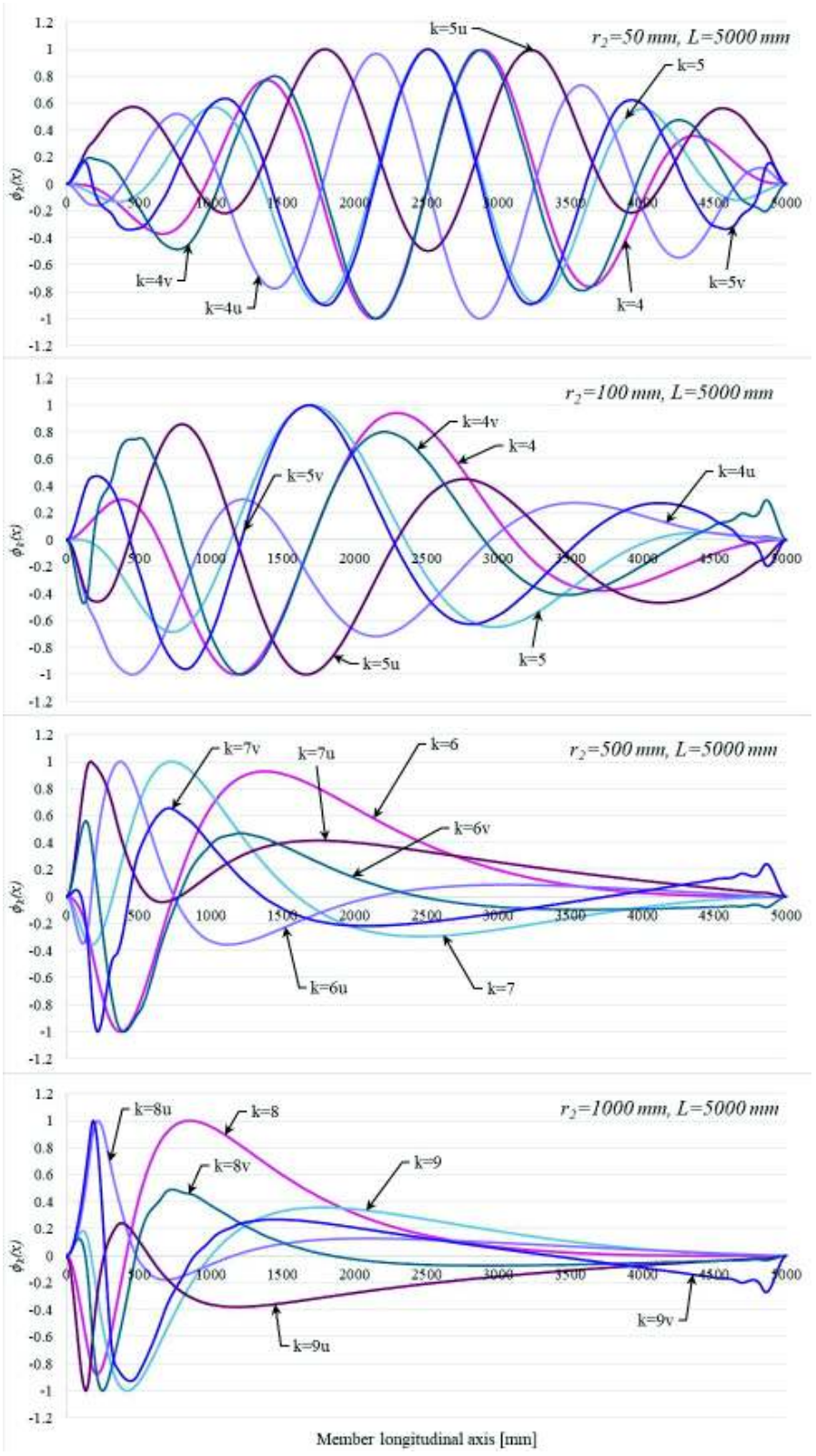

Figure 6.10: Long conical shells under torsion: the graphs of the modal amplitude functions $\phi_k(x)$.

Table 6.3: SFEA vs GBT-FEM results for long conical shells under torsion.

		r_2=50 mm		
***L* [mm]**	**λ_c SFEA**	**λ_c GBT-FEM**	**Differences**	***k***
2000	0.18971	0.1907	0.52%	4+5
5000	0.15796	0.1595	0.97%	4+5
		r_2=100 mm		
***L* [mm]**	**λ_c SFEA**	**λ_c GBT-FEM**	**Differences**	***k***
2000	0.32251	0.326	1.07%	6+7
5000	0.19479	0.1982	1.72%	4+5
		r_2=500 mm		
***L* [mm]**	**λ_c SFEA**	**λ_c GBT-FEM**	**Differences**	***k***
2000	0.75153	0.7523	0.10%	10+11
5000	0.46779	0.4899	4.51%	6+7
		r_2=1000 mm		
***L* [mm]**	**λ_c SFEA**	**λ_c GBT-FEM**	**Differences**	***k***
2000	1.0558	1.0154	3.98%	12+13
5000	0.6733	0.6909	2.55%	8+9

6.3. Conical Shells with Variable Thickness

In this section the analysed conical shells have variable thickness as illustrated in Figure 6.11: in the first half of the structure the thickness is t_1=*1 mm*, while in the second half of the structure the thickness is t_2=*2 mm*. The following sections present conical shells under torsion with variable thickness and having different lengths.

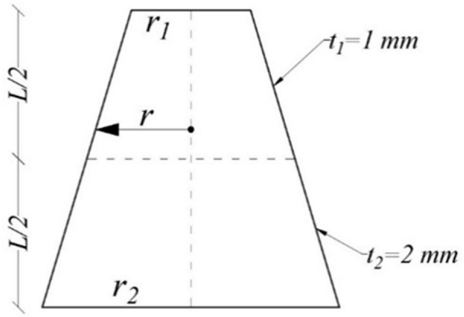

Figure 6.11: The geometry of the conical shell under torsion with variable thickness.

6.3.1. Short Conical Shells

The following section presents short conical shells under torsion with length $L<1000\ mm$. As in the previous case, for each conical shell with a particular bottom radius r_2 value, the following lengths were considered: $L=200\ mm$, $L=400\ mm$ and $L=800\ mm$. Figure 6.12 displays the critical buckling modes, the values of the critical buckling coefficients λ_c and the corresponding cross-section deformation modes k resulting from SFEA, for conical shells with $L=800\ mm$. Figure 6.13 presents the critical buckling modes of the same conical shells resulting from the GBT-based FE procedure performed with Matlab. According to the figures, if the thickness is variable then the value of the critical buckling coefficient is higher than in the previous case, which means that the structure becomes stiffer in general. From the figures one can observe that the largest torsion deformations occur in the area with $t_1=1\ mm$, while in for $t_2=2\ mm$ the deformations are smaller because the cross section is stiffer. Also, in the figures it can be observed that the order of the cross section deformation mode k decreases as the length of the conical shell increases.

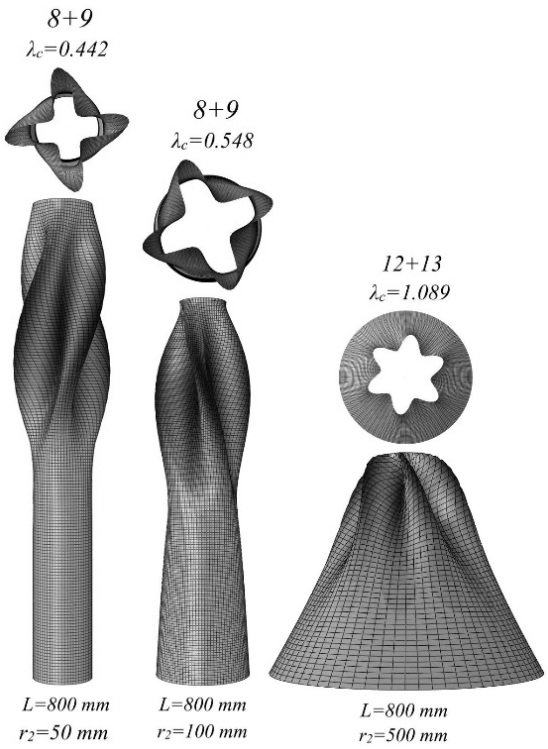

Figure 6.12: The critical buckling modes of short conical shells under torsion with variable thickness having the length $L=800\ mm$ resulting from SFEA.

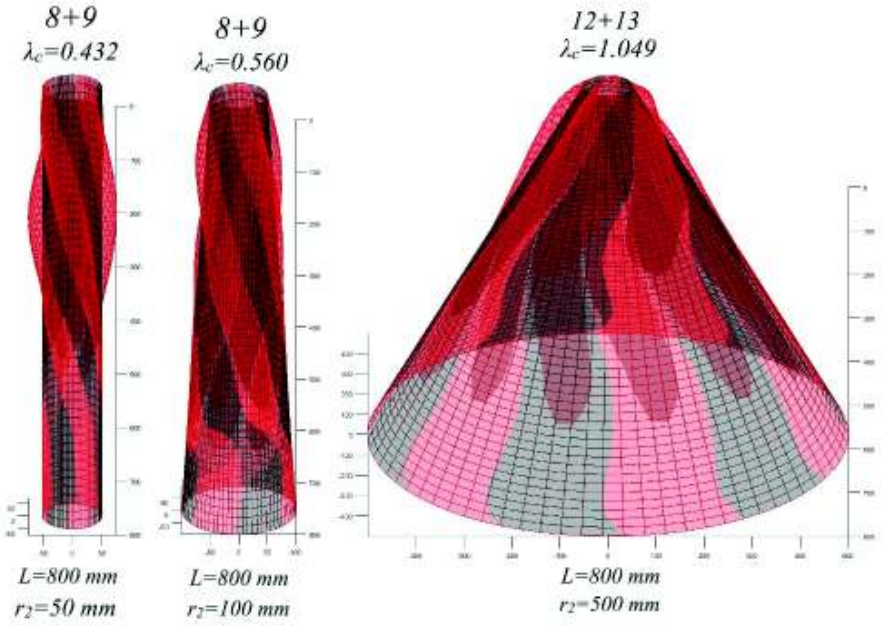

Figure 6.13: The critical buckling modes of short conical shells under torsion with variable thickness having the length *L=800 mm* resulting from the GBT-based FE procedure performed with Matlab code.

Figure 6.14 shows the normalized graphs of the modal amplitude functions $\phi_k(x)$ for conical shells with *L=800 mm* resulting from the GBT-based FE procedure. As in the previous case, the "u" and "v" shear deformation modes occur, besides the shell-type deformation modes, both being coupled. According to Figure 6.14, the graphs of the modal amplitude functions for the "v" shear modes have a jump at the middle of the span, corresponding to the transition from t_1*=1 mm* to t_2*=2 mm*. This shows that in the thickness transition zone there are large transverse shear deformations. The "v" shear modes that have jumps at the middle of the span are, depending on the bottom radius, the following: for r_2*=50 mm* and r_2*=100 mm* is *k=8v+9v* and for r_2*=500 mm* is *k=12v+13v*.

Also, according to Figure 6.14, the longitudinal half-waves concentrate more in the area with t_1*=1 mm* (at the left side of the graph), which means that the area with t_2*=2 mm* is stiffer and less sensitive to buckling. This aspect is clearly shown by the conical shell with r_2*=50 mm*: in Figure 6.4, for r_2*=50 mm* and constant thickness, the longitudinal half-waves are distributed almost evenly, while for the conical shell with r_2*=50 mm* and variable thickness, the longitudinal half-waves are distributed according to the cross section stiffness (the area with smaller thickness has a complex distribution, while the area with larger thickness has simple distribution.

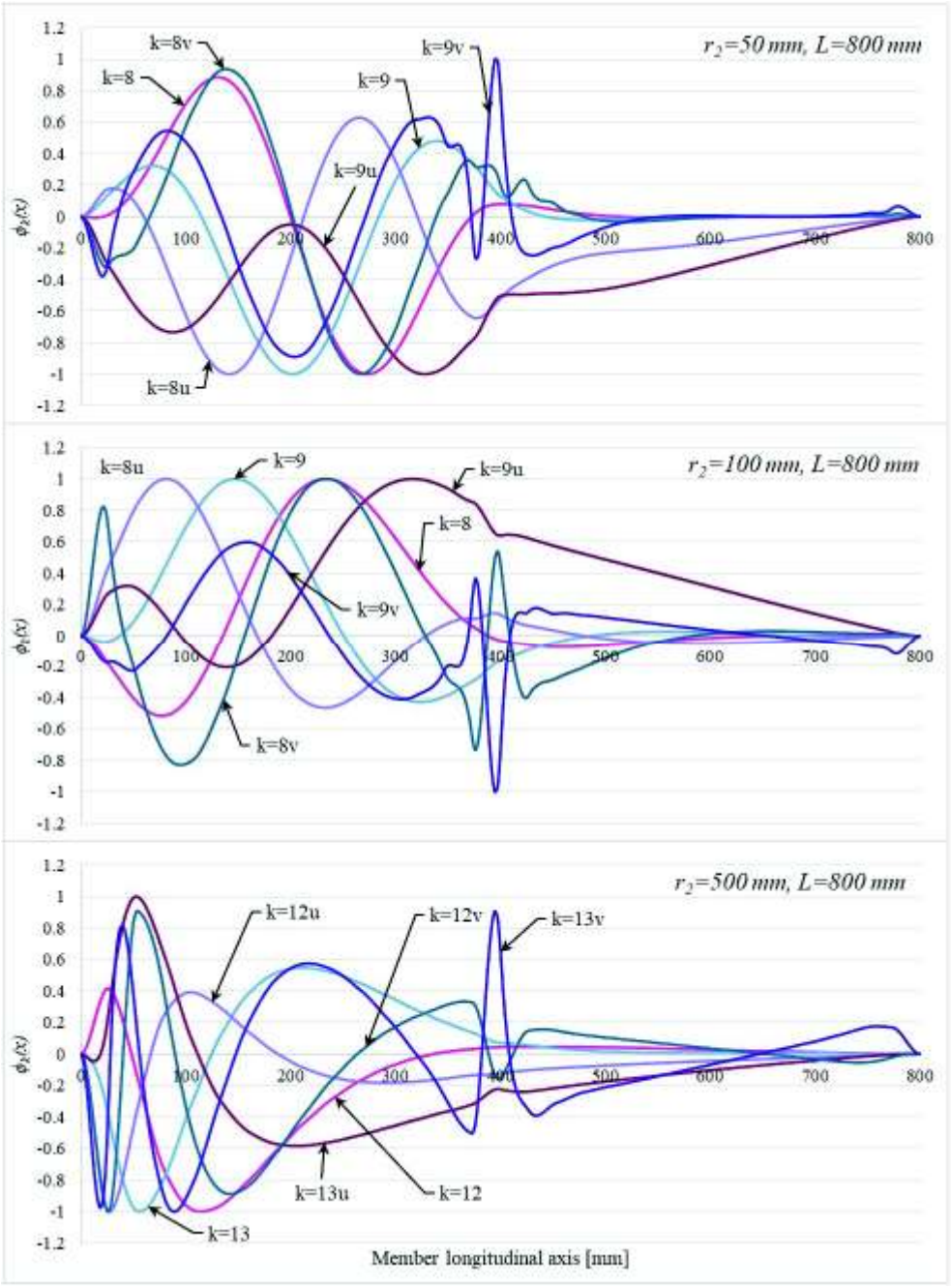

Figure 6.14: Short conical shells under torsion with variable thickness: the graphs of the modal amplitude functions $\phi_k(x)$.

Table 6.4 provides the differences between the results determined by SFEA and the GBT-based FE procedure. According to the table, the differences do not exceed 5%, which means that the proposed formulation can also be applied in the case of conical shells under torsion with variable (stepped) thickness.

Table 6.4: SFEA vs GBT-FEM results for short conical shells under torsion with variable thickness.

r_2=50 mm				
L [mm]	**λ_c SFEA**	**λ_c GBT-FEM**	**Differences**	**k**
200	0.84924	0.8693	2.31%	12+13
400	0.62697	0.6041	3.79%	10+11
800	0.44185	0.432	2.28%	8+9
r_2=100 mm				
L [mm]	**λ_c SFEA**	**λ_c GBT-FEM**	**Differences**	**k**
200	1.1097	1.099	0.97%	14+15
400	0.78469	0.808	2.88%	10+11
800	0.54899	0.5602	2.00%	8+9
r_2=500 mm				
L [mm]	**λ_c SFEA**	**λ_c GBT-FEM**	**Differences**	**k**
800	1.0899	1.0492	3.88%	12+13

6.3.2. Medium Conical Shells

The following case study presents medium conical shells with variable thickness. The length of these structures, in this situation, ranges between *1000 mm* and *2000 mm*. Like in the previous case, for each bottom radius r_2 the following lengths were considered: *L=1000 mm* and *L=1500 mm*.

Figure 6.15 shows the critical buckling modes, the critical buckling coefficients λ_c and the cross section deformation modes k for conical shells with L=1500 mm resulting from SFEA. Figure 6.16 illustrates the critical buckling coefficients for the same conical shells but determined by the GBT-based FE procedure. As in the case of short conical shells with variable thickness, the largest torsion deformations occur in the area with t_1=*1 mm*, because the cross sections are less stiffer than in the area with t_2=*2 mm*.

Figure 6.17 presents the normalized graphs of the modal amplitude functions $\phi_k(x)$ for the conical shells with *L=1500 mm* resulting from the GBT-based FE formulation. As in the case presented in the previous section, the graphs of the modal amplitude functions for the "v" shear modes describe a jump at the middle of the span, in the thickness transition zone. The "v" shear modes which produce jumps at the middle of the span are the following: for r_2=*50 mm* and r_2=*100 mm* is *k=6v+7v*, for r_2=*500 mm* is *k=10v+11v* and for r_2=*1000 mm* is *k=12v+13v*. Also, the largest concentration of longitudinal half-waves is in the area with t_1=*1 mm* (the left side of the graph), where the cross sections are less stiffer.

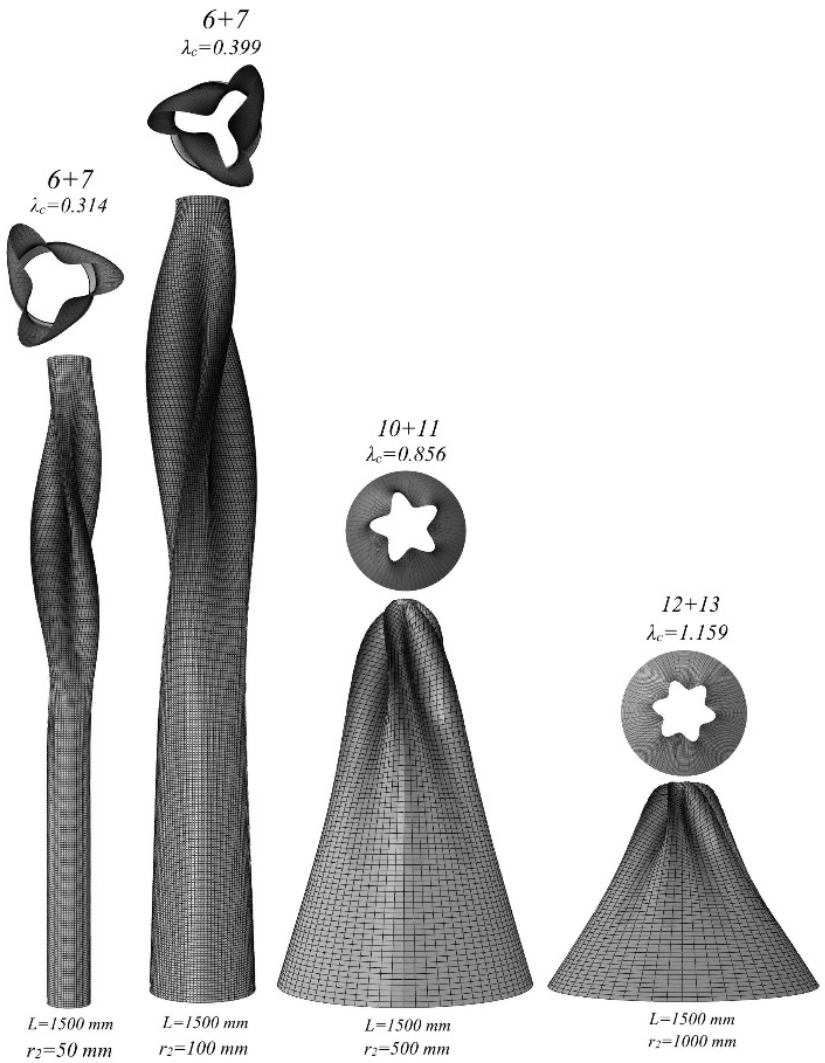

Figure 6.15: The critical buckling modes of medium conical shells under torsion with variable thickness having the length *L=1500 mm* resulting from SFEA.

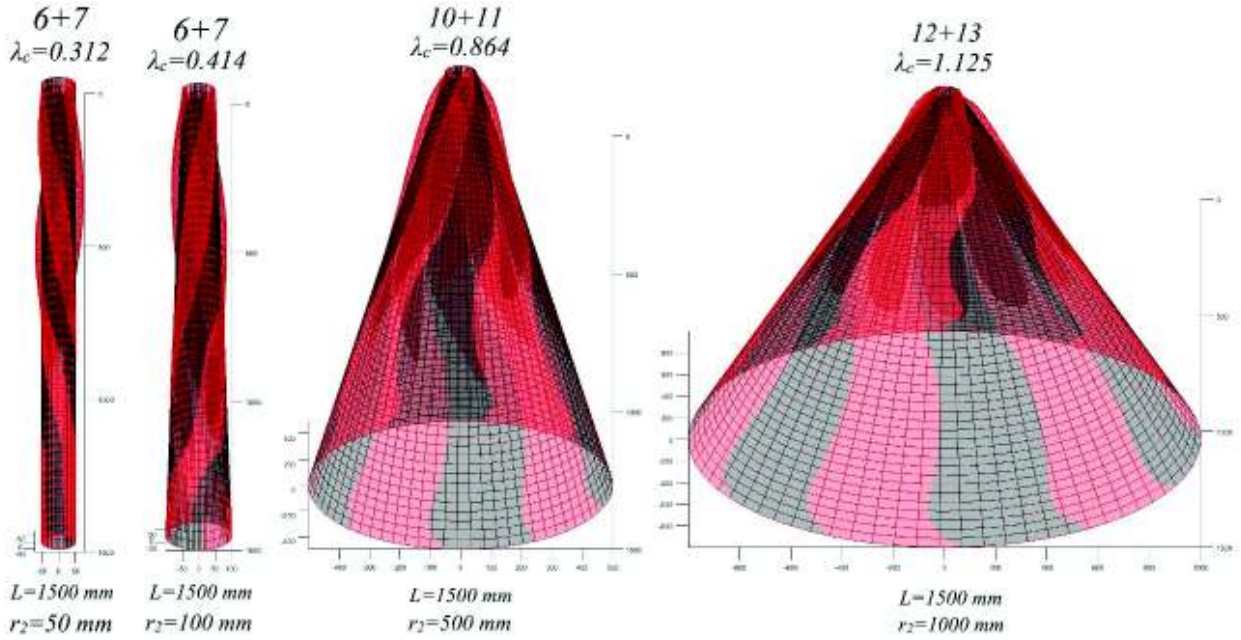

Figure 6.16: The critical buckling modes of medium conical shells under torsion with variable thickness having the length *L=1500 mm* resulting from the GBT-based FE procedure with Matlab code.

Table 6.5 provides the differences between the results determined by SFEA and the ones determined by the GBT-based FE formulation. According to the table the differences between these results do not exceed 5%. According to Table 6.5, in case of conical shells with r_2*=50 mm* and r_2*=1000 mm*, the order of the cross section deformation mode *k* remains unchanged as the length increases: for r_2*=50 mm*, the shell-type deformation modes are *k=6+7*, while for r_2*=1000 mm* the shell-type deformation modes are *k=12+13*. In the two remaining cases the order of the cross section deformation mode *k* decreases as the length increases.

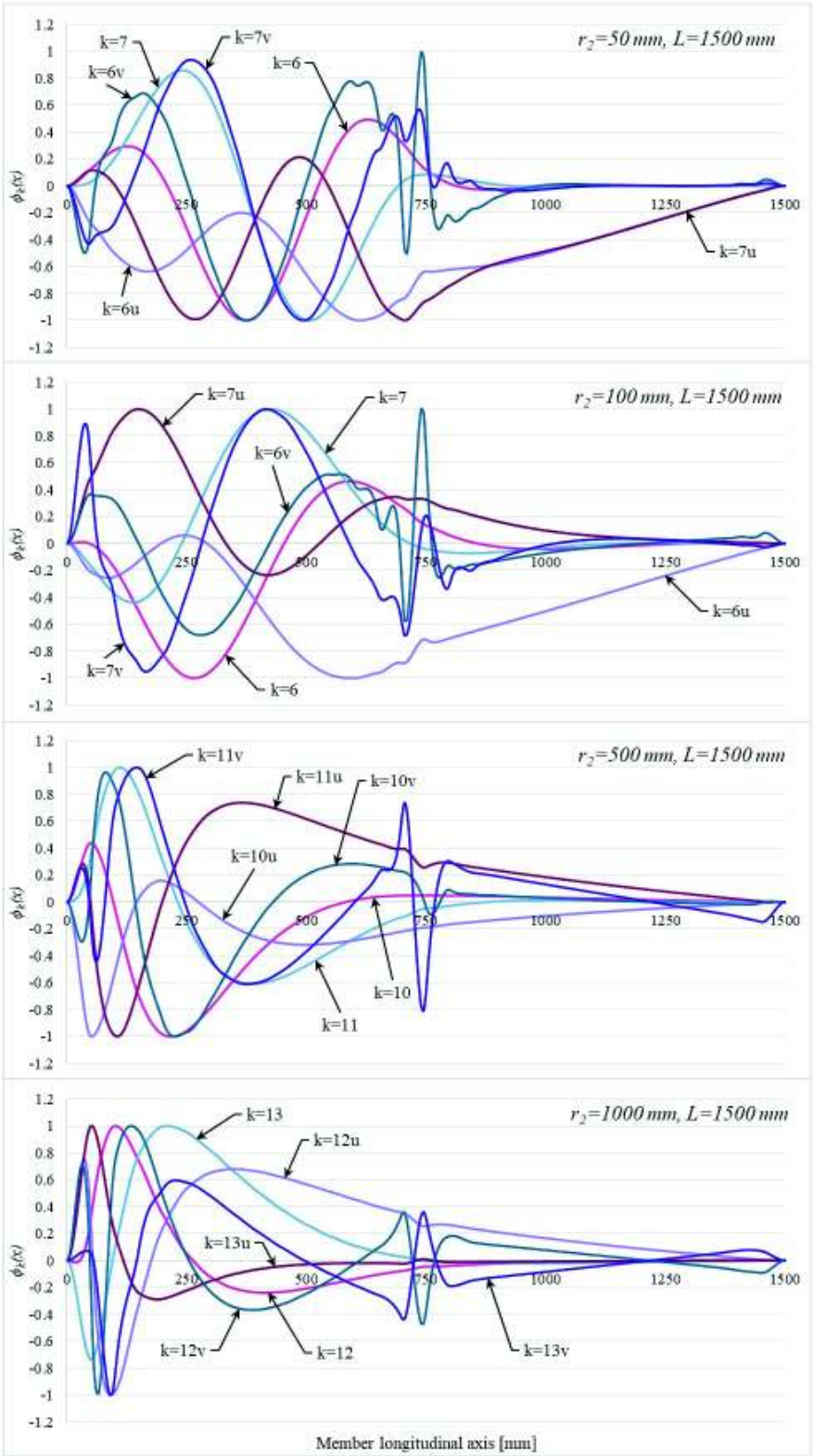

Figure 6.17: Medium conical shells under torsion with variable thickness: the graphs of the modal amplitude functions $\phi_k(x)$.

Table 6.5: SFEA vs GBT-FEM results for medium conical shells under torsion with variable thickness.

r_2=50 mm				
L [mm]	**λ_c SFEA**	**λ_c GBT-FEM**	**Differences**	**k**
1000	0.38421	0.3933	2.31%	6+7
1500	0.31352	0.3124	0.36%	6+7
r_2=100 mm				
L [mm]	**λ_c SFEA**	**λ_c GBT-FEM**	**Differences**	**k**
1000	0.49349	0.4951	0.33%	8+9
1500	0.3993	0.4139	3.53%	6+7
r_2=500 mm				
L [mm]	**λ_c SFEA**	**λ_c GBT-FEM**	**Differences**	**k**
1000	0.94456	0.9799	3.61%	12+13
1500	0.85609	0.8642	0.94%	10+11
r_2=1000 mm				
L [mm]	**λ_c SFEA**	**λ_c GBT-FEM**	**Differences**	**k**
1000	1.1343	1.159	2.13%	12+13
1500	1.1593	1.1251	3.04%	12+13

6.3.3. Long Conical Shells

This section studies long conical shells with variable thickness. The long conical shells have a length $L \geq 2000\ mm$. In the numerical examples presented below, for each conical shell with a bottom radius r_2, the following lengths were considered: $L=2000\ mm$ and $L=5000\ mm$.

Figure 6.18 presents the critical buckling modes, the values of the critical buckling coefficients and the corresponding cross-section deformation modes of conical shells with $L=5000\ mm$ and resulting from SFEA. The critical buckling modes of the same conical shells resulting from the proposed formulation are illustrated in Figure 6.19. The largest torsion deformations occur in the area with $t_1=1\ mm$, as in the cases presented in the previous sections.

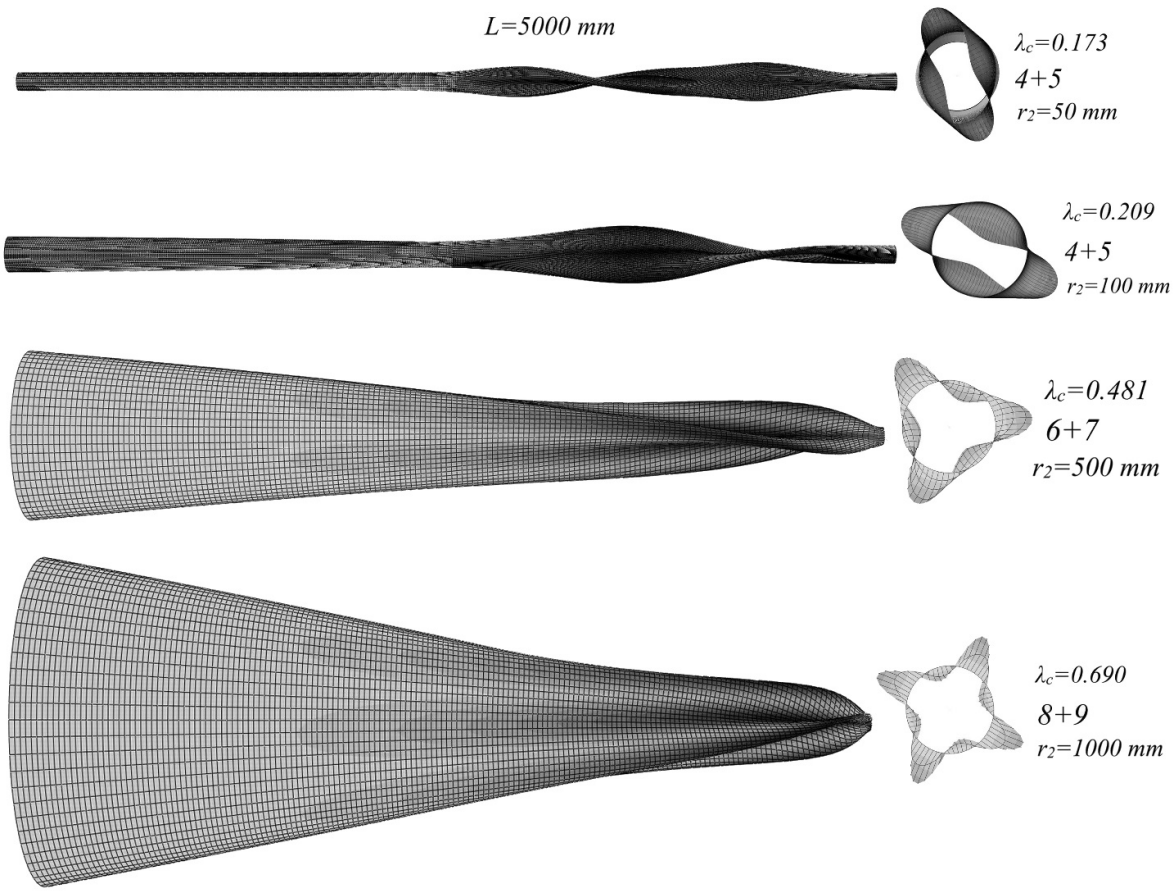

Figure 6.18: The critical buckling modes of long conical shells under torsion with variable thickness having the length *L=5000 mm* resulting from SFEA.

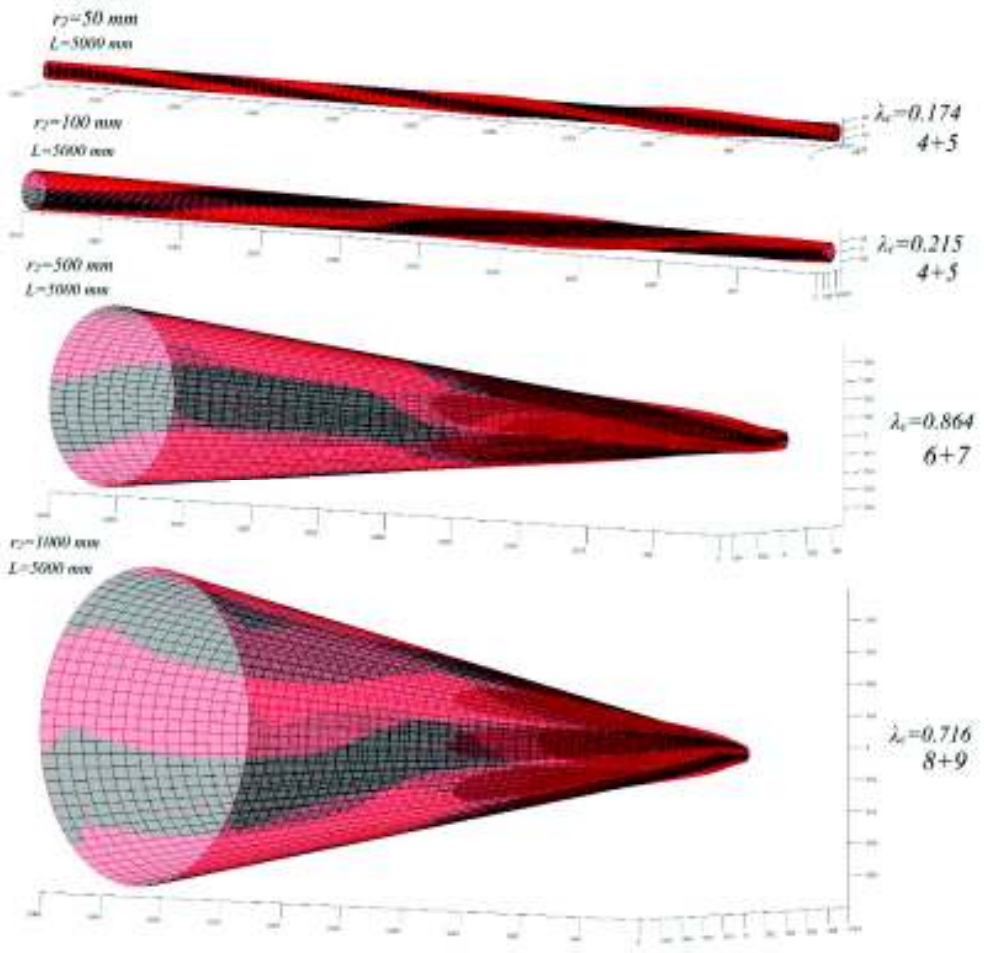

Figure 6.19: The critical buckling modes of long conical shells under torsion with variable thickness having the length *L=5000 mm* resulting from the GBT-based FE procedure performed in Matlab.

Figure 6.20 illustrates the normalized graphs of the modal amplitude functions $\phi_k(x)$ of conical shells with *L=5000 mm* and resulting from the GBT-based FE procedure. As in the previous sections, the graphs of the modal amplitude functions for the "v" shear modes show a jump at the middle of the span, where the thickness transition takes place. In the numerical examples presented in Figure 6.20, the "v" shear modes which produce jumps at the middle of the span are the following: for $r_2=50$ *mm* and $r_2=100$ *mm* is $k=4v+5v$, for $r_2=500$ *mm* is $k=6v+7v$ and for $r_2=1000$ *mm* is $k=8v+9v$. Also, the higher longitudinal half-wave concentrations are in the zone with $t_1=1$ *mm,* at the left side of the graph.

Table 6.6 presents the differences between the results determined by the two buckling analysis procedures. The differences do not exceed 5%. According to Table 6.6, for $r_2=50$ *mm*, the order of the cross section deformation mode *k* remains unchanged and, in this case, is *k=4+5*. In the remaining cases, the order of the cross section deformation mode *k* decreases as the length of the conical shell increases.

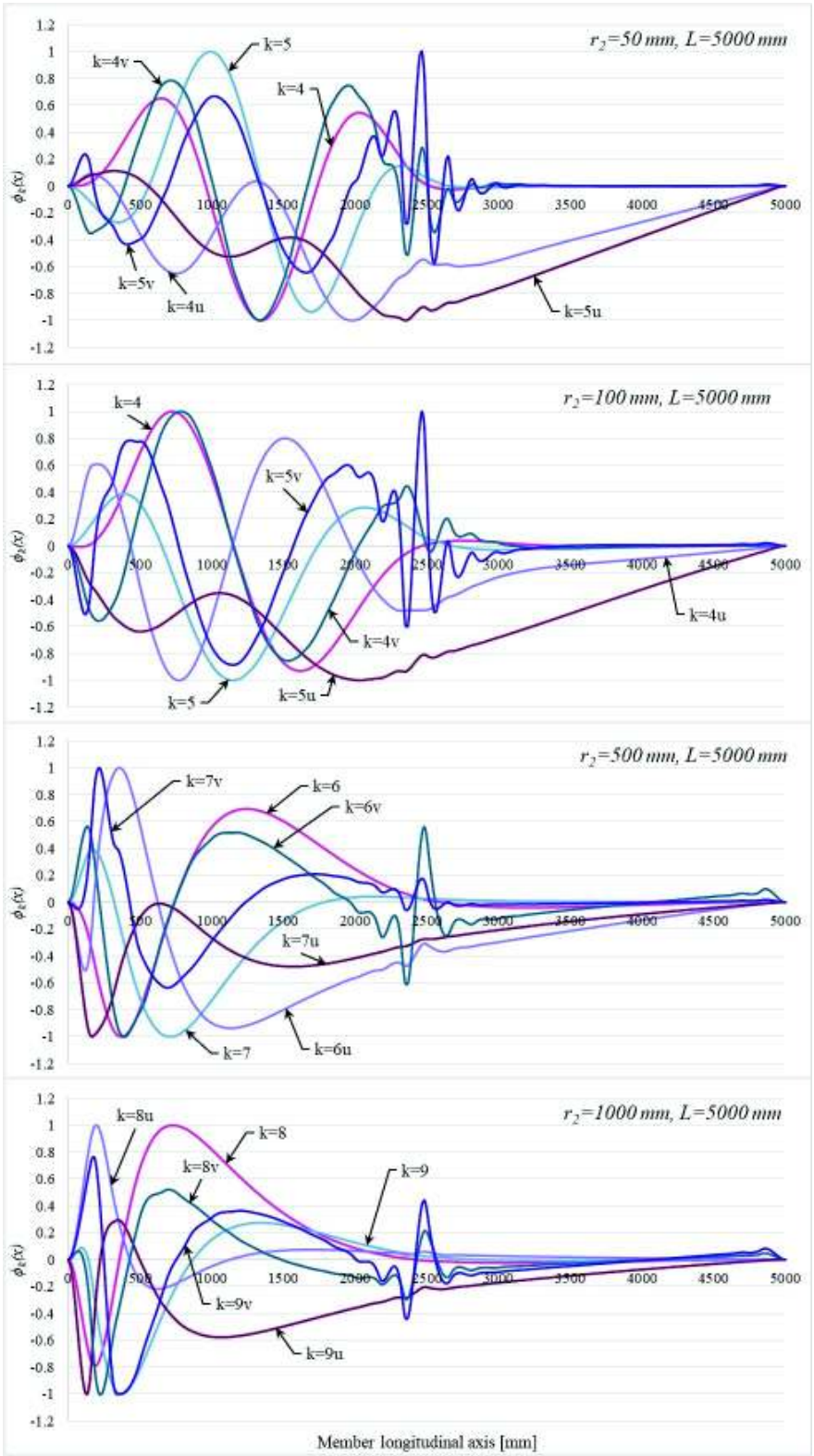

Figure 6.20: Long conical shells under torsion with variable thickness: the graphs of the modal amplitude functions $\phi_k(x)$.

Table 6.6: SFEA vs GBT-FEM results for long conical shells under torsion with variable thickness.

r_2=50 mm				
L [mm]	**λ_c SFEA**	**λ_c GBT-FEM**	**Differences**	**k**
2000	0.31169	0.3124	0.23%	4+5
5000	0.17267	0.1744	0.99%	4+5
r_2=100 mm				
L [mm]	**λ_c SFEA**	**λ_c GBT-FEM**	**Differences**	**k**
2000	0.3529	0.3503	0.74%	6+7
5000	0.2099	0.2155	2.60%	4+5
r_2=500 mm				
L [mm]	**λ_c SFEA**	**λ_c GBT-FEM**	**Differences**	**k**
2000	0.73033	0.7601	3.92%	10+11
5000	0.48142	0.5017	4.04%	6+7
r_2=1000 mm				
L [mm]	**λ_c SFEA**	**λ_c GBT-FEM**	**Differences**	**k**
2000	1.0683	1.0574	1.03%	12+13
5000	0.69041	0.7161	3.59%	8+9

6.4. Conclusions

In the case of conical shells under torsion, unlike the axially compressed conical shell case, the deformation modes are coupled. This means that the GBT system of differential equations is coupled and the unknowns are determined by simultaneously solving all the equations of the system (this poses no problem within a finite element procedure, although the computational cost obviously increases). Also, the geometric matrix X^{τ}_{4ik} (see Eq. (3.39)) is not diagonal. The critical buckling mode resulting from the buckling analysis of conical shells under torsion is a combination of two similar shell-type deformation modes with the same order m. This torsion behavior was also remarked by Silvestre [120]. Besides the shell-type deformation modes, the buckling behavior of conical shells under torsion is also described by the "u" and "v" shear deformation modes. The introduction of shear deformation modes in the Matlab code adapted for conical shells under torsion was necessary to achieve results with differences under 5% with respect to the SFEA.

In order to validate the proposed formulation, the results determined by SFEA were compared to the results determined by the GBT-based FE procedure. The numerical examples were divided into two main categories: (i) conical shells with constant thickness and (ii) conical shells with variable thickness. Then the numerical examples were analysed according to the length of the conical shell as

follows: (i) short conical shells (*L<1000 mm*), medium conical shells (*L* ranges *1000 between 2000 mm*) and long conical shells (*L≥2000 mm*).

According to the results, as the length of the conical shell increases, the critical buckling coefficient λ_c and the order of the cross section deformation mode *k* decrease. There were also exceptions when the order of the cross section deformation mode *k* remained unchanged. For example, in the case of conical shells with constant thickness, for a bottom radius r_2*=50 mm* and length *L≥2000 mm*, the cross section deformation mode *k* remains 4+5 (see Table 6.3). Also, in the case of conical shells with variable thickness, the order of the cross section deformation mode remains unchanged in the following situations: for r_2*=50 mm* and *L* ranging between *1000 and 2000 mm*, *k* stays 6+7 (see Table 6.5), for r_2*=1000 mm* and *L* ranging between *1000 and 2000 mm* (see Table 6.5), *k* stays 12+13 and for r_2*=50 mm* and *L≥2000 mm*, *k* remains 4+5 (see Table 6.6). Also, from the results one can remark that the index of the deformation modes *m* ranges between *2* and *7*, which means that the order of the cross section deformation mode *k* starts from 4+5, in case of long conical shells and small values of the bottom radius r_2, and may reach 14+15 in case of very short conical shells. For example, *k=14+15* for a conical shell with variable thickness,r_2*=100 mm* and *L=200 mm* (see Table 6.4).

In the case of conical shells with variable thickness, according to the SFEA results and the normalized graphs of the modal amplitude functions $\phi_k(x)$, the largest torsion deformations occur in the area of smaller thickness (t_1*=1 mm*), which means that the cross sections at the zone with t_2*=2 mm* are stiffer. Also, in the graphs of the modal amplitude functions for "v" shear deformation modes. a jump occurs at the middle of the span, in the transition zone between thickness values, meaning that the transverse shear deformations have abrupt changes in that region.

The differences between the results determined by SFEA and the ones determined by the GBT-based FE procedure do not exceed 5%, proving once again that the proposed formulation can be applied to other loading and boundary condition cases, no matter the geometric configuration of the analysed shell.

Chapter VII
Conical Shells under Bending

7.1. Introduction

The present chapter studies the case of conical shells under bending. As in the case of conical shells under torsion, the geometric matrix $X_{2ik}^{\sigma x}$, where $j=2$ represents the bending, is not diagonal. As in the previous chapter, the GBT system of differential equations is coupled and the unknowns are determined by solving the equations of the system simultaneously.. As in the previous case, the "u" and "v" shear deformation modes were also inserted in the buckling analysis of conical shells under bending, because the differences between the results determined by SFEA and the ones determined by the GBT-based FE formulation exceeded 5% in their absence. Besides the shell-type and shear deformation modes, in the buckling of conical shells under bending also participate additional deformation modes. The additional deformation modes were inserted in the first order analysis and are mode 1, mode 2 and mode 3, presented in Chapter III, Section 3.3.2.2.

The critical buckling mode of the conical shells under bending is described either by the combination of shell-type deformation modes: 5+6+9+10+13+14+17+18+21+22+25+26, which are symmetric with respect to the bending plane, or 3+4+7+8+11+12+15+16+19+20+23+24, which are non-symmetric with respect to the bending plane. This buckling behavior was initially observed in cylindrical shells by Silvestre [120].

For the numerical examples presented in the following sections the conical shell from Figure 7.1 was considered. The conical shell is made of steel ($E=210$ *GPa*, $\mu=0.3$), the thickness of the wall is $t=1$ *mm* and the top radius is $r_1=50$ *mm*. The bottom radius r_2 ranges between *50 mm* and *1000 mm*, while the length of the structure L ranges between *48 mm* and *5000 mm*. All the conical shells from the numerical examples presented in the next sections are cantilever conical shells. The end section corresponding to the bottom radius r_2 is fixed (i.e. all the displacements are blocked), while the end section corresponding to the top radius r_1 is free.

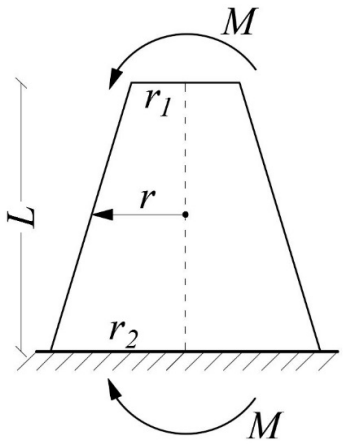

Figure 7.1: The geometry of the conical shell under pure bending.

In order to validate the GBT-based FE formulation for this loading case, the Matlab code [6] was adapted to conical shells under pure bending. Then, the next step was the performance of SFEA using Abaqus [7]. The models created in Abaqus were meshed with S4 shell finite elements and the size of the mesh ranged between *2 mm* and *20 mm*, depending on the geometric configuration of the analysed conical shell.

As in the case of axially compressed conical shells with stress concentrations presented in Chapter V, Section 5.3, the conical shells under bending were analysed in two steps: (i) the first step was the first order analysis from which the normal meridional stresses σ_{xx}^{0}, normal hoop stresses $\sigma_{\theta\theta}^{0}$ and shear stresses $\tau_{x\theta}^{0}$ resulted and (ii) the second step was the buckling analysis of the conical shells using the stresses determined from the first order analysis.

7.2. First Order Analysis of Conical Shells under Bending

The first order analysis of conical shells under bending was run using the algorithm presented in Section 4.3.1 from Chapter IV. In the case of axially compressed conical shells with stress concentrations, the additional deformation modes, described in Chapter III, Section 3.3.2.2, used in the first order analysis are as follows: the axial extension mode, the axisymmetric extension mode and the coupling between the axial extension and axisymmetric modes. In the case of conical shells under bending, the additional deformation modes used in the first order analysis are modes 1, 2 and 3 (see Chapter III, Section 3.3.2.2).

The initial load used in the SFEA and GBT models is applied at the conical shell's free end (at $x=0$) and it is distributed along the cross-section circumference as a sinusoid (see Figure 7.2). The maximum value of the initial stress is $P_{max}=1000\ N/mm^2$ and the variation law is $P=P_{max}\cdot sin\theta$.

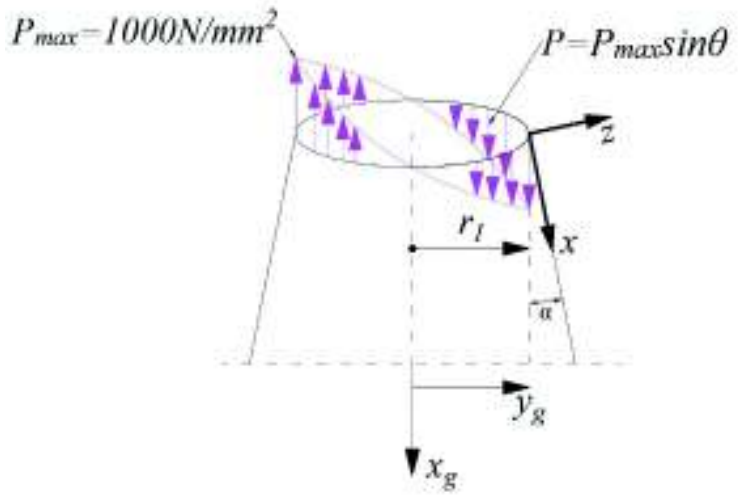

Figure 7.2: The distribution of the load at the free end of a conical shell under bending.

The vector of equivalent nodal forces was determined by Eq. (4.6). Thus, in case of conical shells under bending, the vector of equivalent nodal forces for the first node at the free end of the structure has the following form:

$$f^{(e)} = \{P_0 c \quad 0 \quad 0 \quad 0 \quad 0 \quad 0 \quad 0 \quad 0 \quad 0 \quad -P_0 s \quad 0 \quad 0\}^T \tag{7.1}$$

where $P_0=P_{max}\cdot r_1\cdot\pi$, $c=\cos\alpha$, $s=\sin\alpha$ (see Figure 7.2). The first four components of the vector correspond to mode 1, the next four components correspond to mode 2 and the last four components correspond to mode 3.

As in the case of conical shells under torsion, the conical shells studied in this chapter were divided according to their length into two categories as follows: (i) short conical shells, with *L<1000 mm*, and (ii) long conical shells, with *L≥1000 mm*. The following paragraphs present the first order analysis of conical shells under bending through numerical examples.

7.2.1. Short Conical Shells

The short conical shells considered have a length *L<1000 mm*. In the numerical examples for the first order analysis the following lengths were considered:

(i) for conical shells with the bottom radius r_2*=50 mm* and r_2*=100 mm*, the lengths are as follows: *48 mm*, *240 mm*, *500 mm* and *800 mm*.

(ii) for conical shells with the bottom radius r_2*=500 mm* and r_2*=1000 mm*, the lengths are *500 mm* and *800 mm*.

Conical shells with large values of the bottom radius r_2 and *L<500 mm* are not considered, because in this case these structures would not be able to be considered as "bars", due to the large value of the r_2/L ratio (the slope of the conical shell's meridian is very large).

Figure 7.3 represents the deformed configuration of a conical shell having the bottom radius r_2=*100 mm* and alength *L=48 mm* resulting from SFEA with Abaqus [7], while Figure 7.4 presents the same deformed configuration, this time obtained from the GBT-based FE procedure performed with Matlab. According to the figure, at the free end, where the load is applied, the deformations are very large and also there are stress concentrations. These stress concentrations can be clearly observed in the graphs of Figure 7.5, Figure 7.6 and Figure 7.7. These figures illustrate the normal meridional stresses σ_{xx}^{0}, the normal hoop stresses $\sigma_{\theta\theta}^{0}$ and the shear stresses $\tau_{x\theta}^{0}$ resulting from SFEA and also the GBT-based FE formulation. The stress concentrations are represented on the left side of the graphs.

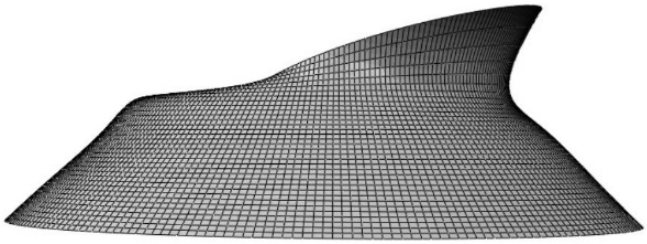

Figure 7.3: The deformed configuration of a short conical shell under bending resulting from SFEA (r_2=*100 mm*, *L=48 mm*).

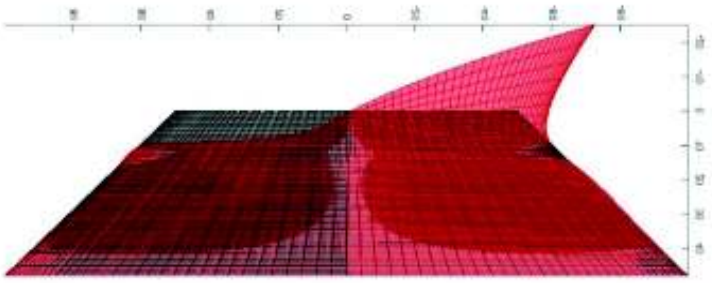

Figure 7.4: The deformed configuration of a short conical shell under bending resulting from the GBT-based FE procedure performed in Matlab (r_2=*100 mm*, *L=48 mm*).

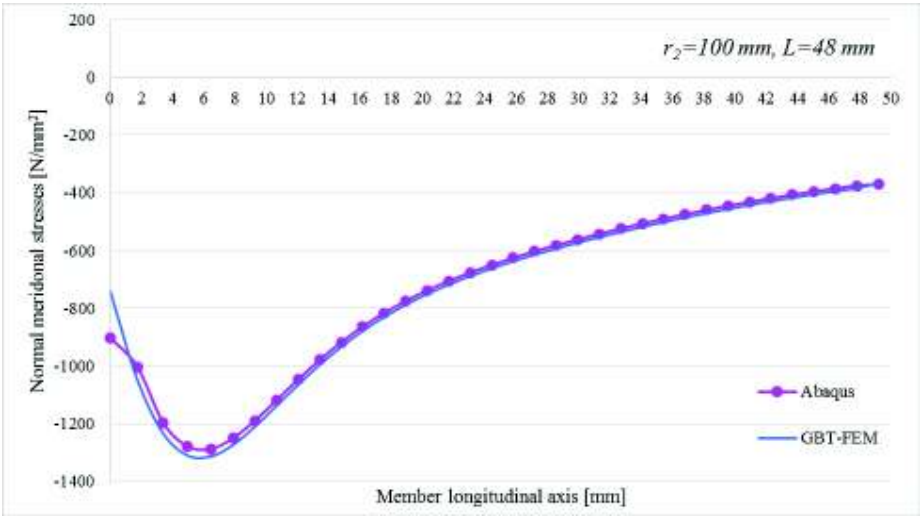

Figure 7.5: The normal meridional stresses σ^{0}_{xx} resulting from SFEA and GBT-based FE formulation for a conical shell with r_2=*100 mm* and *L=48 mm*.

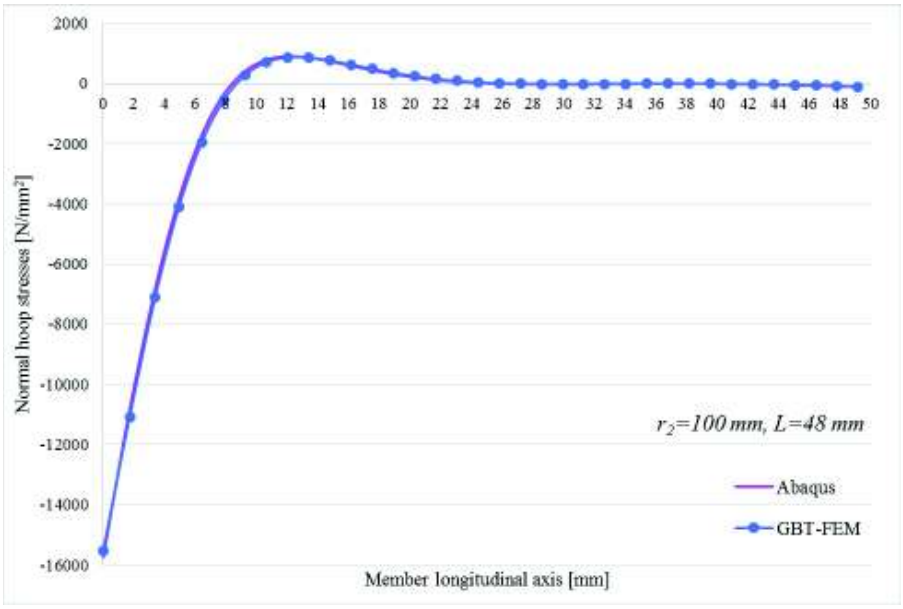

Figure 7.6: The normal hoop stresses $\sigma^{0}_{\theta\theta}$ resulting from SFEA and GBT-based FE formulation for a conical shell with r_2=*100 mm* and *L=48 mm*.

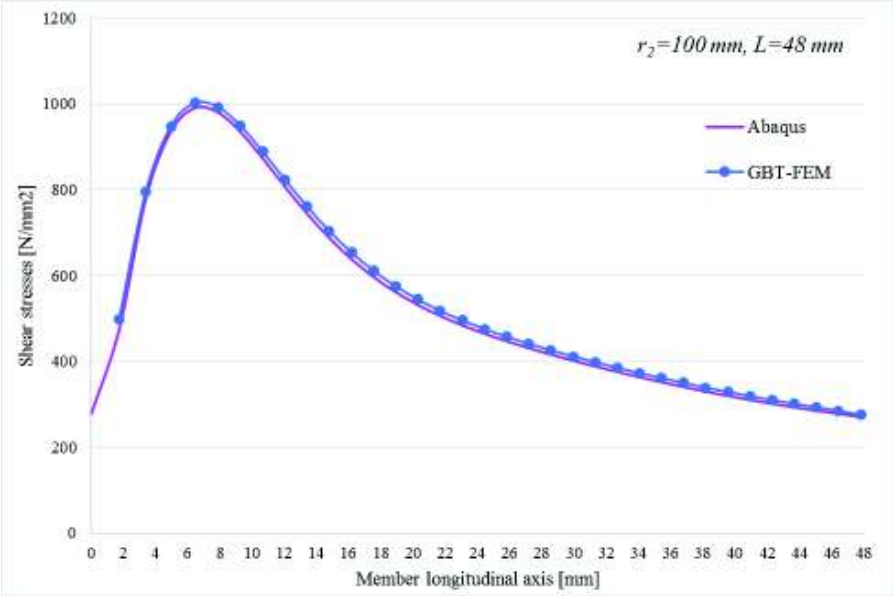

Figure 7.7: The shear stresses $\tau_{x\theta}^{0}$ resulting from SFEA and GBT-based FE formulation for a conical shell with r_2=100 mm și L=48 mm.

7.2.2. Long Conical Shells

Long conical shells have a length $L \geq 1000$ mm. In the first order analysis of the numerical examples the following lengths were considered: *1000 mm*, *2000 mm* and *5000 mm*.

Figure 7.8 illustrates the deformed configuration of a conical shell with a bottom radius r_2=100 mm and length L=1000 mm, resulting from SFEA, while Figure 7.9 presents the first order deformed configuration of the same conical shell, but this time resulting from the GBT-based FE formulation. Unlike the short conical shells (i.e. r_2=100 mm, L=48 mm), in the case of long conical shells the stress concentrations at the free end, where the load is applied, are, generally, smaller. However, the deformations are large, as in the previous case. According to Figure 7.10, which represents the graphs of the normal meridional stresses σ_{xx}^{0} resulting from SFEA and the GBT-based FE procedure, at the free end of the structure (at the left side of the graph) the stress concentrations are so small that they could be neglected. But in the case of normal hoop stresses $\sigma_{\theta\theta}^{0}$ (see Figure 7.11) and shear stresses $\tau_{x\theta}^{0}$ (see Figure 7.12), the stress concentrations at the conical shell's free end cannot be neglected. Also according to Figure 7.11 and Figure 7.12 stress concentrations also occur at the fixed end.

Regardless of the length, the stress concentrations at the end sections must be taken into account in the buckling analysis of conical shells under bending, otherwise the differences between the results determined by the two modeling procedures (i.e. SFEA and GBT-based FE formulation) will exceed 5%.

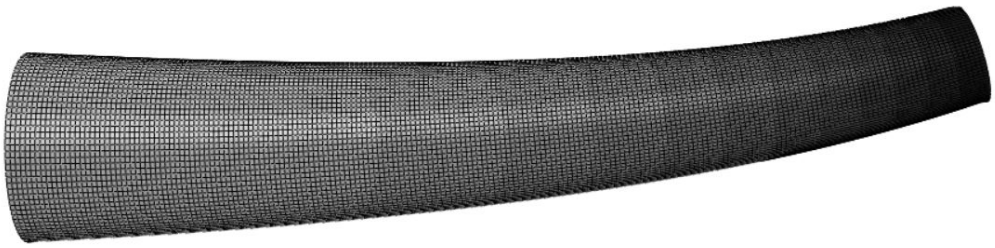

Figure 7.8: The deformed configuration of a long conical shell under bending resulting from SFEA (r_2=*100 mm*, *L=1000 mm*).

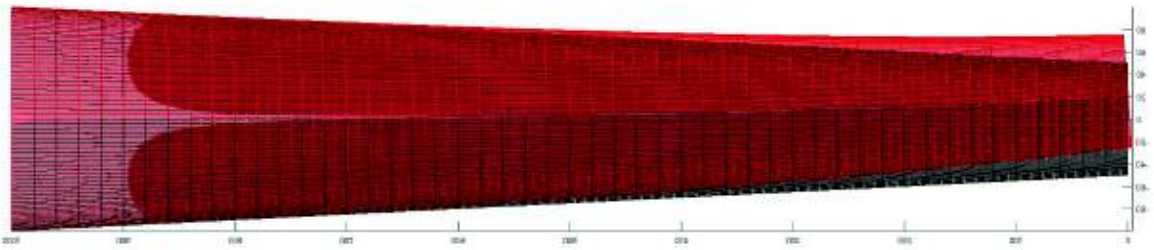

Figure 7.9: The deformed configuration of a long conical shell under bending resulting from the GBT-based FE procedure performed with Matlab code (r_2=*100 mm*, *L=1000 mm*).

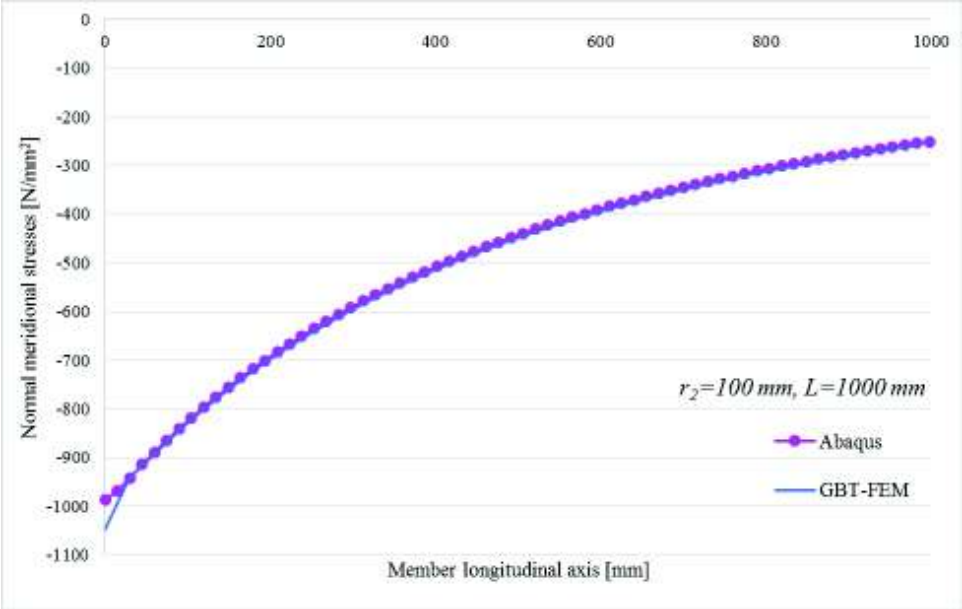

Figure 7.10: The normal meridional stresses σ_{xx}^{0} resulting from SFEA and GBT-based FE formulation for a conical shell with r_2=*100 mm* and *L=1000 mm*.

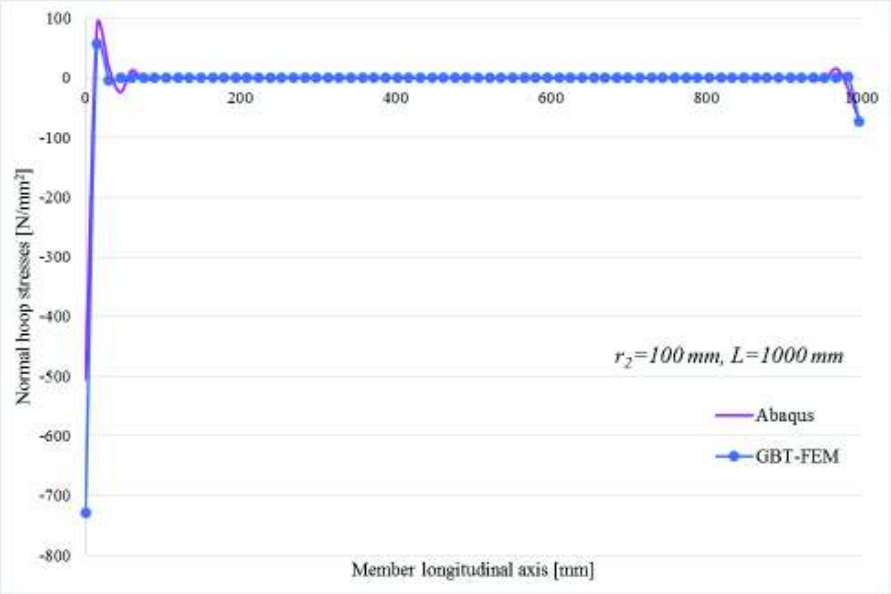

Figure 7.11: The normal hoop stresses $\sigma^0_{\theta\theta}$ resulting from SFEA and GBT-based FE formulation for a conical shell with r_2=*100 mm* and *L=1000 mm*.

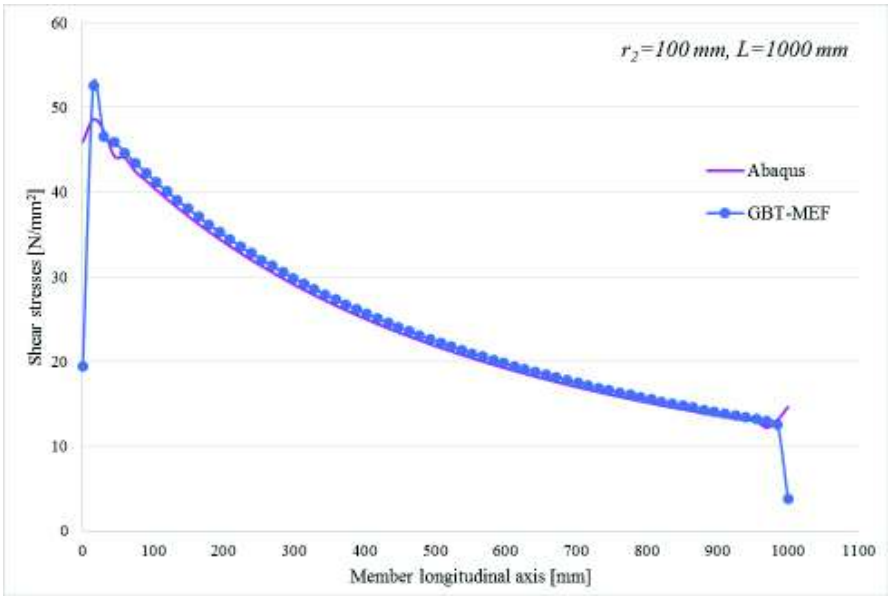

Figure 7.12: The shear stresses $\tau^0_{x\theta}$ resulting from SFEA and GBT-based FE formulation for a conical shell with r_2=*100 mm* și *L=1000 mm*.

7.3. Buckling Analysis of Conical Shells under Bending

The following section presents the buckling analysis of conical shells under bending. The buckling analysis was conducted using the stresses resulting from the first order analysis described in the previous section.. As in the case of conical shells under torsion, the conical shells under bending were divided according to their length, into two categories: (i) short conical shells with *L<1000 mm* and (ii) long conical shells with *L≥1000 mm*.

7.3.1. Short Conical Shells

The short conical shells have a length $L<1000\ mm$. For the numerical examples presented in this section, the following lengths were selected:

(i) for conical shells with a bottom radius $r_2=50\ mm$ and $r_2=100\ mm$, the lengths are: *48 mm*, *240 mm*, *500 mm* and *800 mm*.

(ii) for conical shells with a bottom radius $r_2=500\ mm$ and $r_2=1000\ mm$, the lengths are *500 mm* and *800 mm*.

The conical shells with large values of the bottom radius r_2 do not have lengths $L<500\ mm$, because the r_2/L ratio attains large values. This means that the slope of the conical shell's meridian is large and the structure may no longer be considered as a bar.

Figure 7.13 shows the critical buckling modes of short conical shells under bending with $L=48\ mm$ and a bottom radius r_2 equal to *50 mm* and *100 mm*, and with $L=500\ mm$ and a bottom radius equal to *500 mm*. Figure 7.14 presents the critical buckling modes of the same conical shells resulting from the GBT-based FE procedure performed with Matlab. Besides the critical buckling modes, the figures also illustrate the cross-section deformation modes and the values of the critical buckling coefficients λ_c. In case of bending, the buckling mode is a combination of either one of the following shell-type deformation modes:

(i) Deformation modes symmetric with respect to the bending plane: 5+6+9+10+13+14+17+18+21+22+25+26;

(ii) Deformation modes non-symmetric with respect to the bending plane: 3+4+7+8+11+12+15+16+19+20+23+24.

Figure 7.15, Figure 7.16 and Figure 7.17 represent the normalized graphs of the modal amplitude functions $\phi_k(x)$ for short conical shells under bending and having the bottom radius r_2 equal to *50 mm*, *100 mm* and *500 mm*. According to the graphs, as the value of the bottom radius r_2 increases, the longitudinal half-waves concentrate towards the conical shell's free end (at the left side of the graph). This means that, as the value of the bottom radius r_2 increases, the cross-sections from that area become stiffer.

Table 7.1 presents the differences between the results determined by SFEA and the ones determined by the GBT-based FE procedure. The results obtained with the proposed formulation were obtained with 50 finite elements. According to Table 7.1, the differences between the results do not exceed 5%. Also, according to Table 7.1, the value of the critical buckling coefficient increases as the length of the structure increases, except for conical shells with $r_2=50\ mm$, where the value of the critical buckling coefficient decreases as the length increases.

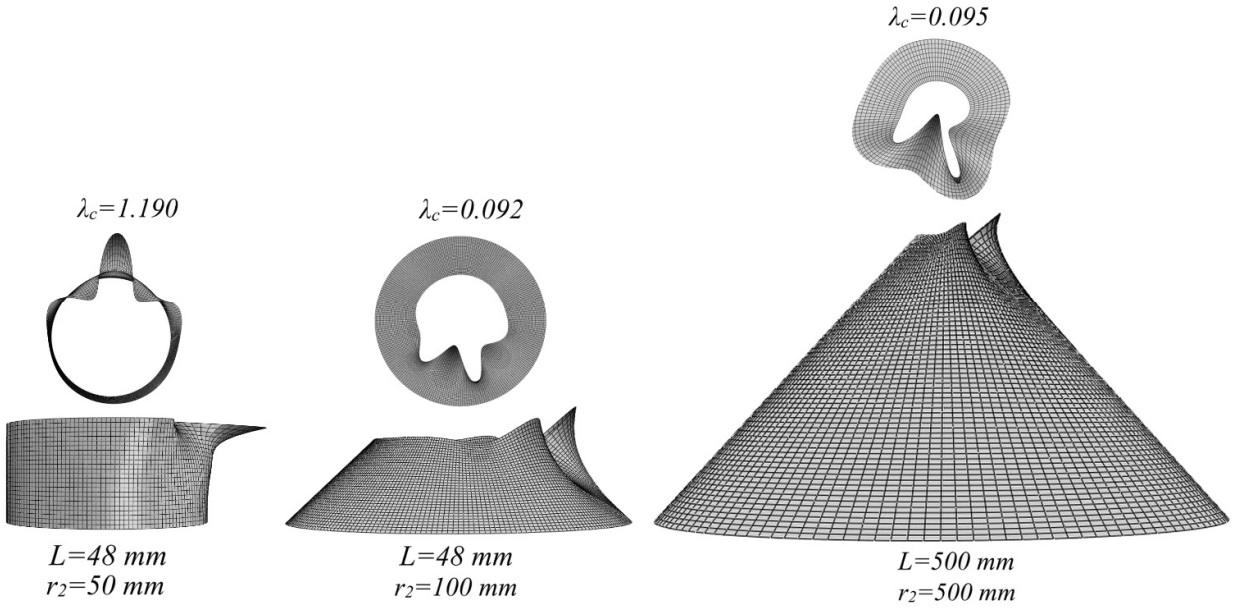

Figure 7.13: The critical buckling modes of short conical shells under bending: *L=48 mm*, r_2*=50 mm* and r_2*=100 mm*, and *L=500 mm*, r_2*=500 mm* and r_2*=1000 mm*, resulting from SFEA.

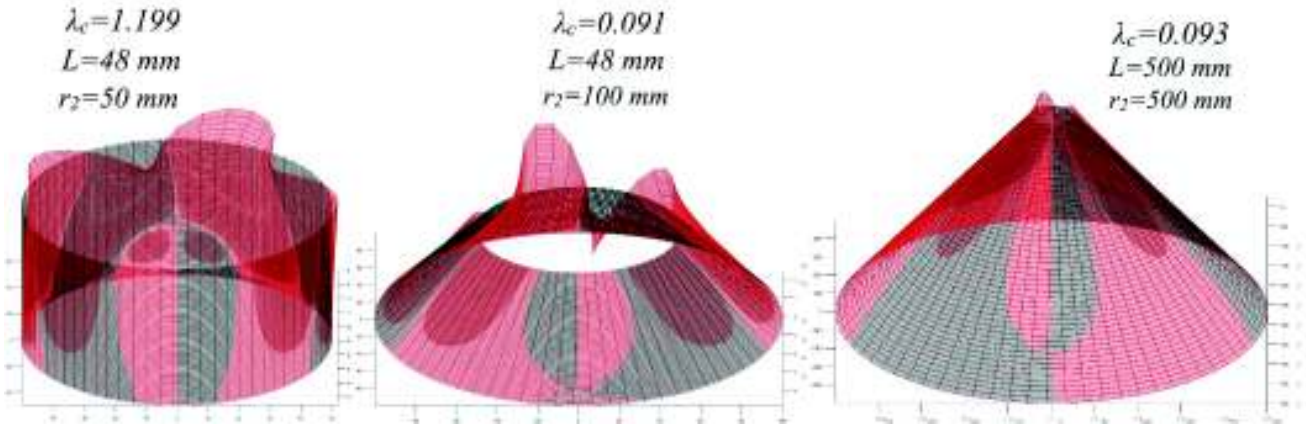

Figure 7.14: The critical buckling modes of short conical shells under bending: *L=48 mm*, r_2*=50 mm* and r_2*=100 mm*, and *L=500 mm*, r_2*=500 mm* and r_2*=1000 mm*, resulting from the GBT-based FE procedure with Matlab code.

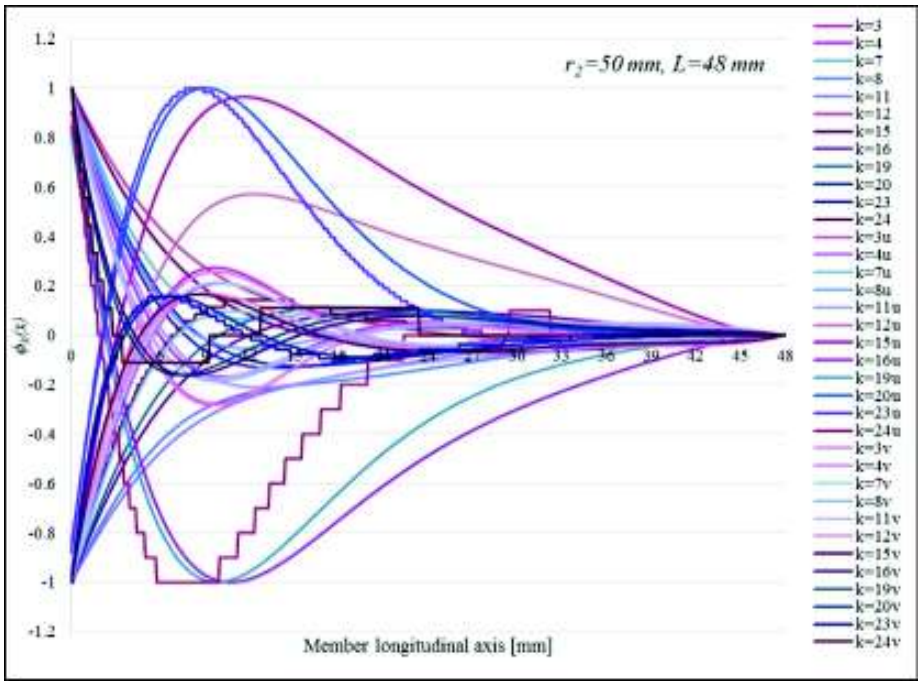

Figure 7.15: Short conical shells under bending (r_2=*50 mm*, *L=48 mm*): the graphs of the modal amplitude functions $\phi_k(x)$.

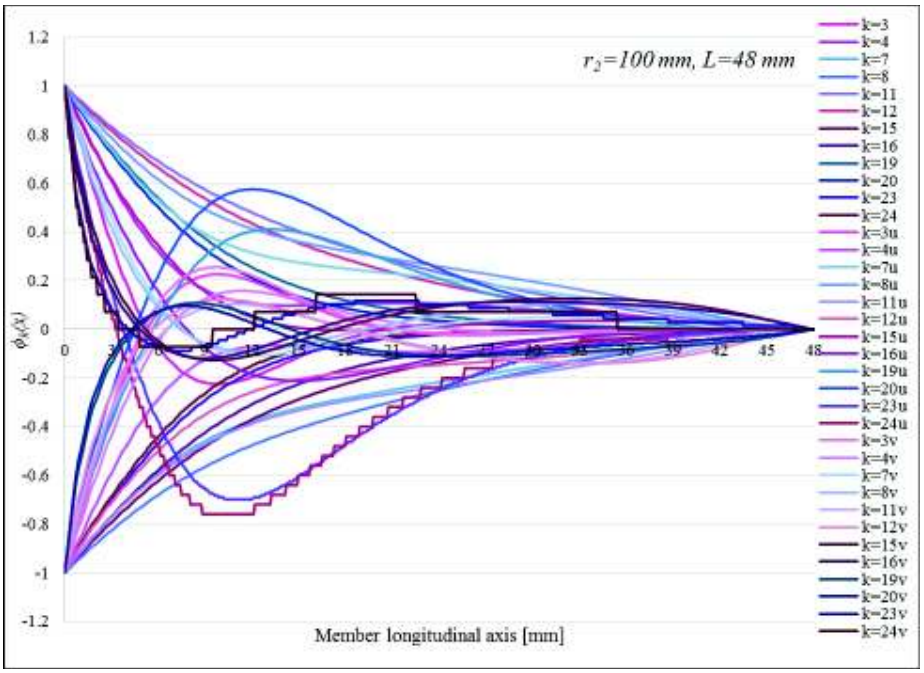

Figure 7.16: Short conical shells under bending (r_2=*100 mm*, *L=48 mm*): the graphs of the modal amplitude functions $\phi_k(x)$.

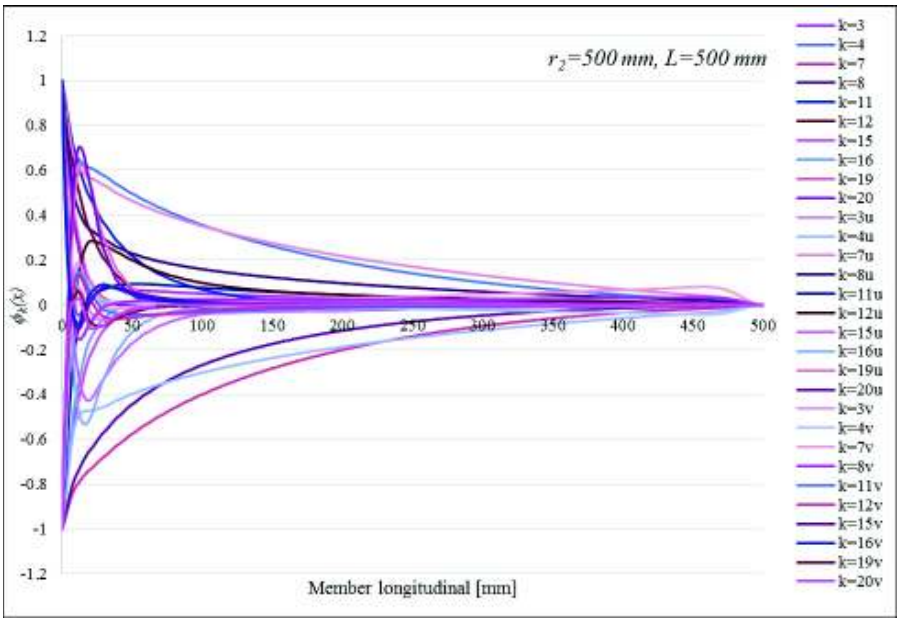

Figure 7.17: Short conical shells under bending (r_2=*500 mm*, *L=500 mm*): the graphs of the modal amplitude functions $\phi_k(x)$.

Table 7.1: SFEA vs GBT-FEM results for short conical shells under bending.

r_2=50 mm			
***L* [mm]**	**λ_c SFEA**	**λ_c GBT-FEM**	**Differences**
48	1.1904	1.1999	0.79%
240	1.0749	1.0831	0.76%
500	1.0575	1.0772	1.83%
r_2=100 mm			
***L* [mm]**	**λ_c SFEA**	**λ_c GBT-FEM**	**Differences**
48	0.0923528	0.0917	0.71%
240	0.34877	0.3556	1.92%
500	0.57953	0.5719	1.33%
r_2=500 mm			
***L* [mm]**	**λ_c SFEA**	**λ_c GBT-FEM**	**Differences**
500	0.094919	0.0938	1.19%
800	0.14984	0.1499	0.04%
r_2=1000 mm			
***L* [mm]**	**λ_c SFEA**	**λ_c GBT-FEM**	**Differences**
500	0.0405264	0.0397	2.08%
800	0.0688067	0.0682	0.89%

7.3.2. Long Conical Shells

Long conical shells have a length $L \geq 1000\ mm$. For the numerical examples presented in this section the following lengths were considered: *1000 mm*, *2000 mm* and *5000 mm*.

Figure 7.18 presents the critical buckling modes of the long conical shells under bending having a length $L=2000\ mm$ and the values of the critical buckling coefficients λ_c resulting from SFEA. Figure 7.19 illustrates the critical buckling modes of the same conical shells resulting from the GBT-based FE procedure performed with Matlab. Figure 7.20, Figure 7.21, Figure 7.22 and Figure 7.23 represent the normalized graphs of the modal amplitude functions $\phi_k(x)$ for long conical shells under bending with $L=2000\ mm$ and r_2 equal to *50 mm*, *100 mm*, *500 mm* and *1000 mm*.

As in the case presented in the previous section, the value of the critical buckling coefficient increases with the length, except for conical shells with $r_2=50\ mm$, where the value of λ_c decreases as the length increases. Also, the buckling mode is a combination of several shell-type deformation modes. In case of long conical shells, the longitudinal half-waves of the modal amplitude functions are concentrated towards the conical shell's free end (at the left side of the graph), which means that the end section, where the load is applied, is the area where most of the buckling deformations are concentrated. Also, according to the graphs of the modal amplitude functions, the shell-type deformation modes 3+4+7+8 have the shape of the deformed cantilever under bending.

Table 7.2 shows the differences between the results determined by the two modeling procedures and analysis (i.e. SFEA and GBT-based FE formulation). The differences do not exceed 5%.

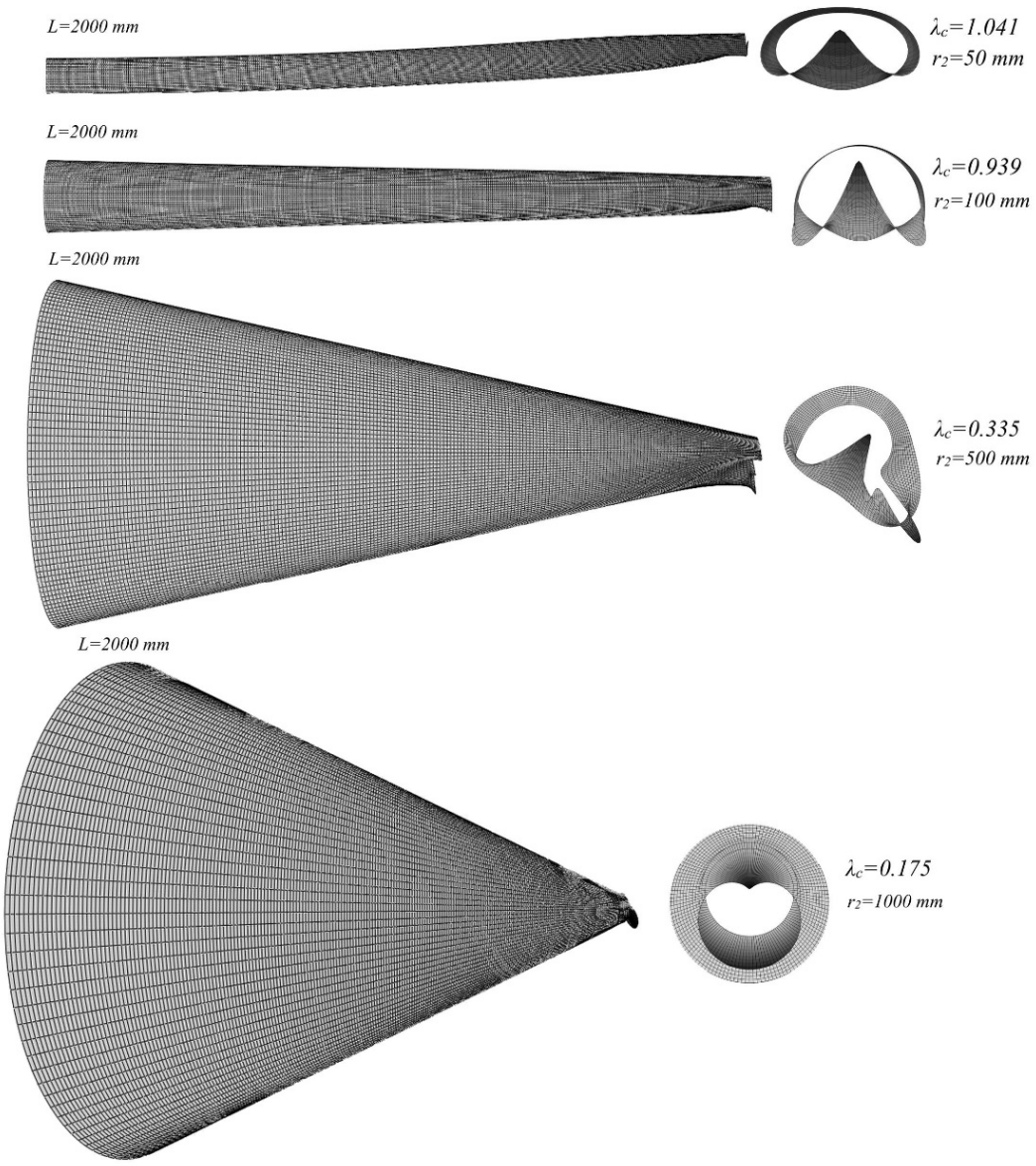

Figure 7.18: The critical buckling modes of long conical shells under bending having the length *L=2000 mm* resulting from SFEA.

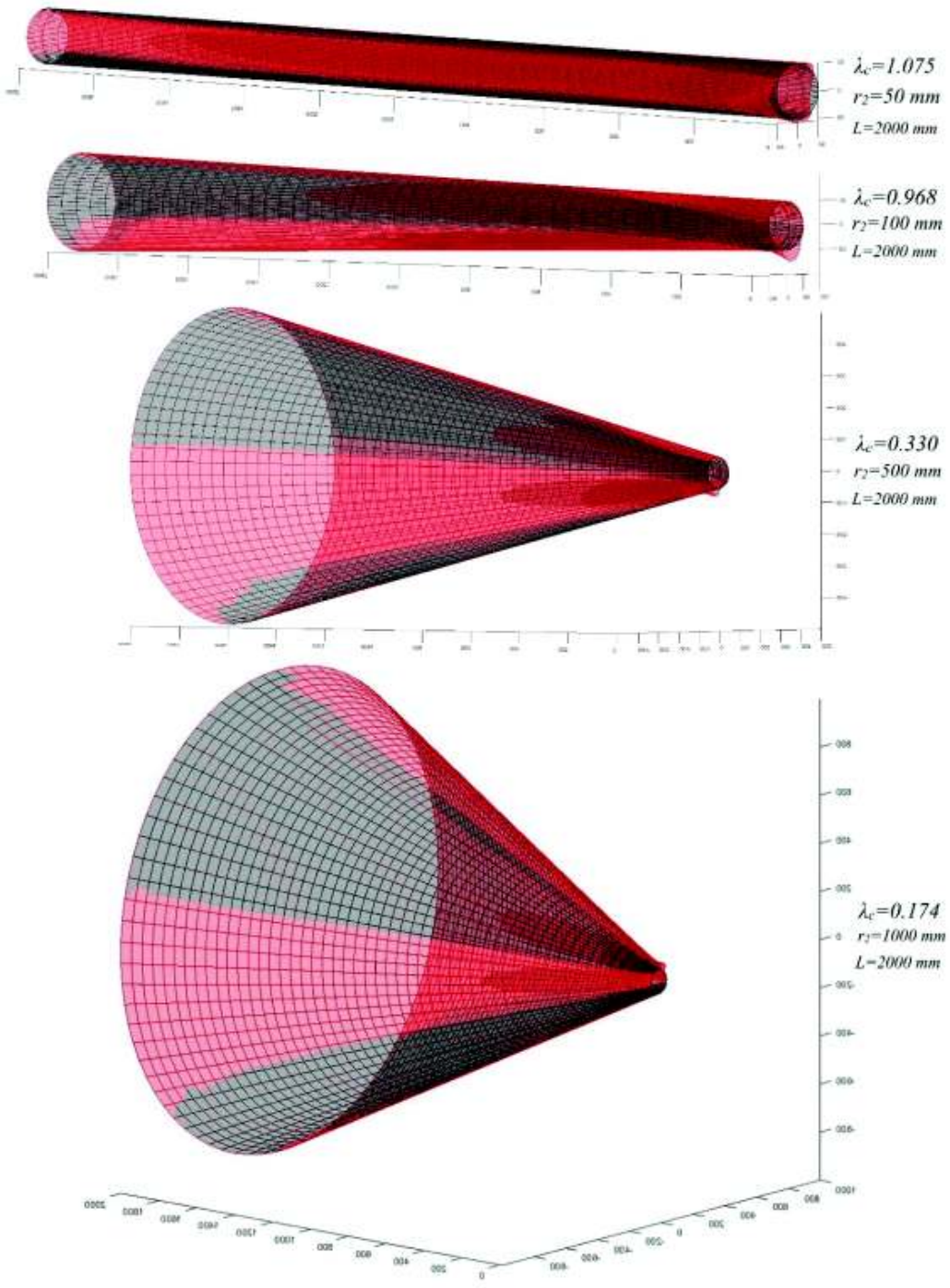

Figure 7.19: The critical buckling modes of long conical shells under bending having the length *L=2000 mm* resulting from the GBT-based FE procedure performed with Matlab code.

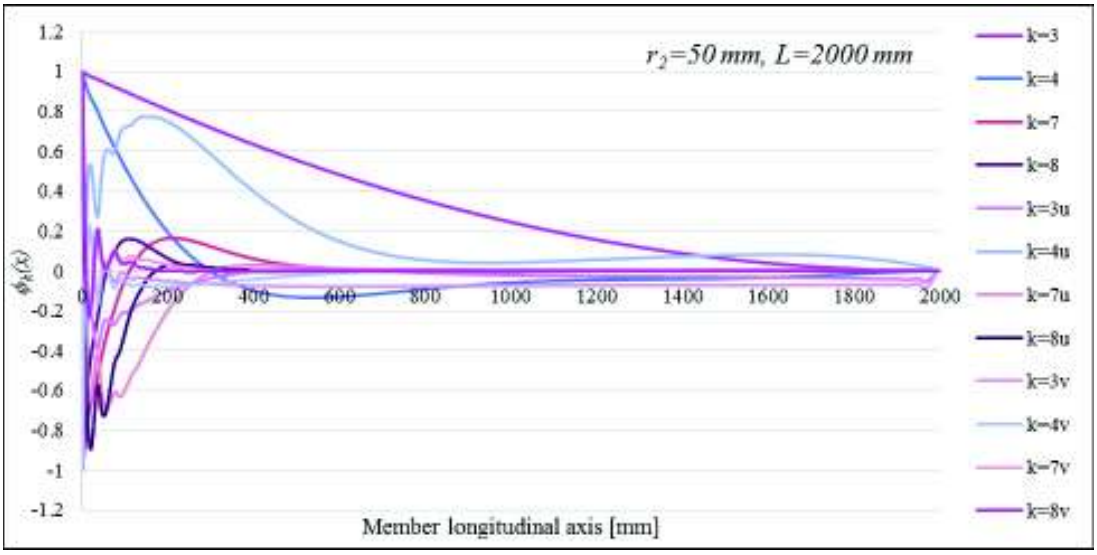

Figure 7.20: Long conical shells under bending (r_2=*50 mm*, *L=2000 mm*): the graphs of the modal amplitude functions $\phi_k(x)$.

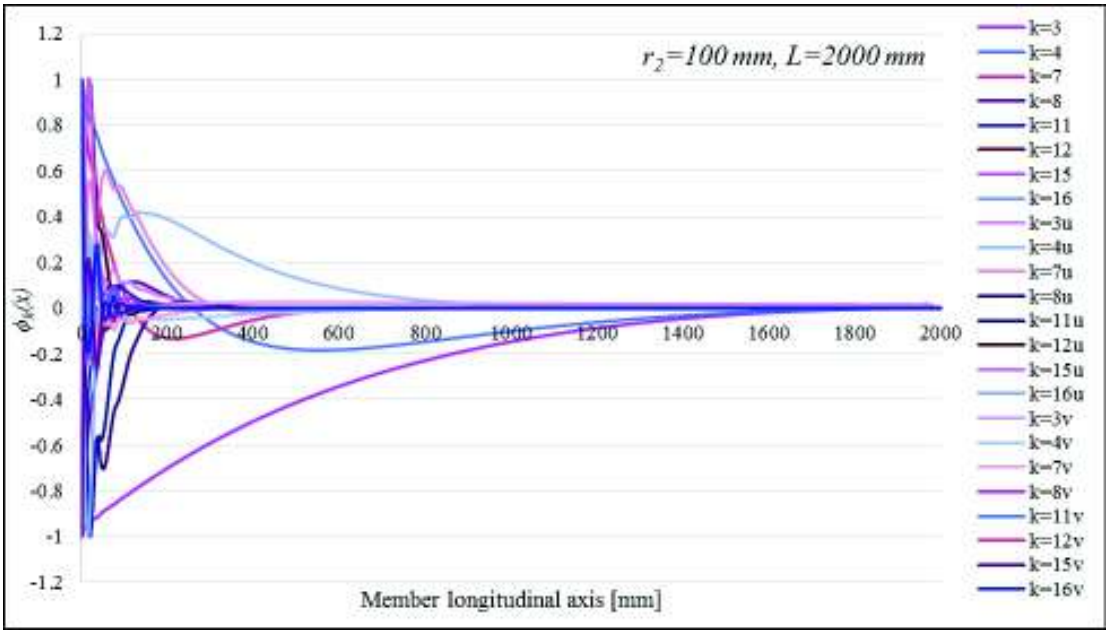

Figure 7.21: Long conical shells under bending (r_2=*100 mm*, *L=2000 mm*): the graphs of the modal amplitude functions $\phi_k(x)$.

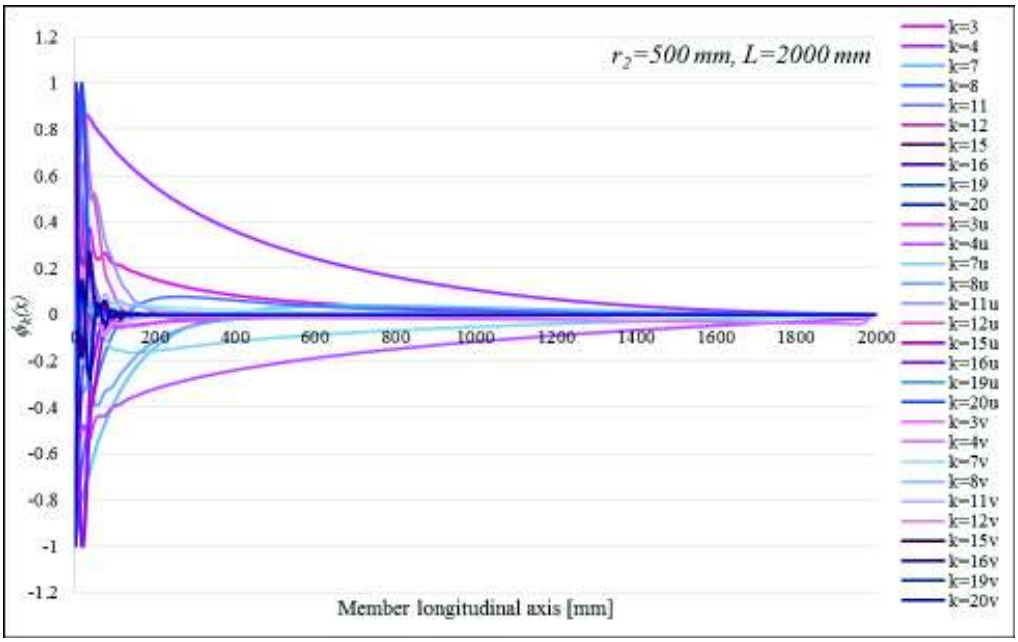

Figure 7.22: Long conical shells under bending (r_2=*500 mm*, *L=2000 mm*): the graphs of the modal amplitude functions $\phi_k(x)$.

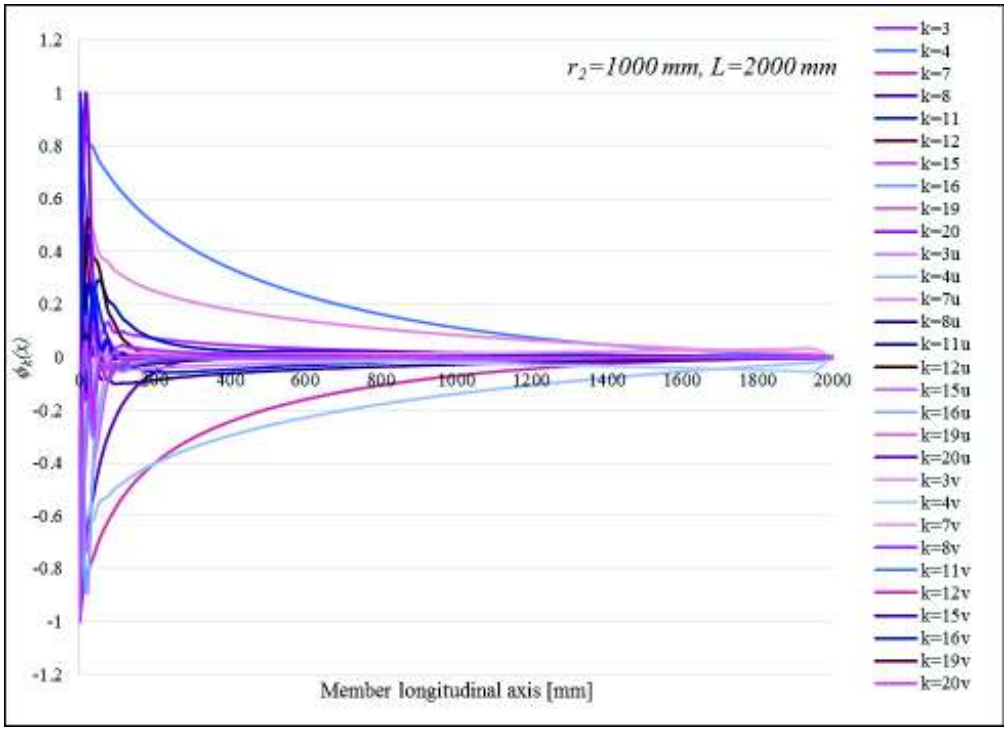

Figure 7.23: Long conical shells under bending (r_2=*1000 mm*, *L=2000 mm*): the graphs of the modal amplitude functions $\phi_k(x)$.

Table 7.2: SFEA vs GBT-FEM results for short conical shells under bending.

r_2=50 mm			
L [mm]	**λ_c SFEA**	**λ_c GBT-FEM**	**Differences**
1000	1.1168	1.0773	3.67%
2000	1.0408	1.0754	3.22%
5000	0.77438	0.8013	3.36%
r_2=100 mm			
L [mm]	**λ_c SFEA**	**λ_c GBT-FEM**	**Differences**
1000	0.79257	0.7755	2.20%
2000	0.93976	0.9684	2.96%
5000	1.1348	1.1409	0.53%
r_2=500 mm			
L [mm]	**λ_c SFEA**	**λ_c GBT-FEM**	**Differences**
1000	0.18484	0.1838	0.57%
2000	0.33473	0.3304	1.31%
5000	0.69759	0.7116	1.97%
r_2=1000 mm			
L [mm]	**λ_c SFEA**	**λ_c GBT-FEM**	**Differences**
1000	0.0881629	0.0869	1.45%
2000	0.17525	0.1744	0.49%
5000	0.41296	0.4338	4.80%

7.4. Conclusions

As in the case of conical shells under torsion, for conical shells under bending the geometric matrix $X_{2ik}^{\sigma x}$ (where *j=2* represents bending) is not diagonal, which means that the GBT system of differential equations is coupled. Unlike conical shells under axial compression or torsion, where the cross-section deformation mode is defined by the number of circumferential half-waves *k*, in the case of conical shells under bending the cross-section deformation mode is a combination of shell-type and shear deformation modes, as follows: (i) deformation modes symmetric with respect to the bending plane: 5+6+9+10+13+14+17+18+21+22+25+26 or (ii) deformation modes non-symmetric with respect the bending plane: 3+4+7+8+11+12+15+16+19+20+23+24.

The analysis of conical shells under bending consisted into two steps, as follows: (i) a first order analysis where the normal meridional, normal hoop and shear stresses were determined and (ii) a buckling analysis using the stresses determined from the first order analysis. Unlike the first order analysis of the axially compressed conical shells with stress concentrations (see Chapter V, Section

5.3), the first order analysis of conical shells under bending is described by the following deformation modes: (i) mode 1 (see Eq. (3.25)), (ii) mode 2 (see Eq. (3.26)) and (iii) mode 3 (see Eq. (3.27)). According to the first order analysis, regardless of the length of the conical shell, at the end sections stress concentrations occur (see Figure 7.5, Figure 7.6, Figure 7.7, Figure 7.11 and Figure 7.12) which must be taken into account in the buckling analysis, in order to have accurate results.

According to the buckling analysis, the value of the critical buckling coefficient λ_c increases along with the length L, except for conical shells with a bottom radius r_2=*50 mm*, where the critical buckling coefficient decreases as the length increases. Also, as the value of the bottom radius r_2 increases, the longitudinal half-waves of the modal amplitude functions $\phi_k(x)$ are concentrating towards the free end of the analysed conical shell, which shows that the cross-sections from the area of the bottom radius r_2 become stiffer as the value of r_2 increases. For long conical shells ($L \geq 1000$ *mm*), the modal amplitude functions of the shell-type deformation modes 3+4+7+8 have the shape of a deformed cantilever beam under pure bending (see Figure 7.20, Figure 7.21, Figure 7.22 and Figure 7.23).

The differences between the results determined by SFEA and the ones determined by the GBT-based FE formulation do not exceed 5%, proving once again that the proposed formulation can be applied in case of more complex loads, such as bending.

Chapter VIII
Conclusions

8.1. Conclusions of the Research

As it was demonstrated in the case studies presented in the previous chapters, the Generalized Beam Theory is a very efficient method to determine the buckling loads and the buckling modes of thin walled structures. Initially it was believed that GBT could only be applied for prismatic thin walled bars with constant cross-section along the longitudinal axis. Recent studies, presented in detail in Chapter II, Sections 2.5.3 and, respectively 2.5.4, have demonstrated that GBT could be extended for other types of thin walled structures such as bars with curved longitudinal axis [98], structures with circular and elliptic cross-section [120], [121] and structures with variable cross-section along the longitudinal axis [3], [4].

The following thesis presented the GBT extension for circular isotropic conical shells and the GBT-based Finite Element (FE) formulation for the first order and buckling analysis of these type of structures. The advantages of the GBT-based FE formulation, compared to SFEA, are the following:

(i) Fewer degrees of freedom are necessary to determine results with a precision similar to that obtained with refined SFEA;

(ii) In coupled instability problems, the proposed formulation provides the degree of modal participation which also provides valuable information regarding the buckling behavior of the analysed structures.

From the numerical examples presented in the previous chapters the following general remarks can be traced:

(i) The differences between the values of the critical buckling coefficients determined by SFEA and the ones determined by the proposed formulation do not exceed 5%, which means that the proposed formulation is considered valid and accurate.

(ii) The proposed formulation can be applied to any type of load, boundary conditions and geometric configurations (i.e. constant thickness or stepped variable thickness), which shows the fact that the GBT-based FE formulation is flexible.

(iii) The shear deformation modes, presented in Chapter III, Section 3.3.2.2., have significant effects on the final results in some load cases, as torsion or pure bending, in some cases of boundary conditions or geometric configuration (for example, in the case of axially compressed short conical shells).

The following sections summarize the conclusions of every case study described in this thesis.

8.1.2. Conclusions Concerning Axially Compressed Conical Shells

For axially compressed conical shells there were two main cases examined: (i) conical shells without stress concentrations and (ii) conical shells with stress concentrations. The conical shells without stress concentrations are the ones who have both end sections supported and the types of supports are fixed end, simple support or combinations between these. In this case, the stress concentrations that occur at the end sections have very low values and can be neglected. Therefore, the normal hoop stresses were neglected, while the normal meridional stresses were approximated by simplified expressions. The conical shells with important stress concentrations are cantilever structures. The axial force is applied at the free end, so at the respective end section stress concentrations occur. In this case, the normal hoop stresses can no longer be neglected, while the normal meridional stresses cannot be approximated by simplified expressions. The analysis of conical shells with stress concentrations had two steps: (i) the first order analysis where the normal merdional and hoop stresses were determined and (ii) the buckling analysis where the stresses determined in the first step were used.

In the case of short conical shells and, respectively conical shells with variable thickness, the differences between the results determined by the proposed formulation and the ones determined by SFEA did not exceed 5% if the shear deformation modes were included in the buckling analysis.

For the axially compressed conical shells, in the case where the shear deformation modes were not included in the analysis, the geometric matrix $X_{1ik}^{\sigma x}$ is diagonal. This means that the GBT system of differential equations is not coupled and the system's unknowns, the modal amplitude functions $\phi_k(x)$, may be determined by solving the equations separately for each deformation mode included in the analysis. This aspect simplifies the buckling analysis of axially compressed conical shells unlike other methods used in current practice, such as SFEA.

8.1.3. Conclusions Concerning Conical Shells under Torsion

Unlike axially compressed conical shells, in case of conical shells under torsion the geometric matrix X_{4ik}^{τ} is not diagonal. This means that the GBT system of differential equations is coupled, therefore the unknowns are determined by solving the system's equations simultaneously (this poses no problem within the developed FEM framework). The buckling mode that results in this case is a combination of two similar deformation modes with the same index *m*.

According to the analysed numerical examples, generally, the value of the critical buckling coefficient and the order of the shell-type deformation mode *k* decrease as the length of the structure increases. In the case of conical shells with variable thickness, in the thickness transition zone, large

deformations occur which are represented in the graphs of the modal amplitude functions. More exactly, deformations are observed in the graphs of the "v" shear modes.

8.1.4. Conclusions Concerning Conical Shells under Bending

The case of conical shells under bending is special since, unlike the two other cases, the buckling phenomenon is more complex. The analysis of conical shells under bending had two steps: (i) the first order analysis where the normal and shear stresses were determined and (ii) the buckling analysis where the stresses determined in the previous step were used.

As in the case of conical shells under torsion, the geometric matrix $X_{2ik}^{\sigma x}$ is not diagonal and the GBT system of differential equations is coupled. Therefore, the unknowns are determined by solving the system's equations simultaneously. The buckling mode that results from the analysis is a combination of shell-type and shear deformation modes as follows: (i) deformation modes symmetric with respect to the bending plane: 5+6+9+10+13+14+17+18+21+22+25+26 or (ii) deformation modes non-summetric with respect to the bending plane: 3+4+7+8+11+12+15+16+19+20+23+24.

According to the results obtained, the value of the critical buckling coefficient increases as the length of the structure increases, except for conical shells with a bottom radius r_2=*50 mm*, where the value of the critical buckling coefficient decreases as the length of the structure increases. This shows that, as the value of the bottom radius r_2 increases, the stiffness of the conical shell under bending increases as well.

8.2. Personal Contributions

The personal contributions of the thesis are as following:

(i) The introduction of the shear deformation modes in case of short conical shells with variable thickness under axial compression, in case of conical shells under torsion and in case of conical shells under bending.

(ii) The introduction of the additional deformation modes for the first order analysis of axially compressed conical shells with stress concentrations and for conical shells under bending.

(iii) The determination of the GBT cross-section stiffness matrices for shear deformation modes.

(iv) Determination of cross-section stiffness matrices for additional deformation modes, showing that the pre-buckling stresses need to be considered.

(v) The adaptation of the GBT based FE formulation to the first order analysis of conical shells under axial compression, torsion and bending.

(vi) The adaptation of the GBT based FE formulation to the buckling analysis of conical shells under axial compression, torsion and bending.

8.3. The Valorification of Results

The results determined from the analysed case studies were published in the following scientific papers:

(i) Adina-Ana Mureșan, Mihai Nedelcu and Rodrigo Gonçalves, „GBT-based FE formulation to analyse the buckling behaviour of isotropic conical shells with circular cross-section", Thin Walled Structures, vol. 134, pp. 84 – 101, Jan. 2019.

(ii) Mihai Nedelcu, Adina-Ana Mureșan, "GBT-based Finite Element formulation for elastic buckling analysis of conical shells", EUROSTEEL 2017, September 13–15, 2017, Copenhagen, Denmark.

(iii) Adina-Ana Mureșan, Mihai Nedelcu, "Analiza la flambaj elastic a structurilor conice folosind formularea în Element Finit bazată pe Teoria Generalizată a Grinzii", A 15-a CONFERINȚĂ NAȚIONALĂ DE CONSTRUCȚII METALICE, IAȘI, 16 – 17 Noiembrie 2017.

(iv) Adina-Ana Mureșan, Rodrigo Gonçalves and Mihai Nedelcu, „GBT Model For The Buckling Analysis Of Conical Shells With Stress Concentrations", Eighth International Conference on THIN-WALLED STRUCTURES, ICTWS 2018, Lisbon, Portugal, July 24-27, 2018.

(v) Adina-Ana Mureșan, Mihai Nedelcu, „The GBT based Finite Element formulation to analyse the buckling behaviour of conical shells", C65 International Conference, "Tradition and Innovation - 65 Years of Constructions in Transilvania", 15 – 17 November 2018, Cluj-Napoca, Romania.

8.4. Future Research

In the following thesis the GBT-based Finite Element formulation was applied to perform buckling analyses of circular conical shells under axial compression, under torsion and under bending. The proposed formulation may be applied to the buckling analysis of conical shells under other types of loads. For example, the proposed formulation may be applied in case of conical shells under eccentric compression. These cases may be the subject of future research, which will contribute to the investigation of the buckling behavior of conical shells.

Also, the GBT and the GBT-based FE formulation may be adapted for the analysis of arbitrary shells of revolution, meaning shells with curved meridian. GBT could also be adapted for thin-walled structures having arbitrary variable cross section.

Annex I

The Analytical Expressions of the Cross Section Stiffness Matrices

The pre-buckling stresses are considered constant along the cross section.

Index definition:

$$
\begin{aligned}
&m = k/2, && k = 2,4,6,...,n \\
&m = (k-1)/2, && k = 3,5,7,...,n+1 \\
&u = k + n \\
&v = k + 2n
\end{aligned}
$$

A. Shell-type Deformation Modes (*k*)

$$C_{kk} = A_{11}\pi r^3 + D_{11}\frac{\pi m^4}{c^2} r$$

$$D^1_{kk} = (A_{11} + 2\tilde{A}_{12} + \tilde{A}_{22})\pi s^2 r + \left[D_{22}\pi m^4 \left(\frac{s}{c}\right)^2 + D_{33}\pi m^2 \left(\frac{2m^2}{c} - c\right)^2 \right]\frac{1}{r}$$

$$D^2_{kk} = D_{12}\pi m^4 \left(1 - \left(\frac{m}{c}\right)^2\right)\frac{1}{r}$$

$$B_{kk} = \tilde{A}_{33}\pi m^2 s^2 \frac{1}{r} + \left[D_{22}\pi m^4 \left(\frac{m^2}{c} - c\right)^2 + D_{33} 4\pi m^2 \left(\frac{m^2}{c} - c\right)^2 s^2 \right]\frac{1}{r^3}$$

$$G_{kk} = \left[D_{22}\pi m^4 \left(1 - \left(\frac{m}{c}\right)^2\right) s - D_{33} 2\pi m^2 \left(2\left(\frac{m^2}{c}\right)^2 - 3m^2 + c^2\right) s \right]\frac{1}{r^2}$$

$$H_{kk} = \left(\tilde{A}_{11} + A_{12}\right)\pi s r^2 + D_{12}\pi m^4 \frac{s}{c^2}$$

$$X^{\sigma x}_{jkk} = \sigma^0_{xx}\pi m^2 \left(\left(\frac{m}{c}\right)^2 + 1\right) tr$$

$$X^{\sigma\theta}_{jkk} = \sigma^0_{\theta\theta}\pi m^2 \left(\frac{m^2}{c} - c\right)^2 \frac{t}{r}$$

$$X^{\tau}_{jkk} = \tau^0_{x\theta}\pi m^3 \left(\left(\frac{m}{c}\right)^2 + 1\right) t$$

B. „u" Shear Modes (*u*)

$$C_{uu} = A_{11}\pi r^3$$
$$D^1_{uu} = \left[(A_{11} + 2\tilde{A}_{12} + \tilde{A}_{22})\pi s^2 + A_{33}\pi m^2 \right] r$$
$$H_{uu} = \left(\tilde{A}_{11} + A_{12} \right) \pi s r^2$$

C. „v" Shear Modes (*v*)

$$D^1_{vv} = A_{33}\pi m^2 r + D_{33}\pi m^2 c^2 \frac{1}{r}$$
$$B_{vv} = \left[A_{22}\pi m^4 + \tilde{A}_{33}\pi m^2 s^2 \right] \frac{1}{r} + \left[D_{22}\pi m^4 c^2 + D_{33} 4\pi m^2 s^2 c^2 \right] \frac{1}{r^3}$$
$$G_{vv} = -\tilde{A}_{33}\pi m^2 s - D_{33} 2\pi m^2 c^2 s$$
$$X^{\sigma x}_{jvv} = \sigma^0_{xx}\pi m^2 t r$$
$$X^{\sigma \theta}_{jvv} = \sigma^0_{\theta\theta}\pi m^2 c^2 \frac{t}{r}$$

D. Shell-type Modes Coupled with "u" Shear Modes

$$C_{ku} = C_{uk} = C_{uu}$$
$$D^1_{ku} = D^1_{uk} = (A_{11} + 2\tilde{A}_{12} + \tilde{A}_{22})\pi s^2 r$$
$$G_{ku} = A_{33}\pi m^2 s$$
$$H_{ku} = \left(\tilde{A}_{11} + A_{12} \right) \pi s r^2$$

E. Shell-type Modes Coupled with "v" Shear Modes

$$D_{kv}^{1} = D_{vk}^{1} = D_{33}\pi m^2\left(c^2 - 2m^2\right)\frac{1}{r}$$

$$D_{kv}^{2} = A_{12}\pi m^2 r + D_{12}\pi m^4\frac{1}{r}$$

$$B_{kv} = \tilde{A}_{33}\pi m^2 s^2\frac{1}{r} + \left[D_{22}\pi m^4\left(c^2 - m^2\right) + D_{33}4\pi m^2\left(c^2 - m^2\right)s^2\right]\frac{1}{r^3}$$

$$G_{kv} = -A_{33}\pi m^2 s + \left[-D_{33}2\pi m^2\left(c^2 - m^2\right)s\right]\frac{1}{r^2}$$

$$G_{vk} = \left(A_{12} + \tilde{A}_{22}\right)\pi m^2 s + \left[D_{22}\pi m^4 s - D_{33}2\pi m^2\left(c - \frac{m^2}{c}\right)cs\right]\frac{1}{r^2}$$

$$X_{jkv}^{\sigma x} = X_{jvk}^{\sigma x} = \sigma_{xx}^{0}\pi m^2 tr$$

$$X_{jkv}^{\sigma\theta} = X_{jvk}^{\sigma\theta} = \sigma_{\theta\theta}^{0}\pi m^2 c^2\frac{t}{r}$$

$$X_{jkv}^{\tau} = \tau_{x\theta}^{0}\pi m^3 t$$

F. „u" Shear Modes Coupled with „v" Shear Modes

$$D_{uv}^{1} = D_{vu}^{1} = -A_{33}\pi m^2 r$$

$$D_{vu}^{2} = A_{12}\pi m^2 r$$

$$G_{vu} = -\left(A_{12} + \tilde{A}_{22}\right)\pi ms + \tilde{A}_{33}\pi m^2 s$$

Annex II
The List of Figures

Chapter I: Introduction

Chapter III: Generalized Beam Theory

Chapter IV: The GBT-based Finite Element Formulation

Chapter V: Axially Compressed Conical Shells

Chapter VI: Conical Shells under Torsion

Chapter VII: Conical Shells under Bending

Annex III
The List of Tables

Chapter V: Axially Compressed Conical Shells

Chapter VI: Conical Shells under Torsion

Chapter VII: Conical Shells under Bending

References

[1] W.-W. Yu and R. A. LaBoube, Cold-Formed Steel Design, 4th ed. United States of America: Wiley. John Wiley & Sons Inc., 2010.

[2] "Eurocod 3: Proiectarea structurilor din oțel. Partea 1-3: Reguli generale - Reguli suplimentare pentru elementele structurale și table formate la rece," Asociația de Standardizare din România, SR EN 1993-1-3, Feb. 2008.

[3] M. Nedelcu, "GBT formulation to analyse the behaviour of thin-walled members with variable cross-section," Thin-Walled Struct., vol. 48, no. 8, pp. 629–638, Aug. 2010.

[4] M. Nedelcu, GBT formulation to analyse the buckling behaviour of isotropic conical shells, Thin-Walled Structures, 49 (7) (2011) 812–818.

[5] R. Schardt, Verallgemeinerte Technische Biegetheorie. Lineare Probleme. Springer-Verlag Berlin. Heidelberg New York, London, Paris, Tokyo, Hong Kong, 1989.

[6] MATLAB, version 7.10.0 (R2010a), The MathWorks Inc., Massachusetts, 2010.

[7] Hibbit, Karlsson and Sorensen Inc. ABAQUS Standard (Version 6.3), 2002.

[8] W. W. Yu, Cold-Formed Steel Structures, Chen Wai-Fah. Boca Raton: CRC Press LLC, 1999.

[9] C. C. Weng and T. Pekoz, "Residual Stresses in Cold-Formed Steel Members," J. Struct. Eng., vol. 116, no. 6, Jun. 1990.

[10] G. P. Mulligan and T. Pekoz, "Locally Buckled Thin-Walled Columns," J. Struct. Eng., vol. 110, no. 11, Nov. 1984.

[11] T. H. Miller and T. Pekoz, "Load-Eccentricity Effects on Cold-Formed Steel Lipped-Channel Columns," J. Struct. Eng., vol. 120, no. 3, Mar. 1994.

[12] V. Kalyanaraman and T. Pekoz, "Analytical Study of Unstiffened Elements," J. Struct. Div., vol. 104, no. 9, pp. 1507–1524, 1978.

[13] B. W. Schafer, Z. Li, and C. D. Moen, "Computational modeling of cold-formed steel," Thin-Walled Struct., vol. 48, no. 10–11, pp. 752–762, Nov. 2010.

[14] G. J. Hancock, Y. B. Kwon, and E. S. Bernard, "Strength design curves for thin-walled sections undergoing distortional buckling," J. Constr. Steel Res., vol. 31, no. 2–3, pp. 169–186, 1994.

[15] R. M. Lucas, F. G. A. Al-Bermani, and S. Kitipomchai, "Modelling of cold-formed purlin-sheeting systems— Part 1: Full model," Thin-Walled Struct., vol. 27, no. 3, pp. 223–243, Mar. 1997.

[16] P. W. Key and G. J. Hancock, "A theoretical investigation of the column behaviour of cold-formed square hollow sections," Thin-Walled Struct., vol. 16, no. 1–4, pp. 31–64, 1993.

[17] B. Young and K. J. R. Rasmussen, “Behaviour of cold-formed singly symmetric columns,” Thin-Walled Struct., vol. 33, no. 2, pp. 83–102, Feb. 1999.

[18] H. B. Blum and K. J. R. Rasmussen, “Elastic buckling of columns with a discrete elastic torsional restraint,” Thin-Walled Struct., vol. 129, pp. 502–511, Aug. 2018.

[19] B. Young and E. Ellobody, “Design of cold-formed steel unequal angle compression members,” Thin-Walled Struct., vol. 45, no. 3, pp. 330–338, Mar. 2007.

[20] J. M. Davies, P. Leach, and A. Taylor, “The design of perforated cold-formed steel sections subject to axial load and bending,” Thin-Walled Struct., vol. 29, no. 1–4, pp. 141–157, Dec. 1997.

[21] A. Ghersi, R. Landolfo, and F. M. Mazzolani, “Buckling modes of double-channel cold-formed beams,” Thin-Walled Struct., vol. 19, no. 2–4, pp. 353–366, 1994.

[22] “AISI – American Iron and Steel Institute: Cold-formed steel design manual,” American Iron and Steel Institute, Washington D.C., 1996.

[23] J. Loughlan, “Thin-walled cold-formed sections subjected to compressive loading,” Thin-Walled Struct., vol. 16, no. 1–4, pp. 65–109, 1993.

[24] A. Tomà, G. Sedlacek, and K. Weynand, “Connections in cold-formed steel,” Thin-Walled Struct., vol. 16, no. 1–4, pp. 219–237, 1993.

[25] J. F. A. Madeira, J. Dias, and N. Silvestre, “Multi objective optimization of cold-formed steel columns,” Thin-Walled Struct., vol. 96, pp. 29–38, 2015.

[26] G. Zagari, G. Zucco, A. Madeo, V. Ungureanu, R. Zinno, and D. Dubina, “Evaluation of the erosion of critical buckling load of cold-formed steel members in compression based on Koiter asymptotic analysis,” Thin-Walled Struct., vol. 108, pp. 193–204, Nov. 2016.

[27] L. Bertocci, D. Comparini, G. Lavacchini, M. Orlando, L. Salvatori, and P. Spinelli, “Experimental, numerical, and regulatory P-Mx-My domains for cold-formed perforated steel uprights of pallet-racks,” Thin-Walled Struct., vol. 119, pp. 151–165, Oct. 2017.

[28] N. Tondini and A. Morbioli, “Cross-sectional flexural capacity of cold-formed laterally-restrained steel rectangular hollow flange beams,” Thin-Walled Struct., vol. 95, pp. 196–207, Oct. 2015.

[29] C. Basaglia, D. Camotim, and H. Coda, “Behaviour, failure and DSM design of cold-formed steel beams: Influence of the load point of application,” Thin-Walled Struct., vol. 81, pp. 78–88, Aug. 2014.

[30] Z. Sadovský and J. Kriváček, “Influence of boundary conditions and load eccentricity on strength of cold-formed lipped channel columns,” Thin-Walled Struct., vol. 131, pp. 556–565, Jul. 2018.

[31] J. Bonada, M. Casafont, F. Roure, and M. M. Pastor, “Selection of the initial geometrical imperfection in nonlinear FE analysis of cold-formed steel rack columns,” Thin-Walled Struct., vol. 51, pp. 99–111, Feb. 2012.

[32] T. Vraný, “Effect of loading on the rotational restraint of cold-formed purlins,” Thin-Walled Struct., vol. 44, no. 12, pp. 1287–1292, Dec. 2006.

[33] R. J. Kasperska, K. Magnucki, and M. Ostwald, “Bicriteria optimization of cold-formed thin-walled beams with monosymmetrical open cross sections under pure bending,” Thin-Walled Struct., vol. 45, no. 6, pp. 563–572, Jun. 2007.

[34] D. Dubina and R. Zaharia, “Cold-formed steel trusses with semi-rigid joints,” Thin-Walled Struct., vol. 29, no. 1–4, pp. 273–287, Dec. 1997.

[35] R. Zaharia and D. Dubina, “Stiffness of joints in bolted connected cold-formed steel trusses,” J. Constr. Steel Res., vol. 62, no. 3, pp. 240–249, Mar. 2006.

[36] D. Dubina, V. Ungureanu, and L. Gilia, “Experimental investigations of cold-formed steel beams of corrugated web and built-up section for flanges,” Thin-Walled Struct., vol. 90, pp. 159–170, Mar. 2015.

[37] D. Dubina, “Structural analysis and design assisted by testing of cold-formed steel structures,” Thin-Walled Struct., vol. 46, no. 7–9, pp. 741–764, Sep. 2008.

[38] D. Dubina and V. Ungureanu, “Behaviour of multi-span cold-formed Z-purlins with bolted lapped connections,” Thin-Walled Struct., vol. 48, no. 10–11, pp. 866–871, Nov. 2010.

[39] R. Lorenz, Achsensymmetrische verzerrungen in dünnwandingen hohlzzylindern. Z Vereines Deutscher Ing 52 (43) (1908) 1706–1713.

[40] L.H. Donnel, A New Theory for the Buckling of Thin Cylinders Under Axial Compression and Bending, Transactions of the American Society of Mechanical Engineers, 12 (56) (1934) 795–806.

[41] J.L. Sanders, Nonlinear theories for thin shells, The Quarterly Journal of Mathematics, 21 (1) (1963) 21–36.

[42] W. Flügge, Stresses in Shells, second ed. Springer, Berlin, 1973.

[43] V.V. Novozhilov, Foundations of the Nonlinear Theory of Elasticity, Graylock Press, Rochester, NY, USA (now available from Dover, NY, USA), 1953.

[44] S. Timoshenko, J.M. Gere, Theory of elastic stability, McGraw-Hill Book Company, New York, 1961.

[45] Y. Goldfeld, Imperfection sensitivity of laminated conical shells, Solids and Structures, 44 (2007) 1221–1241.

[46] T. von Karman, H.-S. Tsien, The Buckling of Thin Cylindrical Shells Under Axial Compression, Aeronautical Sciences, 8 (8) (1941), 303–312.

[47] L.H. Donnel, C.C. Wan, Effect of imperfections on the buckling of thin cylinders and columns under axial compression, Applied Mechanics, 1 (17) (1950), 73–83.

[48] J. Arbocz and J. M. A. M. Hol, “Collapse of axially compressed cylindrical shells with random imperfections,” Thin-Walled Struct., vol. 23, no. 1–4, pp. 131–158, 1995.

[49] T. A. Winterstetter and H. Schmidt, “Stability of circular cylindrical steel shells under combined loading,” Thin-Walled Struct., vol. 40, no. 10, pp. 893–910, Oct. 2002.

[50] T. Rahman and E. L. Jansen, “Finite element based coupled mode initial post-buckling analysis of a composite cylindrical shell,” Thin-Walled Struct., vol. 48, no. 1, pp. 25–32, Jan. 2010.

[51] S. Singh, B. P. Patel, and Y. Nath, “Postbuckling of angle-ply laminated cylindrical shells with meridional curvature,” Thin-Walled Struct., vol. 47, no. 3, pp. 359–364, Mar. 2009.

[52] J. M. Alexander, “An approximate analysis of the collapse of thin cylindrical shells under axial loading,” Q. J. Mech. Appl. Math., vol. 13, no. 1, pp. 10–15, Jan. 1960.

[53] P. Seide and V. I. Weingarten, “On the Buckling of Circular Cylindrical Shells Under Pure Bending,” J. Appl. Mech., vol. 28, no. 1, pp. 112–116, Mar. 1961.

[54] C. A. Schenk and G. I. Schuëller, “Buckling analysis of cylindrical shells with random geometric imperfections,” Int. J. Non-Linear Mech., vol. 38, no. 7, pp. 1119–1132, Oct. 2003.

[55] H. Shen and T. Chen, “Buckling and postbuckling behaviour of cylindrical shells under combined external pressure and axial compression,” Thin-Walled Struct., vol. 12, no. 4, pp. 321–334, 1991.

[56] M. Jabareen and I. Sheinman, “Effect of the nonlinear pre-buckling state on the bifurcation point of conical shells,” Int. J. Solids Struct., vol. 43, no. 7–8, pp. 2146–2159, Apr. 2006.

[57] P.E. Tovstik, Some problems of the stability of cylindrical and conical shells, Applied Mathematics and Mechanics, 47 (5) (1983) 657–663.

[58] K. Chandrashekhara and M. S. Karekar, “Bending analysis of a truncated conical shell subjected to asymmetric load,” Thin-Walled Struct., vol. 13, no. 4, pp. 299–318, 1992.

[59] M. K. Chryssanthopoulos, C. Poggi, and A. Spagnoli, “Buckling design of conical shells based on validated numerical models,” Thin-Walled Struct., vol. 31, no. 1–3, pp. 257–270, May 1998.

[60] M. K. Chryssanthopoulos and A. Spagnoli, “The influence of radial edge constraint on the stability of stiffened conical shells in compression,” Thin-Walled Struct., vol. 27, no. 2, pp. 147–163, Feb. 1997.

[61] M. A. Kouchakzadeh, M. Shakouri, Stability analysis of joined isotropic conical shells under axial compression, Thin-Walled Structures, 72 (2013) 20–27.

[62] I. Ecsedi, “Torsional stiffness of conical membrane shells,” Mech. Res. Commun., vol. 27, no. 4, pp. 403–406, Aug. 2000.

[63] M. Maali, A. C. Aydın, H. Showkati, and M. Sağıroğlu, “The effect of longitudinal imperfections on thin-walled conical shells,” J. Build. Eng., vol. 20, pp. 424–441, Aug. 2018.

[64] H. Maan Jawad, Theory and design of plate and shell structures. London: Chapman & Hall; 1994. 344–346.

[65] A. H. Sofiyev and N. Kuruoglu, "Buckling analysis of nonhomogeneous orthotropic thin-walled truncated conical shells in large deformation," Thin-Walled Struct., vol. 62, pp. 131–141, Jan. 2013.

[66] S. L. Veldman, "Wrinkling prediction of cylindrical and conical inflated cantilever beams under torsion and bending," Thin-Walled Struct., vol. 44, no. 2, pp. 211–215, Feb. 2006.

[67] G. Watts, M. K. Singha, and S. Pradyumna, "Nonlinear bending and snap-through instability analyses of conical shell panels using element free Galerkin method," Thin-Walled Struct., vol. 122, pp. 452–462, Jan. 2018.

[68] M. Shakouri, A. Spagnoli, and M. A. Kouchakzadeh, "Re-interpreting simultaneous buckling modes of axially compressed isotropic conical shells," Thin-Walled Struct., vol. 84, pp. 360–368, Nov. 2014.

[69] W.T. Koiter, The stability of elastic equilibrium, in DTIC Document, 1970.

[70] P. Seide, "On the Buckling of Truncated Conical Shells in Torsion," J. Appl. Mech., vol. 29, no. 2, pp. 321–328, May 1961.

[71] F. Shadmehri, S. V. Hoa, and M. Hojjati, "Buckling of conical composite shells," Compos. Struct., vol. 94, no. 2, pp. 787–792, Jan. 2012.

[72] I.F. Correia Pinto, C.M. Soares Mota, C.A. Soares Mota. Analysis of laminated conical shell structures using higher order models. Compos Struct 2003; 62(3–4):383–90.

[73] E.J. Barbero, J.N. Reddy, J.L. Teply. General two-dimensional theory of laminated cylindrical shells. AIAA J 1990; 28(3):544.

[74] M. Nedelcu, "Buckling mode identification of perforated thin-walled members by using GBT and shell FEA," Thin-Walled Struct., vol. 82, pp. 67–81, Sep. 2014.

[75] M. Nedelcu and H. L. Cucu, "Buckling modes identification from FEA of thin-walled members using only GBT cross-sectional deformation modes," Thin-Walled Struct., vol. 81, pp. 150–158, Aug. 2014.

[76] "AISI – American Iron and Steel Institute: North American Specification for the Design of Cold-Formed Steel Structural Members with Commentary," American Iron and Steel Institute, Washington D.C., 2011.

[77] "AS/NZS 4600 – Australian/New Zealand Standards. Cold-formed Steel Structures," Sydney, 1996.

[78] "AISI – American Iron and Steel Institute: Supplement 2004 to the North American Specification for the Design of Cold-Formed Steel Structural Members 2001 Edition: Appendix 1, Design of

Cold-Formed Steel Structural Members Using Direct Strength Method," American Iron and Steel Institute, Washington D.C., 2004.

[79] "CUFSM: Elastic Buckling Analysis of Thin-Walled Members by Finite Strip Analysis, CUFSM v2.6."

[80] S. Ádány and B. W. Schafer, "A full modal decomposition of thin-walled, single-branched open cross-section members via the constrained finite strip method," J. Constr. Steel Res., vol. 64, no. 1, pp. 12–29, Jan. 2008.

[81] J.P. Papangelis and G.J. Hancock, Cross-Section Analysis and Finite Strip Analysis and Direct Strength Design of Thin-Walled Structures − THIN-WALL (version 2.1), Center for Advanced Structural Analysis, School of Civil and Mining Engineering, University of Sydney, 2005. (Its website is http://www.civil.usyd.edu.au/case/thinwall)

[82] R. Schardt, "Generalized beam theory—an adequate method for coupled stability problems," Thin-Walled Struct., vol. 19, no. 2–4, pp. 161–180, 1994.

[83] J. M. Davies, "Recent research advances in cold-formed steel structures," J. Constr. Steel Res., vol. 55, no. 1–3, pp. 267–288, Jul. 2000.

[84] D. Camotim, N. Silvestre, R. Gonçalves, and P. B. Dinis, "GBT Analysis of Thin-Walled Members: New Formulations and Applications, Thin-Walled Structures: Recent Advances and Future Trends in Thin-Walled Structures Technology", J. Loughlan. Bath: Canopus Publishing, 2004.

[85] "GBTUL 1.0b Buckling and Vibration Analysis of Thin-Walled Members."

[86] J. M. Davies and P. Leach, "First-Order Generalised Beam Theory," J. Construct. Steel Research, vol. 31, pp. 187–220, Jan. 1994.

[87] J. M. Davies and P. Leach, "Second-Order Generalised Beam Theory," J. Construct. Steel Research, vol. 31, pp. 221–241, Jan. 1994.

[88] R. Bebiano, C. Basaglia, D. Camotim, and R. Gonçalves, "GBT buckling analysis of generally loaded thin-walled members with arbitrary flat-walled cross-sections," Thin-Walled Struct., vol. 123, pp. 11–24, Feb. 2018.

[89] N. Silvestre and D. Camotim, "First-order generalised beam theory for arbitrary orthotropic materials," Thin-Walled Struct., vol. 40, no. 9, pp. 755–789, Sep. 2002.

[90] N. Silvestre and D. Camotim, "Second-order generalised beam theory for arbitrary orthotropic materials," Thin-Walled Struct., vol. 40, no. 9, pp. 791–820, Sep. 2002.

[91] N. Silvestre and D. Camotim, "Shear Deformable Generalized Beam Theory for the Analysis of Thin-Walled Composite Members," J. Eng. Mech., vol. 139, no. 8, Aug. 2013.

[92] R. Gonçalves and D. Camotim, "Buckling behaviour of thin-walled regular polygonal tubes subjected to bending or torsion," Thin-Walled Struct., vol. 73, pp. 185–197, Sep. 2013.

[93] R. Gonçalves and D. Camotim, "GBT deformation modes for curved thin-walled cross-sections based on a mid-line polygonal approximation," Thin-Walled Struct., vol. 103, pp. 231–243, Jun. 2016.

[94] R. Gonçalves, R. Bebiano, and D. Camotim, "On the shear deformation modes in the framework of Generalized Beam Theory," Thin-Walled Struct., vol. 84, pp. 325–334, Nov. 2014.

[95] R. Bebiano, R. Gonçalves, and D. Camotim, "A cross-section analysis procedure to rationalise and automate the performance of GBT-based structural analyses," Thin-Walled Struct., vol. 92, pp. 29–47, Jul. 2015.

[96] N. M. F. Silva, N. Silvestre, and D. Camotim, "GBT formulation to analyse the buckling behaviour of FRP composite open-section thin-walled columns," Compos. Struct., vol. 93, no. 1, pp. 79–92, Dec. 2010.

[97] S. de Miranda, A. Gutiérrez, R. Miletta, and F. Ubertini, "A generalized beam theory with shear deformation," Thin-Walled Struct., vol. 67, pp. 88–100, Jun. 2013.

[98] N. Peres, R. Gonçalves, and D. Camotim, "First-order generalised beam theory for curved thin-walled members with circular axis," Thin-Walled Struct., vol. 107, pp. 345–361, Oct. 2016.

[99] P. Natário, N. Silvestre, and D. Camotim, "Localized web buckling analysis of beams subjected to concentrated loads using GBT," Thin-Walled Struct., vol. 61, pp. 27–41, Dec. 2012.

[100] J. M. Davies, P. Leach, and A. Taylor, "The Design of Perforated Cold-Formed Steel Sections Subject to Axial Load and Bending," Thin-Walled Struct., vol. 29, no. 1–4, pp. 141–157, 1997.

[101] J. Jönsson and M. J. Andreassen, "Distortional eigenmodes and homogeneous solutions for semi-discretized thin-walled beams," Thin-Walled Struct., vol. 49, no. 6, pp. 691–707, Jun. 2011.

[102] G. Piccardo, G. Ranzi, and A. Luongo, "A direct approach for the evaluation of the conventional modes within the GBT formulation," Thin-Walled Struct., vol. 74, pp. 133–145, Jan. 2014.

[103] G. Garcea et al., "Deformation modes of thin-walled members: A comparison between the method of Generalized Eigenvectors and Generalized Beam Theory," Thin-Walled Struct., vol. 100, pp. 192–212, Mar. 2016.

[104] S. Ádány, N. Silvestre, B. W. Schafer, and D. Camotim, "GBT and cFSM: two modal approaches to the buckling analysis of unbranched thin-walled members," Adv. Steel Constr., vol. 5, no. 2, pp. 195–223, 2009.

[105] J. Cai and C. D. Moen, "Elastic buckling analysis of thin-walled structural members with rectangular holes using generalized beam theory," Thin-Walled Struct., vol. 107, pp. 274–286, Oct. 2016.

[106] R. Bebiano, N. Silvestre, and D. Camotim, "GBT formulation to analyse the buckling behaviour of Thin-walled members subjected to non-uniform bending," Int. J. Struct. Stab. Dyn., vol. 7, no. 1, pp. 23–54, Mar. 2007.

[107] N. Silvestre and D. Camotim, "GBT Buckling Analysis Of Pultruded FRP Lipped Channel Members," Comput. Struct., pp. 1889–1904, Feb. 2003.

[108] C. Basaglia and D. Camotim, "Buckling Analysis of Thin-Walled Steel Structural Systems Using Generalized Beam Theory (GBT)," Int. J. Struct. Stab. Dyn., vol. 15, no. 1, 2015.

[109] C. Basaglia, D. Camotim, and N. Silvestre, "GBT-based local, distortional and global buckling analysis of thin-walled steel frames," Thin-Walled Struct., vol. 47, no. 11, pp. 1246–1264, Nov. 2009.

[110] C. Basaglia, D. Camotim, and N. Silvestre, "Post-buckling analysis of thin-walled steel frames using generalised beam theory (GBT)," Thin-Walled Struct., vol. 62, pp. 229–242, Jan. 2013.

[111] M. Nedelcu, "GBT-based buckling mode decomposition from finite element analysis of thin-walled members," Thin-Walled Struct., vol. 54, pp. 156–163, May 2012.

[112] D. Camotim, N. Silvestre, C. Basaglia, and R. Bebiano, "GBT-based buckling analysis of thin-walled members with non-standard support conditions," Thin-Walled Struct., vol. 46, no. 7–9, pp. 800–815, Sep. 2008.

[113] C. Basaglia, D. Camotim, and N. Silvestre, "Global buckling analysis of plane and space thin-walled frames in the context of GBT," Thin-Walled Struct., vol. 46, no. 1, pp. 79–101, Jan. 2008.

[114] C. Basaglia, D. Camotim, R. Gonçalves, and A. Graça, "GBT-based assessment of the buckling behaviour of cold-formed steel purlins restrained by sheeting," Thin-Walled Struct., vol. 72, pp. 217–229, Nov. 2013.

[115] D. Henriques, R. Gonçalves, and D. Camotim, "GBT-based finite element to assess the buckling behaviour of steel–concrete composite beams," *Thin-Walled Struct.*, vol. 107, pp. 207–220, Oct. 2016.

[116] EN 1994-1-1:2004, Eurocode 4: Design of Composite Steel and Concrete Structures – Part 1-1: General Rules and Rules for Buildings, CEN, Brussels, Belgium, 2004.

[117] D. Henriques, R. Gonçalves, and D. Camotim, "A physically non-linear GBT-based finite element for steel and steel-concrete beams including shear lag effects," Thin-Walled Struct., vol. 90, pp. 202–215, May 2015.

[118] C. Schardt, Zur berechnung des kreiszylinders mit ansätzen der Verallgemeinerten Technischen Biegetheorie, vol. Diplomarbeit Institut für Mechanik. TU Darmstadt, 1985.

[119] R. Schardt, C. Schardt, Anwendungen der Verallgemeinerten Technischen Biegetheorie im Leichtbau, Wiley-VCH Verlag, Stahlbau 70 (9), 2001.

[120] N. Silvestre, “Generalised beam theory to analyse the buckling behaviour of circular cylindrical shells and tubes,” Thin-Walled Struct., vol. 45, no. 2, pp. 185–198, Feb. 2007.

[121] N. Silvestre, Buckling behaviour of elliptical cylindrical shells and tubes under compression, Solids and Structures, 45 (16) (2008) 4427–4447.

[122] U.M. Ascher, R.M.M. Mattheij, R.D. Russell, Numerical Solution of Boundary Value Problems for Ordinary Differential Equations, Society for Industrial and Applied Mathematics, 1995.

[123] D.O. Brush and B.O. Almroth (1975). Buckling of Bars, Plates and Shells, McGraw-Hill, New York.

[124] V.Z. Vlasov (1959). Thin-Walled Elastic Bars, Fizgmatiz, Moscow. (in Russian; translation to English: Israel Program for Scientific Translation, Jerusalem, 1961).

[125] R. A. Silva Bebiano, Stability and dynamics of thin-walled members. Application of Generalised Beam Theory. PhD Thesis - Universidade Técnica De Lisboa. Instituto Superior Técnico, 2010.

[126] M. Nedelcu and H. Mociran, Metoda elementelor finite. Indrumator de laborator. Cluj-Napoca: U.T. Press, 2016.